Title
Ligand regulation of peroxisome proliferator-activated receptor-[gamma] induction

Author
Person, Eric C.

Publication Date
2001

Peer reviewed|Thesis/dissertation

Ligand Regulation of Peroxisome Proliferator-Activated Receptor-γ Induction

by

Eric C. Person

DISSERTATION

Submitted in partial satisfaction of the requirements for the degree of

DOCTOR OF PHILOSOPHY

in

BIOPHYSICS

in the

GRADUATE DIVISION

of the

UNIVERSITY OF CALIFORNIA SAN FRANCISCO

Date University Librarian

Degree Conferred: .....

Dedicated to my family for their love and support.

Acknowledgments

First and foremost, I owe my gratitude to my graduate advisor, Professor Thomas S. Scanlan. Tom has been a wonderful mentor and teacher, whose continued support and advice have provided a nurturing environment in which to develop my scientific skills.

I also wish to express my gratitude to Professors Keith Yamamoto and Paul Ortiz de Montellano for providing their time and effort to serve on both my thesis and orals committees. I credit their advice and feedback as being instrumental in bringing my studies to a successful conclusion.

I wish to thank all the members of the Scanlan laboratory, especially Ross Weatherman. They have helped make my graduate experience rewarding.

I wish to thank my collaborators, Leslie Waite and Professor Robert Taylor, for sharing their results regarding pregnancy serum with us. Our collaboration on this topic led to two papers, and was instrumental in bringing my project to a successful completion.

I wish to thank Russ Huber from the Fletterick laboratory for his help and advice. He provided specific assistance in the expression and purification of the hPPARγ LBD described in Chapter 5 as well as general advice on the albumin binding assay.

Ligand Regulation of Peroxisome Proliferator-Activated Receptor-γ Induction

Eric C. Person

Abstract

This thesis focuses on the question of ligand regulation of PPARγ. The project started with the design and synthesis of rosiglitazone and novel thiazolidinedione derivatives based on the extension hypothesis. The second phase of the project involved finding useful transfection and binding assays for the evaluation of these and other ligands. Due to difficulties obtaining reasonable signal-to-noise levels from conventional transient transfection cell assays, a stable cell line with endogenous PPARγ expression and response and a transfected PPRE driven luciferase reporter gene was generated and characterized. EP-JEG cells, as we have called them, were found to yield better reproducibility both within and between experiments than the transient transfection experiments. EP-JEG cells were used to identify and evaluate a serum factor responsible for inhibiting $15dJ_2$ induction of PPARγ. In the presence of serum $15dJ_2$ gave 2-15 fold induction of PPARγ, while in the absence of serum $15dJ_2$ was found to lead to 150-700 fold induction of PPARγ. Bovine serum albumin was found to bind $15dJ_2$ with a K_d of 870 ± 70 nM. Through this binding interaction albumin significantly reduces the free $15dJ_2$ concentration available to activated transcription through PPARγ, leading to the observed inhibition of $15dJ_2$ induction of PPARγ. The potential interaction of albumin with other PPARγ ligands should be considered when selecting techniques to isolate and characterize PPARγ ligands, and may be important in understanding the function of PPARγ *in vivo*.

Table of Contents

List of Tables

List of Figures

List of Terms and Abbreviations

$15dJ_2$	15-deoxy-$\Delta^{12,14}$-prostaglandin J_2 (11-oxo-prosta-5Z,9,12E,14Z-tetraen-1-oic acid)
AF-1	activation function-1
AF-2	activation function-2
aP2	adipocyte lipid binding protein
APS	ammoniumpersulfate
ATCC	American Type Culture Collection
BCA	bicinchoninic acid
BSA	bovine serum albumin
CBP	CREB binding protein
DBD	DNA binding domain
DMEM	Debecalo's modified essential medium H-21
DMSO	dimethylsulfoxide
DTT	dithiothreitol
EDTA	ethylenediaminetetraacetic acid
ER	estrogen receptor
EtOH	ethanol
FBS	fetal bovine serum
G418	Geneticin (neomycin)
HPLC	high performance liquid chromatography
HSA	human serum albumin
HTFBS	heat treated (80°C, 20 min) FBS
HTNCS	heat treated (80°C, 20 min) NCS
LBD	ligand binding domain
LCMS	liquid chromatography-mass spectrometry
LDL	low density lipoprotein
MEM Earle's BSS	minimal essential medium with Earle's balanced salt solution
NCoR	nuclear corepressor
NCS	newborn calf serum
NIDDM	non insulin dependent diabetes mellitus
oxLDL	oxidized low density lipoprotein
PBP	PPAR binding protein
PBS	phosphate buffered saline 0.1 g/L $CaCl_2$, 0.1 g/L $MgCl_2 \cdot 6H_2O$, 0.2 g/L KCl, 0.2 g/L KH_2PO_4, 8.0 g/L NaCl, 2.16 g/L $Na_2HPO_4 \cdot 7H_2O$.
PBS, calcium and magnesium free	phosphate buffered saline without calcium or magnesium salts 0.2 g/L KH_2PO_4, 2.16 g/L $Na_2HPO_4 \cdot 7H_2O$, 0.2 g/L KCl, 9.0 g/L NaCl.
PGD_2	Prostaglandin D_2
PGE_2	Prostaglandin E_2
PGH_2	Prostaglandin H_2
PMSF	phenylmethylsulfonyl fluoride

PPAR	peroxisome proliferator-activated receptor
PPRE	Peroxisome proliferator response element
PVDF	polyvinylidene difluoride
Rosiglitazone	BRL49653 Avandia™ (Z)-5-(4-(2-(methyl-2-pyridinylamino)ethoxy)benzyl)-2,4-thiazolidinedione
RT-PCR	reverse transcriptase-polymerase chain reaction
RXR	retinoic x receptor
SDS	sodium dodecyl sulfate
SDS-PAGE	SDS-polyacrylamide gel electrophoresis
SRC-1	steroid receptor coactivator-1
STV	standard trypsin (0.05%) and versine (0.02%)
TBS	Tris buffered saline 100 mM Tris pH 7.5, 0.9% (w/v) NaCl
TEMED	N,N,N,N'-tetramethylethylenediamine
TIF-2	transcriptional intermediate protein
TNFα	tumor nucrosis factor α
β-gal	β-galactosidase

Chapter 1: Introduction

Nuclear hormone receptors are ligand inducible transcription factors. As a family, they bind their small hydrophobic ligands within the hydrophobic core of their ligand binding domain (1, 2). Nuclear receptors typically form either homodimers or heterodimers with the retinoic x receptor (RXR) and bind to short stretches of DNA in the promoter regions of receptor regulated genes known as response elements. Upon ligand binding, RXR heterodimers release corepressors and recruit coactivators resulting in activation of transcription (3-5). While the endogenous high affinity ligands of many nuclear receptors are known, a large number of these receptors do not have known high affinity ligands (6). These orphan receptors are potentially important drug targets due to the critical role nuclear receptors play in gene transcription and regulation of physiological effects (7).

Peroxisome Proliferator-Activated Receptor-γ

Background and History

The peroxisome proliferator-activated receptors (PPARs) are orphan nuclear receptors that heterodimerize with RXR and bind to peroxisome proliferator response elements (PPREs), which consist of a direct repeat of the AGGTCA half site with a one spacer nucleotide(8-10). In the recently proposed unified nomenclature of nuclear receptors, PPARs (NR1C) form group C in subfamily 1, which also includes the thyroid hormone receptor and other RXR heterodimers (11). Like other nuclear receptors, the PPARs consist of an N-terminal region, which contains the activation function-1 (AF-1), a DNA-binding domain (DBD), which is responsible for recognition and binding of the

DNA response elements, a short hinge region, and a ligand binding domain (LBD), which contains the ligand dependent activation function-2 (AF-2) (12-14).

There are three subtypes of PPAR. PPARα (NR1C1) was first identified as a protein upregulated by a class of compounds known as peroxisome proliferators, and was shown to mediate the activities of the compounds (13). PPARδ (also called PPARβ, NUC-1 and FAAR) (NR1C2) and PPARγ NR1C3) were identified shortly thereafter (12). It has been suggested that each PPAR subtype may have similar but chemically distinct ligands (15), based on both the relatively low similarity of the ligand binding domains of PPARs (60% identity for PPARs versus 82% identity for thyroid hormone receptor (16)) and the observed subtype specificity of known agonists.

Genomic Structure

PPARα, PPARδ, and PPARγ are encoded on distinct single copy genes located on human chromosomes 22, 6 and 3 respectively (17-19). Alternate promoter usage and gene splicing generates three transcripts from the PPARγ gene (20, 21). These three PPARγ transcripts differ only in the 5' region corresponding to the N-terminal domain. The third transcript, PPARγ3 yields a protein identical to that of PPARγ1.

Mouse PPARγ2 differs from PPARγ1 in that it has an additional 30 N-terminal amino acids (22). Rosiglitazone has an EC_{50} of 30 nM for PPARγ1 and 100 nM for PPARγ2, but pioglitazone has the same activity with expression with PPARγ2 expressed primarily in white and brown adipose tissue (23). As several coactivators and corepressors are known to interact with the N-terminal domain (24), and the N-terminal domain is known to affect ligand activity (24-30), it is likely that these two PPARγ isoforms have overlapping but distinct roles *in vivo*.

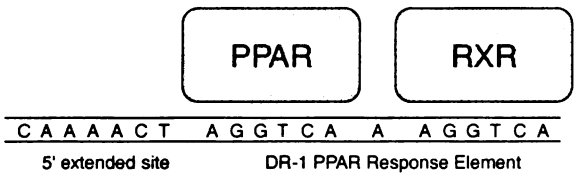

Figure 1.1: The Consensus Sequence of the PPAR Response Element

Shown is the consensus sequence of the peroxisome proliferator response element (PPRE) including the extended 5' recognition site reported by June-Aubrey (10). Unlike other RXR heterodimers, PPARs binds at the 5' half site.

DNA Binding and Recognition

Like other nuclear receptors, the PPAR DBDs use two zinc finger motifs to bind DNA. The PPAR P-box is identical to that of other receptors that form RXR heterodimers, all of which recognize the AGGTCA half site (6, 31, 32). PPAR dimerzies with RXR and recognizes response elements consisting of a direct repeat of this half site with one spacer nucleotide, but differs from other RXR heterodimers in that PPAR is located 5' of RXR (Figure 1.1) (12, 33-35). This may be due to differences in the PPAR D-box, where PPAR has only three of the five amino acids found in most other nuclear receptors (9).

The PPAR/RXR dimer binding is improved if the spacer nucleotide is an A, and if an extended 5' site is included (Figure 1.1) (9, 10). PPARγ binding is less dependent on the 5'-flanking sequence than PPARα binding, so the extended recognition site may provide potential subtype specificity (10). The PPREs found in the promoters of several genes expressed in adipocytes, including phosphoenolpyruvate carboxykinase (PEPCK) and adipocyte lipid binding protein (aP2), do not match the consensus sequence for this extended 5' site and show preferential binding of PPARγ (10).

Tissue Specific Expression

In humans, PPARα is expressed in the liver, heart, kidney, skeletal muscle, intestine, pancreas, and to a lesser extent in placenta, lung, and adipose tissue (36, 37).

The expression of PPARα in the human liver is lower than the expression observed in rodents (38). PPARδ is expressed in most tissues, with higher levels of receptor found in the brain (36, 37). PPARγ1 is found in adipose tissue, skeletal muscle, liver, heart, bone marrow stromal cells, placenta, ovaries, lung, colonic mucosa, mammary gland, and urinary bladder (18, 36, 37, 39-43). Particularly high levels of PPARγ are expressed in cancerous colon, breast, lung and prostate tumors (41, 44-49). PPARγ2 is expressed at high levels in both white and brown adipose tissue (23).

Along with ligand subtype specificity and the possibility of promoter specificity, the tissue specific expression provides a molecular mechanism whereby the different subtypes can exert different physiological effects.

Ligand Binding and Recognition

Synthetic PPARγ Ligands

Rosiglitazone was the first identified high affinity ligand for the PPARs, binding to PPARγ with a K_d of 43 nM and activating transcription in reporter gene assays with an EC_{50} of 80 nM (50, 51). Interestingly, many of the anti-diabetic compounds known as thiazolidinediones (Figure 1.2, Table 1.1) were found to be specific PPARγ ligands with low to sub micromolar affinities (50-54). The origin of the thiazolidinedione drugs is discussed in more detail below. Rosiglitazone and AD-5075 are still two of the highest affinity PPARγ specific ligands, which have been reported to date.

Several non-steroidal anti-inflammatory drugs (NSAIDs) activate PPARγ-regulated transcription, compete with rosiglitazone for PPARγ binding, and induce adipogenesis in culture. The chemical structures for ibuprofen, fenoprofen, flufenamic

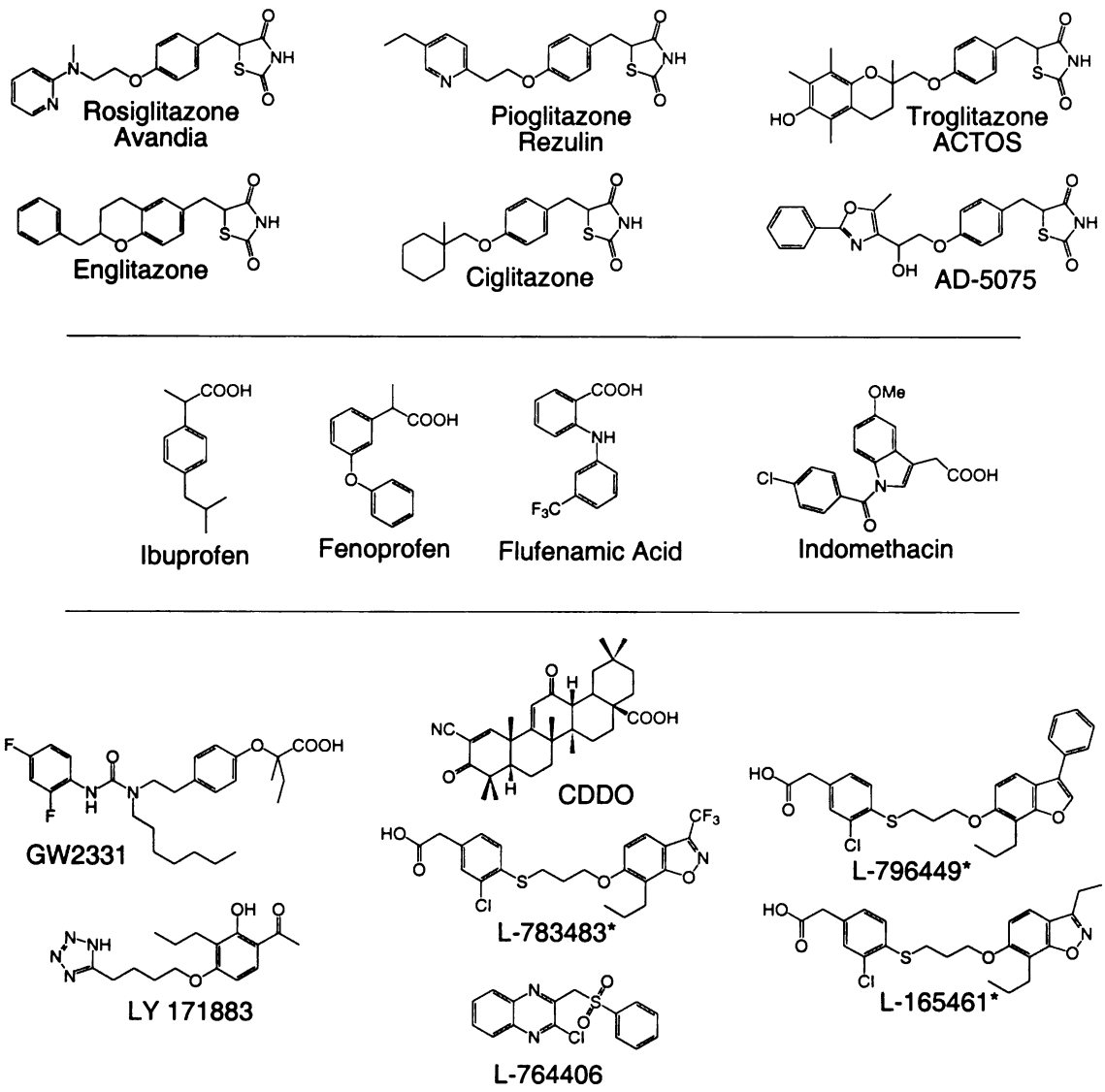

Figure 1.2: PPARγ Synthetic Agonists

The chemical structures of synthetic compounds known to induce PPARγ regulated transcription are shown. The thiazolidinediones (top) are insulin sensitizers useful in treating diabetes. The activities of these compounds are listed in Table 1.1.

acid, and indomethacin are shown in Figure 1.2, and their PPARγ activities are listed in Table 1.1. They are all extremely weak ligands, with the best, indomethacin, requiring greater than10 μM concentrations to obtain full activation (55).

A variety of synthetic compounds other than thiazolidinediones have been shown to activate transcription of PPARγ responsive genes (54-59). A partial list, comprised of

Compound Name	EC_{50} /K_i	Reference(s)
Rosiglitazone	30-80 nM / 43 nM	(50-52)
Pioglitazone	400 nM /	(50, 51, 60)
Troglitazone	83 nM /	(53, 61-63)
Englitazone	> 2 μM	(50)
Ciglitazone	> 2 μM	(50)
AD-5075	1 nM / 11 nM (K_d)	(54, 57, 64)
Ibuprofen	> 10 μM	(55)
Fenoprofen	> 10 μM	(55)
Flufenamic Acid	> 10 μM	(55)
Indomethacin	40 μM / 100 μM	(55)
GW2331	300 nM / 300 nM	(59)
GW0072	110 nM / 70 nM partial agonist 15-25%	(65)
LY 171883	activates at 30 μM	(58)
L-783483	40 nM / 14 nM	(57)
L-764406	69 nM / 70 nM partial agonist 25%	(54)
L-796449	15 nM / 2 nM	(57)
L-165461	40 nM / 15 nM	(57)
CDDO	10 nM / 12 nM partial agonist 30%	(56)

Table 1.1: PPARγ Synthetic Agonists

The activity of synthetic compounds known to induce PPARγ regulated transcription are shown. The chemical structures of these compounds are listed in Figure 1.2.

some of the higher affinity ligands are shown in Figure 1.2 and their activities are listed in Table 1.1.

The fibrates, a family of peroxisome proliferators are typically PPARα ligands (15). Drug discovery efforts at Glaxo-Wellcome using combinatorial techniques have identified novel fibrates as ligands for both PPARδ (66, 67) and PPARγ (59, 65, 66). Some other noteworthy compounds include a series of carboxylic acids developed by Merck Laboratories, which activate both PPARδ and PPARγ (54, 57). Several of these compounds, shown in Figure 1.2 and listed in Table 1.1, bind and activate the receptor in the low nM range, making them among the highest affinity reported ligands for PPARs.

One of the Merck ligands, L-764406 (Figure 1.2, Table 1.1) binds irreversibly by forming a covalent complex with Cys^{313} of PPARγ (54). The thiazolidinedione AD-5075 cannot bind to the covalent complex, with the relatively small L-764406 bound in the ligand pocket. L-764406 has an apparent IC_{50} of 70 nM, and an EC_{50} of 69 nM, but only 25% of AD-5075 maximal activation, and is therefore only a partial agonist.

Another partial agonist, which was reported recently, is the synthetic triterpenoid, CDDO (Figure 1.2, Table 1.1) (56). Both CDDO and its methyl ester (CDDO-Me) (Figure 1.3, Table 1.2) bind to PPARγ, but CDDO shows partial agonist activity and CDDO-Me is an antagonist. CDDO has an EC_{50} of approximately 10 nM and a K_i of 12 nM, but only results in 30% of the maximal activation shown by 1 μM rosiglitazone. CDDO-Me can inhibit rosiglitazone induction of PPARγ with an IC_{50} of approximately 100 nM, consistent with its K_I of 130 nM. The differences in activity of these ligands and rosiglitazone were shown to be connected to recruitment of cofactors. While rosiglitazone and CDDO release corepressor on binding, CDDO-Me does not. The partial agonism of CDDO appears to be due to a weaker affinity for coactivator (56).

The crystal structure of GW0072 (Figure 1.3, Table 1.2), another synthetic PPARγ antagonist, bound to PPARγ has been solved (65). GW0072 blocks rosiglitazone (100 nM) induction of PPARγ and rosiglitazone induced adipogenesis. GW0072 does not directly affect the positioning of helix 12 or residues involved in coactivator recruitment, as observed for the estrogen receptor (ER) antagonist structures (68-70), but causes the receptor to adopt a conformation similar to the unliganded receptor (65).

BADGE (Figure 1.3, Table 1.2), a component of epoxy resins, was identified by Wright as a synthetic ligand for PPARγ (71). BADGE shows no ability to activate

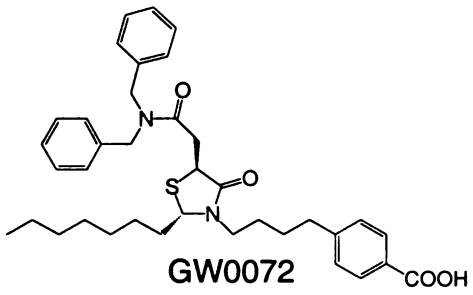

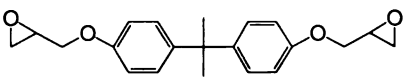

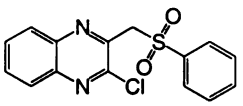

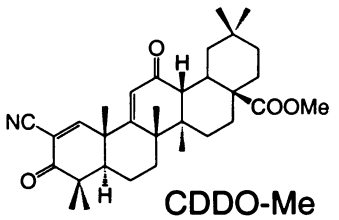

Figure 1.3: PPARγ Antagonists

The chemical structures of synthetic compounds known to block induction of PPARγ regulated transcription are shown. The activities of these compounds are listed in Table 1.2.

Compound Name	IC_{50} / K_I	Reference(s)
BADGE	70% inhibition & 50% displacement at 100 μM	(71)
GW0072	110 nM / 70 nM partial agonist 15-25%	(65)
L-764406	69 nM / 70 nM partial agonist 25%	(54)
CDDO-Me	100 nM / 130 nM	(56)

Table 1.2: PPARγ Antagonists

The activity of synthetic compounds known to block induction of PPARγ regulated transcription are shown. The chemical structures of these compounds are listed in Figure 1.3.

PPARγ mediated transcription, but can antagonize the ability of rosiglitazone to induce PPARγ. Limited affinity and solubility prevents complete blockage, and hence the determination of an IC_{50} and K_i. BADGE also inhibits adipocyte differentiation, demonstrating that PPARγ is required for hormonally induced adipocyte differentiation (71).

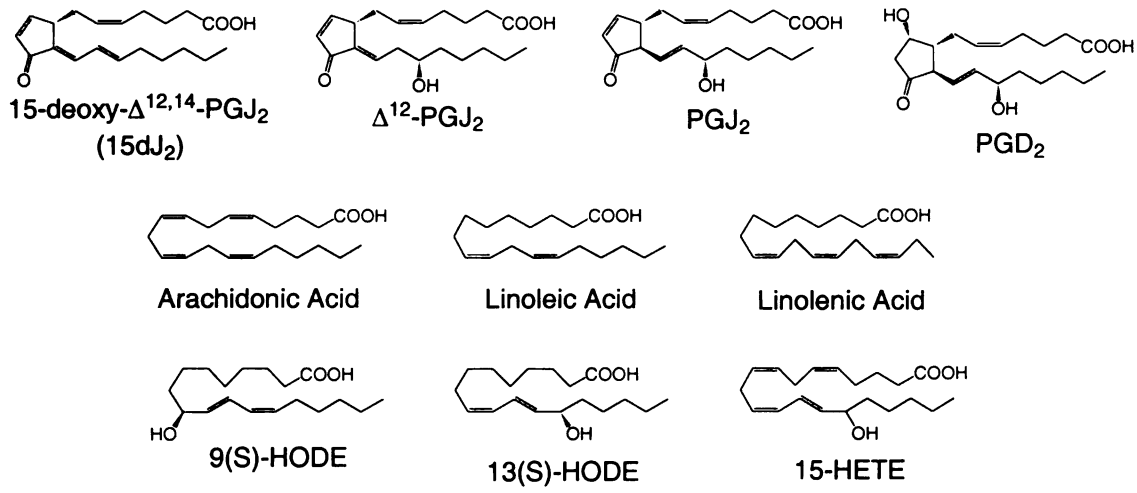

Figure 1.4: PPARγ Endogenous Agonists

The chemical structures of fatty acids known to induce PPARγ regulated transcription are shown. These ligands have not been demonstrated to be present at sufficient concentrations to activate PPARγ transcription in vivo. The activities of these compounds are listed in Table 1.3.

Endogenous Ligands

Though several high affinity synthetic PPARγ ligands have been identified, an endogenous ligand with an affinity sufficient to allow activation by endogenous levels of ligand has not been identified at this time. Some authors have proposed that PPARγ may be a generic fat sensor, responding to a wide range of fatty acids with only moderate receptor affinity (72). The endogenous high affinity hormones of other members of the nuclear receptor superfamily bind in the low- to sub-nanomolar range (7), in contrast to the micromolar affinities for most of the endogenous compounds that have been shown to activate PPARγ (43, 73-76). It is important to note that failure to find an endogenous high affinity PPARγ activator, or the existence of weak activators, does not preclude the existence of a single sub-nanomolar ligand for PPARγ.

In 1995 the arachidonic acid metabolite 15-deoxy-$\Delta^{12,14}$-Prostaglandin J_2 ($15dJ_2$) (Figure 1.4, Table 1.3) was identified as a PPARγ specific agonist (51, 77). $15dJ_2$ binds

Compound Name	EC_{50} / K_I	Reference(s)
15-deoxy-$\Delta^{12,14}$-Prostaglandin J_2	2 μM / 2.5 μM	(51, 62, 63, 76-78)
Δ^{12}-Prostaglandin J_2	> 5 μM	(51, 77)
Prostaglandin J_2	> 5 μM	(51, 77)
Prostaglandin D_2	> 5 μM	(51, 77)
Arachidonic Acid	activity at 100 μM	(59)
Linoleic acid	activity at 100 μM	(59)
Linolenic acid	activity at 100 μM	(59)
9-HODE	activity at 67 μM	(75)
13-HODE	activity at 30 μM	(74, 75)
15-HETE	activity at 30 μM	(74)

Table 1.3: PPARγ Endogenous Agonists

The activity of fatty acids known to induce PPARγ regulated transcription are listed. These ligands have not been demonstrated to be present at sufficient concentrations to activate PPARγ transcription *in vivo*. The chemical structures of these compounds are shown in Figure 1.4.

to PPARγ with a K_I of 2.5 μM and activates transcription with an EC_{50} of 2 μM (51, 77). Though it had not been observed *in vivo* at that time, it was originally reported as an albumin catalyzed degradation product of Prostaglandin D_2 (PGD_2) (79, 80), and was proposed as an endogenous ligand for PPARγ. $15dJ_2$ has since been observed in both human inflamed lung tissue (78) and the duck uropygial gland (76). While PPARγ is expressed in both of these tissues, the reported ligand concentration is not sufficient to result in receptor activation if the *in vivo* activity of $15dJ_2$ is consistent with the activity observed in reporter gene assays.

Oxidized metabolites of linoleic and arachidonic acid, present in oxidized low density lipoprotein (oxLDL) have been identified as endogenous PPARγ ligands (Figure 1.4, Table 1.3) (74, 75). Like $15dJ_2$, 9-HODE, 13-HODE, and 15-HETE all have PPARγ activity in the micromolar range.

The production of endogenous ligands in several PPARγ expressing tissues has been reported. PPARγ can be activated by the ADD1/SREBP1 transcription factor,

which is expressed early in adipogenesis, through production of an endogenous ligand (73). The ligand and ADD1/SREBP1 target gene have not been identified, but may provide a useful experimental approach to higher affinity endogenous PPARγ ligands. Treatment of ducks with estrogen induces the formation of $15dJ_2$ by the uropygial gland (76).

The Taylor lab has recently reported the presence of a PPAR activator in serum drawn from pregnant women (43). Preliminary experiments suggest that the activator is not a protein (81), but the activating factor has not yet been isolated. The activator has not been proven to function through PPARγ, but inhibition of activation by TNF-α is consistent with the activating factor being an endogenous PPARγ ligand (43). The activating factor in serum from pregnant women is present at 10-fold higher concentrations than are required to see activation in reporter gene assays (43). This suggests that it is likely to have higher affinity than previously reported endogenous activators, and may be the most promising approach to the identification of a physiologically relevant endogenous PPARγ activator.

LBD Structure

The crystal structures of PPARγ LBD has been solved in the absence and presence of the synthetic ligand rosiglitazone (72, 82), and shows similar structure to the PPARδ LBD structure (67). The overall fold of the PPAR LBD is formed by 13 helices and a small β-sheet consisting of four strands (Figure 1.5). The only major difference between the PPAR LBD fold and other nuclear receptors is the additional helix, designated 2', located between the first β-strand and helix 3. Like other nuclear receptors, the β-sheet region of the receptor structure forms part of the binding pocket.

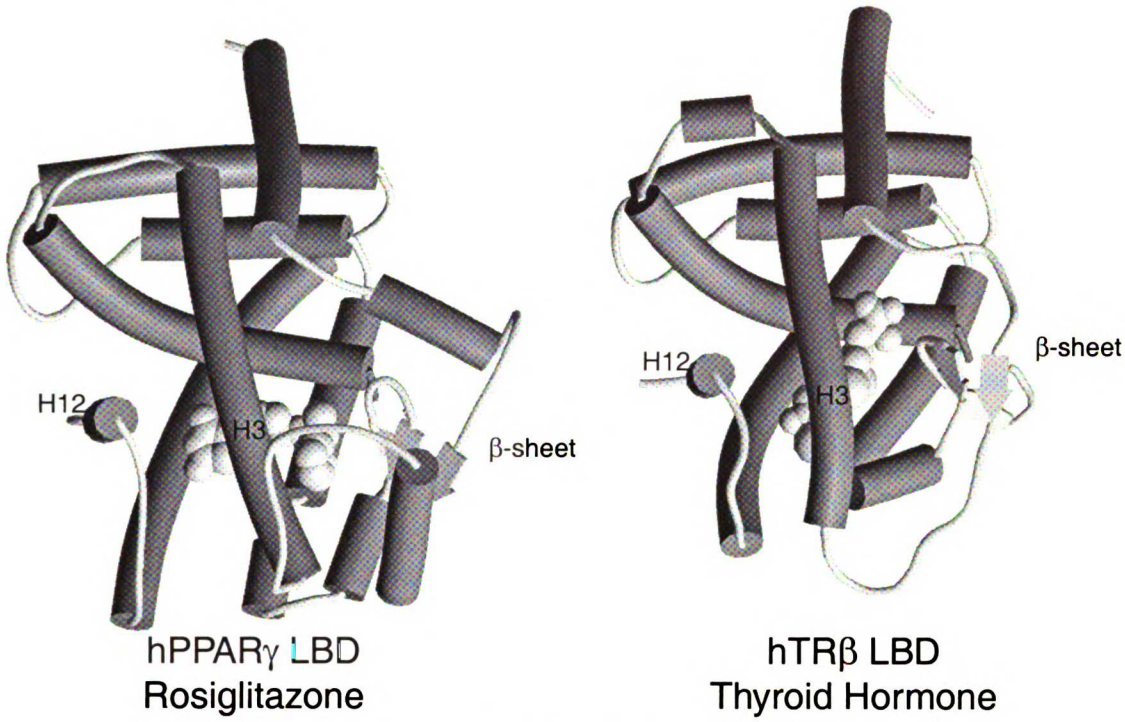

Figure 1.5: hPPARγ and hTRβ LBD Crystal Structures

Schematics of the hPPARγ and hTRβ crystal structures are shown. The bound ligands, rosiglitazone and Thyroid Hormone respectively (shown as white space-fill models), are found in the hydrophobic core of the protein. The β-sheet region of the PPARγ LBD (bottom right) is expanded relative to the TRβ structure, allowing for the increased volume of the observed PPARγ ligand binding pocket. The thiazolidinedione ring of rosiglitazone is found the left where it makes contact with helix 12. The pyridine ring is bent around helix 3 where it binds between helix 3 and the β-sheet region.

The temperature factors in this region of the PPARγ structure are higher than other regions of the structure, and there is poor density between helix 2' and helix 3 (72).

Like other nuclear receptor structures the ligand is bound in a hydrophobic pocket comprising the core of the bottom half of the ligand binding domain (Figure 1.5) (2, 72, 83). In contrast to other nuclear receptors, the ligand-binding cavity is considerably larger, a volume of approximately 1300 $Å^2$ (72, 82) compared to approximately 600 $Å^2$ for TR (83). The ligand-binding cavity, which is present in both the apo and halo structures, forms a t-shape between helices 3-7 and 10. Rosiglitazone, whose molecular volume is comparable to other nuclear receptor agonists (84), occupies roughly 40% of

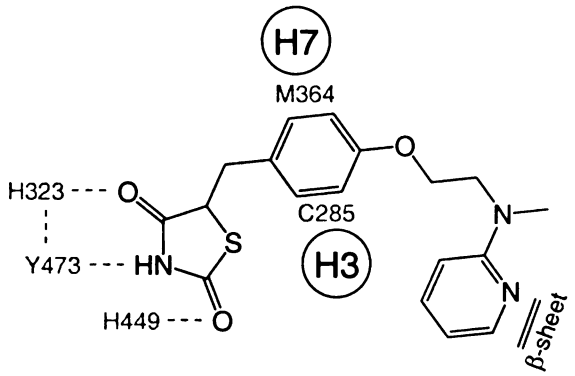

Figure 1.6: Rosiglitazone Binding Contacts

A schematic of some of the noteworthy rosiglitazone PPARγ LBD binding contacts is shown. Rosiglitazone is bound in a U-shaped conformation around helix 3. H232, Y473, and H449 are within hydrogen bonding distance of the thiazolidinedione ring of rosiglitazone. The phenyl ring is bound in a narrow pocket between C285 on helix 3 and M364 on helix 7. The pyridine ring is bound in a hydrophobic pocket between helix 3 and the β–sheet.

the ligand-binding site in the ternary complex (72). It is bound in a U-shaped conformation (Figure 1.6), wrapping around helix 3 with its central benzene ring directly behind helix 3 and the thiazolidinedione head group and pyridine ring wrapped around helix 3. The thiazolidinedione head group makes several specific interactions with amino acids in helices 3, 4, 10 and 12. The carbonyl groups of the thiazolidinedione ring form hydrogen bonds with two histidine residues, H323 and H449. The nitrogen is within hydrogen bonding distance of helix 12, specifically Y473, which also forms a secondary hydrogen bond with H323. The sulfur atom is positioned in a hydrophobic pocket. The thiazolidinedione's chiral carbon is in the S confirmation, though racemic rosiglitazone was used to form the crystals. The central benzene ring fits through a narrow pocket between C285 (helix 3) and M364 (helix 7). The pyridine ring binds between helix 3 and the β-sheet. While the thiazolidinedione and benzene ring are well conserved among the anti-diabetic thiazolidinediones, the pyridine ring of rosiglitazone is not. There is a considerable amount of unoccupied space in the t-shaped binding pocket near the pyridine ring, which could easily accommodate the variety of hydrophobic structures observed in the thiazolidinediones.

The authors suggest that this large binding site may be optimized to bind a variety of endogenous ligands with moderate affinity, rather than a single high affinity ligand as is the case with other nuclear receptors (72). As the volumes of nuclear receptor ligands are well conserved and other agonist bound ligand binding domains show binding pockets with volumes comparable to their ligands (84), there are remaining questions regarding the ligand binding pocket observed in the PPARγ rosiglitazone structure. While not certain, the receptor bound to an endogenous high affinity activator, or another synthetic ligand, may adopt the more stable compact structure typical of the nuclear receptors (Figure 1.5).

Regardless of whether the rosiglitazone bound structure allows proper formation of the β-sheet region and the ligand binding cavity that would be observed with the endogenous activator bound, rosiglitazone allows proper folding of helix-12. Upon ligand binding helix-12 forms the hydrophobic cleft comprising the coactivator binding site with helices 3 and 4 (72). A 88 amino acid peptide containing the NR-box 1 and 2 of Steroid Receptor Coactivator-1 (SRC-1) binds with one NR-box bound in each of two neighboring LBDs in the crystal. The LXXLL motifs, which comprise the NR-boxes bind in this hydrophobic cleft in a helical structure making use of a charge clamp formed by E471 and K301 (Figure 1.7) (72).

Coactivators and Corepressors

PPARγ ligand binding activates transcription through the recruitment of coactivators to the coactivator binding site formed by helices 3, 4 and 12. The PPARγ LBD is known to interact with both SRC-1 (72, 85) and the CREB-binding protein CBP/p300 (24, 56) in a ligand-dependent manner. Both SRC-1 and CBP/p300 have

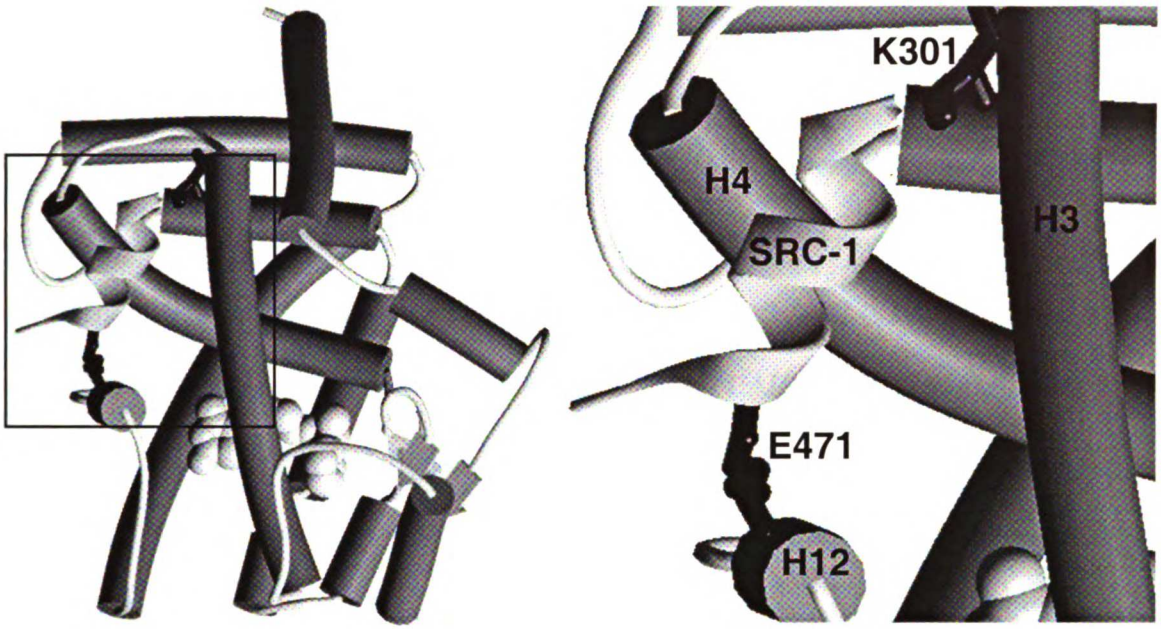

Figure 1.7: PPARγ Crystal Structure - Coactivator Binding

A schematic of the hPPARγ crystal structure is shown on the left. Rosiglitazone is bound in the hydrophobic core (shown as a white space-fill model). A peptide from the coactivator SRC-1 (shown as a white ribbon) is recruited by the ligand bound structure. An enlargement of the region of the structure showing the bound coactivator is shown on the right. The coactivator peptide binds in a hydrophobic cleft formed by helices 3, 4, and 12. Lysine 301 and glutamate 471 stabilize the coactivator helix by forming a charge clamp.

intrinsic histone deacetylase activity (86-89), as well as interacting with other cofactors including each other (3, 90). Both SRC-1 and CBP/p300 are also known to interact with the N-terminal region of PPARγ (24, 91).

Ligand binding also produces conformational changes in the receptor that effect the release of corepressors (5). The nuclear corepressor (NCoR) has been shown to be released from PPARγ upon rosiglitazone binding (56, 65). Two of the partial agonists described above, GW0072 and CDDO, release corepressor upon binding to PPARγ, but fail to recruit coactivators with sufficient affinity to achieve maximal activation (56, 65). CDDO-Me is an antagonist in part because it fails to effect release of NCoR (56). The potential of novel ligands to interact specifically with certain coactivators or corepressors, which in turn could have tissue dependent expression patterns, provides a complex

variety of ways ligands could have tissue selectivity in addition to receptor subtype specificity.

Several other proteins, including the transcriptional intermediate factor 2 (TIF2) and the PPAR-binding-protein (PBP), which has been identified as a component of multiprotein activation complexes such as TRAP, DRIP and ARC (92-95), have been identified as ligand dependent coactivators (95-97) for PPARγ. PBP is of particular interest because of recent deletion studies in transgenic mice, which show the same embryonic lethality observed in PPARγ null mice (98), indicating that PBP plays a critical role in development (95). Kodera showed that PPARγ can recruit both SRC-1 and TIF-2 when bound to $15dJ_2$, but cannot recruit either cofactor when bound to trogltiazone (96). This demonstrates that receptor cofactor interactions can be ligand specific, and may provide an explanation of observed differences in the biological activity of the thiazolidinediones and $15dJ_2$ (96).

AF-1 Modulation of Ligand Activity

Though the N-terminal region is often regarded as the ligand independent activation function (AF-1), it is becoming clear that the N-terminal region of PPAR plays a role in regulating the ligand dependent activation of the ligand binding domain. Treatment of cells with insulin results in the MAP-kinase mediated phosphorylation of serine 12 and 21 in PPARα, and serine 112 in PPARγ. Phosphorylation enhances transcriptional activation of PPARα (25, 27) and lowers the transcriptional activity of PPARγ2 (26, 28-30). The decreased activity of PPARγ2 appears to be a result of about a ten fold decrease in the binding affinity of PPARγ ligands for the phosphorylated form of the receptor, due to stabilization of the ligand free receptor (99). Peptides or hormones

that cause or inhibit MAP kinase-mediated Ser^{112} phosphorylation of PPARγ would affect insulin's regulation PPARγ activity and could cause resistance to insulin (29). Consistent with the phosphorylation results for PPARγ, deletion of the N-terminal region of PPARγ2 results in greater adipogenic potential in transfected cells as compared to the wild type receptor (100).

The N-terminal region of PPARγ2 also regulates receptor activation in a ligand independent manner. Mutation of proline 12 of PPARγ2 to alanine results in decreased binding of the receptor to DNA (101).

The N-terminal region has also been shown recently to interact with both corepressors and coactivators. For example, the p300 coactivator has been shown to interact in a ligand independent manner with the N-terminal region of the receptor (24). As this coactivator also interacts with the ligand binding domain in a ligand dependent fashion (24) it provides another way for the N-terminal region to affect the receptors ligand dependent transcriptional activity.

Phosphorylation, mutation, or modification of the N-terminal region of PPARγ or interacting proteins, such as p300, could affect both the N-terminal region's ligand independent activation function, as well as its effect on ligand dependent activation of the receptor.

Physiology

The class of compounds known as peroxisome proliferators, for which PPAR was named, mediate peroxisome proliferation in the liver and are ligands for the first PPAR characterized, PPARα (15). PPARα regulates a number of genes in the liver, which are

Target Gene	Response Element	Gene Function	References
aP2, adipocyte lipid - binding protein	ARE6, ARE7	fatty acid binding	(23, 102)
Fatty acid binding protein	FABP	fatty acid binding	(103)
Apolipoprotein C-III	APO CIII(B)	fatty acid transport	(104)
Acyl-CoA synthetase	ACS(CI)	peroxisomal β-oxidation	(105)
Acyl-CoA oxidase	ACOA, ACOB	peroxisomal β-oxidation	(12, 35, 104, 106)
Enoyl-CoA hydratase/3-OH-acyl-CoA dehydrogenase (bifunctional enzyme)	BIF (HD)	peroxisomal β-oxidation	(104, 107, 108)
CYP4A1/P450 IV	CYP4A1	microsomal ω-oxidation	(109)
CYP4A6/P450 IV	CYP4A6(Z)	microsomal ω-oxidation	(104, 110)
3-Hydroxy-3-methyl-glutaryl-CoA-synthase	HMG (MTHMGS)	ketone body synthesis	(111)
Malic enzyme	MEp, MEd	fatty acid synthesis	(112)
Phosphoenolpyruvate carboxykinase	PEPCK1, PEPCK2	glycerogenesis (adipose), gluconeogenesis (liver)	(113)
Liver-specific type I sugar transporter	Ti-LPT	sugar transport	(114)
Uncoupling protein-1	UCP-1	thermoregulation	(115)
Uncoupling protein-2	UCP-2	thermoregulation	(115)
Uncoupling protein-3	UCP-3	thermoregulation	(115)
Lipoprotein lipase	LPL	fatty acid metabolism	(116)
Medium chain acyl-CoA dehydrogenase	MCAD	fatty acid synthesis	(117)

Table 1.4: PPAR Regulated Genes and their Response Elements

PPAR regulated genes with known PPREs and their functions are listed.

important in regulating lipid catabolism (15). While both PPARδ and PPARγ can also activate expression at these response elements (58, 102), many of the peroxisome proliferators are specific PPARα ligands and the tissue specific expression of PPAR subtypes favors PPARα in the liver (15), where these effects are seen.

Table 1.4 is a list of genes with identified PPRE(s) in their promoter. One of the most extensively studied promoters of peroxisome proliferator-activated genes belongs to acyl-CoA oxidase (9, 10, 12, 35, 104, 106, 118). This enzyme is involved in peroxisomal

β-oxidation. The promoter contains two PPREs, whose consensus sequence is used as the synthetic PPRE sequence in the tk-PPRE$_3$-LUC reporter gene of Evans (50, 51, 58), which is the most extensively used full length PPAR reporter gene in the literature.

The earliest clues about the physiological role of PPARγ came from the discovery that a class of anti-diabetic drugs collectively known as thiazolidinediones were the first known high affinity ligands for any of the PPARs (50, 51). The effect of these drugs in lowering lipid levels in mouse models of non-insulin dependent diabetes mellitus (NIDDM) suggested a connection of PPARγ and insulin sensitization. The thiazolidinediones, which are PPARγ specific, are discussed in more detail in the next section.

Adipogenesis

The use of thiazolidinediones, and the PPARγ specific prostaglandin ligand 15dJ$_2$, allowed the study of the role of PPARγ activation in fatty acid homeostasis. This led to the discovery of the role of PPARγ in promoting adipogenesis, the terminal differentiation of adipocytes (100, 119, 120). Both adipocytes and their precursors express high levels of PPARγ (12). Treatment of preadipocytes, such as 3T3 L1 cells, with PPARγ ligands results in the terminal differentiation of these cells (100, 102). The role of PPARγ ligands in inducing adipogeneis is strong enough that treatment of both bone and muscle precursors with PPARγ ligands leads to terminal differentiation of these cells into adipocytes (121, 122). The strong adiopogenic effects of PPARγ ligands might lead to the potentially serious inclusion of fat bodies in bone marrow and muscle tissue (123). Interestingly, a variety of cancer cell lines undergo adipogenesis upon treatment with PPARγ ligands (45, 47).

The process of adipogenesis can be monitored in several ways. The expression of adipocyte markers, including the aP2 gene and adapsin, are considered indications of adipogenesis (51, 65, 71, 102, 122). Another common assay involves the staining of lipids. Because adipocytes accumulate large fat droplets, staining of cells with a lipid stain such as Oil-Red-O allows a qualitative colorametric determination of the extent of adipogenesis (51, 65, 71, 102, 122). In fact, these lipid droplets are so large, they can often be seen under a tissue culture microscope at standard magnification as yellow bodies in the cytoplasm (122).

Though the initial link between PPARγ and adipogenesis hinged on the activation by PPARγ specific ligands, this hypothesis has been supported directly by more recent experiments. For example, PPARγ antagonists show the ability to block adipogenesis induced by PPARγ ligands in cell culture experiments (65, 71).

PPARγ Knockout Mouse

Genetic elimination of PPARγ leads to fatal placental defects, indicating a critical role for PPARγ in placental development and pregnancy (98). The results from these studies pertaining to pregnancy are discussed in the following section on PPARγ and pregnancy. These fatal defects can be avoided by restoring PPARγ to the placenta through tetraploid chimeras. Null embryos with PPARγ in the placenta were viable. The PPARγ null pup maintained 70% of the body weight of its sibling for 4 days, but died within a week. After four days the null pup showed dehydration, severe weight loss (20%/day), and lethargy (98).

The PPARγ null pup lacked all adipose tissue, confirming other results that PPARγ was essential for adipogenesis of both brown and white adipose tissue. PPARγ

was not required for the early establishment of brown adipose tissue, but rather for its elaboration (98). These null pups showed extremely high liver fatty acid concentrations. Liver cells showed increased cell size, as well as inclusion of lipid droplets in the cytoplasm (98). Severe intestinal bleeding and numerous focal hematomas throughout the brain, the later is quite likely related to the rapid deterioration of the health of the null pup (98).

Intestinal bleeding and hemorrhages are consistent with the fatty acid induced endothelial cell damage that is observed in diseases with abnormally high levels of circulating lipids (124, 125). High circulating lipid levels and the accumulation of fat bodies in the liver and are consistent with a failure of fat storage and regulation mechanisms. Together the animal and tissue experiments point to the critical role PPARγ plays in fat storage and regulation through mediating adipogenesis.

Apoptosis and Cell Death

Though several tissues have been shown to respond to treatment with PPARγ ligands by undergoing differentiation, other cell lines respond by activation of the apoptotic pathways. Apoptosis is typically monitored by measuring the mitocondrial activity using the MTT assay (49, 126, 127). Apoptosis in some cell lines can be monitored optically by evaluating a change in shape of the cells to identify cytoplasmic rounding and membrane blebbing (127).

PPARγ induced apoptosis was first observed upon treatment of several cell lines, including JEG-3, ECV-304, HUVEC, and BMEC-b cells, with 10 μM $15dJ_2$ (126, 127). This effect has recently been observed in several human lung cancer cell lines (49). It is

not yet clear what cellular factors determine if cells respond to PPARγ ligand by apoptosis or adipogenesis.

Cytokines and the Immune System

Treatment of monocytes / macrophages with PPARγ results in inhibition of inflammatory cytokines, such as TNFα, IL-1β and IL-6 (62, 63). PPARγ activation results in inhibition of multiple steps in the NF-kB signaling pathway (128). PPARγ inhibition of cytokine production and these signaling pathways results in inhibition of the activation of macrophages and T-lymphocytes (63, 129). Studies on PPARγ inhibition of the synthesis of nitric oxide synthase, showed that PPARγ activation antagonizes activation of the transcription factors AP-1, STAT, and NF-κB (63).

Cytokines also have transcriptional effects on PPARγ signaling. TNFα is in turn a physiological inhibitor of PPARγ activation (43, 130-133). The effects of cytokine inhibition can be seen in both PPARγ mediated adipogenesis as well as in PPARγ reporter gene assays.

Non steroidal anti-inflammatory drugs (NSAIDS) show extended benefits in reducing cytokine production by monocytes when taken at higher doses than are required for inhibition of COX-2, their primary target (134). As shown in Table 1.1, NSAIDS are weak ligands for PPARγ (55), which when considered with the role of PPARγ in cytokine inhibition, may provide an explanation for the benefits of high doses in treating some chronic inflammatory diseases (134).

The feedback mechanism formed by this mutual inhibition may play an important role in regulating the immune response in a variety of tissues (8).

PPARγ and Heart Disease

PPARγ has both beneficial anti-inflammatory and undesirable pro-atherogenic effects as relate to heart disease(134, 135).

In addition to the general anti-inflammatory effects discussed above, by inhibiting macrophage activation, PPARγ ligands reduce secretion of the matrix metalloproteinase-9, which is associated with the increased rupture of atherosclerotic plaques (48, 136). Ruptured atherosclerotic plaques can lead to blood clotting resulting in heart failure or stroke (137).

Through its interaction with macrophages, PPARγ also plays a detrimental role in facilitating the formation of those same atherosclerotic plaques (134). PPARγ is expressed throughout the plaques in macrophage cells, the epithelial layer, the vascular smooth muscle, and at high levels in the foam cells (63, 136, 138). These macrophages can become lipid-laden foam cells, which contribute to the formation of highly damaging oxidized low density lipoproteins (oxLDL) through the secretion of oxidizing enzymes and agents (135, 139).

Oxidized LDL has been shown to activate transcription of PPARγ (75). Several PPARγ ligands, listed in Table 1.3, have been isolated from oxLDL and shown to activate PPARγ transcription (75). These and other PPARγ ligands can induce monocytes to differentiate into macrophages, and eventually to the lipid laden foam cells that form these plaques (138). Treatment of macrophages, and presumably foam cells as well, PPARγ activation by oxLDL or other ligands results in the expression of the CD36 oxLDL scavenger receptor (138). This receptor in turn bestows these cells with the ability to bind and internalize oxLDL. This in turn provides higher cellular levels of

PPARγ ligands. This positive feedback for lipid accumulation may explain the ability of PPARγ to induce foam cell formation (135).

Cancer

Recently PPARγ has been shown to be expressed at high levels in several cancer tumors, often at higher levels that the surrounding epithelial tissue (41, 44, 45, 47, 49). The ability to target these tissues, due to their high expression levels is intriguing, but it is unclear at this point what effect activation and repression of PPARγ in these tissues has in humans (48, 134, 140, 141). Several cancers, including colon, breast, and prostate cancer show significant increases in risk for patients with high fat diets (41, 142-144).

Recently the effect of PPARγ ligands on a variety of human cancer cell lines has been studied in culture (43, 45-48, 126). The first of these experiments involved the treatment of several colon cancer cell lines with PPARγ ligands (45). PPARγ ligands lead to a dramatic reduction in linear or clonogenic cell growth. PPARγ ligands promoted a broad and salient reprogramming of colon cancer cells towards a more-differentiated, less-malignant phenotype, but maintained high levels of PPARγ expression. The treated cells showed a program that is characteristic of colonic maturation and differentiation (45). These are strong effects occurring at thiazolidinedione concentrations achieved in patients undergoing treatment with these drugs for NIDDM (145). Sarraf has reported recently that colon cancer is associated with a loss of function mutation in PPARγ (146).

Other epithelial cancer cell lines have also shown beneficial effects of treatment with PPARγ ligands. Several lung cancer cell lines undergo apoptosis upon treatment with PPARγ ligands (49). Like colon cancer cells, breast cancer cells undergo

adipogenesis on treatment with PPARγ ligands, but also show interesting protective effects at lower concentrations (47). The Maspin protease inhibitor, which is expressed in high levels in normal breast tissue and absent in many breast tumors has been shown to have tumor suppressor activity (47, 147). Treatment of breast cancer cells with PPARγ ligands results in increased expression of Maspin, and tumor suppression. This protective effect lasts for several days after treatment with PPARγ ligands, consistent with the induced expression of a tumor suppressing protein (47). 21MT, which was the only breast cancer cell line resistant to treatment with PPARγ ligands, had an activated MAP-kinase cascade that inhibited PPARγ induction of Maspin gene expression. The inclusion of MAP-kinase inhibitors with PPARγ activators showed similar tumor suppression and Maspin gene expression as the other cell lines (47).

In support of the protective role for PPARγ observed in tissue culture, PPARγ ligands are reported to induce apoptosis and fibrosis of breast and prostate tumor cell injected into mice, and can attenuate the tumor incidence of mice subjected to chemical carcinogens (48).

Though experiments in human cells are potentially more therapeutically relevant, experiments in C57BL/6J-APC^{Min}/+ mice, which have a nonsense mutation in the adenomatous polyposis coli (APC) tumor suppressor gene, develop about 30 tumors throughout the intestinal tract, and show reduced lifespans as a result of this cancer (41, 44). Treatment of these animals with PPARγ ligands, either rosiglitazone or troglitazone, results in a significant increase in both the number and size of polyps in the colon, but does not appear to affect the rest of the intestinal tract (41, 44). The colon is the only part of the intestine with high levels of PPARγ, where it is found mainly in the epithelium

(44), and is often expressed at higher levels in the tumor than in the normal epithelium (41).

A role for PPARγ in causing colon cancer is indirectly supported by a strong correlation between the intake of fatty acids of animal origin and several cancers including breast, colon, and prostate cancer (140, 143, 144). Though the molecular mechanism has not been determined, based on these data, PPARγ may play a role in nutritionally sensitive tumors such as colon cancer(41). A decrease in prostaglandin production, seen in mice with mutations in the cyclooxygenase 2 (COX-2) gene and in animals and humans treated with COX inhibitors, prevents or attenuates colon cancer development (148-150).

Though the experiments in human cells could be considered more therapeutically relevant due to differences in signaling in rodents and humans, there are also potential differences between the results seen in tissue culture and what would be observed *in vivo*. It is important to recognize that the effect of ligands on cells injected into mice, or in tissue culture could be very different than the effect of ligands on these tumor cells in otherwise healthy epithelial tissue which expresses PPARγ. More experiments are required to determine if these differences are a result of species differences in PPARγ signaling or a different response to ligands *in vivo* and *in vitro*.

Diabetes and Obesity

Several lines of evidence connect the antidiabetic properties of thiazolidinediones to PPARγ. Each of the thiazolidinedione drugs binds to and activates PPARγ at a similar concentration range to that required for anti-diabetic activity (151). There is a linear correlation between the antidiabetic activity, measured as the ED_{50} for glucose lowering

in db/db mice, of thiazolidinediones and other PPARγ ligands with their PPARγ binding affinity (57). Several non-thiazolidinedione PPARγ ligands also show anti-diabetic activity and fit this same linear correlation. Activation of PPARγ with thiazolidinediones or other PPARγ ligands is sufficient for insulin sensitization, while activation by PPARα or PPARδ can not confer this effect (57). No other receptor for thiazolidinediones has been identified. And finally a P12A mutation in the human PPARγ gene is observed in diabetic Caucasians (152).

Though it is clear that the antidiabetic properties of the thiazolidinediones are mediated by PPARγ, and NIDDM was one of the first diseases linked to PPARγ, the mechanism by which PPARγ ligands improve insulin sensitivity remains unclear (123, 134).

Obesity, a condition clearly linked to NIDDM is primarily a disorder of energy balance, where energy intake exceeds use (123, 134). Activation of PPARγ with thiazolidinediones does not result in significant weight gain, instead treatment is thought to increase the number of adipocytes, and reduce the average cell size accordingly (153). As smaller cells are typically more sensitive to insulin, this shift in cell size would improve the insulin sensitivity of the adipose tissue (153).

Though PPARγ is expressed in much higher levels in adipose tissue than it is in either muscle or liver, the insulin sensitizing effects of thiazolidinediones extend to these peripheral tissues. Though expression of PPARγ is much higher in adipocytes, it is expressed in both muscle and liver tissues (42, 154). In fact treatment of dog muscle tissue directly with thiazolidinediones restores insulin sensitivity (155). Studies in a

mouse model of lipodystrophy confirm that thiazolidinedione sensitization can occur independent of fat tissue (156).

In addition to the ability to directly effect the insulin sensitivity of peripheral tissues, the activation of PPARγ in adipocytes can have distal effects on the insulin sensitization of peripheral tissues. By facilitating the storage of free fatty acids in adipose tissue, PPARγ acts to regulate the circulating levels of free fatty acid. As high circulating fatty acid levels can confer insulin resistance on peripheral tissues, reductions in circulating fatty acid levels effected by PPARγ ligands can result in the insulin sensitization of peripheral tissues (157, 158). TNFα, whose synthesis is inhibited by PPARγ activity, is overexpressed in obesity and insulin resistance (159). Neutralization of TNFα in obese animals with systemic insulin sensitivity showed significant improvement in systemic insulin sensitivity (160). It would be reasonable to conclude that by inhibiting TNFα, PPARγ ligands could improve systemic insulin sensitivity. Leptin, another gene that is down regulated by PPARγ ligands in adipose tissue (161, 162), has been proposed to interfere with insulin signaling in some cells (163), providing another mechanism whereby PPARγ ligands can improve insulin sensitivity.

There is certainly no requirement for PPARγ to function exclusively through any one of these pathways, so many or all of these mechanisms are likely to play a role in the *in vivo* insulin sensitization of thiazolidinediones. As discussed above, by activating the MAP-kinase cascade insulin can inhibit full PPARγ activation through the phosphorylation of Ser-112 (29).

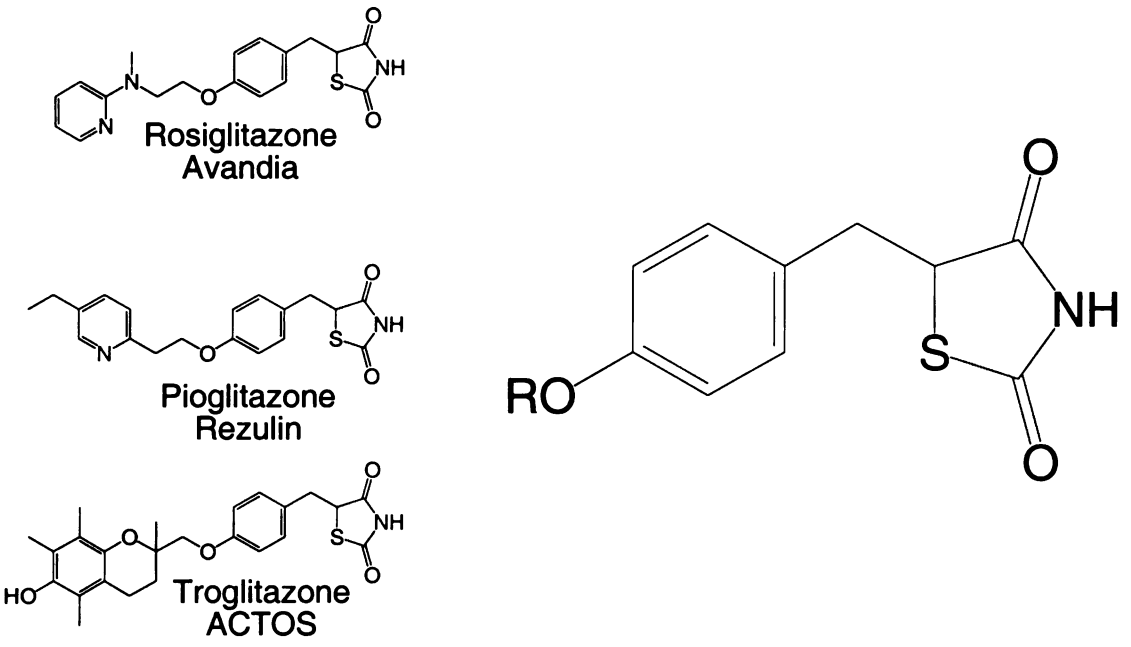

Figure 1.8: Conserved Structure of Antidiabetic Thiazolidinediones

The structures of three FDA approved thiazolidinediones are shown on the left. The thiazolidinedione and phenyl rings common to these and other thiazolidinedione s are shown on the right.

Thiazolidinediones: Clinically Useful PPARγ Ligands

The thiazolidinedione compounds were originally developed in a pharmaceutical company by screening large numbers of compounds in mouse models of obesity and diabetes for serum glucose and lipid lowering effects (164-175). The most potent compounds were found to have a conserved thiazolidinedione ring connected by one methylene unit to a phenyl ring, though the remainder of the molecules tolerate a variety of hydrophobic or aromatic structures (Figure 1.8).

The connection of the thiazolidinedione drugs to PPARγ began with the observation that pioglitazone increased transcriptional activity from the aP2 enhancer (176). Upon identification and cloning of the responsible transcription factor, the thiazolidinedione drugs were identified as high affinity PPARγ agonists (50, 51).

As discussed above, it is not clear how thiazolidinediones affect insulin sensitization *in vivo*, but it is clear that PPARγ mediates this response. Several thiazolidinediones have been approved for treatment in patients suffering from NIDDM (52, 60, 61).

Rosiglitazone (Avandia™) is administered orally twice daily in 2-4 mg doses. The half-life of rosiglitazone in circulation is approximately 6 days. It is completely metabolized by N-demethylation and hydroxylation followed by conjugation with sulfate and glucuronic acid before secretion. None of the major metabolites show activity (52).

Rosiglitazone, like the other thiazolidinedione drugs can lead to the resumption of ovulation in premenopausal, anovulatory women. Treatment leads to statistically significant increases in plasma volume (1.8 mL/kg). This may explain decreases in hemoglobin and white blood cell counts (52). Animal experiments at high doses showed increased incidence of adipose hyperplasia, increased incidence of benign adipose tissue tumors, and increased heart weight (52).

The most serious side effects of this class of drugs may be hepatotoxic effects. Troglitzone (Rezulin) was removed from market after incidences of idiosyncratic hepatotoxicity, and liver failure (52, 61). These problems have resulted in both liver transplants and death. Though no liver toxicity has been observed in trials with rosiglitazone, the manufacturer recommends regular monitoring of liver enzymes (52).

As discussed above, PPARγ-bound troglitazone fails to recruit SRC-1 and TIF-2, cofactors that are recruited by the PPARγ bound to $15dJ_2$ (96). Because different tissues express different coactivators in different amounts, the ability of ligands to distinguish between these coactivators may provide tissue specific receptor activation. The

development of ligands showing selective recruitment of coactivators or release of corepressors, could eventually lead to the identification of a ligand that would maintain the insulin sensitizing properties of thiazolidinediones, but avoid some of the side effects.

PPARγ and Pregnancy

Recent work suggests that PPARγ may play a role in healthy pregnancy, in particular hemochorial placentation.

Studies by Barak et al. (98) on PPARγ deficient mice demonstrate that PPARγ is essential for normal placental development. Embryos without this gene show massive placental defects that lead to fatality between 9.5 and 12.5 days of gestation. PPARγ is expressed at high levels in the placenta as early as a gestational age of 8.5 days and is not expressed in any other tissue for 3-4 days. The observed PPARγ related fatality is consistent with the notion that fetal death around 9.5 days is a common consequence of defects in extraembryonic tissues (177). Barak et al. were able to rescue the placental defects of PPARγ null embryos by restoration of the PPARγ gene in the placenta via tetraploid chimeras (98), demonstrating that the PPARγ dependence resides in the placenta. Defects observed in the trophoblast-formed vascular structures in the PPARγ-null placentas show that PPARγ is required for trophoblast terminal differentiation associated with their barrier function. This could be expected to result in deficient nutrient exchange. Additionally PPARγ null placentas failed to accumulate lipid droplets observed in healthy trophoblast tissue. This is consistent with the role PPARγ plays in lipid uptake in other tissues (75, 100, 138). Interestingly, a knockout of the PPARγ coactivator PBP shows similar defects in the development of the placental vascular structure to those seen in the PPARγ null mice (95).

Lim et al. (178) found that prostacyclin synthesis is essential for implantation and decidualization in mice, and that its actions appear to involve PPARδ. PPARδ expression appears to precede PPARγ expression, appearing as early as day 4. Disruption of the COX-2 gene prevents proper implantation, which can then be restored by treatment with PGI_2 or the synthetic PPARδ agonist L-165041 (178). Though these results do not directly implicate PPARγ, PPARδ activation could lead to increased expression of PPARγ. Activation of PPARγ in JEG-3 cells upregulates PPARγ mRNA (43, 81). As the PPAR subtypes activate transcription at many of the same response elements (9, 10, 102), activation of PPARδ in mice embryos could upregulate PPARγ leading to detectable levels of PPARγ expression 4 days after PPARδ first appears (98, 178).

Treatment of rats with rosiglitazone did not affect implantation, but was associated with fetal death and growth retardation and placental pathology on treatment in mid-late gestation (52). The observed placental defects are consistent with a separate observation of PPARγ mediated apoptosis in JEG-3 cells, a choriocarcinoma cell line derived from placental trophoblasts (126).

While substantial placental anatomical differences exist between mice and humans, *in vitro* studies using human cells complement the findings in mice. PPARγ expression has been observed in human placental tissue (40, 43). PPARγ mRNA (43, 126), PPARδ mRNA (81, 179) and PPARγ expression (43) have been observed in JEG-3 cells. Additionally, transient transfection experiments using JEG-3 cells show that the endogenous levels of receptor are sufficient to observe useful levels of PPARγ ligand induction of reporter gene expression (43).

Treatment of JEG-3 cells with serum from pregnant women leads to increased PPARγ expression and PPRE-regulated reporter gene activation (43). The observed PPARγ expression in human placental trophoblasts and observed PPAR activating factor in serum from pregnant women suggest that PPARγ plays an important role in the human placenta and pregnancy, as it does in mice.

Dramatic maternal physiological changes in human pregnancy necessitate modified regulation of glucose and lipid metabolism. During normal pregnancy, maternal energy and lipid metabolism are profoundly altered (180). The developing fetus utilizes glucose as its predominant energy source, which puts a continuous demand on the mother to provide this substrate (181). Problems with sugar metabolism, such as hypoglycemia, or alternatively gestational diabetes, are not uncommon during pregnancy. Lipid metabolism also changes in pregnancy. Levels of circulating free fatty acids are in the normal range during most of pregnancy, but rise dramatically during the final weeks of pregnancy, and drop precipitously at term (182). Additionally, maternal triglyceride levels triple during pregnancy (183). Prostaglandin metabolism also is altered, with levels of vasorelaxants such as prostacyclin increasing, while vasoconstrictive prostaglandins decrease (184-186). These changes and the role of PPARs in energy, glucose, and fat homeostasis suggest an additional role for PPARs, and the activator found in serum from pregnant women, in the pregnant mother.

Failure of these alterations in gene expression to occur may lead to pregnancy complications (e.g. preeclampsia) (187, 188). The placental beds of women with preeclampsia resemble those of acute graft rejection (189, 190). Elevated concentrations of immunoactive TNF-α, which participates with PPARγ in a feedback mechanism (62,

63, 130-133), are observed in blood of women with preeclampsia (191-193). Placental decidua from women with preeclampsia show high levels of IL-2, while decidua from women with normal pregnancies do not (194). These and several other lines of evidence suggest that failure of the local immune suppression in normal pregnancy may result in an immune response (195). The release of PPARγ ligands by placental tissues or the higher levels of PPARγ ligands in serum of pregnant women could activate PPARγ in tissues where it would suppress the immune response (8, 62, 63, 128, 129). This immune response would in turn result in the endothelial cell damage and resulting symptoms observed in virtually all maternal organs (187, 195).

In addition to PPARγ's role in suppressing the immune response, specifically inhibition of cytokine production and macrophage activation (62, 63), several of the risk factors of preeclampsia may be related to PPARγ function. Patients with diabetes, obesity, lupus, hypertension, multiple gestation, renal disease, and patients living at high altitudes are all more likely to develop preeclampsia than the general population (196, 197).

JEG-3 cells treated with serum taken from patients with preeclampsia in the third trimester show significantly lower PPARγ expression levels than cells treated with serum from patients with normal pregnancies (81). Further study is needed to determine whether PPARγ participates as a mediator of symptoms, or if it is in some way a cause of the syndrome.

PPARγ may also be involved in other aspects of the female reproductive system. As mentioned above, PPARγ is expressed in human placental cytotrophoblasts and ovaries (40, 43). In addition to the role of PPARγ in placental development and invasion

described above, some of the reported effects of the thiazolidinedione insulin lowering drugs, which are specific PPARγ ligands, suggest a possible role for PPARγ in ovarian tissue.

Elevated insulin levels, which correlate with fertility related endocrine abnormalities, in patients with polycystic ovarian syndrome (PCOS) can be treated with anti-diabetic drugs such as troglitazone. These drugs lower insulin levels, reduce hair loss, help weight loss and normalize elevated blood pressure, but also restore regular menstruation and fertility(198). Though this effect was originally attributed to the insulin lowering properties of the thiazolidinedione drugs, it is now clear that thiazolidinediones also act directly on ovarian porcine granulosa cells to inhibit progesterone production (199). Similar progesterone lowering effects, in addition to estradiol lowering effects are reported in experiments where both rats and monkeys were treated with rosiglitazone (52).

Troglitazone appears to lead to the resumption of ovulation in premenopausal anovulatory patients with insulin resistance (61). Troglitazone, when administered with oral contraceptives (ethinyl estradiol and norethindrone), reduced the plasma concentrations of the contraceptives by approximately 30% and resulted in loss of contraception in some patients (61).

PPAR/RXR heterodimers can compete with ER homodimers for binding to the estrogen response elements (EREs) of the vitellogenin A2 and pS2 genes (33, 200-202). While PPAR can activate these response elements in some synthetic promoters construct, it does not activate the response element in the context of the natural promoter (33, 200-202). ER is clearly important in pregnancy and both PPAR and RXR are present in

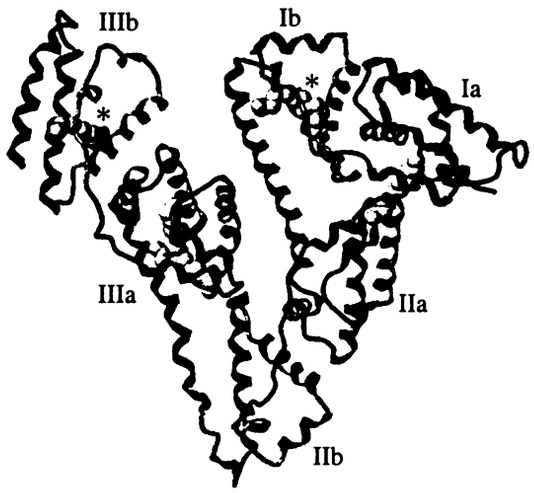

Figure 1.9: Human Serum Albumin Crystal Structure

A ribbon diagram of the crystal structure of human serum albumin shows the three domains, each with two subdomains, forming a heart shaped structure. Each a subdomain is shown in dark gray, while the b subdomains are shown in a lighter gray. Five myristate molecules (white space fill) are observed in the structures. The Ib and IIIb sites (marked with an *) are 17 Å hydrophobic tunnels, open at each end of the domain.

reproductive tissues, so PPAR inhibition of ER induction may indicate another role for PPARγ in pregnancy (201).

Serum Albumin

Albumin (for reviews see 203, 204, 205) was originally identified as a major component of blood as early as 1839 (203, 206). Crystallization conditions were known as early as 1894 (203, 207), and were studied extensively during World War II, as a means of providing a stable human blood substitute (203). The first X-ray structural studies using albumin crystals were performed in the early 1950's, which included some of the first demonstrations that protein crystals contained large percentages of solvent (203, 208, 209). Since the initial studies of albumin structure, several high-resolution crystal structures of human serum albumin (HSA) have been solved (204, 210, 211).

Serum albumin is a 67 kD 585 amino acid protein with three similar helical domains forming a heart shaped molecule (210, 211). There are a total of 17 disulfide bridges and one free cystine. Each of the three domains, numbered I, II, and III, can be further divided into two subdomains, a and b (Figure 1.9). The structure of albumin complexed with myristic acid, confirms observations of potential binding sites on previous crystal structures, with an asymmetric distribution of five fatty acid binding sites

on domains Ib, Ia/IIa, two in IIIa, and IIIb (210). The Ib and IIIb binding sites form deep pockets extending ~ 17Å through the domain. Tri-iodobenzoic acid, which is characteristic of the group of aromatic compounds which bind to albumin, binds in two binding sites: one on Ib contacts the myristate binding site; another on IIa. The other three sites are formed in hydrophobic pockets of the protein surface. In each case the fatty acid is bound within a deep hydrophobic pocket with the carboxylate making favorable charged or hydrogen-bonding interactions with two or three charged or polar receptors near the surface of the protein. The electron density for the myristate is strongest near the carboxylates(210).

This structure is remarkably stable, surviving pasteurization temperatures of 60 °C for 10 hours (203). At neutral pH albumin has a net charge of –18 with an asymmetric distribution of –10, -8, and 0 for domains I, II, and III respectively (205). This is of note as three of the five observed fatty acid binding sites are found on the domain with the lowest net charge.

The abundance of albumin in blood and the ease of purification allowed huge strides in the development of protein structure determination techniques, but has also led to its use as a generic stabilizing protein (203-205). In fact, albumin plays many diverse roles *in vivo*.

Albumin is in every tissue and bodily secretion (203). About 60% of albumin is in the circulatory system where it is the major component of human blood. Due to its concentration, about 40 mg/mL or 60% of the total protein, it is a major contributor to the maintenance of osmotic blood pressure (203) as well as being primarily responsible for

the maintenance of blood pH (212). It is expressed primarily in the liver (213) and has a half-life in circulation of approximately 19 days (214).

Analbuminemia, or the absence of albumin, is rare. The few patients who have been identified experience chronic fatigue, hyperlipidemia, mild diarrhea, and mild odema (203, 215). An analbuminemic rat was identified amongst a population of hypercholesterolemic rats, and through breeding a mutant strain of analbuminemic rats was established (216). These rats show both analbuminemia, with barely detectable levels of albumin, and hyperlipidemia, with increased serum cholesterol and triglycerides. Despite missing albumin, the blood osmolality and blood glucose and electrolyte levels are unaffected. This mutation also showed a dramatic increase in the susceptibility of the mice to the formation of bladder, kidney, stomach, intestine and subcutis tumors upon treatment with chemical carcinogens (215).

One of the major roles of albumin, and a remarkable demonstration of the utility of the albumin binding sites, is the binding and transport of a wide variety of endogenous and exogenous compounds. Pages 177-180 of Carter's review contain an extensive list of known albumin binding constants (203). Albumin binds a wide variety of saturated and unsaturated fatty acids, of various lengths, in the 100 nM to 100 μM range. Through binding these lipids albumin allows the transport of fatty acids that would otherwise be insoluble, and protects endothelial cells from polyunsaturated fatty acid induced injury (124, 125).

In addition to binding a variety of fatty acids, albumin also binds many other small molecules. It sequesters oxygen radicals, and inactivates toxic lipophilic metabolites such as bilirubin (217). Albumin has also been shown to be a key reservoir

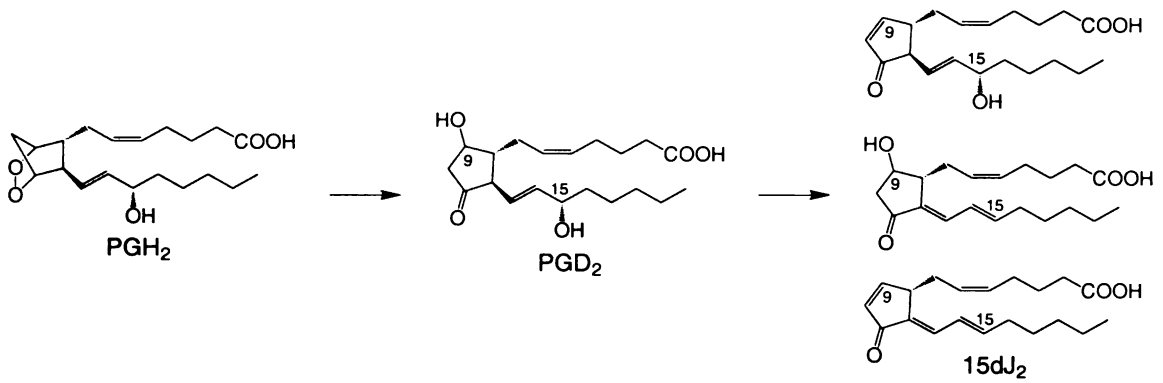

Figure 1.10: Albumin Catalyzed Formation and Metabolism of Prostaglandin D_2

The albumin catalyzed formation of Prostaglandin D_2 from Prostaglandin H_2, and the chemical structures of the Prostaglandin D_2 metabolites are shown.

and transporter of nitric oxide (218). Though most of its binding interactions are reversible, albumin forms covalent adducts with cystine, pyridoxyl phosphate, and glutathione (203).

As might be expected, albumin interactions can show stereoselectivity. The affinity for L-tryptophan is 100-fold higher than the affinity for D-tryptophan (203, 205). In some cases binding to albumin can result in a chemical change in ligands, although slower than typical enzymatic transformations (205).

Albumin binding of has been shown to stabilize the structures of several buffer labile prostaglandins (219). Albumin has also been shown to play an active role in the formation and degradation of prostaglandin D_2 (PGD_2).

Incubation of prostaglandin H_2 (PGH_2) in human plasma or purified albumin results in the formation of both prostaglandin E_2 and PGD_2 (Figure 1.10). Only PGD_2 formation is dependent on the amount of added albumin, and can be abolished by prior boiling (220). This reaction proceeds with a rate of 0.87 M/min and a K_m for PGH_2 of 6 μM, which could be completely abolished by treatment at 70 °C for 5 minutes.

Albumin also catalyzes the *in vitro* dehydration of PGD_2 into three metabolites (79, 80). First-order reaction rates were proportional to the albumin content of the buffer. After 30 hours at 37 °C in the presence of 10 mg/mL of albumin 90+% of the initial PGD_2 had been consumed. The three observed PGD_2 metabolites are the product of dehydration of PGD_2 at the 9 and or 15 positions shown in (Figure 1.10). The PPARγ specific ligand $15dJ_2$, results from dehydration at both the 9 and 15 positions.

In addition to analbuminema, several diseases show lowered circulating albumin levels including cirrhosis of the liver, nephrotic syndrome, protein losing enteropathy, malnutrition, and AIDS (137, 221). In all of these diseases the expression of other serum proteins is dramatically increased to maintain the osmolality of blood. As albumin is present in blood essentially at the solubility limit, no diseases have been reported with increased levels of circulating albumin.

In addition to diseases with quantitatively reduced levels of circulating albumin, several diseases show modified forms of albumin. Non-insulin dependent diabetes mellitus (NIDDM) for example shows increased levels of nonenzymatic glucosylation (Figure 1.11) of albumin (222, 223). Lys-525 is though to be the principal glucosylation site (224). In healthy patients between seven and eight percent of circulating albumin is glucosylated. Patients with poorly controlled diabetes can show levels as high as 30% glucosylation. As the nonenzymatic glucosylation of albumin is concentration dependent, it may reflect a short-term control of hyperglycemia(222).

Changes in ratio of albumin to free fatty acids, or the degree of saturation of the albumin binding sites is observed in several diseases including coronary heart disease (225, 226) and preeclampsia (124, 227). The resulting change in albumin can be

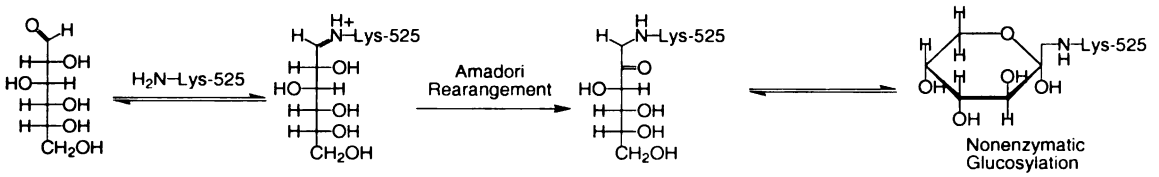

Figure 1.11: Nonenzymatic Glucosylation

The mechanism for the nonenzmatic glucosylation of serum albumin at Lys-525 is shown.

observed as a pI shift, from 5.6 to 4.8, upon binding of the negatively charged fatty acids (125).

Modification of albumin may affect any or all of the roles of albumin, including pH regulation, binding, catalysis, drug clearance, and receptor regulation. Whether defects in the regulation of albumin expression or mutations in albumin directly cause these diseases, the altered levels and forms of albumin are likely to lead to some of the symptoms.

Chapter 2: The Design and Synthesis of Rosiglitazone Derivatives

The synthesis of rosiglitazone and twelve derivatives with extensions at the thiazolidinedione location is discussed. The beginning of synthetic routes for adding extensions to the phenyl ring location are also discussed.

Introduction and Experimental Approach

The peroxisome proliferator-activated receptor-γ (PPARγ) is an orphan nuclear receptor. Although the endogenous high affinity activator for the receptor is unknown, varieties of synthetic compounds have been identified as specific PPARγ agonists (8, 43, 50, 51, 59, 75, 116, 126, 228). There were no known antagonists for PPARγ when this project began, but three have since been proposed (56, 65, 71).

Diseases are commonly associated with both abnormally high and low activity of nuclear receptors (7). Specific ligands activating, or inhibiting activation, of these receptors have potential use in the treatment of these diseases depending on their side-effect profiles. These side effects can be related to factors such as activity through other receptors, other subtypes of the same receptor, or activity of the receptor in a different tissue. The specific PPARγ ligand rosiglitazone (Figure 2.1), also known as Avandia™ or BRL 49653, and several related thiazolidinediones are currently used in treating poorly

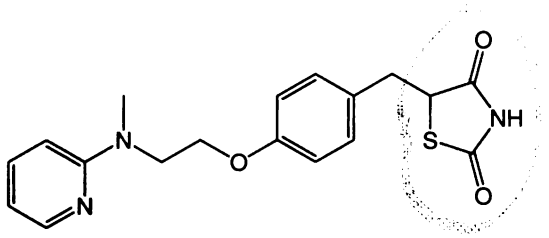

Figure 2.1: Rosiglitazone

The chemical structure of the thiazolidinedione rosiglitazone is shown. It is also known as Avandia™ and BRL 49653. The thiazolidinedione head group, after which this class of compound is named, is circled in gray.

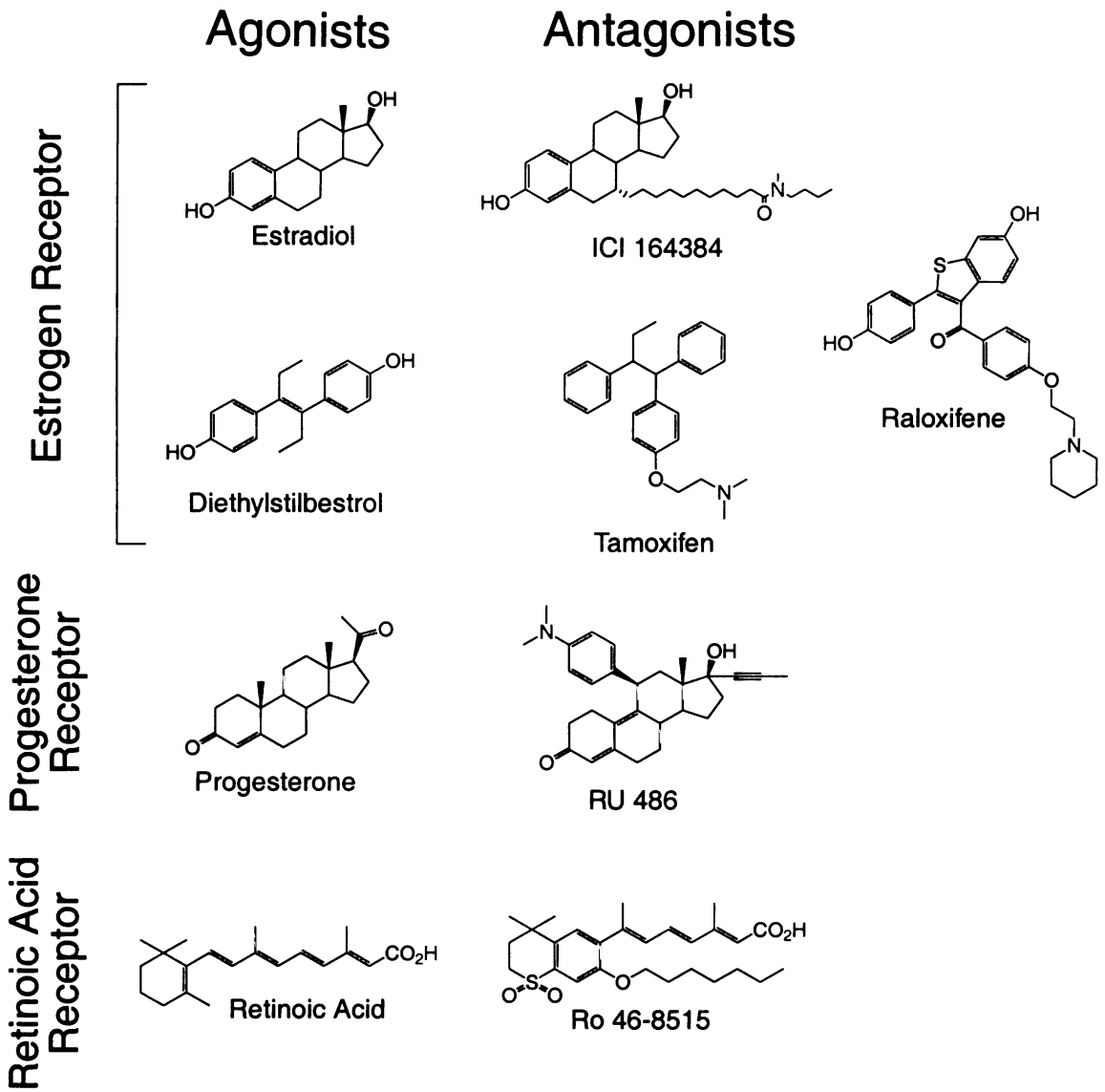

Figure 2.2: Antagonists and Agonists

The chemical structures of some known nuclear receptor agonists and antagonists are shown. The chemical structures of antagonists are related to the agonist structure with an extension from the central portion of the molecule.

controlled non-insulin dependent diabetes mellitus (NIDDM). PPARγ has also been implicated as playing a role in other diseases including atherosclerosis, colon cancer, preeclampsia, and obesity (8, 41, 44, 45, 75, 81, 98, 141, 229). It is likely that novel PPARγ ligands, whether they function as agonists or antagonists, will be medically

Figure 2.3: Extension Hypothesis

A schematic representation of the extension hypothesis that agonists can be generated by adding an extension to the central portion of an agonist structure.

relevant in characterizing, if not treating, these and other disease states related to PPARγ activity.

While many synthetic agonists for PPARγ have been described, no antagonists had been published when this project was started, making them a desirable synthetic target. Our approach to design of antagonists for PPARγ was based on the chemical structures of known antagonists for other nuclear receptors (Figure 2.2). Antagonists appear to be structurally related to agonists for the same receptor with an extension from the 'central portion of the molecule.' The average volume of known nuclear receptor antagonists is approximately 25% larger than the highly conserved nuclear receptor agonist volume (84). These observations led to the Extension Hypothesis (Figure 2.3), which states that a nuclear receptor antagonist can be generated by adding an extension to the 'central portion' of the scaffold of a known high affinity agonist for the receptor.

Like other nuclear receptors, PPARγ binds its ligand within the hydrophobic core of the protein, where the ligand is sequestered from solvent (68, 70, 72, 82, 83). With the binding pocket for the nuclear receptor ligands completely defined by the receptor, there is not room for the extension, and the associate extra ligand volume, within the binding pocket. Crystal structures of the estrogen receptor (ER) with its antagonists show that the antagonist's extension is located where helix-12 is found in the agonist structure (68, 70). In the ER crystal structures with bound Raloxifene or Tamoxifen, helix-12 is found in the coactivator binding site, preventing the recruitment of the coactivators required for

transcription. This explains why the bound antagonist does not activate transcription. Because it competes with agonists for receptor binding without resulting in transcriptional activation, the antagonist is able to inhibit induction of the receptor by agonists. While disruption of the folding of helix-12 is not the only way to block activation, it is representative of a more general mechanism of antagonist action through binding the receptor and preventing proper folding of a receptor surface important for function.

The Extension Hypothesis suggests that antagonists of PPARγ can be synthesized by adding extensions to a known high affinity agonist. The general application of this hypothesis experimentally is guided by four basic principles.

First, and most important, the compound, derivatization position, and chosen extensions must be accessible synthetically. Not all hypothetical chemical structures are stable and many others can not be experimentally synthesized. Furthermore, in order to make a small library of compounds it is important that the addition of extensions be accomplished in one of the last synthetic steps.

Second, based on the structures of known antagonists for other nuclear receptors, the extension should be added to the 'central portion' of the agonist scaffold. We do not expect the disruption of the folding of the receptor surface to be a precise process. The specific requirements likely arise from the interaction of the side chain with the protein surface, as stabilizing interactions in this region of the molecule could have important effects on the binding affinity, and hence activity, of the ligand.

Third, it will be important to test a variety of extensions. While known antagonists all show the existence of an extension and consistency in the general location

of the extension, there is considerable variety in the types of extensions found in these molecules. Because it is unclear how the receptor will react structurally to the ligand, it is also unclear what potential extension interactions are available. Screening extensions containing a range of functionalities will allow exploration of possible stabilizing interactions with the disrupted protein.

Finally, it is necessary to evaluate the activity of candidate ligands and use that data in guiding the synthesis of new candidate ligands. Because of the range of possible interactions, it is unlikely that the best possible compound will be found on the first try. Evaluating the binding and activity of the first series of compounds can produce information about what beneficial interactions are available. For instance if a negative charge binds well, a new series of compounds might change the charged group, the length of the chain, and other variables to maximize the energetic benefit of this interaction.

We chose to apply the Extension Hypothesis and these principles to PPARγ antagonist design and synthesis using rosiglitazone as an agonist scaffold. Rosigltiazone is part of a family of compounds known as thiazolidinediones that were first developed in the early 1980s as antihyperglycaemic agents in mice (164-175, 230, 231). When the PPARs were discovered in the early 1990s (13), they were found to be the highest affinity ligands known for PPARγ. Several of these compounds have been used clinically. Rosiglitazone has one of the highest reported affinities for PPARγ, and a reported synthesis, making it the most desirable starting point for a scaffold. The phenyl ring, in the central portion of the scaffold, appeared to be a good site for derivatization by the incorporation of an additional functional group on the benzaldehyde used in the published synthetic route.

The goal of this project was to further understanding of the structural basis of antagonism of the nuclear receptor superfamily by designing an antagonist for PPARγ based on the chemical structure of rosiglitazone (Figure 2.1), and the extension hypothesis (Figure 2.3). Attempts at the characterization of these derivatives are described in subsequent chapters.

Experimental Procedures

Reagents & General Procedures

Unless otherwise specified, all chemicals were obtained from Fisher Scientific (Pittsburgh PA) or Sigma-Aldrich (St. Louis MO). Proton and carbon nuclear magnetic resonance spectra (^{1}H-NMR, ^{13}C-NMR) were obtained on a General Electric 300 MHz instrument; ^{1}H-NMR chemical shifts are reported as δ values in parts per million (ppm) downfield from internal tetramethylsilane. ^{13}C-NMR chemical shifts are reported as δ values in parts per million (ppm) referenced to the solvent peak. Deuterated dimethyl sulfoxide (DMSO-d_6) and acetone were purchased from Aldrich in sealed ampules with 98%+ isotopic purity. Deuterated chloroform ($CDCl_3$) was purchased from Aldrich with 99%+ isotopic purity. Mass spectrometry (MS) and high resolution mass spectrometry (HRMS) were performed by the National Bio-Organic, Biomedical Mass Spectrometry Resource at UCSF. Flash chromatography on crude products was performed using 230-400 mesh silica gel (Aldrich). Purity of compounds and extent of reaction were determined by thin layer chromatography (TLC), using commercial silica gel plates (Alltech, Alugramb Sil B/UV 254), and by ^{1}H-NMR. Glassware was oven or flame-dried

before use. Anhydrous dimethylformamide (DMF) and tetrahydrafuran (THF) were purchased from Aldrich in Sure-Seal bottles.

2-Methyl-2-pyridinylaminoethanol (1)

Following the procedure of Cantello (164, 231), a stirred mixture of 2-chloropyridine (12.05 g, 106 mmol, 1eq.) in 2-methylaminoethanol (100 mL, 11.7 eq.) was heated under nitrogen to 120°C for 45 hours. The mixture was cooled to room temperature, added to 200 mL of ice water, and extracted with ethyl acetate. The combined organic extracts were washed with brine, dried using sodium sulfate, and evaporated to dryness under reduced pressure. The residual oil was vacuum distilled (b.p. = 118°C at 1 torr) to yield the alcohol **1** (12.5446 g, 82.4 mmol, 77.8% yield).

^{1}H-NMR (300.68 MHz) ($CDCl_3$): δ 3.05 (s, 3H), 3.69 (t, 2H, J = 5.0 Hz), 3.83 (t, 2H, J = 5.0 Hz), 5.44 (br s, 1H), 6.51-6.58 (m, 2H), 7.46 (td, 1H, J = 1.9, 7.4 Hz), 8.04 (d, 1H, J = 3.9 Hz) ppm. ^{13}C-NMR (75.59 MHz) ($CDCl_3$): δ 37.80, 54.16, 62.70, 106.17, 106.27, 112.05, 112.15, 137.59, 137.74, 146.93, 146.99, 159.15 ppm. MS exact mass calculated for $C_8H_{12}N_2O$: 152.1, MH^+ found: 153.1.

4-(2-(Methyl-2-pyridinylamino)ethoxy)benzaldehyde (2)

Following the procedure of Cantello (164, 231), **1** (6.0237 g, 39.6 mmol, 1 eq.) was dissolved and stirred continuously in anhydrous DMF (150 mL). Sodium hydride (1.7717 g, 44.3 mmol, 1.1 eq.), 60% in mineral oil, was weighed, rinsed with hexanes to remove the mineral oil, suspended in anhydrous DMF (10 mL), and added portionwise over 20 minutes to the reaction under argon inert atmosphere. After vigorous reaction was complete (no bubbling) freshly distilled 4-fluorobenzaldehyde (5.4816 g, 44.2 mmol,

1.1 eq.), dissolved in anhydrous DMF (50 mL), was added dropwise under argon inert atmosphere over 90 minutes. After reaction stopped (10 hours), reaction was added to 600 mL of ice water, extracted with ethyl acetate, washed with brine, dried over sodium sulfate and evaporated under reduced pressure. The crude product was purified on a flash column using a solvent gradient increasing from 10% ethyl acetate in hexane to 50% ethyl acetate in hexane. 500 mL fractions were collected, screened by thin layer chromatography, and evaporated under reduced pressure giving the aldehyde **2** (4.9837 g, 19.4 mmol, 49% yield) as an oil which solidified after storage at 4°C overnight.

^{1}H-NMR (300.68 MHz) ($CDCl_3$): δ 3.14 (s, 3H), 4.01 (t, 2H, J = 5.0 Hz), 4.27 (t, 2H, J = 5.0 Hz), 6.52 (d, 1H, J = 8.4), 6.572 (t, 1H, J = 5.1), 6.997 (d, 2H, J = 8.4), 7.462 (td, 1H, J = 1.5, 7.2 Hz), 7.80 (d, 2H, J = 8.4), 8.16 (d, 1H, J = 4.2 Hz), 9.857 (s, 1H) ppm. ^{13}C-NMR (75.59 MHz) ($CDCl_3$): δ 37.867, 49.224, 66.638, 105.657, 111.876, 114.730, 129.832, 131.891, 137.303, 147.772, 158.085, 163.845, 190.637 ppm. No mass spectrometry data is available.

(Z)-5-((4-(2-(Methyl-2-pyridinylamino)ethoxy)phenyl)-methylene-2,4-thiazolidinedione (3) Method A

Based on procedure of Cantello (164, 231), a mixture of **2** (3.8305 g, 14.9 mmol, 1 eq.) and 2,4-thiazolidinedione (1.75 g, 14.9 mmol, 1 eq.) in toluene (80 mL) with a catalytic amount of piperidinium acetate (0.128 g, 1.49 mmol, 0.1 eq.) was refluxed for two hours with a Dean-Stark water trap. The solution was cooled and filtered. The precipitate was washed with ether and dried under vacuum to yield the thiazolidinedione **3** (3.8896 g, 10.94 mmol, 73.4% yield).

^{1}H-NMR (300.68 MHz) (DMSO-d_6): δ 3.07 (s, 3H), 3.93 (t, 2H, J = 5.7 Hz), 4.22 (t, 2H, J = 5.7 Hz), 6.57 (t, 1H, J = 5.4 Hz), 6.65 (d, 1H, J = 8.6 Hz), 7.10 (d, 2H, J = 8.7 Hz), 7.48-7.55 (m, 1H), 7.54 (d, 2H, J = 8.5 Hz), 7.73 (s, 1H), 8.08 (d, 1H, J = 4.6), 12.5 (br s, 1H) ppm. ^{13}C-NMR (75.59 MHz) (DMSO-d_6): δ 37.07, 48.34, 65.81, 105.75, 111.60, 115.32, 120.61, 125.62, 131.54, 132.05, 137.34, 147.53, 157.98, 160.11, 167.75, 168.09 ppm. MS exact mass calculated for $C_{18}H_{17}N_3O_3S$: 355.1, MH^+ found: 356.0.

(Z)-5-((4-(2-(Methyl-2-pyridinylamino)ethoxy)phenyl)-methylene-2,4-thiazolidinedione (3) Method B

Based on the procedures of Tanis, Cantello, and Shoda (164, 175, 230, 231), a mixture of **2** (1.3567 g, 5.29 mmol, 1 eq.) and 2,4-thiazolidinedione (0.6217 g, 5.31 mmol, 1 eq.) in ethanol (10 mL) with a catalytic amount of piperidine (0.25 mL, 2.53 mmol, 0.48 eq.) was refluxed for four hours. The solution was cooled to 4°C overnight. The yellow precipitate was filtered, washed with ether, and dried under vacuum to yield the thiazolidinedione **3** (1.317 g, 3.7 mmol, 70% yield).

5-(4-(2-(Methyl-2-pyridinylamino)ethoxy)benzyl-2,4-thiazolidinedione (4) Method A

Based on the procedure of Cantello (164, 231), 0.5337 g of magnesium turnings was added to a flask and oven dried overnight. The flask was allowed to cool to room temperature in a desiccator, and stirred vigorously for 30 minutes under an argon inert atmosphere without solvent to activate the turnings. 15 mL of methanol was added to magnesium turnings before **3** (1.0103 g, 2.84 mmol, 1 eq.) was added as a suspension in 110 mL of methanol. The reaction was warmed to approximately 40 °C. An additional 0.5224 g of oven dried magnesium (total = 1.0561 g, 43.45 mmol, 15.3 eq.) were added

portionwise over 2 hours. During course of reaction, canary yellow precipitate in suspension changed to a cloudy pale yellow solution. After reaction was complete, 75 mL of $CHCl_3$ and 75 mL of 1 M hydrochloric acid were added to reaction mixture. Concentrated hydrochloric acid was added dropwise with vigorous stirring until solution cleared. The pH was adjusted back to approximately pH 6 and extracted with $CHCl_3$. The extracts were filtered using a silica gel plug. Crude 4 was eluted from the plug using 4% methanol in $CHCl_3$, and then evaporated under reduced pressure until immediately before solidification of the oil. Addition of 10 mL of cold ether to this oil resulted in a fluffy white precipitate, which was filtered and dried under vacuum yielding **4** (0.8971 g, 2.51 mmol, 88% yield).

^{1}H-NMR (300.68 MHz) (DMSO-d_6): δ 3.09-3.44 (ABX, 2H), 3.14 (s, 3H), 3.96 (t, 2H, J = 5.3 Hz), 4.01-4.17 (m, 2H), 4.48 (ABX, 1H), 6.52 (d, 1H, J = 8.5 Hz), 6.56 (t, 1H, J = 4.8 Hz), 6.82 (d, 2H, J = 8.9 Hz), 7.12 (d, 2H, J = 8.8 Hz), 7.45 (td, 1H, J = 1.5, 6.7), 8.13 (d, 1H, J = 5) ppm. ^{13}C-NMR (75.59 MHz) (DMSO-d_6): δ 37.89, 38.11, 49.73, 53.90, 66.45, 106.04, 111.96, 114.90, 127.79, 130.56, 137.59, 147.87, 158.39, 158.49, 170.66, 174.43 ppm. MS exact mass calculated for $C_{18}H_{19}N_3O_3S$: 357.1, found: 357.1.

5-(4-(2-(Methyl-2-pyridinylamino)ethoxy)benzyl-2,4-thiazolidinedione (4) Method B

The thiazolidinedione **3** (1.1 g, 3.1 mmol, 1 eq.) was added to a 100 mL Paar Shaker Flask and dissolved in 23 mL of acetic acid giving a rich canary yellow color. 0.27 g of 20% Paladium hydroxide on carbon (wet) catalyst was added to the flask. It was then subjected to 40 lbs. of hydrogen gas in the Paar shaker apparatus for 24 hours. An additional 0.33 g of catalyst was added after 9 hours. After completion, the reaction was filtered through celite to remove the palladium catalyst. The celite was washed with

acetic acid and chloroform. The resulting solution was clear, though it maintained a faint yellow tint. Solvent was removed under reduced pressure. Coevaporation with toluene removed last traces of solvent, giving the acetate salt of **4** (1.3 g, 3.1 mmol, 100%).

^{1}H-NMR (300.68 MHz) (DMSO-d_6): δ 2.36 (s, 3H), 3.09-3.44 (ABX, 2H), 3.14 (s, 3H), 3.96 (t, 2H, J = 5.3 Hz), 4.01-4.17 (m, 2H), 4.48 (ABX, 1H), 6.52 (d, 1H, J = 8.5 Hz), 6.56 (t, 1H, J = 4.8 Hz), 6.82 (d, 2H, J = 8.9 Hz), 7.12 (d, 2H, J = 8.8 Hz), 7.45 (td, 1H, J = 1.5, 6.7), 8.13 (d, 1H, J = 5) ppm. HRMS exact mass calculated for $C_{18}H_{19}N_3O_3S$: 357.114714, found: 357.115268.

3-Bromo-4-(2-(methyl-2-pyridinylamino)ethoxy)-benzaldehyde (2Br)

Based on the procedure of Cantello (164, 231), the alcohol **1** (1.5186 g, 9.98 mmol, 1 eq.) was dissolved and stirred continuously in anhydrous DMF (30 mL). Sodium hydride (0.4510 g, 11.3 mmol, 1.1 eq.), 60% in mineral oil, was weighed, rinsed with hexanes to remove the mineral oil, suspended in anhydrous DMF (10 mL), and added portionwise over 20 minutes to the reaction under argon inert atmosphere. After vigorous reaction was complete (no bubbling) the alkoxide was transferred by pipette to a solution of 4-fluoro-3-bromo-benzaldehyde (2.233 g, 11.1 mmol, 1.1 eq.) in 10 mL DMF over 40 minutes. Transfer by siphon through a bent pipette was intended, but clogging required intervention with a standard pipette. After 20 hours the reaction had stopped and was added to 150 mL of ice water, extracted with ethyl acetate, washed with brine, dried over sodium sulfate and evaporated under reduced pressure. TLC analysis showed that the reaction did not proceed to completion, presumably due to incomplete formation of the alkoxide. The crude product was purified on a flash column using 2% methanol in dichloromethane. Column purification did not resolve the product from the reactants.

Subsequent columns were run with 1% methanol in dichloromethane, in an attempt to purify the residue further. Pure **2Br** was eventually obtained after crystalization upon standing. Unfortunately the crystalized product was not weighed or submitted for mass spectrometry, so an accurate yield and molecular weight determination are not available. The product was identified by ^{1}H and ^{13}C-NMR after comparison to the chemical shifts of the starting materials and aldehyde **2**.

^{1}H-NMR (300.68 MHz) ($CDCl_3$): δ 3.23 (s, 3H), 4.11 (t, 2H, J = 5.15 Hz), 4.36 (t, 2H, J = 5.18 Hz), 6.52-6.60 (m, 2H), 7.03 (d, 1H, J = 8.47), 7.48 (td, 1H, J = 1.71, 7.82 Hz), 7.78 (dd, 1H, J = 1.77, 8.54), 8.08 (d, 1H, J = 1.77), 8.16 (d, 1H, J = 3.97 Hz), 9.832 (s, 1H) ppm. ^{13}C-NMR (75.59 MHz) ($CDCl_3$): δ 38.407, 49.155, 68.267, 105.734, 111.846, 112.210, 112.646, 130.559, 131.169, 134.380, 137.367, 147.737, 157.991, 160.088, 189.418, 189.621 ppm.

(Z)-5-((4-Chloro-3-nitrophenyl)methylene)-2,4-thiazolidinedione (5)

Based on the condensation procedure of Cantello (164, 231), 4-chloro-3-nitrobenzaldehyde (2.9580 g, 25.26 mmol, 1 eq.) was dissolved in 55 mL of toluene. 2,4-thiazolidinedione (4.6620 g, 25.12 mmol, 1 eq.) and p-toluene sulfonic acid (0.4590 g, 2.413 mmol, 0.1 eq.) were added to the reaction. The reaction was refluxed for 42 hours with a Dean-Stark trap to remove the water released by the condensation. Heat was removed and the reaction was allowed to cool to 4 °C. Precipitate was filtered to remove toluene, and then dissolved in 500 mL acetone to allow removal of the boiling chips. Acetone was evaporated under reduced pressure. The resulting crystalline solid was washed with water and dried under high vacuum giving **5** (3.9988 g,14.05 mmol, 55.9% yield) as a yellow crystalline solid.

^{1}H-NMR (300.68 MHz) (DMSO-d_6): δ 7.84-7.95 (m, 3H), 8.326 (d, 1H, J = 1.67), 12.813 (brs, 1H) ppm. HRMS exact mass calculated for $C_{10}H_5SN_2O_4Cl$: 283.965856, found: 283.965963.

4-(2-(Methyl-2-pyridinylamino)ethoxy)-3-nitrobenzaldehyde (8)

Based on the generic dioxolane deprotection conditions reported in Greene (232), the protected benzaldehyde **10** (4.7320 g, 13.7 mmol, 1 eq.) was dissolved in acetone (35 mL). 125 mL of 1 M hydrochloric acid was added converting the orange solution to a cloudy pale yellow color. After stirring for 3.5 hours at room temperature, the reaction had cleared to a salmon color. 20 mL of 6M sodium hydroxide was added to neutralize the reaction. 200 mL of ethyl acetate and 100 mL of bicarbonate were added and the aqueous layer was extracted with ethyl acetate. The organic extract was washed with bicarbonate, water, and brine before drying over sodium sulfate. Evaporation to dryness under reduced pressure gave the aldehyde **8** (3.5369 g, 11.7 mmol, 86% yield).

^{1}H-NMR (300.68 MHz) (Acetone-d_6): δ 3.224 (s, 3H), 4.149 (t, 2H, J = 5.49), 4.615 (t, 2H, J = 5.51), 6.641 (t, 1H, J = 5.07), 6.710 (d, J = 8.60), 7.575 (td, 1H, J = 1.91, 8.78), 7.703 (d, 1H, J = 8.76), 8.181 (dd, 1H, J = 1.1, 4.76), 8.248 (dd, 1H, J = 1.97, 8.70), 8.4395 (d, 1H, J = 1.96), 10.069 (s, 1H) ppm. HRMS exact mass calculated for $C_{15}H_{15}N_3O_4$: 301.106256, found: 301.106552.

4-Chloro-3-nitrophenyl-1,3-dioxolane (9)

Based on the generic ethylene glycol protection conditions reported in Greene (232), 4-chloro-3-nitrobenzaldehyde (1.1163 g, 6.016 mmol, 1 eq.), ethylene glycol (1.8707 g, 30.01 mmol, 5 eq.), and catalytic p-toluenesulfonic acid (0.3487 g, 1.83 mmol,

0.3 eq.) were dissolved in toluene (60 mL). The reaction was refluxed for 12 hours with a Dean-Stark trap to remove the water released in the reaction. 240 mL of ethyl ether was used to wash the last traces of the reaction out of the flask and added to the reaction mixture, which was then washed with bicarbonate to remove the catalytic acid. After washing with brine and drying over sodium sulfate the organic layer was evaporated under reduced pressure to give the protected aldehyde **9** (1.3747 g, 5.99 mmol, quantitative).

^{1}H-NMR (300.68 MHz) (Acetone-d_6): δ 3.950-4.118 (m, 4H), 5.833 (s, 1H), 7.713 (s, 2H), and 8.003 (s, 1H) ppm. HRMS exact mass calculated for $C_9H_8ClNO_4$: 229.01419, found: 228.991342.

4-(2-(Methyl-2-pyridinylamino)ethoxy)-3-nitrophenyl-1,3-dioxolane (10)

Based on the procedure of Cantello (164, 231), the alcohol **1** (0.3079 g, 2.02 mmol, 1 eq.) was dissolved and stirred continuously in anhydrous THF (5 mL). Sodium hydride (0.0894 g, 2.24 mmol, 1.1 eq.), 60% in mineral oil, was weighed, rinsed with hexanes to remove the mineral oil, suspended in anhydrous THF (5 mL), and added portionwise to the reaction under argon inert atmosphere. After vigorous reaction was complete (2.5 hours), the protected benzaldehyde **9** (0.5044 g, 2.20 mmol, 1.1 eq.), dissolved in anhydrous THF (2 mL), was added dropwise under argon inert atmosphere. After stirring overnight the reaction was added to 30 mL of a saturated aqueous ammonium chloride solution, extracted with ethyl acetate, washed with brine, dried over sodium sulfate and evaporated under reduced pressure. The crude extracts were purified using flash chromatography, after dry loading extracts onto silica, in a mobile phase of 30% ethyl acetate in hexanes with 1% triethylamine. Evaporation of the fractions

containing product under reduced pressure yielded the protected aldehyde **10** (0.3044 g, 0.88 mmol, 44% yield).

^{1}H-NMR (300.68 MHz) (Acetone-d_6): δ 3.217 (s, 3H), 4.043-4.201 (m, 6H), 4.486 (t, 2H, J = 5.52), 5.842 (s, 1H), 6.628 (td, 1H, J = 1.9, 5.94), 6.703 (d, 1H, J = 8.58), 7.483 (d, 1H, J = 8.70), 7.566 (t, 1H, J = 6.93), 7.759 (dd, 1H, J = 2.05, 8.66), 7.968 (d, 1H, J = 1.99), and 8.172 (dd, 1H, J = 1.07, 4.49) ppm. HRMS exact mass calculated for $C_{17}H_{19}N_3O_5$: 345.132471, found: 345.132828.

4-(2-(Methyl-2-pyridinylamino)ethoxy)-3-aminophenyl-1,3-dioxolane (15)

The protected aldehyde **10** (0.0362 g, 0.105 mmol, 1 eq.) was dissolved, with the assistance of sonication, in 1.5 mL of ethanol in a 5 mL vial. The palladium catalyst (0.0333 g 10% Pd/C) was added and the reaction was subjected to 30 lbs. of hydrogen gas in a Paar shaker apparatus for 5 hours. At this time, the reaction had lost the yellow color indicating reaction of the nitro group. TLC indicated complete conversion to a new slower running spot. The reaction was filtered through celite to remove the palladium catalyst. The celite was washed with ethyl acetate and ethanol. The combined organic flow-through was evaporated under reduced pressure giving the aniline **15** (0.0303 g, 0.096 mmol, 91.5% yield).

^{1}H-NMR (300.68 MHz) ($CDCl_3$): δ 3.13 (s, 3H), 3.93-4.23 (m, 12H, 8H assigned), 5.68 (s, 1H), 6.52-6.57 (m, 2H), 6.74-6.84 (m, 3H), 7.45 (td, 1H, J = 2.12, 8.97), and 8.15 (d, 1H, J = 3.96) ppm. ^{13}C-NMR (75.59 MHz) ($CDCl_3$): δ 37.64, 49.56, 65.33, 66.62, 104.03, 105.90, 111.04, 112.01, 113.01, 116.92, 130.80, 136.44, 137.47, 147.36, 148.07, and 158.64 ppm. No mass spectrometry data is available.

5-(4-(2-(Methyl-2-pyridinylamino)ethoxy)benzyl-N-octyl-2,4-thiazolidinedione (101)

Sodium iodine (175.5 mg, 1.16 mmol, 2.2 eq.) was dissolved in acetone (12 mL), which had been dried overnight with sodium sulfate. 1-bromooctane (90 μL, 0.521 mmol, 1 eq.) was added as a liquid. After two hours a white precipitate had formed. The precipitate and supernatant were evaporated under reduced pressure and dissolved in ethyl ether (50 mL). The organic layer was washed with 5% sodium sulfite, washed with brine, dried over sodium sulfate, and evaporated under reduced pressure. A crude NMR showed approximately 80% formation of 1-iodooctane.

Based on the phthalimide alkylation conditions of Sheehan (233), the thiazolidinedione **4** (51.4 mg, 0.144 mmol, 1 eq.) was dissolved in 1 mL DMF. Potasium hexamethyldisilazide (KHMDS) (345 μL of 0.5 M in toluene, 0.173 mmol, 1.2 eq.) was added dropwise. After stirring for 4 hours to ensure complete formation of the alkoxide, 1-iodooctane (52 μL, ~0.200 mmol, ~1.4 eq.) was added dropwise. After stirring overnight, reaction was diluted into ethyl acetate (20 mL), added to bicarbonate, and extracted with ethyl acetate. The combined organic layers were washed with bicarbonate, washed with brine, dried over sodium sulfate, and evaporated under reduced pressure. The residue was then dry loaded onto silica gel and purified by flash chromatography in a mobile phase of 20% ethyl acetate in hexanes with 1% ammonium hydroxide yielding the derivatized thiazolidinedione **101** (44.6 mg, 0.095 mmol, 66% yield).

^{1}H-NMR (300.68 MHz) ($CDCl_3$): δ 0.88 (t, 3H, J = 6.8), 1.24 (brs, 13H (10 assigned), 1.48 (m, 2H), 3.02 - 3.44 (ABX, 2H), 3.14 (s, 3H), 3.52 (t, 2H, J = 6.36), 3.97 (t, 2H, J = 5.47), 4.15 (t, 2H, J = 5.35), 4.39 (dd, 1H, J = 3.86, 9.35), 6.50 - 6.57 (m, 2H), 6.82 (d, 2H, J = 8.69), 7.10 (d, 2H, J = 8.62), 7.45 (td, 1H, J = 2.57, 8.68), and 8.14 (d,

1H, J = 4.7) ppm. HRMS exact mass calculated for $C_{26}H_{35}N_3O_3S$: 469.239914, found: 469.239617.

5-(4-(2-(Methyl-2-pyridinylamino)ethoxy)benzyl-N-(2-(bromomethyl)anthroquinone)-2,4-thiazolidinedione (102)

Based on the phthalimide alkylation conditions of Sheehan (233), the thiazolidinedione **4** (51.6 mg, 0.144 mmol, 1 eq.) was dissolved in 1 mL DMF. KHMDS (315 μL of 0.5 M in toluene, 0.157 mmol, 1.1 eq.) was added dropwise. After stirring for 30 minutes, 2-(bromomethyl)anthroquinone (52.5 mg, 0.174 mmol, 1.2 eq.) was added. An orange precipitate formed upon stirring overnight. The reaction was filtered, and the precipitate was washed with ethyl ether, and dried under high vacuum yielding the derivatized thiazolidinedione **102** (56.9 mg, 0.098 mmol, 68% yield).

^{1}H-NMR (300.68 MHz) ($CDCl_3$): δ 3.11 (s, 3H), 3.11-3.40 (ABX, 2H), 3.88-3.98 (m, 2H), 4.09 (t, 2H, J = 6.46), 4.52 (dd, 1H, J = 3.12, 7.68), 4.84 (s, 2H), 6.49-6.56 (m, 2H), 6.73 (d, 2H, J = 8.61), 7.06 (d, 2H, J = 8.51), 7.43 (td, 1H, J = 1.59, 6.99), 7.50 (d, 1H, J = 7.87), 7.80-7.82 (m, 2H), 8.13 (d, 1H, J = 4.61), 8.19-8.24 (m, 2H), and 8.32-8.34 (m, 2H) ppm. HRMS exact mass calculated for $C_{33}H_{29}N_3O_5S$: 579.1828, found: 442.074544 ($-C_8H_{13}N_2$).

5-(4-(2-(Methyl-2-pyridinylamino)ethoxy)benzyl-N-benzyl-2,4-thiazolidinedione (103)

Based on the phthalimide alkylation conditions of Sheehan (233), the thiazolidinedione **4** (53.6 mg, 0.150 mmol, 1 eq.) was dissolved in 1 mL DMF. KHMDS (40.2 mg, 0.202 mmol, 1.3 eq.) was added portionwise. After stirring for 20 minutes,

benzylbromide (21 μL, 0.177 mmol, 1.2 eq.) was added. After stirring overnight, the reaction was diluted into ethyl acetate (15 mL), added to 1 M sodium hydroxide (10 mL), and extracted with ethyl acetate. The combined organic layers were washed with 1 M sodium hydroxide, washed with brine, dried over sodium sulfate, and evaporated under reduced pressure. The residue was then dry loaded onto silica gel and purified by flash chromatography in a mobile phase of 15% ethyl acetate in hexanes with 1% ammonium hydroxide yielding the derivatized thiazolidinedione **103** (49.8 mg, 0.11 mmol, 76% yield).

^{1}H-NMR (300.68 MHz) ($CDCl_3$): δ 3.06-3.40 (ABX, 2H), 3.16 (s, 3H), 3.99 (t, 2H, J = 5.50), 4.15 (t, 2H, J = 5.61), 4.43 (dd, 1H, J = 3.91, 8.57), 4.69 (d, 2H, J = 3.92), 6.52-6.59 (m, 2H), 6.75 (d, 2H, J = 8.56), 7.04 (d, 2H, J = 8.67), 7.26 (brs, 5H), 7.46 (t, 1H, J = 7.13), and 8.17 (d, 1H, J = 3.38) ppm. HRMS exact mass calculated for $C_{25}H_{25}N_3O_3S$: 447.161664, found: 447.160303.

5-(4-(2-(Methyl-2-pyridinylamino)ethoxy)benzyl-N-(4-nitrobenzyl)-2,4-thiazolidinedione (104)

Based on the phthalimide alkylation conditions of Sheehan (233), the thiazolidinedione **4** (33.0 mg, 0.092 mmol, 1 eq.) was dissolved in 1 mL DMF. KHMDS (26.5 mg, 0.133 mmol, 1.44 eq.) was added portionwise. After stirring for 60 minutes, 4-nitrobenzylbromide (32.3 mg, 0.150 mmol, 1.62 eq.) was added. After stirring overnight, the reaction was diluted into ethyl acetate (15 mL), added to 1 M sodium hydroxide (10 mL), and extracted with ethyl acetate. The combined organic layers were washed with 1 M sodium hydroxide, washed with brine, dried over sodium sulfate, and evaporated under reduced pressure. The residue was then dry loaded onto silica gel and

purified by flash chromatography in a mobile phase of 20% ethyl acetate in hexanes with 1% ammonium hydroxide yielding the derivatized thiazolidinedione **104** (14.4 mg, 29.2 μmol, 32% yield).

^{1}H-NMR (300.68 MHz) ($CDCl_3$): δ 3.16 (s, 3H), 3.16-3.36 (ABX, 2H), 4.00 (t, 2H, J = 5.52), 4.14 (t, 2H, J = 6.10), 4.51 (dd, 1H, J = 3.87, 7.81), 4.74 (d, 2H, J = 5.46), 6.52-6.57 (m, 2H), 6.74 (d, 2H, J = 8.69), 7.06 (d, 2H, J = 8.54), 7.28 (d, 2H, J = 7.98), 7.46 (t, 1H, J = 7.06), and 8.11-8.16 (m, 3H) ppm. HRMS exact mass calculated for $C_{25}H_{24}N_4O_5S$: 492.146742, found: 492.147262.

5-(4-(2-(Methyl-2-pyridinylamino)ethoxy)benzyl-N-(4-tolunitrile)-2,4-thiazolidinedione (105)

Based on the phthalimide alkylation conditions of Sheehan (233), the thiazolidinedione **4** (53.6 mg, 0.150 mmol, 1 eq.) was dissolved in 1 mL DMF. KHMDS (52.9 mg, 0.265 mmol, 1.8 eq.) was added portionwise. After stirring for 30 minutes, α-bromo-p-tolunitrile (42.5 mg, 0.217 mmol, 1.4 eq.) was added. After stirring overnight, the reaction was diluted into ethyl acetate (50 mL), added to 5% sodium bicarbonate, and extracted with ethyl acetate. The combined organic layers were washed with water, washed with brine, dried over sodium sulfate, and evaporated under reduced pressure. The residue was then dry loaded onto silica gel and purified by flash chromatography in a mobile phase of 25% ethyl acetate in hexanes with 1% ammonium hydroxide yielding the derivatized thiazolidinedione **105** (32.9 mg, 70 μmol, 46% yield).

^{1}H-NMR (300.68 MHz) ($CDCl_3$): δ 3.09-3.37 (ABX, 2H), 3.16 (s, 3H), 3.99 (t, 2H, J = 5.42), 4.15 (t, 2H, J = 6.17), 4.48 (dd, 1H, J = 3.95, 7.80), 4.69 (d, 2H, J = 3.16), 6.52-6.57 (m, 2H), 6.75 (d, 2H, J = 8.66), 7.04 (d, 2H, J = 8.57), 7.27 (d, 2H, J = 8.91),

7.45 (t, 1H, J = 9.61), 7.56 (d, 2H, J = 8.98), and 8.14 (d, 1H, J = 4.73) ppm. HRMS exact mass calculated for $C_{26}H_{24}N_4O_3S$: 472.156913, found: 472.157106.

5-(4-(2-(Methyl-2-pyridinylamino)ethoxy)benzyl-N-naphthyl-2,4-thiazolidinedione (107)

Based on the phthalimide alkylation conditions of Sheehan (233), the thiazolidinedione **4** (56.5 mg, 0.158 mmol, 1 eq.) was dissolved in 1 mL DMF. KHMDS (345 μL of 0.5 M in toluene, 0.173 mmol, 1.1 eq.) was added dropwise. After stirring for 30 minutes, 2-(bromomethyl)naphaline (41.1 mg, 0.186 mmol, 1.2 eq.) was added. After stirring overnight, reaction was diluted into ethyl acetate (20 mL), added to bicarbonate (10 mL), and extracted with ethyl acetate. The combined organic layers were washed with bicarbonate, washed with brine, dried over sodium sulfate, and evaporated under reduced pressure. The residue was then dry loaded onto silica gel and purified by flash chromatography yielding the derivatized thiazolidinedione **107** (47.2 mg, 0.095 mmol, 60% yield).

^{1}H-NMR (300.68 MHz) ($CDCl_3$): δ 3.05-3.37 (ABX, 2H), 3.12 (s, 3H), 3.91-4.05 (m, 4H), 4.42 (dd, 1H, J = 4.08, 8.49), 4.85 (s, 2H), 6.49-6.57 (m, 2H), 6.63 (d, 2H, J = 8.49), 6.99 (d, 2H, J = 8.71), 7.36-7.46 (m, 3H), 7.73-7.81 (m, 3H), and 8.16 (d, 1H, J = 4.67) ppm. HRMS exact mass calculated for $C_{29}H_{27}N_3O_3S$: 497.177314, found: 497.177459.

(Z)-5-((4-(2-(Methyl-2-pyridinylamino)ethoxy)phenyl)-methylene-N-octyl-2,4-thiazolidinedione (121)

Based on the phthalimide alkylation conditions of Sheehan (233), the thiazolidinedione **3** (0.3566 g, 1.00 mmol, 1 eq.) was suspended in 10 mL DMF. KHMDS (0.55 mL of 0.5 M in toluene, 0.275 mmol, 0.27 eq.) was added dropwise. The remaining suspended thiazolidinedione **3** went into solution upon addition of the base. After stirring for 30 minutes, 1-bromooctane (0.195 mL, 1.13 mmol, 1.1 eq.) was added. An additional aliquot of KHMDS (1.65 mL of 0.5 M in toluene, 0.825 mmol, 0.82 eq.) was added dropwise resulting in a dark red solution. The reaction was not complete after stirring at room temperature overnight, so more KHMDS (2.0 mL of 0.5 M in toluene, 1.0 mmol, 1 eq.) and 1-bromooctane (0.175 mL, 1 mmol, 1 eq.) were added. After stirring overnight the reaction was diluted with 20 mL of chloroform, then added to 80 mL of water, and then extracted with chloroform. The combined organic extracts were washed with 1M sodium hydroxide, water, and brine. The organic layer was dried over sodium sulfate before evaporating under reduced pressure. TLC of the residue showed five major spots. The residue was dry loaded onto silica gel and purified by flash chromatography with a mobile phase of 30% ethyl acetate in hexane with 1% ammonium hydroxide. The derivatized thiazolidinedione **121** was collected only from the fractions containing no contaminants. Unfortunately, the purified product was not weighted, so an accurate yield could not be determined.

^{1}H-NMR (300.68 MHz) (DMSO-d_6): δ 0.84 (brs, 3H), 1.17-1.25 (m, 15H (10 assigned), 1.57 (m, 2H), 3.09 (s, 3H), 3.64 (t, 2H, J = 7.10), 3.94 (t, 2H, J = 5.70), 4.24 (t, 2H, J = 6.10), 6.58 (t, 1H, J = 6.10), 6.66 (d, 1H, J = 8.60), 7.12 (d, 2H, J = 8.42), 7.52 (t,

1H, J = 7.22), 7.58 (d, 2H, J = 8.39), 7.88 (s, 1H), and 8.09 (d, 1H, J = 4.83) ppm. HRMS exact mass calculated for $C_{26}H_{33}SN_3O_3$: 467.224264, found: 467.222773.

(Z)-5-((4-(2-(Methyl-2-pyridinylamino)ethoxy)phenyl)-methylene-N-(2-(bromomethyl)anthroquinone)-2,4-thiazolidinedione (122)

Based on the phthalimide alkylation conditions of Sheehan (233), the thiazolidinedione **3** (50.5 mg, 0.142 mmol, 1 eq.) was suspended in 1 mL DMF. KHMDS (315 μL of 0.5 M in toluene, 0.157 mmol, 1.1 eq.) was added dropwise. The remaining suspended thiazolidinedione **3** went into solution upon addition of the base. After stirring for 20 minutes, 2-(bromomethyl)anthroquinone (53 mg, 0.176 mmol, 1.2 eq.) was added. An orange precipitate formed upon stirring overnight. The reaction was filtered, the precipitate was washed with ethyl ether, and dried under high vacuum yielding the derivatized thiazolidinedione **122** (73.3 mg, 0.127 mmol, 89% yield).

^{1}H-NMR (300.68 MHz) ($CDCl_3$): δ 3.09 (s, 3H), 4.01 (t, 2H, J = 5.52), 4.26 (t, 2H, J = 5.35), 5.06 (s, 2H), 6.51 (d, 1H, J = 8.55), 6.57 (t, 1H, J = 5.41), 6.98 (d, 1H, J = 8.55), 7.42-7.45 (m, 3H), 7.79-7.82 (m, 3H), 7.89 (s, 1H), 8.16 (d, 1H, J = 4.69), and 8.29-8.31 (m, 3H) ppm. HRMS exact mass calculated for $C_{33}H_{27}N_3O_5S$: 577.1671, found: 442.071932 ($-C_8H_{11}N_2$).

(Z)-5-((4-(2-(Methyl-2-pyridinylamino)ethoxy)phenyl)-methylene-N-benzyl-2,4-thiazolidinedione (123)

Based on the phthalimide alkylation conditions of Sheehan (233), the thiazolidinedione **3** (0.3551 g, 1.00 mmol, 1 eq.) was suspended in 10 mL DMF. KHMDS (0.55 mL of 0.5 M in toluene, 0.275 mmol, 0.27 eq.) was added dropwise. The

remaining suspended thiazolidinedione **3** went into solution upon addition of the base. After stirring for 30 minutes, benzyl bromide (0.175 mL, 1.47 mmol, 1.47 eq.) was added. An additional aliquot of KHMDS (1.65 mL of 0.5 M in toluene, 0.825 mmol, 0.82 eq.) was added dropwise. The reaction was not complete after stirring at room temperature overnight, so more KHMDS (2.0 mL of 0.5 M in toluene, 1.0 mmol, 1 eq.) and benzyl bromide (0.120 mL, 1 mmol, 1 eq.) were added. After stirring overnight the reaction was diluted with chloroform, added to 0.1 M sodium hydroxide (100 mL), and extracted with ethyl acetate. The combined organic extracts were washed with 1 M sodium hydroxide, washed with brine, dried over sodium sulfate, and evaporated under reduced pressure. The residue was dry loaded onto silica gel and purified by flash chromatography with a mobile phase of 25% ethyl acetate in hexane with 1% ammonium hydroxide yielding the derivatized thiazolidinedione **123** (0.1184 g, 0.27 mmol, 27% yield).

^{1}H-NMR (300.68 MHz) ($CDCl_3$): δ 3.07 (s, 3H), 3.93 (t, 2H, J = 5.60), 4.23 (t, 2H, J = 6.14), 4.83 (s, 2H), 6.57 (t, 1H, J = 6.83), 6.65 (d, 1H, 8.94), 7.12 (d, 2H, J = 8.83), 7.29-7.35 (m, 5H), 7.50 (td, 1H, J = 1.63, 8.49), 6.58 (d, 2H, J = 8.84), 7.92 (s, 1H), and 8.08, (d, 1H, J = 4.13) ppm. HRMS exact mass calculated for $C_{25}H_{23}SN_3O_3$: 445.1460, found: 311.061566 ($-C_8H_{11}N_2$).

(Z)-5-((4-(2-(Methyl-2-pyridinylamino)ethoxy)phenyl)-methylene-N-(4-nitrobenzyl)-2,4-thiazolidinedione (124)

Based on the phthalimide alkylation conditions of Sheehan (233), the thiazolidinedione **3** (1.0051g, 2.83 mmol, 1 eq.) was suspended in 12 mL DMF. KHMDS (6.2 mL of 0.5 M in toluene, 3.10 mmol, 1.1 eq.) was added dropwise. The

remaining suspended thiazolidinedione **3** went into solution upon addition of the base. After stirring for 20 minutes, the reaction was cooled to 0°C, and 4-nitrobenzylbromide (0.6913 g, 3.20 mmol, 1.1 eq.) was added. After stirring overnight, the reaction was filtered, the precipitate was washed with ethyl ether and hexanes, and dried under high vacuum yielding the derivatized thiazolidinedione **124** (1.3712 g, 2.79 mmol, 98% yield).

^{1}H-NMR (300.68 MHz) ($CDCl_3$): δ 3.14 (s, 3H), 4.01 (t, 2H, J = 5.54), 4.26 (t, 2H, J = 5.69), 4.97 (s, 2H), 6.51 (d, 1H, J = 8.6), 6.57 (t, 1H, J = 4.76), 6.99 (d, 2H, J = 8.83), 7.42-7.49 (m, 3H), 6.58 (d, 2H, J = 8.67), 7.87 (s, 1H), 8.16 (d, 1H, J = 4.59), and 8.19 (d, 2H, J = 8.61) ppm. HRMS exact mass calculated for $C_{25}H_{22}N_4O_5S$: 490.131092, found: 490.131339.

(Z)-5-((4-(2-(Methyl-2-pyridinylamino)ethoxy)phenyl)-methylene-N-(4-tolunitrile)-2,4-thiazolidinedione (125)

Based on the phthalimide alkylation conditions of Sheehan (233), the thiazolidinedione **3** (0.3613 g, 1.02 mmol, 1 eq.) was dissolved in 10 mL DMF. KHMDS (0.2236 g, 1.12 mmol, 1.1 eq.) was added portionwise. The remaining suspended thiazolidinedione **3** went into solution upon addition of the base. After stirring overnight, α-bromo-p-tolunitrile (0.2149 g, 1.10 mmol, 1.1 eq.) was added. After stirring overnight, the reaction was filtered. The precipitate was dissolved in 80 mL of 1M sodium hydroxide and extracted with ethyl acetate, and evaporated under reduced pressure to yield the derivatized thiazolidinedione **125** (0.2917 g, 0.620 mmol, 61% yield).

^{1}H-NMR (300.68 MHz) (DMSO-d_6): δ 3.07 (s, 3H), 3.93 (t, 2H, J = 5.72), 4.24 (t, 2H, J = 5.92), 4.92 (s, 2H), 6.57 (dd, 1H, J = 5.18, 7.09), 6.65 (d, 1H, J = 8.59), 7.12 (d, 2H, J = 8.82), 7.48-7.53 (m, 3H), 7.59 (d, 2H, J = 8.83), 7.82 (d, 2H, J = 8.67), 7.93 (s,

1H), and 8.08 (d, 1H, J = 3.67) ppm. HRMS exact mass calculated for $C_{26}H_{22}N_4O_3S$: 470.1413, found: 337.059208 ($-C_8H_9N_2$).

(Z)-5-((4-(2-(Methyl-2-pyridinylamino)ethoxy)phenyl)-methylene-N-allyl-2,4-thiazolidinedione (126)

Based on the phthalimide alkylation conditions of Sheehan (233), the thiazolidinedione **3** (0.3584 g, 1.01 mmol, 1 eq.) was suspended in 10 mL DMF. KHMDS (0.55 mL of 0.5 M in toluene, 0.275 mmol, 0.27 eq.) was added dropwise. The remaining suspended thiazolidinedione **3** went into solution upon addition of the base. After stirring for 30 minutes, allyl bromide (0.125 mL, 1.44 mmol, 1.43 eq.) was added. An additional aliquot of KHMDS (1.65 mL of 0.5 M in toluene, 0.825 mmol, 0.82 eq.) was added dropwise. The reaction was not complete after stirring at room temperature overnight, so more KHMDS (2.0 mL of 0.5 M in toluene, 1.0 mmol, 1 eq.) and allyl bromide (0.90 mL, 1 mmol, 1 eq.) were added. After stirring overnight the reaction was diluted with chloroform, added to 1 M sodium hydroxide (80 mL), and extracted with ethyl acetate. The combined organic extracts were washed with 1 M sodium hydroxide, washed with brine, dried over sodium sulfate, and evaporated under reduced pressure. The residue was dry loaded onto silica gel and purified by flash chromatography with a mobile phase of 20% ethyl acetate in hexane with 1% ammonium hydroxide yielding the derivatized thiazolidinedione **126** (0.0895 g, 0.23 mmol, 23% yield).

^{1}H-NMR (300.68 MHz) (DMSO-d_6): δ 3.07 (s, 3H), 3.93 (t, 2H, J = 5.55), 4.22-4.26 (m, 4H), 5.11-5.18 (m, 2H), 5.80-5.89 (m, 1H), 6.57 (dd, 1H, J = 4.81, 6.88), 6.65 (d, 1H, J = 8.44), 7.12 (d, 2H, J = 8.91), 7.51 (td, 1H, J = 2.02, 8.81), 7.58 (d, 2H, J =

8.87), 7.90 (s, 1H), and 8.08 (d, 1H, J = 4.29) ppm. HRMS exact mass calculated for $C_{21}H_{21}SN_3O_3$: 395.130364, found: 395.130579.

Results and Discussion

Rosiglitazone Synthesis

Rosiglitazone ((Z)-5-(4-(2-(methyl-2-pyridinylamino)ethoxy)benzyl-2,4-thiazolidinedione (**4**)), which is also known as Avandia™ or BRL 49653, is a potent agonist of PPARγ (50, 51). I sought to obtain a useful synthetic route to provide both rosiglitazone for our cell assays and precursors for the synthesis of novel derivatives of rosiglitazone. I began the synthesis of rosiglitazone following the synthetic approach outlined by Cantello (164, 231) and made modifications as needed. The synthetic route

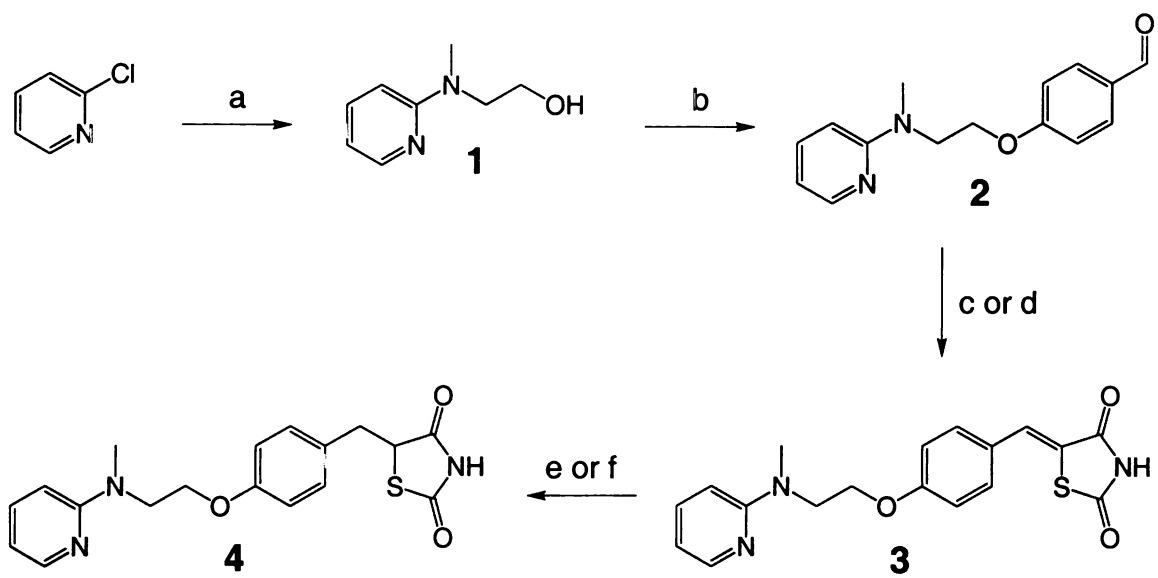

Figure 2.4: Rosiglitazone Synthesis.

The synthetic route for rosiglitazone (5-(4-(2-(methyl-2-pyridinylamino)ethoxy)benzyl-2,4-thiazolidinedione) is shown. a) 2-methylaminoethanol (11 eq.) 120 °C 45 hours 78%. b) i) sodium hydride (1.1 eq.), DMF 2 hours ii) 4-fluorobenzaldehyde (1.1 eq.) 10 hours 49%. c) 2,4-thiazolidinedione (1 eq.), piperidinium acetate (0.1 eq.), toluene reflux -H_2O 2 hours 73%. d) 2,4-thiazolidinedione (1 eq.), piperidine (0.5 eq.), ethanol reflux 4 hours 70%. e) activated magnesium turnings, methanol 40 °C 88%. f) catalytic palladium on carbon, H_2 (30-40 lbs.), acetic acid room temperature overnight 100%.

and conditions are shown in Figure 2.4.

The first step in Cantello's synthesis, the addition of N-methylaminoethanol to 2-chloropyridine to give the alcohol **1**, has worked consistently. As I typically did this reaction on relatively large scales, one of the challenges was the volume used in the extraction procedure. The purification by fractional distillation was difficult, at the time, because our vacuum pump was not giving stable pressure, and the viscosity of the alcohol resulted in bumping when it gathered in the condenser. The use of a larger separatory funnel (4L), and a better vacuum distillation procedure, perhaps involving the use of a Kügelrohr apparatus, would make this reaction easier and might significantly improve the yield.

The second step in Cantello's synthesis, the addition of **1** to 4-fluorobenzaldehyde to give the aldehyde **2**, did not work in my hands as well. The major problems appeared to be incomplete alkoxide formation, and difficulty separating the alcohol **1** from the product **2** using flash chromatography due to streaking of the alcohol **1**. The incomplete alkoxide formation is likely due to two factors: water contamination of the solvent; air exposure of the sodium hydride. The use of solvent stills, or a better source of anhydrous solvents, and increasing the equivalents of base used would be easy first steps in improving the extent of alkoxide formation and hence the reaction yield. Because the sodium hydride needs to be rinsed with hexanes to remove the mineral oil, posing the risk of exposure to the water in air, the use of an alternative non-nucleophilic base, such as KHMDS, has the potential to improve the yield and consistency of the reaction. Reducing the amount of unreacted alcohol is the best way to ease the purification of the product **2**., but careful attention to prevent overloading the column in also important.

The third step in Cantello's synthesis provided reasonable yields, but inconsistent results. If the temperature used to reflux the toluene is too high, thermal decomposition leads to a red insoluble wax that hinders or prevents isolation of the precipitate **3**. The reaction also appears to be prone to drying out, resulting in a charcoal like solid. The use of smaller Dean-Stark traps with jacketed necks wrapped in aluminum foil for insulation and a good water jacketed condenser helped to reduce the temperature required to fill the trap, and minimized solvent loss. Addition of toluene to the trap before starting the reaction also helped prevent the reaction from drying out. If the wax resulting from thermal decomposition is avoided, the product is relatively pure upon precipitation from the toluene, but the precipitation is incomplete, so the yield decreases with increasing reaction volumes. Column purification of this product was difficult, did not significantly increase the purity, and did not give good recovery of material, presumably due to the low solubility of this compound in most solvents.

Alternative conditions for the thiazolidinedione condensation reaction using ethanol as a solvent and piperidine as a catalytic base avoids the thermal decomposition problem and the use of the Dean-Stark trap. Use of a good condenser and careful control of the temperature is still important to prevent the reaction from drying out. The precipitate from this reaction is more crystalline in character than the toluene method, and still quite pure, making it easier to handle.

The final step in Cantello's synthesis, the dissolving magnesium reduction of the αβ-unsaturated double bond of **3**, is technically difficult but gives good yields when conducted successfully. One of the major difficulties is keeping the magnesium active during the reaction. Mechanical agitation with a glass rod during the reaction and

Cantello's suggested activation with elemental iodide did not work well in my hands. I was successful with oven drying the magnesium overnight and then stirring it vigorously under inert atmosphere without solvent to mechanically break the turnings open and expose a reactive metal surface. With this magnesium preparation, I was able to avoid most of the complications of the insolubility of **3**. During the course of the reaction, the suspension of **3** was replaced with a cloudy pale yellow solution. Addition of the reaction to the aqueous acid resulted in a gel that hampered stirring, and complicated the accurate neutralization of the reaction. The thiazolidinedione **3** and some of its derivatives are the least soluble compounds I have made. Reduction of **3** to **4** improves the solubility considerably, but does not eliminate solubility problems and the associated synthetic difficulties. Flash chromatography of this product was difficult due to its limited solubility, and did not significantly increase the purity of the product.

The alternative palladium catalyzed hydrogenation is easier than the dissolving magnesium reduction technically, but is complicated by the poisoning of the palladium catalyst, presumably by either the amidine or sulfur present in the thiazolidinediones **3** and **4**. The use of a palladium hydroxide catalyst reduced the poisoning problems, but still required the use of large amounts of catalyst. Thorough washing of the celite with acetic acid and chloroform is required to recover the product **4** due to its limited solubility.

A radiolabeled rosiglitazone would be useful for PPARγ competitive binding assays. The hydrogenation in the last step of the synthesis is a logical point to incorporate tritium. Unfortunately, both of the conditions I have used for the reduction are not suitable for tritiation reactions with the equipment available to us.

In summary, I was able to synthesize rosiglitazone following the published route, with minor modifications to the conditions in the last two steps of the synthesis.

Phenyl Derivatives

The first attempts at derivatization of rosiglitazone centered around incorporating a functional group on the phenyl ring that could later be used to add a variety of extensions in one of the last few steps of the synthesis. The choice of the phenyl ring as a derivatization site centered on empirical evaluations of the chemical structures of known antagonists (Figure 2.2). Antagonist chemical structures resemble the structures of agonists for the same receptor with an extension from the "central portion" of the molecule (Figure 2.3). Two synthetic pathways were tested with limited success. The first pathway used a phenylhalide (Figure 2.5) as a synthetic handle to be used in a variety cross coupling reactions. The second pathway used an aromatic nitrobenzene (Figure 2.6) that could be reduced along with the αβ-unsaturated double bond neighboring the thiazolidinedione ring in the last step of the rosiglitazone synthesis to give an aniline. The aniline could then be coupled with a variety of alkylating or acetylating reagents.

The synthetic approach to a halide derivative of rosiglitazone centered on the incorporation of the halide by coupling the alcohol **1** to a different commercially available benzaldehyde (Figure 2.5). The use of 4-fluoro-3-bromobenzaldehyde gave the bromo analog of aldehyde **2**, **2Br**, in a reasonable yield. Unfortunately, attempts to conduct a palladium catalyzed Sonigashira cross coupling reaction (234, 235) on this reagent did not work. Sonigashira cross coupling reactions using the 4-fluoro-3-bromobenzaldehyde substrate did not work either. One possible problem is the lower

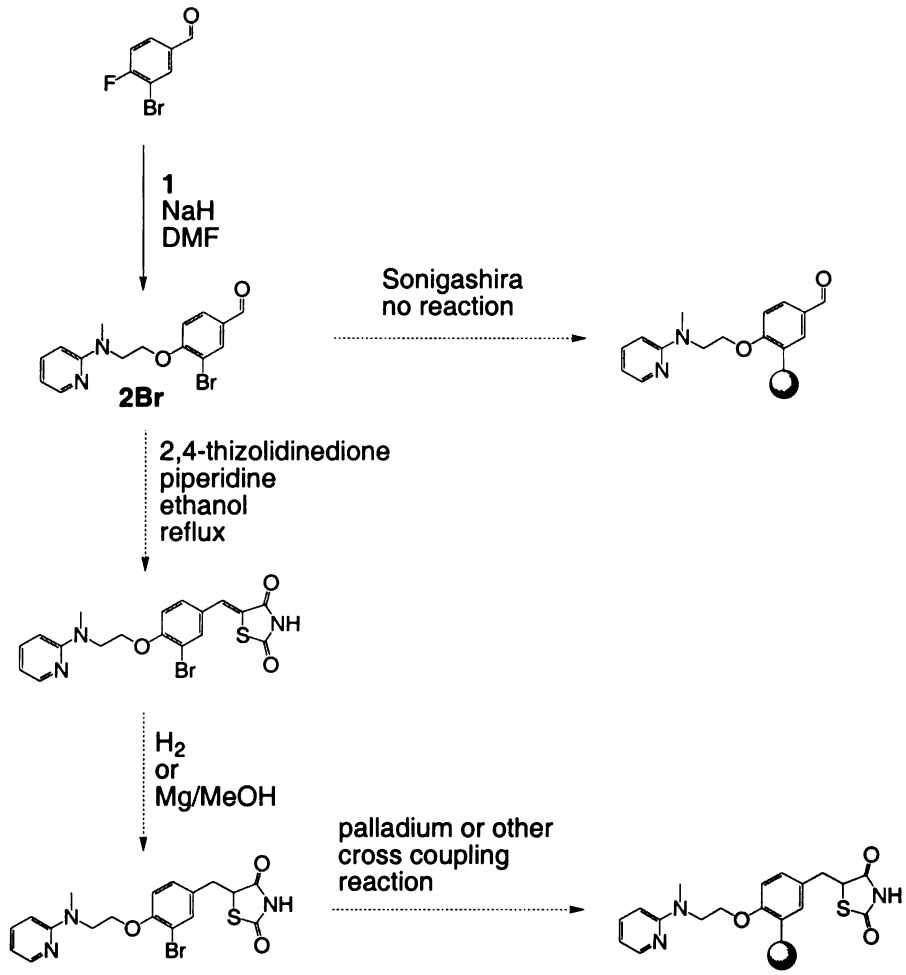

Figure 2.5: The Synthesis of Phenyl Derivatives Using Halide Chemistry

An approach for the synthesis of phenyl ring derivatives of rosiglitazone using cross coupling chemistry and a halide derivative is shown.

reactivity of the bromine relative to iodine in these reactions. Attempts at iodinating either 4-fluorobenzaldehyde or the benzaldehyde **2** were not successful. In hindsight, the use of a different cross coupling reaction or conversion of the halide to another functional handle, such as an alcohol, might have worked better. Alternatively, addition of the thiazolidinedione and the subsequent reduction, though they might introduce solubility problems, might have sufficiently changed the electronic properties of the phenyl ring to allow a coupling reaction to work.

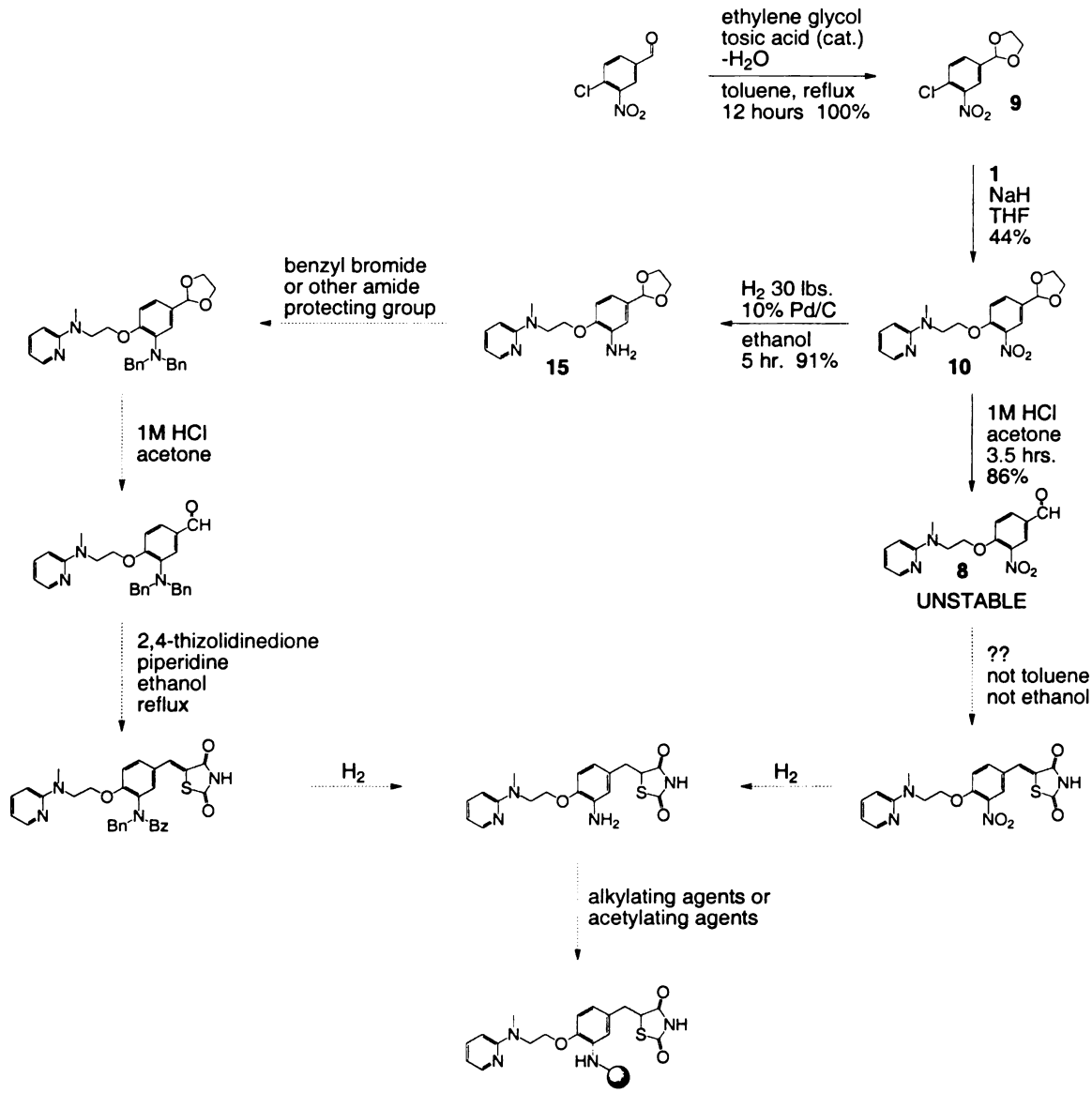

Figure 2.6: The Synthesis of Aniline Derivatives

An approach for the synthesis of phenyl ring derivatives of rosiglitazone using an aniline functionality is shown.

The synthetic approach to an aniline derivative of rosiglitazone centered on the incorporation of an aromatic nitro group by coupling the alcohol **1** to a different commercially available benzaldehyde (Figure 2.6). This aromatic nitro group incorporated using 4-chloro-3-nitrobenzaldehyde would later be reduced to an aniline functionality.

Attempts at the addition of 4-chloro-3-nitrobenzaldehyde directly to the alcohol **1** were not successful resulting in the alcohol **1** and what appeared to be 4-hydroxy-3-nitrobenzaldehyde based on the ^{1}H-NMR and color of that compound. While the condensation of 2,4-thiazolidinedione with 4-chloro-3-nitrobenzaldehyde to give **5** worked well, the coupling of **5** with the alcohol **1** did not work. The solubility limitations of **5** along with the lower reactivity of the chloro functionality in the nucleophilic aromatic substitution reaction, relative to a fluoride group, may have contributed to this.

Protection of 4-chloro-3-nitrobenzaldehyde with ethylene glycol gave **9** in excellent yield, but it was quite difficult to separate the product from the last traces of ethylene glycol. Several attempts at finding appropriate column conditions were not fruitful due to severe streaking of ethylene glycol on silica. The largest factor in obtaining relatively pure product was waiting for the reaction to reach complete protection of the aldehyde and a careful extraction with sufficient volumes. Purification by vacuum distillation was attempted, but was limited by apparent thermal decomposition, viscosity, and variability in the vacuum pressure. The use of an apparatus such as a Kügelrohr apparatus along with a better vacuum pump would reduce the temperatures necessary for purification, reduce problems of bumping, and might make this a useful means of purifying **9**.

The protected aldehyde **9** was coupled with alcohol **1** to give the protected benzaldehyde **10**. The use of THF, instead of the more viscous DMF, made this reaction much easier to handle than the previously described couplings. Sodium hydride was used as the base in this reaction, and an incomplete reaction again limited the yield. The use

of KHMDS or another non-nucleophilic base and completely anhydrous solvent, perhaps from a still, might significantly improve the yield of the reaction.

Deprotection of **10** to give the benzaldehyde **8** was accomplished using 1 M hydrochloric acid. Unfortunately, this deprotection reaction has not been very reproducible, often leading to decomposition yielding the alcohol **1** and what appears to be 4-hydroxy-3-nitrobenzaldehyde. This decomposition reaction proceeds within a week if the benzaldehyde **8** is left at room temperature. The compound does not survive either of the conditions used for the 2,4-thiazolidinedione condensation reaction in the rosiglitazone synthesis.

We suspect that the decomposition is aided by the electron withdrawing properties of the nitro group, particularly when coupled with the electron withdrawing properties of the aldehyde. To avoid these problems we pursued the possibility of reducing the nitro group to give the aniline, which we could then protect if necessary. The nitro group of the protected benzaldehdye **10** is rapidly reduced by catalytic hydrogenation to give the aniline **15**. Based on the color change, only 20 minutes may suffice for this reaction, which was only attempted once.

TZD Derivatives

While I was still pursuing the phenyl derivative, the crystal structure of a PPARγ LBD construct bound to rosiglitazone was published (72). This structure showed the thiazolidinedione head group (Figure 2.1) participating in hydrogen bonding interactions with residues on helix-12. As the molecular mechanism of antagonism of estrogen receptor by tamoxifen and raloxifene appears to be disruption of helix-12 based on crystal structures of the estrogen receptor with these compounds bound (68, 70). The

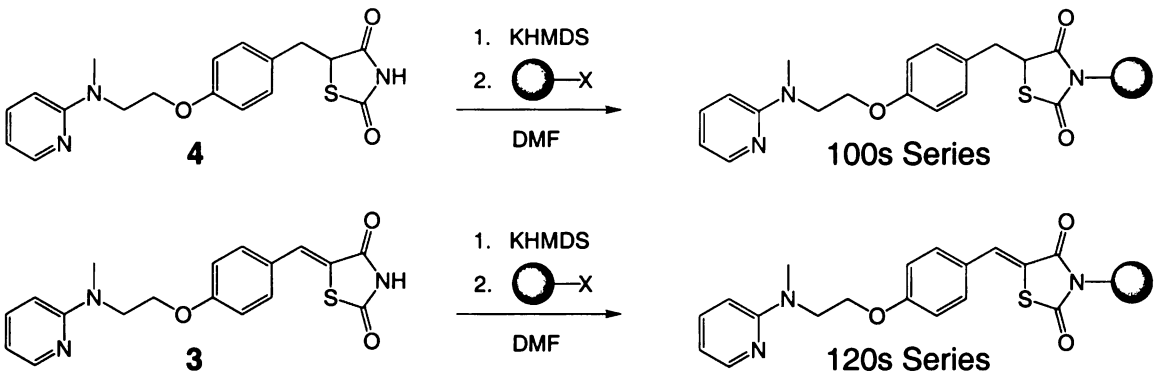

Figure 2.7: The Synthesis of Thiazolidinedione Derivatives

Derivatization of the thiazolidinedione head group with bromo or iodo compounds is accomplished in a single step. Compounds in the 100s are derivatives of rosiglitazone, while compounds in the 120s are derivatives of the thiazolidinedione **3**.

thiazolidinedione functionality can be derivatized in a single reaction by deprotonation of the nitrogen and addition of organic bromides (233). Due to the relative ease of generating derivatives at this position, and the suspicion based on the crystal structure that these extensions might interact with helix-12, I shifted my focus to derivatization of the thiazolidinedione site (Figure 2.7).

Alkylation under these conditions typically worked well, but the purification and isolation was often difficult due to solubility constraints, resulting in yields between 23% and 98% (Figure 2.8). In general, the derivatives of **3** showed lower solubility than the derivatives of **4**, with **122**, **124**, and **125** showing visible amounts of precipitate at 1 mM concentrations in every solvent tested, including cell culture media. The octyl derivatives showed the best solubility, while the anthroquinone derivatives showed the worst solubility of the derivatives made. As a class, the thiazolidinedione derivatives typically showed sufficient solubility in chloroform or DMSO to obtain proton NMR, but insufficient concentrations for obtaining carbon spectra with our instrument.

Of the compounds that were made, many were toxic to cultured cells or showed limited solubility making their characterization in cell assays difficult. Some cell data for

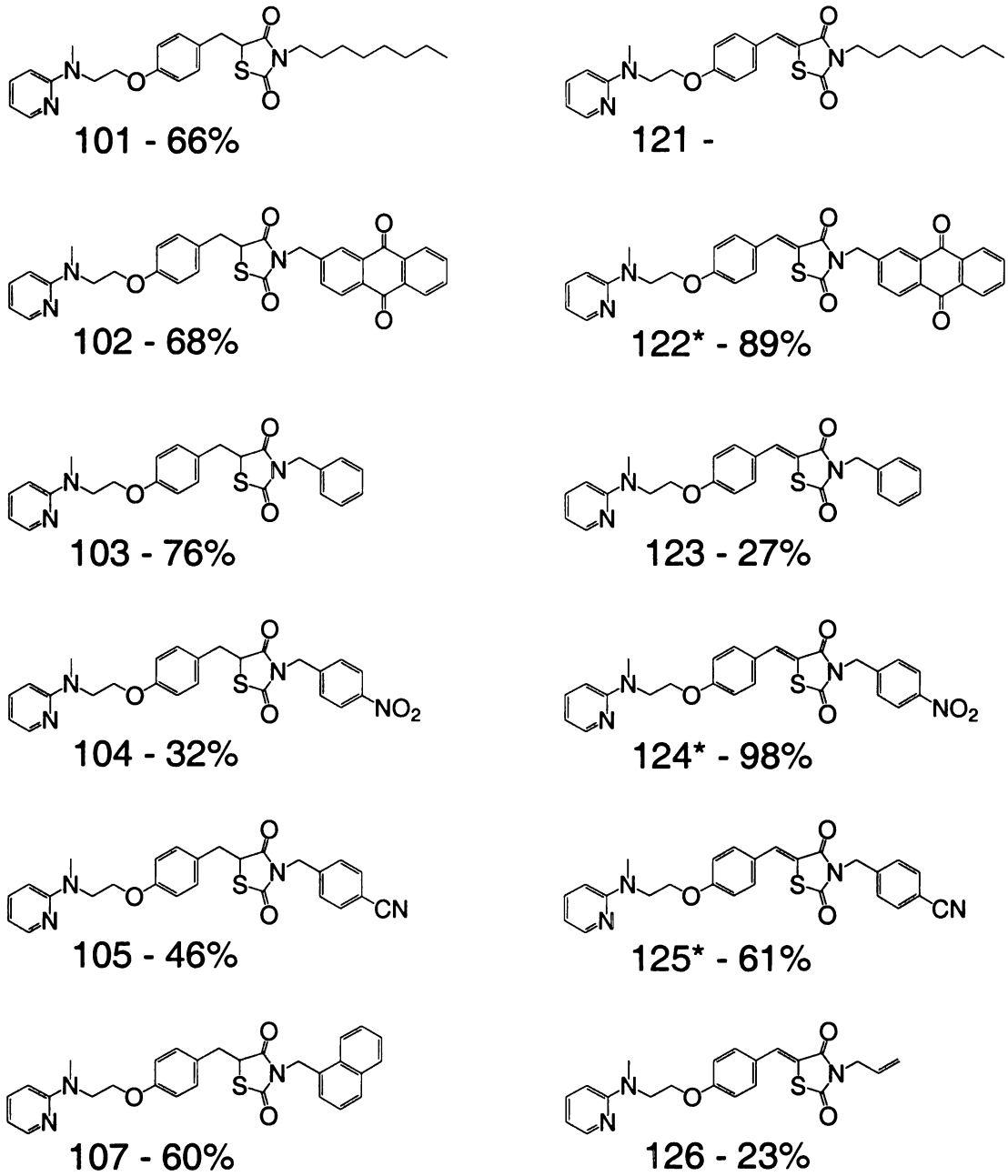

Figure 2.8: Thiazolidinedione Derivatives

The chemical structures and yields of the 100s and 120s series thiazolidinedione derivatives are shown. Compounds showing low solubility in all solvents tested are designated by an *.

these compounds is found in Chapter 3. Because the solubility of these compounds relates to their use in cell assays, any future efforts at generating derivatives at this location should focus on generating derivatives with reasonable solubility properties.

Because **4** gives more soluble products, and is a tighter binding itself than **3**, it would be the best choice for a scaffold. Extensions should focus more on the aliphatic chains than on the aromatic chains, as they appear to be likely to show better solubility properties.

Chapter 3: Transient Transfection PPARγ Reporter Gene Assays

JEG-3 cells express high levels of PPARγ and contain an endogenous PPARγ transcriptional response. HeLa cells do not express PPARγ and require cotransfection of a PPARγ expression vector. Large error levels in these experiments prevented the evaluation of the transcriptional response of the rosiglitazone derivatives using these cell lines.

Introduction

Though binding assays are used to confirm that ligands interact directly with the receptor, they are not sufficient to evaluate the receptor activation properties of candidate ligands. Reporter gene assays can be used to detect ligand induced gene expression, as is seen for agonists, or inhibition of gene expression induced by a known agonist, as is the case for antagonists. In these assays, a response element from the promoter of a receptor-regulated gene, or a synthetic consensus response element, is inserted in the promoter region of a plasmid containing a reporter gene, such as luciferase. Measurement of the enzymatic activity in the cell lysate, after incubation of transfected cells with ligands, will provide a quantitative measure of ligand induction of receptor mediated gene expression. Because many cell lines do not contain sufficient endogenous levels of receptors to yield measurable levels of reporter gene induction, a constitutive mammalian expression vector for the receptor is often cotransfected.

A second reporter gene, whose activity can be assayed independently, in a constitutive expression plasmid is often cotransfected as a control for transfection.

Normalization of the experimental data to expression of the control can help correct for the inherent variability in transfection efficiency and cell density.

There are currently two reporter gene systems used extensively for the evaluation of PPAR-regulated transcription. The first is a full-length mouse PPAR used with a peroxisome proliferator response element (PPRE) reporter construct (50, 51, 58), and the second is a Gal4-PPARγ ligand binding domain (LBD) fusion protein used with a Gal4 response element (50, 51, 77). While the Gal4 fusion protein is reported to give excellent responses, it lacks the DNA binding domain (DBD) and N-terminal regions of the PPARγ receptor. As the role of these regions in regulating ligand activity has not been clearly defined, and they may play a different role in the activity of novel ligands, their elimination limits the physiological relevance of the results.

A full-length PPAR reporter construct, which has been used successfully in several labs, is the tk-$PPRE_3$-LUC reporter gene construct of Evans (50, 51, 58). This construct contains three copies of a synthetic response element (AGGACA-A-AGGTCA) based on the PPRE sequence from the acyl-CoA oxidase promoter inserted upstream of a firefly luciferase reporter gene. This reporter gene construct has been shown to respond to all three PPAR subtypes (58, 102).

CV-1, HeLa and a variety of other cell lines have all been reported to give ligand induced transcriptional response when transfected with this full-length receptor construct (9, 10, 29, 50, 51, 55, 58, 62, 63, 65, 73-75, 102, 116, 127-129, 138, 236). Of these cell lines, the CV-1 monkey kidney cell line has been reported most frequently for ligand screening assays, while the others are commonly used as models for physiological responses. The most commonly used full-length receptor expression vectors are the three

mouse PPARs developed by Evans (58). Because there are reported differences for several ligands in the response of human and mouse PPARγ (40, 48), it would be more relevant from a therapeutic standpoint to use a human PPARγ construct in cell assays. This is particularly relevant since the reporter gene assays use human (HeLa) or monkey (CV-1) cell lines. The human PPARγ gene has been cloned and its LBD has been inserted into the Gal4 fusion constructs, but a full-length human expression vector has not been reported.

While a cell line with little or no endogenous receptor, such as CV-1 or HeLa cells, is necessary for testing receptor mutants, it is not a requirement for screening ligands. JEG-3 cells express high levels of endogenous PPARγ and have an active PPARγ response without a transfected receptor expression plasmid. While an endogenous PPARγ response has inherent complications related to the activity of unknown associated proteins and activation through other receptor subtypes, it is the most physiologically relevant system available. Compared to the experiments using overexpressed PPARγ, the endogenous response is more likely to have sufficient levels of associated proteins to follow the same molecular mechanism of transcriptional activation as endogenous activation of PPARγ would follow *in vivo*.

In this chapter, I report the generation of human expression vectors, their use in a transient transfection reporter gene assay in HeLa cells, and a transient transfection reporter gene assay using the endogenous receptor in JEG-3 cells. I also report the transcriptional activity of the thiazolidinedione derivatives reported in Chapter 2 in each of these reporter gene assays.

Experimental Procedures

Reagents

Unless otherwise specified, all chemicals were obtained from Fisher Scientific (Pittsburgh PA) or Sigma-Aldrich (St. Louis MO). 15-Deoxy-$\Delta^{12,14}$-prostaglandin J_2 ($15dJ_2$) was obtained from Cayman Chemical Company (Ann Arbor MI). cis-Parinaric Acid (CPA)was obtained from Molecular Probes (Eugene OR). Chlorophenol red-β-D-galactopyranoside (CPRG) was obtained from Roche Molecular Biochemicals (Indianapolis IN). Molecular biology reagents and enzymes were obtained from Promega (Madison WI) or New England Biolabs (Beverly MA) unless otherwise specified. Cell culture media and buffers were obtained from the UCSF Cell Culture Facility (San Francisco CA) unless otherwise specified. Rosiglitazone (BRL 49653) and its derivatives were synthesized as described in Chapter 2. Fetal Bovine Serum (FBS) was obtained from Hyclone (Logan UT).

Plasmids

The tk-$PPRE_3$-LUC luciferase reporter plasmid and the pCMX-mPPARγ expression plasmid were gifts from Dr. Ronald Evans (50, 51, 58). The pCRII-hPPARγ2 plasmid was a gift from Dr. Alex Elbrecht (237). The pCI, pSI, and pCIneo expression vectors were purchased from Promega. The RSV-β-gal plasmid was a gift from Dr. Keith Yamamoto. The pσ-Luc plasmid was a gift from Dr. Peter Kushner.

The human PPARγ expression plasmids were generated from the cDNA in the pCRII-hPPARγ2 plasmid using standard molecular biology techniques, following the manufacturers' supplied protocols. Briefly, the hPPARγ cDNA was excised from the

pCRII-hPPARγ2 plasmid by digestion with Spe I and Not I, and was subsequently purified on an agarose gel. Promega's expression vectors were digested with both Xba I (a Spe I isoschizomer) and Not I, purified on an agarose gel, and treated with alkaline phosphatase to prevent religation. Based on the relative visual intensities of the bands on the ethidium bromide stained agarose gel, the opened vectors and approximately four to five molar equivalents of the insert were added to T4 DNA Ligase reactions. After transformation and ampicillin selection, six colonies grown from each plasmid were screened and each showed the expected BamHI digestion sites. A single clone was selected, and subsequent digestions were also consistent with the insertion of a single copy of the insert in the expected orientation. The sequences surrounding the ligation sites were determined by the UCSF Biomolecular Resource using either the ABI/PE dGTP mix or the ABI/PE "Big Dye" protocols, and showed the expected sequences. These sequences also allowed the determination of the missing sequence from a short region of the insert DNA following the PPARγ2 gene, not determined for the pCRII-hPPARγ2 plasmid, and obtain a complete sequence for all three plasmids. The plasmid maps for each expression vector are included in the appendix and the sequences for each vector are included as GCG sequence files on the data CD.

Cell Culture

CV-1 and HeLa cells were obtained from the UCSF Cell Culture Facility (San Francisco, CA). CV-1b cells were obtained from Dr. Keith Yamamoto. JEG-3 cells were obtained from the American Type Culture Collection (ATCC, Manassus VA).

CV-1 and CV-1b cells were cultured at 37°C with 5% CO_2 in Debecalo's modified minimal essential medium (H-21 DMEM) containing 10% FBS, penicillin (100

U/mL), streptomycin (100 μg/mL), and MEM non-essential amino acid solution (Sigma #M7145). HeLa cells were cultured at 37°C with 5% CO_2 in Debecalo's modified minimal essential medium (H-21 DMEM) containing 10% FBS, penicillin (100 U/mL), streptomycin (100 μg/mL), and glutamine (20 mM). JEG-3 cells were cultured at 37°C with 5% CO_2 in Eagle's minimal essential medium with Earle's salts containing 10% FBS, penicillin (100 U/mL), and streptomycin (100 μg/mL). All cells were passaged no more than 10 times after being thawed from a common stock.

Western Blot Protocol

Cells were grown in 24 well plates to near confluence (approximately $1.5x10^5$ cells per well). Cells were washed twice with calcium and magnesium free PBS and then 50 μL lysis buffer (50 mM Tris pH 7.5, 150 mM NaCl, 1% Nonidet P-40, 2 mM ethylenediaminetetraacetic acid (EDTA), 2 μg/mL aprotinin, 100 μg/mL phenylmethylsulfonyl fluoride (PMSF), 2 mM dithiothreitol (DTT), 1 mM Na orthovanadate) was added. Dishes were shaken to coat cells with lysis buffer and then incubated on ice for 30 minutes, ensuring that plates were flat enough for the lysis buffer to remain covering the cells. The dish was rinsed with the lysate and the pipette tip was used to scrape cells from the dish. Four separate wells were combined for each condition.

The lysate was transferred to a labeled microcentrifuge tube and put on ice while running a BCA (bicinchonic acid) protein assay (Pierce #23225, Rockford IL) to determine the total protein concentration of the lysate. Briefly, 5 μL protein assay samples were measured in duplicate at two dilutions to determine protein concentration. 195 μL of BCA assay solution was added to each well, and the plate was incubated at

37°C for 30 minutes. The plate was then read and analyzed using a programmed BCA protocol on a Labsystems (Helsinki, Finland) Multiscan MCC/340 Microtiterplate Reader. The BCA program mixes the plate for 5 seconds then takes a single reading at 560 nm and analyzes the data using a linear regression of BSA standards to determine protein concentration of the unknown samples.

The volume of lysate containing 20 μg total protein was calculated and added, along with 5 μL of 5x gel loading buffer (250 mM Tris pH 6.8, 500 mM DTT, 10% sodium dodecyl sulfate (SDS), 0.5% bromophenol blue, 50% glycerol), to fresh microcentrifuge tubes and boiled for 3 minutes, after which tubes were immediately transferred to ice. There was only sufficient protein for the JEG-3 cells with transfected mPPARγ sample to load approximately 5 μg.

Two SDS-polyacrylamide gel electrophoresis (SDS-PAGE) gel was poured using the Bio-Rad (Martinez, CA) Mini-Protean II system. The resolving gel was composed of 10% acrylamide (29:1 acrylamide:bis-acrylamide) in 0.38 M Tris pH 8.8, 0.1% SDS, 0.1% ammonium persulfate (APS), and polymerized using 0.04% N,N,N,N'-tetramethylenediamine (TEMED). The stacking gel was composed of 4% acrylamide (29:1 acrylamide:bis-acrylamide) in 0.13 M Tris pH 6.8, 1% SDS, 1% APS, and polymerized using 0.1% TEMED.

Samples were then loaded into wells 2-9 of each gel using a Hamilton syringe. Molecular weight markers were loaded into lane 10 of each gel. The gels were run in run buffer (0.063 M Tris-base, 0.2 M glycine, 1 % SDS) using Bio-Rad Mini-Protean II system at a constant current of 25 mA.

Proteins were transferred to nitrocellulose membranes at 4°C and 50V for 2 hours in transfer buffer (25 mM Tris-base, 200 mM glycine, 15% methanol) using the Bio-Rad Mini-Protean II system. The blots were submerged in tris buffered saline (TBS) and marked with a china pencil to show the outline of the gel and the molecular weight makers locations. The blots were then blocked overnight at 4°C in blocking buffer (TBS, 0.2% tween-20, 5% nonfat dried milk).

The membrane was rinsed twice with wash buffer (TBS, 0.2% tween-20, 0.2% nonfat dried milk) and then incubated overnight with 50 μL of the primary antibody (Santa Cruz #7273, mouse anti-PPARγ antibody, Santa Cruz CA) in 5 mL of antibody buffer (TBS, 1% nonfat dried milk, 0.2% tween-20). The blots were then rinsed twice quickly with wash buffer and then washed with wash buffer once for 15 minutes and three times for 5 minutes to remove excess antibody. The blot was then incubated with 2 μL of the secondary antibody (Santa Cruz #2005, goat anti-mouse IgG horseradish peroxidase) in 20 mL of antibody buffer for 1 hours at room temperature. The blot was imaged using Kodak (Rochester NY) Bio Max film and the Amersham Pharmacia ECL Western Blotting Detection Reagents (RPN2109, Piscataway NJ). The film was then marked with the gel outline and the location of the molecular weight markers.

HeLa Transient Transfection Assays

HeLa cells (2 million cells / cuvette) were suspended in electroporation buffer (calcium and magnesium free PBS, 0.1% glucose, 0.01% Biobrene) with the specified hPPARγ mammalian expression vector (1 μg / million cells), tk-PPRE$_3$-LUC (2.5 μg / million cells), a PPRE driven luciferase reporter gene, and RSV-βgal (1 μg / million cells), a β-galactosidase transfection control. Cells were then electroporated in BioRad

(Hercules, California) Gene Pulser Cuvettes (cat# 165-2088, 4 mm electrode gap) using a BioRad Gene Pulser (0.35V, 960 μFD, 200 Ω). Electroporated cells were promptly resuspended in media and plated into either 6-well or 24-well plates (1.5-2 plates / cuvette). Cells were allowed to attach for 2-4 hours before media was aspirated. Cells were then rinsed with PBS and treated in triplicate for 48 hours with media containing the specified concentrations of $15dJ_2$, rosiglitazone, thiazolidinedione derivatives, or 0.1% vehicle (DMSO).

JEG-3 Transient Transfection Assays

JEG-3 cells (1-2 million cells / cuvette) were suspended in electroporation buffer (calcium and magnesium free PBS, 0.1% glucose, 0.01% Biobrene) with tk-$PPRE_3$-LUC (2.5 μg / million cells), a synthetic PPAR response element driven luciferase reporter gene, and RSV-βgal (1 μg / million cells), a β-galactosidase transfection control. Cells were then electroporated in BioRad (Hercules, California) Gene Pulser Cuvettes (cat# 165-2088, 4 mm electrode gap) using a BioRad Gene Pulser (0.35V, 960 μFD, 200 Ω). Electroporated cells were promptly resuspended in media and plated into 24-well plates (1.5-2 plates / cuvette). Cells were allowed to attach for 2-4 hours before media was aspirated. Cells were then rinsed with PBS and treated in quadruplicate for 24 hours with media containing the specified concentrations of $15dJ_2$, rosiglitazone, thiazolidinedione derivatives, or 0.1% vehicle (DMSO).

HeLa Luciferase Activity Assays

Cleared cell lysates were analyzed using the Roche luciferase reporter gene assay (Roche #1 814 036, Indianapolis IN). Briefly, JEG-3 cells were washed with 1 mL of

PBS and then lysed with either100 μL (6-well) or 55 μL (24-well) of the supplied lysis buffer. The cells were subjected to two freeze-thaw cycles and scraped with a rubber policeman.

The lysate was first used to rinse the wells, and was then transferred to microcentrifuge tubes and cleared for 6 minutes at maximum speed. 45 μL of the cleared lysate was analyzed for luciferase activity. A 5 μL aliquot of the cleared lysate was used to determine protein concentration using the BCA Protein Assay. After subtraction of the luciferase activity observed in lysis buffer alone, the luciferase activity was normalized to the protein concentration before averaging and calculation of the fold induction by normalization to the activity observed for the vehicle control.

JEG-3 Luciferase Activity Assays

Cleared cell lysates were analyzed using the Roche luciferase reporter gene assay. Briefly, JEG-3 cells were washed with 1 mL of PBS and then lysed with 55 μL of the supplied lysis buffer at room temperature for 15 minutes.

The lysate was first used to rinse the wells, and was then transferred to microcentrifuge tubes and cleared for 6 minutes at maximum speed. 45 μL of the cleared lysate was analyzed for luciferase activity. A 5 μL aliquot of the cleared lysate was used to determine protein concentration using the BCA Protein Assay. After subtraction of the luciferase activity observed in lysis buffer alone, the luciferase activity was normalized to the protein concentration before averaging and calculation of the fold induction by normalization to the activity observed for the vehicle control.

β-Galactosidase Transfection Control

Based on the protocol of Dr. Beatrice Darimont (238), 20 μL of the cleared cell lysate was added to a 96 well plate. CPRG, 0.5 mM, was diluted 1:1000 in Z Buffer (120 mM Sodium phosphate pH 7.0, 10 mM potasium chloride, 1 mM magnesium sulfate, 20 mM β-mercaptoethanol). 180 μL of the CPRG / Z Buffer mixture was added to the cell lysate and the reaction rate was measured. A Labsystems (Helsinki Finland) Multiscan MCC/340 Microtiterplate Reader was used to measure the absorbance of each well at 550 nm once every minute for 60 minutes. The maximal slope over 20 data points was expressed in mOD / minute and used as the initial rate for normalization of the luciferase data.

Results

I initially attempted to reproduce a PPARγ reporter gene assay in CV-1 cells. I tried several lipofection reagents and electroporation as a transfection method, and CV-1 cells from two sources, but I was unable to obtain consistent activation in this cell line (data not shown). Though I was able to consistently observe luciferase activity of the constitutive luciferase expression plasmid pσ-Luc, the levels of activity were quite variable (data not shown). A β-galactosidase control also showed inconsistent levels of activity, lower than expected activity, and was unable to correct for the variability in the observed reporter gene activity (data not shown). Some combination of the cell line, cell density, transfection conditions, lysis procedure, incubation time, and assay protocol are potential causes of these problems.

HeLa cells were a good candidate for an alternate cell line because of literature reports of their use in PPARγ assays (10, 75, 128), and our labs experience with them in

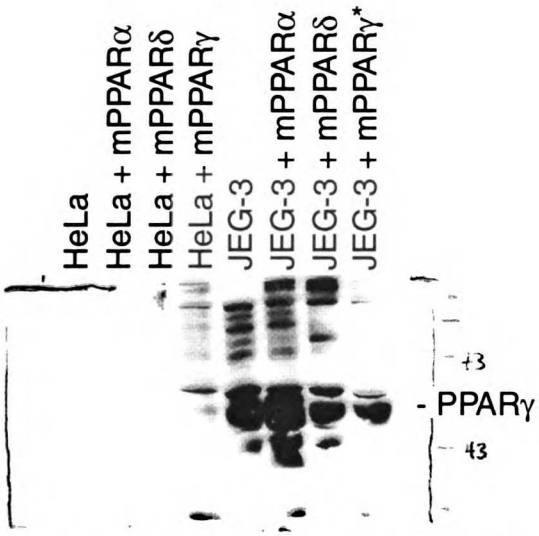

Figure 3.1: PPARγ Expression Levels in HeLa and JEG-3 Cells

HeLa (lanes 2-5) or JEG-3 (lanes 6-9) cells were transfected with the indicated PPAR expression plasmids or left untreated. Cells were lysed and the total protein in the lysate was quantified and 20 mg was added to each well of an SDS-PAGE gel, with the exception of JEG-3 and mPPARγ where there was not enough protein. Protein was visualized after blotting using a PPARγ specific mouse antibody and an anti-mouse peroxidase chemical visualization system. Markers were run both in lane 10, their positions were transferred to the film by hand using a pen, and the molecular weights are noted on the right side. The observed bands are consistent with the presence of full length PPARγ receptor, but not conclusive due to numerous non-specific bands.

reporter gene assays for other nuclear receptors. JEG-3 cells were also considered a good candidate for an alternate cell line based on preliminary results from the Taylor lab, which have since been published (43), showing that they express high quantities of PPARγ. HeLa cells would be cotransfected with a constitutive PPARγ expression plasmid, while the JEG-3 cells could offer a complementary assay with endogenous levels of receptor.

To determine the relative endogenous and transfected expression levels of the cell lines, CV-1, CV-1b, HeLa and JEG-3 cells were electroporated with no plasmid, pCMX-mPPARα, pCMX-mPPARδ or pCMX-mPPARγ. After overnight incubation the cells were lysed, and the cell lysates were analyzed for PPARγ expression by western blot with and anti-PPARγ antibody. The western blot showed numerous non-specific bands, particularly in the JEG-3 lanes (Figure 3.1). There were no observed bands in any of the lanes on the gel containing the CV-1 and CV-1b cell lines (data not shown). The results, though inconclusive due to the non-specific bands, are consistent with other experiments showing high endogenous expression levels

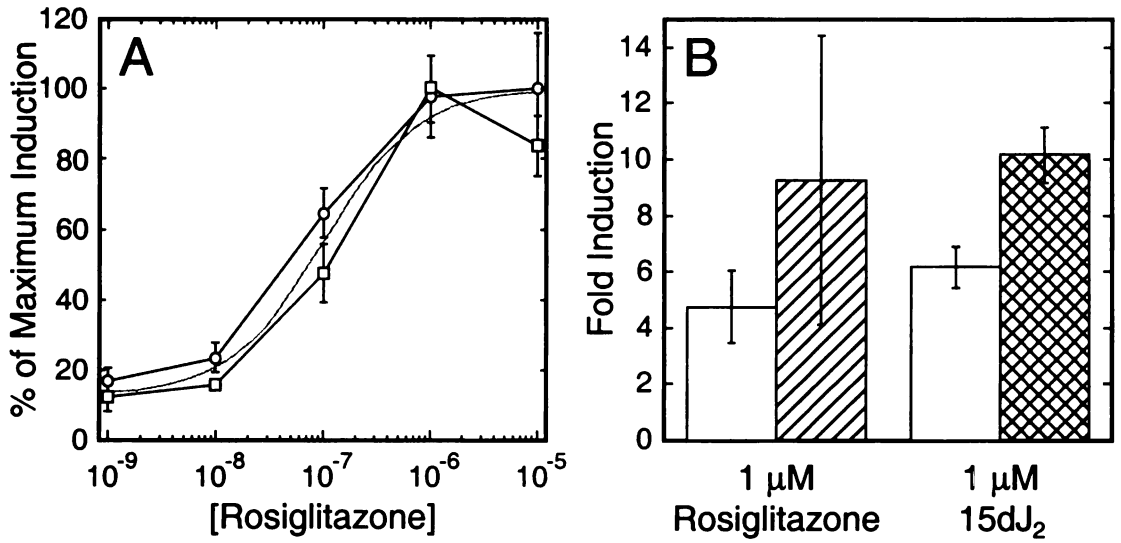

Figure 3.2: Induction by hPPARγ Mammalian Expression Vectors

Transiently transfected HeLa cells were incubated with media containing the specified concentration of rosiglitazone, $15dJ_2$, or 0.1% (v/v) vehicle alone. Luciferase data was normalized to the β-galactosidase expression level for each sample, quadruplicate wells were averaged, and then fold induction was calculated relative to vehicle alone. (A) Fold induction data for pCIhPPARγ2 (open circles) and pSIhPPARγ2 (open squares) were normalized to the maximal response of each curve to give the percent of maximal induction, which is plotted on the vertical axis. A sigmoidal fit of the data is shown in gray. (B) The fold induction for pCIhPPARγ2 (white) or pSIhPPARγ2 (hatched) after incubation with 1 μM rosiglitazone with β-galactosidase as a control is plotted on the left. The fold induction for pCIhPPARγ2 (white) or pCIneohPPARγ2 (double hatched) after incubation with 1 μM $15dJ_2$ with total protein levels as a control is plotted on the right.

of PPARγ in JEG-3 cells (Figure 4.8) (43, 81). No endogenous PPARγ expression was observed in HeLa cells, but there were several faint bands in the lane transfected with the mPPARγ expression plasmid, which could be consistent with plasmid driven mPPARγ expression.

Unlike the JEG-3 cell line, HeLa cells do not express detectable levels of endogenous PPARγ, and require transfection of a mammalian PPARγ expression vector along with the luciferase reporter gene and control plasmid. Because of concerns about differences in the physiological response of rodent and human PPARs and the use of the human HeLa cell line, I generated a human PPARγ mammalian expression vector. The human cDNA for PPARγ2 obtained from Elbrecht (237) was inserted into three

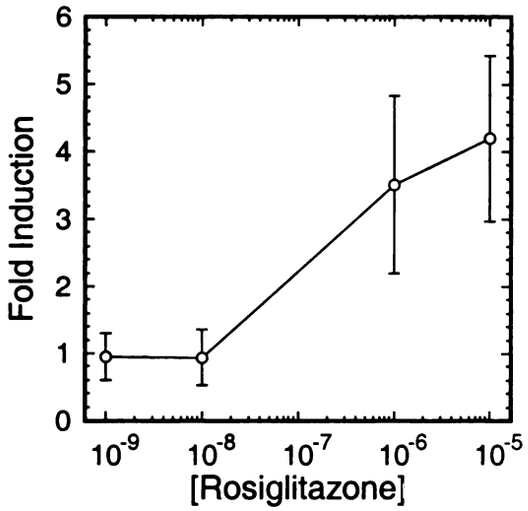

Figure 3.3: Induction of Endogenous PPARγ in JEG-3 Cells

JEG-3 cells were transiently transfected with the tk-$PPRE_3$-LUC luciferase reporter, but no PPARγ expression plasmid. Cells were then incubated with media containing the specified concentration of rosiglitazone or 0.1% vehicle alone (DMSO). Fold induction was calculated relative to 0.1% vehicle.

commercial mammalian expression vectors. Restriction digests and sequencing of the plasmids (data not shown) confirmed successful insertion of a single copy of the hPPARγ2 cDNA in the proper orientation into the multiple cloning site of the expression vectors. Transient transfection assays, using HeLa cells, the new PPARγ expression vectors, tk-$PPRE_3$-LUC, and the RSV-β-galactosidase control plasmid showed ligand dependant induction of transcription with both rosiglitazone and $15dJ_2$ (Figure 3.2). Control experiments without the expression vector showed no ligand dependant induction of reporter gene expression (data not shown), consistent with the lack of endogenous receptor expression observed in the western blot experiment (Figure 3.1).

Preliminary experiments by the Taylor lab, which have since been published, had shown that lipofection of JEG-3 cells with the tk-$PPRE_3$-LUC luciferase reporter plasmid showed $15dJ_2$ dependant induction of reporter gene expression (43, 81). To avoid use of the lipofection reagents, which could potentially affect the observed activity of candidate ligands, JEG-3 cells were electroporated with the tk-$PPRE_3$-LUC luciferase reporter plasmid and a β-galactosidase control. Subsequent treatment of these cells with rosiglitazone showed ligand dependent induction of gene expression (Figure 3.3)

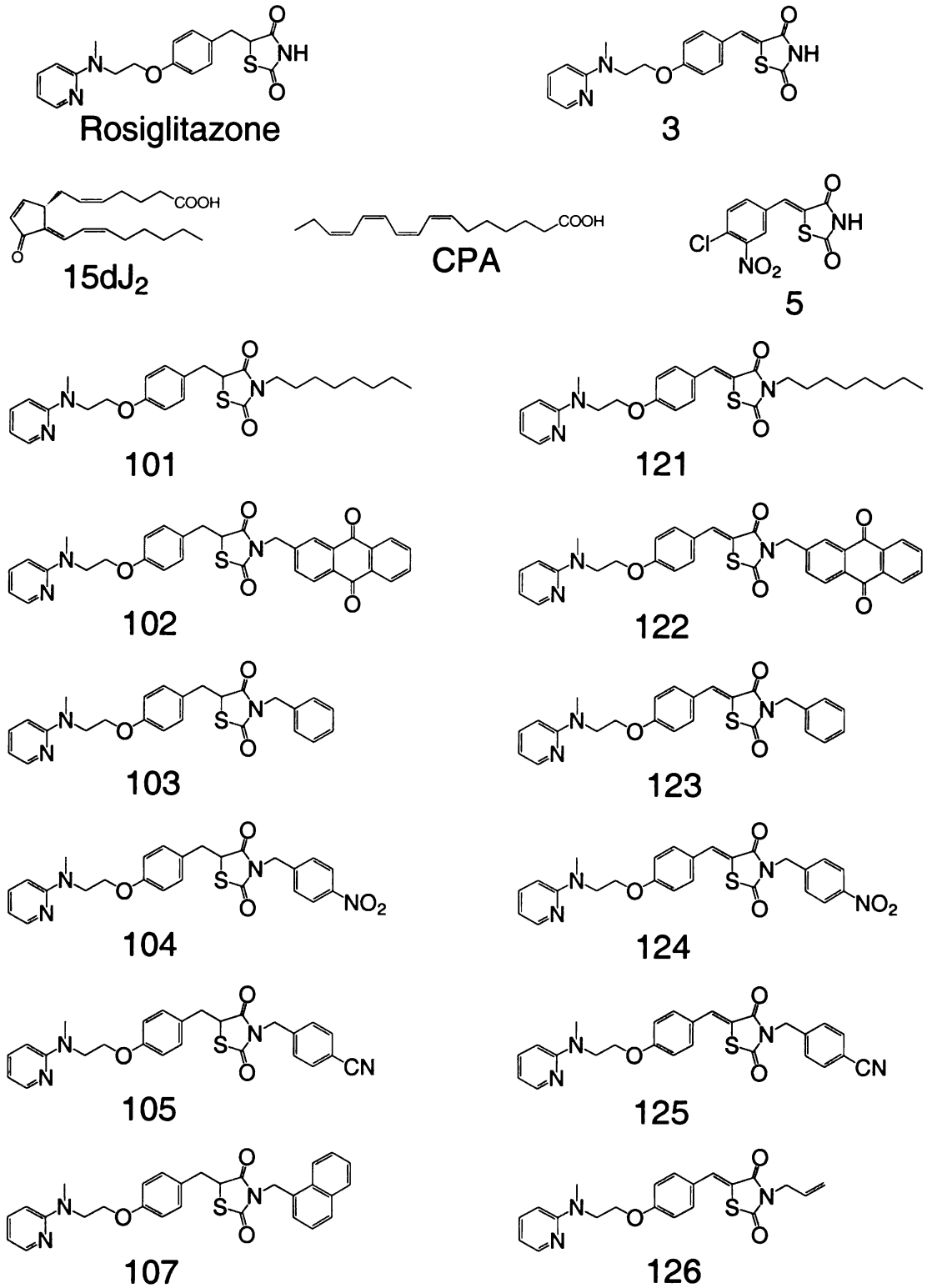

Figure 3.4: Thiazolidinedione Derivatives - Chemical Structure

The chemical structures of compounds tested in Figure 3.5 are shown.

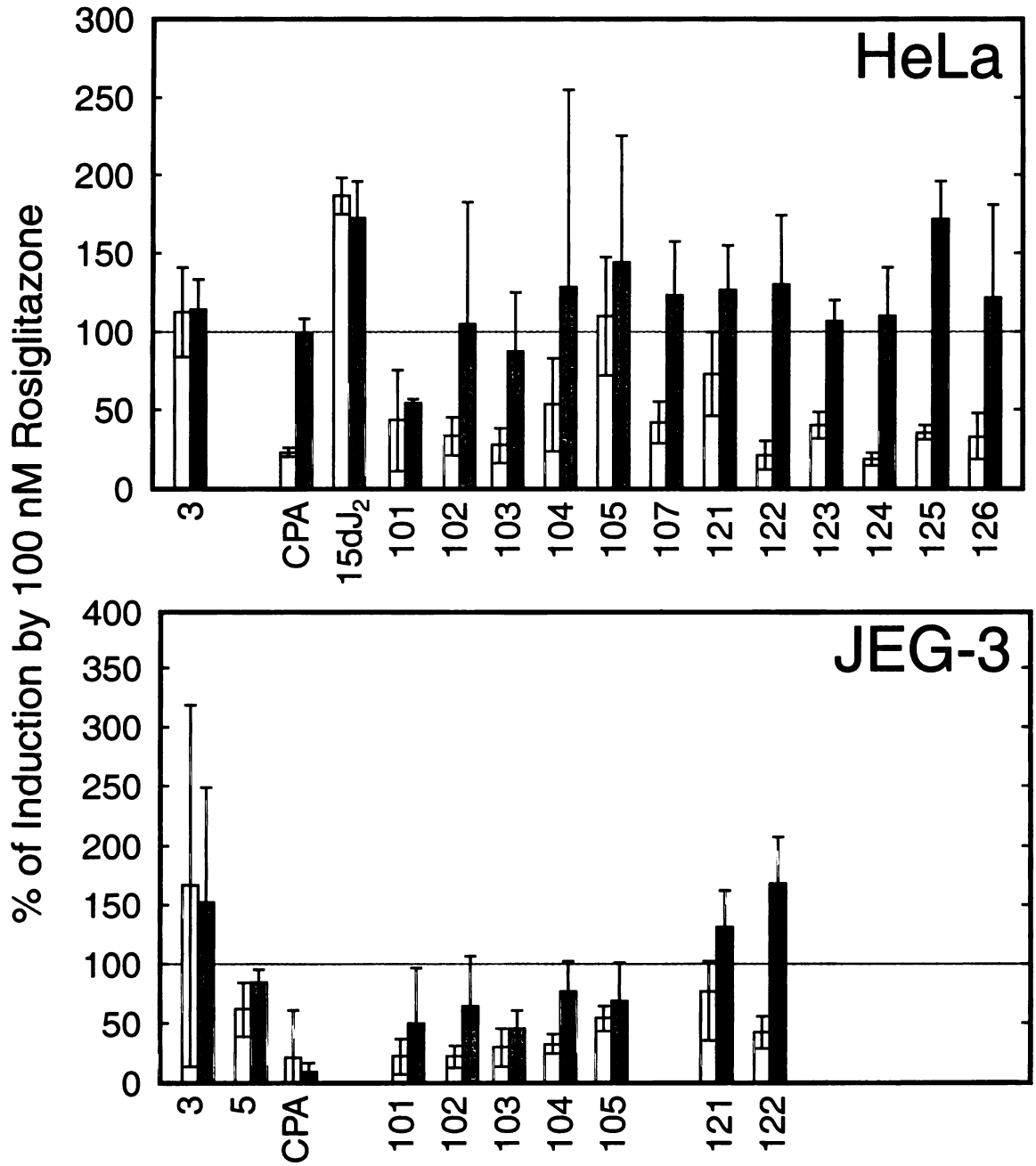

Figure 3.5: Thiazolidinedione Derivatives - Transcriptional Activity

HeLa cells were transiently transfected with the PPARγ expression plasmid pCIhPPARγ, the luciferase reporter plasmid tk-PPRE$_3$-LUC and a β-galactosidase control plasmid (top panel). JEG-3 cells were transiently transfected with the luciferase reporter plasmid tk-PPRE$_3$-LUC and a β-galactosidase control plasmid (bottom panel). Cells were treated for 16 hours with 10 μM of the specified compound (white bars) or 100 nM of rosiglitazone and 10 μM of the specified compound (gray bars). Luciferase and β-galactosidase activity were measured. After normalization to the β-galactosidase control, data were normalized to the observed induction of 100 nM rosiglitazone.

consistent with the rosiglitazone EC_{50} of approximately 100 nM observed in the HeLa transient transfection assays (Figure 3.2) and reported in the literature (50). In contrast, $15dJ_2$ did not show reliable induction above error levels in the JEG-3 assays (data not shown).

Using HeLa and JEG-3 transient transfection assays, the thiazolidinedione derivatives described in Chapter 2 (Figure 3.4) were screened for agonist and antagonist activity. HeLa cells were transiently transfected with pCI-hPPARγ, tk-$PPRE_3$-Luc, and RSV-βgal. JEG-3 cells were transiently transfected with tk-$PPRE_3$-Luc and RSV-βgal. Transfected cells were treated with 10 μM of the specified compound alone or in competition with 100 nM of rosiglitazone. The observed induction was compared to that seen with 100 nM of rosiglitazone alone (Figure 3.5). Large error values prevented definitive conclusions, but several compounds, particularly 101 and 103 showed promise. Compound 103 was tested in titration experiments, but showed considerable error and variability, which prevented interpretation of the data. In general, the JEG-3 cell assays showed lower relative activation levels for the 100 series compounds than the HeLa assays. A combination of the low solubility of the thiazolidinedione derivatives, their low affinity, and apparent toxicity likely contributed to the error and variability of these experiments.

Because of the intrinsic error and variability associated with these transient transfection reporter gene assays, my attention shifted to the generation of a stably transfected reporter gene assay, which is described in Chapter 4.

Discussion

Though the use of CV-1 cells in reporter gene assays for PPARγ has been reported extensively (10, 50, 51, 55, 58, 59, 65, 75, 77, 102, 138, 236), I was unable to use them in a working assay. I was able to develop working transient transfection reporter gene assays using both HeLa cells, which require a cotransfectd PPARγ expression vector, and JEG-3 cells, which contain an endogenous PPARγ response. Both of these assays showed high variability and error. Several aspects of these experiments are likely to contribute to the observed error and variability.

The reporter plasmid, and potentially the mouse expression plasmid, obtained from Evans never gave reliable activation. The reporter plasmid used in the HeLa and JEG-3 transient transfections I have shown was obtained from the Taylor lab, which in turn obtained it from Evans. When I obtained the reporter from the Taylor lab, my original stock of the reporter plasmid did not match the stock obtained from the Taylor lab. It is unclear at what point the plasmid was switched, or if the correct plasmid was obtained from Evans. The use of the new stock of tk-PPRE$_3$-Luc, and the new human PPARγ expression vectors could potentially allow transient transfection experiments using the CV-1 cell line.

I used the same electroporation procedure for each cell line. While it worked well for the HeLa and JEG-3 cells, alternative conditions may be required for the CV-1 cells. Lipofection of CV-1 cells did not produce reliable levels of expression of the constitutive control plasmid. If this variability is related to the transfection, calcium phosphate precipitation or alternative electroporation conditions could be useful. The reported lysis conditions appeared to work well for both the HeLa and JEG-3 cells, but may have been

a problem for the CV-1 cells. If incomplete or variable lysis of the CV-1 cells was responsible, optimization of the lysis procedure may improve the experiments.

The β-galactosidase control used in these assays gave a weak signal and did not always help clairify the variability and error in the data. An alternate control assay, such as Roche's chemiluminescent β-galactosidase assay or Promega's Dual Luciferase Assay, could improve the normalization for transfection efficiency. Improvements in the transfection and lysis procedures described above would also be likely to improve the control assay.

Along with changes to the assay protocol, improving the statistics of the experimental design would likely improve the data quality. Using more replicate wells, more data points on titration curves, and averages of multiple independent experiments all have the potential to offer significant improvements in both the accuracy and error of the experiments.

I observed ligand dependent activation of the luciferase reporter gene in assays using both HeLa and JEG-3 cells. While JEG-3 cells use endogenously expressed PPARγ that is likely to be in balance with other endogenous transcription factors and coactivators, HeLa cells use artificial levels of receptor expression and a potentially simpler response. Assays using these two cell lines provide complementary data.

The pCI-hPPARγ and pSI-hPPARγ mammalian expression plasmids are primarily useful in these transient transfection assays, but the pCIneo-hPPARγ plasmid contains the neomycin selection marker, which could be used to generate a stably transfected cell line. The use of human PPARγ expression plasmids, instead of mouse PPARγ, allows experiments that are more relevant from a therapeutic standpoint.

Though the HeLa and JEG-3 reporter gene assays worked well with the known activator rosiglitazone, they did not work well for testing the thiazolidinedione derivatives. The thiazolidinedione derivatives' toxicity and low solubility likely contributed to the observed error. It is possible that some of the improvements described above could make the assay useful for testing these compounds. At this stage, I sought to generate a stable cell line using the endogenous response of the JEG-3 cell line. A stable cell line would eliminate the variability in transfection efficiency, one of the largest sources of experimental error for transient transfection reporter gene assays.

Chapter 4: Design and Optimization of Stably Transfected Reporter Gene Cell Assays for the Characterization of PPARγ Ligands

Stable transfection of the tk-PPRE$_3$-LUC reporter plasmid into JEG-3 cells yielded several cell lines showing PPARγ inducible luciferase expression. One cell line was chosen because it showed useful levels of ligand induction and the best consistency between experiments. This cell line, EP-JEG cells, allows a functional PPARγ reporter gene assay without the transfection step and the associated error and variability.

Introduction

Transient transfection reporter gene assays are a common method for the evaluation of peroxisome proliferator activated receptor (PPAR) ligands. There are currently two PPARγ reporter gene systems used extensively. The first is a full-length mouse PPAR used with a peroxisome proliferator response element (PPRE) reporter construct (50, 51, 58), and the second is a Gal4-PPARγ ligand binding domain (LBD) fusion protein used with a Gal4 response element (50, 51, 77). While the Gal4 fusion protein gives good responses, it lacks the DNA binding domain (DBD) and N-terminal regions of the PPAR receptor. Since the role of these regions in regulating ligand activity has not been clearly defined, their elimination further reduces the physiological relevance of the results.

A full-length PPAR reporter construct, which has been used successfully in several labs, is the tk-PPRE$_3$-LUC reporter gene construct of Evans (50, 51, 58). This construct contains three copies of a synthetic response element (AGGACA-A-AGGTCA)

based on the PPRE from the acyl-CoA oxidase promoter upstream of a firefly luciferase reporter gene. It can be used with expression vectors for each of the three PPAR subtypes to get a useful response (58, 102).

I have used CV-1 cells (10, 50, 51, 58, 75, 77, 102), a monkey kidney cell line, and HeLa cells (10, 75, 116), a human cervical cell line, in transient transfection assays. Both yield a useful level of activation by known PPARγ ligands when they are transiently transfected with a PPARγ expression plasmid and the tk-$PPRE_3$-LUC reporter construct. Neither of these cell lines contains a measurable endogenous PPAR response, making them useful as model systems using overexpressed receptor. This type of model system allows measurement of the response of either a single PPAR subtype or a controlled mix of the subtypes. While the use of full-length receptor is an improvement over the use of Gal4 proteins, it is still limited in application because it is an artificial response with receptor levels out of proportion with coactivators and the other components of the transcriptional response.

The use of cell lines that contain endogenous PPARγ responses opens another option for the evaluation of PPAR ligands. One such cell line is the JEG-3 choriocarcinoma cell line (43, 126, 179). Like the primary placental trophoblasts they are related to, JEG-3 cells transcribe PPARγ mRNA (126) and express high levels of PPARγ (43). The JEG-3 cell line provides a useful model system for studying the activity of ligands in a natural PPAR response, particularly for the study of the role of PPARγ ligands in pregnancy and pregnancy diseases (43, 98, 126, 178).

Transient transfection of JEG-3 cells with the tk-$PPRE_3$-LUC reporter plasmid yields useful levels of ligand induced expression of luciferase even when reporter

plasmid is transiently transfected without any receptor (43). While PPARγ is known to be expressed in a wide range of tissues (8, 239), I am not aware of a another system where a PPARγ response can be observed by a reporter plasmid independent of transfection of the cells with a receptor expression plasmid. While a different complement of transcription factors may be involved in the PPARγ response in other cell lines, JEG-3 cells are a more natural system to study than the overexpession of receptor in cell lines with no natural response.

Use of the JEG-3 cell line for ligand assays is, however, limited by the possibility that ligands could be acting entirely, or in part, through other receptors resulting in the generation of an autocrine signaling factor ultimately responsible for the activation of the reporter plasmid. Ligands could also potentially activate the reporter gene through one of the other PPAR subtypes (58, 81, 102, 126, 179).

One of the limitations of transient transfection assays in general is variation in the transfection efficiency. This can lead not only to variability between experiments, but can also result in local variation in efficiency within a single experiment. As the amount of the reporter gene, as well as the amount of the receptor, will affect the observed signal along with any ligand treatment, variability in transfection efficiency provides a substantial source of experimental error and variability. There are several experimental controls for transfection efficiency including constitutive β-galactosidease (β-gal) (50, 51, 58) and renilla-luciferase (74) expression plasmids. The activity of these controls can be assayed independently of the firefly luciferase of the reporter plasmid. When co-transfected, these plasmids allow the correction of some of the variability of transfection efficiency, but they also add another source of experimental error to the assays.

Particularly with the addition of the transfection control experiments, transient transfection assays can be relatively labor intensive, expensive, and cumbersome. In order to simplify my ligand assays, I sought to generate stably transfected cell lines, which would eliminate the transient transfection step, and the accompanying error and variability from my cell assays. These stable cell lines would provide an easier experimental system, and while still be subject to variation in plating efficiency, would not be subject to the error and variability resulting from the transfection step.

Experimental Procedures

Reagents

Unless otherwise specified, all chemicals were obtained from Fisher Scientific (Pittsburgh PA) or Sigma-Aldrich (St. Louis MO). 15-Deoxy-$\Delta^{12,14}$-prostaglandin J_2 ($15dJ_2$) was obtained from Cayman Chemical Company (Ann Arbor MI). Rosiglitazone (BRL 49653) was synthesized as described in Chapter 2. Cell culture media and buffers were obtained from the UCSF Cell Culture Facility (San Francisco CA) unless otherwise specified. Fetal Bovine Serum (FBS) was obtained from Hyclone (Logan UT).

Plasmids

The plasmid tk-$PPRE_3$-LUC, a luciferase reporter plasmid driven by three synthetic PPAR response elements (AGGACA-A-AGGTCA), was a gift of Dr. Ronald Evans (50, 51, 58). The plasmid pGK-Neo, a constitutive neomycin resistance plasmid, was a gift of Dr. Keith Yamamoto (240). The PPARγ mammalian expression plasmids pCI-hPPARγ and pCIneo-hPPARγ were constructed as described in Chapter 3.

Cell Culture

JEG-3 cells were obtained from the ATCC (Manassus VA). HeLa cells were obtained from the UCSF Cell Culture Facility.

JEG-3 cells and the stable cell lines derived from this cell line were cultured at 37°C with 5% CO_2 in Eagle's minimal essential medium with Earle's balanced salt solution (MEM Earle's BSS) containing 10% FBS, penicillin (100 U/mL), and streptomycin (100 μg/mL). JEG-3 and derived cells were separated from plates by washing with phosphate buffered saline (PBS), incubating with a minimal volume of standard trypsin and versene (STV) for 4 minutes at room temperature, and then washed off the plates using fresh media. They were then pelleted at 1000g for 3 minutes, residual media was aspirated, and cells were suspended in fresh media, and split 1 to either 3 or 4.

HeLa cells and the stable cells derived from this cell line were cultured at 37°C with 5% CO_2 in Debecalo's modified essential medium H-21 (DMEM H-21) containing 10% FBS, penicillin (100 U/mL), and streptomycin (100 μg/mL). HeLa and derived cells were separated from plates by washing with PBS, incubating with 4 mL of STV for 4 minutes at 37°C, and then washed off the plates and diluted into fresh media. They were then pelleted at 1000g for 3 minutes, residual media was aspirated, and cells were suspended in fresh media, and split 1 to between 4 and 8.

JEG-3 Derived Stable Cell Assays

Stable cells were washed with PBS, incubated with a minimal volume of trypsin for 4 minutes at room temperature, then washed off the plates using media. After counting cells using a hemacytometer, cells were pelleted at 1000g for 3 minutes. Cells were then resuspended in fresh media, and plated onto 6 or 24-well plates at a density of

$1x10^6$ cells per plate. After overnight incubation, unless otherwise specified, cells were washed with PBS, and then treated in triplicate or quadruplicate for 16 hours, unless otherwise specified, with media containing the specified concentrations of $15dJ_2$, rosiglitazone, or 0.1% vehicle (dimethyl sulfoxide (DMSO)) as specified for each experiment. Rosiglitazone and $15dJ_2$ were delivered in DMSO. Other lipids were delivered in ethanol. I have observed no difference in activity among ethanol, DMSO, or media alone (data not shown).

JEG-3 Derived Stable Cell Luciferase Activity Assay

Cleared cell lysates were analyzed using a luciferase reporter gene assay (Roche #1 814 036, Indianapolis IN). Briefly, cells were washed with 1 mL of PBS and then lysed with 200 µL (6-well) or 55 µL (24-well) of the supplied lysis buffer at room temperature for 15 minutes.

The lysate was used to wash wells and was then transferred to microcentrifuge tubes and cleared for 6 minutes at maximum speed. 50 µL (6-well) or 45 µL (24-well) of the cleared lysate was analyzed for luciferase activity. After subtraction of the luciferase activity observed in lysis buffer alone, fold induction was calculated by dividing the hormone response by that of vehicle alone.

JEG-3 Derived Stable Cell Selection

5 million JEG-3 cells were electroporated with 1.8 µg of pGK-Neo and 18.2 µg of tk-$PPRE_3$-LUC after linearization of the plasmids with the restriction endonuclease XmnI. Geneticin (G418, Gibco BRL #3069, Rockville MD), a neomycin analog, was used for selection. A control under the same conditions, but without the neomycin

resistance plasmid was included to check that the G418 concentration was sufficient to kill non-resistant cells.

The transfected cells were allowed to attach for 4 hours before the media was replaced with 1 mg/mL G418. Media was replaced with fresh selection media every 3-4 days until colonies were visible to the naked eye (about 3 weeks). The majority of cells on the control plate were dead and detached within 2 days and all were dead within 4 days.

Media was replaced with a thin layer of PBS, after marking individual well-separated colonies on the bottom of the culture dish with a pen. Colonies were promptly picked by drawing up into a Ranin (Woburn MA) P200 Pipetteman and then suspended in 1 mL of normal media in a single well of a 24 well plate. The isolated colonies were numbered EP-1 to EP-48. These isolates were grown in normal media until the most confluent wells were approximately 90% confluent, when they were lifted from the plate using STV and split into 3 wells, each on separate 24 well plates.

Two of these plates were used for a luciferase screen and the third was maintained for propagation. Media was replaced with fresh media containing either 10 μM rosiglitazone or 0.1% DMSO. After 48 hours media was aspirated and luciferase activity was measured as described.

The 10 colonies that showed luciferase activity above background, along with two colonies showing no activity (EP-14 & EP-37) as controls, were grown into 100 mm then into 150 mm plates. Cells were plated into 24 well plates as described, allowed to attach overnight, and then the media was replaced with fresh media containing either 10 μM rosiglitazone or 0.1% DMSO alone. Quadruplicate wells were assayed after 2, 8, 16, or

24 hours as described.

Four lines were selected for extensive testing (EP-17, EP-31, EP-32, and EP-39). Each of these lines was grown up to make freezer stocks. When cells were approximately 90% confluent cells were removed from plates using STV. Cells were pelleted, media was aspirated, and cells were suspended in fresh media at a density of 2 mL/plate. Cells were aliquoted into 1 mL samples in screw cap freezer tubes, 50 µL DMSO (5%) was added to tubes, tubes were mixed thoroughly, and immediately placed on ice. Cells were frozen slowly by placing in a styrofoam box overnight in a -80°C freezer. They were then transferred to liquid nitrogen for long term storage. These four cell lines were then tested to determine their usefulness for my experiments.

Western Blot Protocol

Cells were grown in 10 cm dishes to near confluence (about $5x10^6$ cells) to ensure sufficient protein for loading onto the gel. Cells were washed twice with calcium and magnesium free PBS and then 200 µL lysis buffer (50 mM Tris pH 7.5, 150 mM NaCl, 1% Nonidet P-40, 2 mM ethylenediaminetetraacetic Acid (EDTA), 2 µg/mL aprotinin, 100 µg/mL phenylmethylsulfonyl fluoride (PMSF), 2 mM dithiothreitol (DTT), 1 mM Na orthovanadate) was added. Dishes were shaken to coat cells with lysis buffer and then incubated on ice for 30 minutes, ensuring that plates were flat enough for the lysis buffer to remain covering the cells. The dish was rinsed with the lysate and the pipette tip was used to scrape cells from the dish. Lysate was transferred to a labeled microcentrifuge tube and put on ice while running a BCA (bicinchonic acid) protein assay (Pierce #23225, Rockford IL) to determine the total protein concentration of the lysate. Briefly, protein assay samples were measured in duplicate at two dilutions to determine protein

concentration. A BSA standard curve was generated by dilution of BSA in lysis buffer to allow determination of the protein concentration. 195 µL of BCA assay solution was added to each well, and the plate was incubated at 37°C for 30 minutes. The plate was then read and analyzed using a programmed BCA protocol on a Labsystems (Helsinki, Finland) Multiscan MCC/340 Microtiterplate Reader. The BCA program mixes the plate for 5 seconds then takes a single reading at 560 nm and analyzes the data using a linear regression of BSA standards to determine protein concentration of the unknown samples.

The volume of lysate containing 20 µg total protein was calculated and added, along with 5 µL of 5x gel loading buffer (250 mM Tris pH 6.8, 500 mM DTT, 10% sodium dodecyl sulfate (SDS), 0.5% bromophenol blue, 50% glycerol), to fresh microcentrifuge tubes and boiled for 3 minutes, after which tubes were immediately transferred to ice.

A SDS-polyacrylamide gel electrophoresis (SDS-PAGE) gel was poured using a Hoefer Scientifgic Instruments (San Francisco CA) Mighty Small SE 200 Gel Caster. The resolving gel was composed of 15% acrylamide (29:1 acrylamide:bis-acrylamide) in 0.38 M Tris pH 8.8, 0.1% SDS, 0.1% ammonium persulfate (APS), and polymerized using 0.04% N,N,N,N'-Tetramethylenediamine (TEMED). The stacking gel was composed of 4% acrylamide (29:1 acrylamide:bis-acrylamide) in 0.13 M Tris pH 6.8, 1% SDS, 1% APS, and polymerized using 0.1% TEMED.

Samples were then loaded into wells 2 and 4-7 of the gel using a Hamilton syringe. Molecular weight markers were loaded into lanes 1 and 8. The gel was run in run buffer (0.063 M Tris-base, 0.2 M glycine, 1 % SDS) using a Hoefer Scientific

Instruments Mighty Small SE250 Gel Apparatus at a constant voltage of 60V until samples reached the resolving gel when the voltage was increased to 100V.

Proteins were transferred to a Millipore (Bedford MA) Immobilon-P polyvinylidene difluoride (PVDF) membrane, prepared according to the manufacturer's instructions, at 50V for 2 hours in transfer buffer (25 mM Tris-base, 200 mM glycine, 15% methanol) using a Hoefer Scientific Instruments TE22 Transfer Apparatus. The blot was submerged in tris buffered saline (TBS) and marked with a china pencil to show the outline of the gel and the molecular weight makers locations. The blot was then blocked overnight at 10°C in blocking buffer (TBS, 0.2% tween-20, 5% nonfat dried milk).

The membrane was rinsed twice with wash buffer (TBS, 0.2% tween-20, 0.2% nonfat dried milk) and then incubated with 50 μL of the primary antibody (Santa Cruz #7273, mouse anti-PPARγ antibody, Santa Cruz CA) in 5 mL of antibody buffer (TBS, 1% nonfat dried milk, 0.2% tween-20) for 2 hours at room temperature. After 90 minutes an additional 50 μL of the primary antibody in 5 mL of antibody buffer was added. The blot was then rinsed twice quickly with wash buffer and then washed with wash buffer once for 15 minutes and three times for 5 minutes to remove excess antibody. The blot was then incubated with 2 μL of the secondary antibody (Jackson Immunoresearch Laboratories #715-035-150 donkey anti-mouse peroxidase antibody, West Grove PA) in 20 mL of antibody buffer for 1 hours at room temperature. The blot was imaged using Kodak (Rochester NY) Bio Max film and the Pierce Super Signal Kit (Pierce #34080, Rockford IL) according the supplied instructions. The film was then marked with the gel outline and the location of the molecular weight markers.

HeLa Stable Cell Attempt

5 million HeLa cells were electroporated with 1.8 μg of pGK-Neo, 18.2 μg of pCI-hPPARγ, and 18.2 μg of tk-$PPRE_3$-LUC after linearization of the plasmids with the restriction endonuclease XmnI (pGK-Neo and tk-$PPRE_3$-LUC) or FspI (pCI-hPPARγ). A control was electroporated under the same conditions, but without the neomycin resistance plasmid was included to check that the G418 concentration was sufficient to kill non-resistant cells.

The transfected cells were allowed to attach before the media was replaced with 1 mg/mL G418. Cells were too dense to allow isolation of colonies so they were split by a factor of 5 and immediately submitted to G418 selection. Media was replaced with fresh selection media every 3-4 days until colonies were visible to the naked eye (about 4 weeks). Some yeast (clear needle like growths) contamination was visible, but was removed by aspiration before continuing with the selection of colonies.

After marking individual well-separated colonies on the bottom of the culture dish with a pen, media was replaced with a thin layer of PBS. Colonies were promptly picked by drawing up into a Ranin P200 Pipetteman and then suspended in 1 mL of normal media in a single well of a 12 well plate. The isolated colonies were numbered EP-101 to EP-136. These isolates were grown in normal media until the most confluent wells were approximately 90% confluent. Extensive yeast contamination of some wells only allowed assaying 13 of the 36 colonies, which were renumbered 1-13.

The surviving 13 colonies were grown up in 10 cm dishes, plated in triplicate in 12-well plates at a density of $1x10^6$ cell per plate, allowed to attach overnight, and then incubated with media containing either 10 μM rosiglitazone or 0.1% DMSO. After 24

hours media was aspirated and luciferase activity was measured and normalized to the measured total protein for each well.

Two other attempts at a HeLa stable cell line resulted in no surviving colonies. The first used the same plasmids described above, but at lower concentrations (6.63 μg tk-PPRE$_3$-LUC, 5.73 μg pCI-hPPARγ, and 0.7 μg pGK-Neo). The second attempt included an expression plasmid containing a built in neomycin resistance (18.2 μg tk-PPRE$_3$-LUC, 1.8 μg pCIneo-hPPARγ). In both of these cases there was no observed difference in the survival of the cells relative to the control plate with no resistance.

Results

JEG-3 Derived Stable Cell Line Isolation and Characterization

As the transient transfection assays were not giving sufficient signal-to-noise I sought to generate a stably transfected cell line for the evaluation of PPARγ ligands. As described in Chapter 3, JEG-3 cells express high levels of endogenous PPARγ (Figure 3.1), which leads to useful levels of PPARγ induced transcription when only the tk-PPRE$_3$-LUC reporter plasmid is transfected (Figure 3.3). Based on these results I concluded that JEG-3 cells were a promising candidate for the generation of a stable cell line for evaluating the PPARγ activity of potential ligands. Rosiglitazone was selected for screening the cells because of its PPARγ selectivity, stability, and my relatively large supply.

JEG-3 cells were transfected with the tk-PPRE$_3$-LUC reporter plasmid along with the pGK-Neo neomycin resistance plasmid, and submitted to G418 selection. 48 single colonies were isolated and grown up. Cells were first screened for rosiglitazone

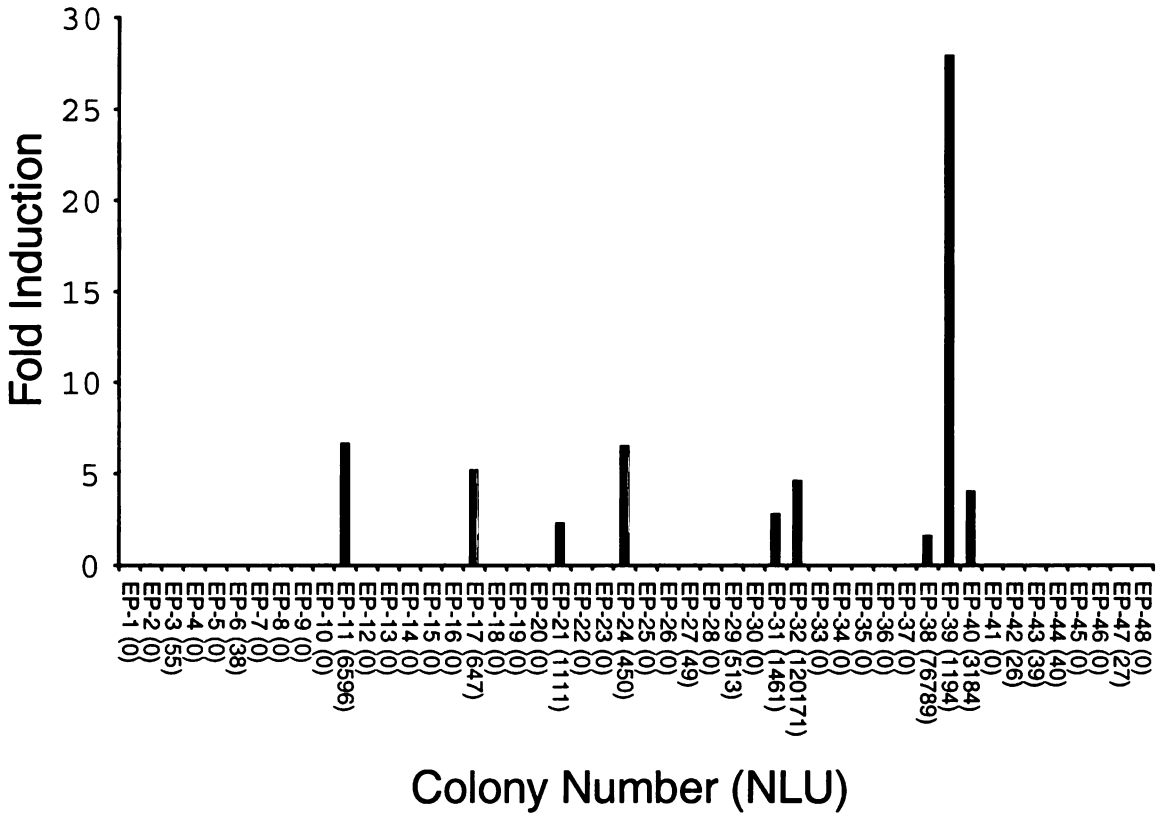

Figure 4.1: Initial Screen of JEG-3 Derived Stable Cell Colonies

Single wells of the isolated colonies were incubated for 48 hours with media containing either 10 μM rosiglitazone or vehicle alone (0.1% DMSO). Fold induction was calculated after subtracting background, and plotted on the vertical axis. The normalized light units, after subtraction of background, are shown as text in parenthesis below the horizontal axis.

induction. When the most confluent cell lines were about 90% confluent, single wells of isolates were incubated for 24 hours with media containing either 10 μM rosiglitazone or vehicle alone (0.1% DMSO). 10 colonies showed luciferase activity above background (Figure 4.1). As these measurements were from single wells, I had no indication of error levels, and drew no conclusions based on the relative induction levels.

These 10 colonies along with EP-14 and EP-37, which did not show luciferase activity and were included as controls, were tested to see if the incubation time was critical for any of these colonies. Colonies were plated in quadruplicate into 24 well plates and incubated with either 10 μM rosiglitazone or vehicle alone (0.1% DMSO) for

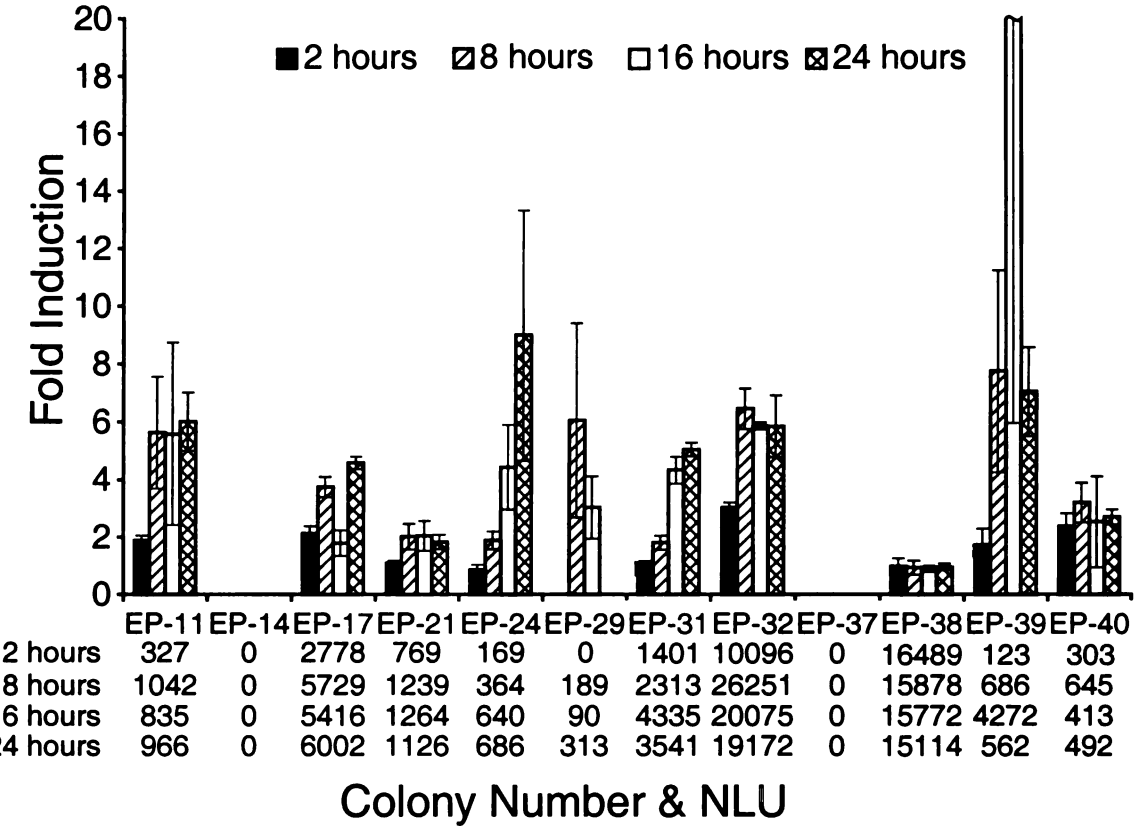

Figure 4.2: Time Dependence of Response

Isolates were incubated in quadruplicate with media containing either 10 μM rosiglitazone or vehicle alone (0.1% DMSO). After 2 (black), 8 (hatched), 16 (white), or 24 (double hatched) hours cells were assayed for luciferase activity. Fold induction was calculated after subtracting background, and plotted on the vertical axis. The normalized light units, after subtraction of background, are shown as text below the horizontal axis. Error bars represent the standard deviation of the individual measurements. EP-14 and EP-37 were included as controls, and did not show any activity in the initial screen.

2, 8, 16, or 24 hours. All 10 colonies showing activity in the first screen, and neither of the two control colonies, again showed PPARγ induction (Figure 4.2). The high induction level of EP-39 cells 16 hour time point was accompanied by a large error value, and was not considered distinct from the induction observed at the 8 and 24 hour time points. Four cell lines, EP-17, 31, 32, and 39, showed significant induction by rosiglitazone accompanied by reasonably high activity, and were selected for further testing. Some lines, such as EP-38, showed high signal but little or no induction, and others, such as EP-24, showed induction, but very low signal and were considered to not

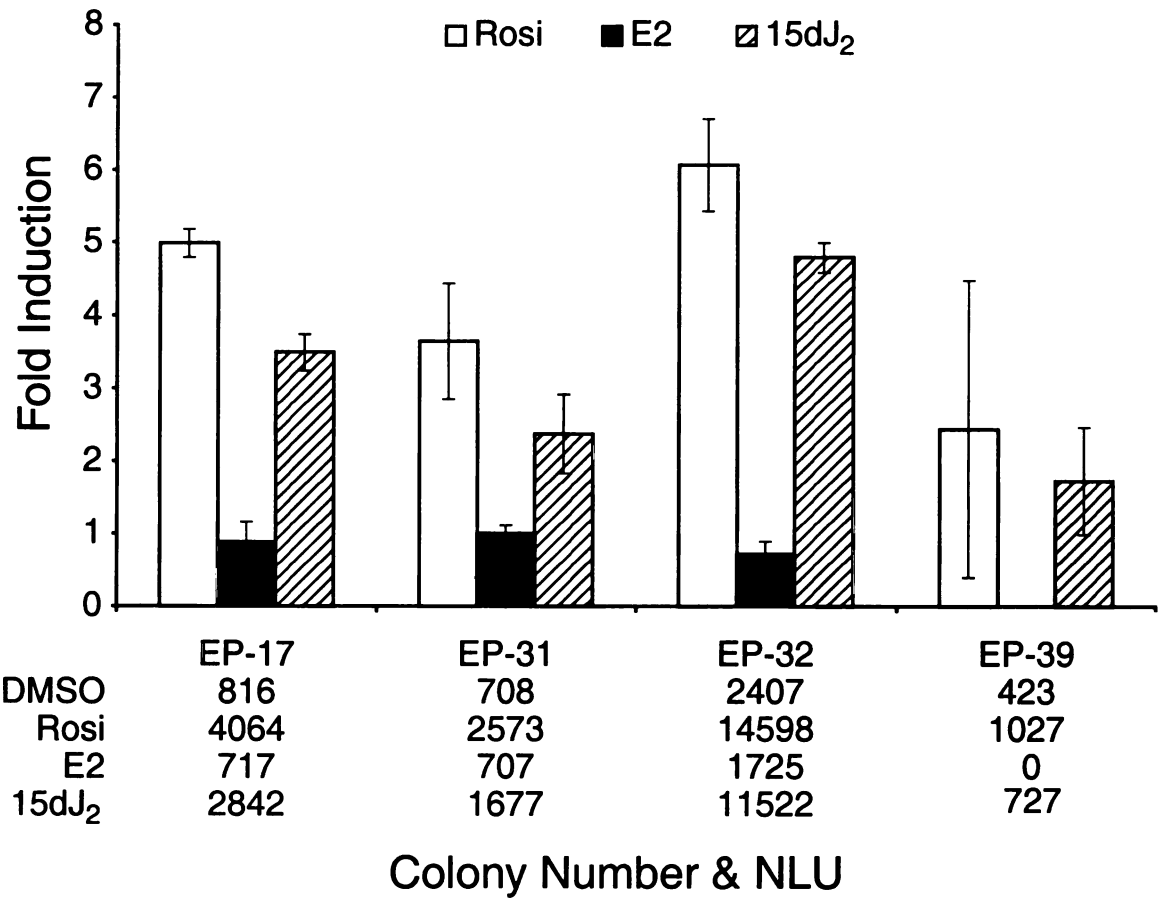

Figure 4.3: Initial Ligand Screen

Stable cell lines were incubated in triplicate for 16 hours with media containing vehicle alone (0.1% DMSO), 10 μM rosiglitazone (white), 1 μM estradiol (black), or 1 μM $15dJ_2$ (hatched). Fold induction was calculated after subtracting background, and plotted on the vertical axis. The normalized light units, after subtraction of background, are shown as text below the horizontal axis. Error bars represent the standard deviation of the individual measurements.

be useful for ligand assays. For each of the four selected cell lines 16 to 24 hours incubation gave good levels of induction, so 16 hours was selected as an incubation time for the remainder of the characterization experiments.

I next checked to see if these cell lines were activated by other ligands. I used 6-well plates in this experiment to see if they improved the observed signal and error levels observed when using the 24-well plates. Cells were plated in triplicate into 6 well plates and incubated with media containing vehicle (0.1% DMSO), 10 μM rosiglitazone, 1 μM estradiol, and 1 μM $15dJ_2$ (Figure 4.3). As expected, estradiol did not activate any of the

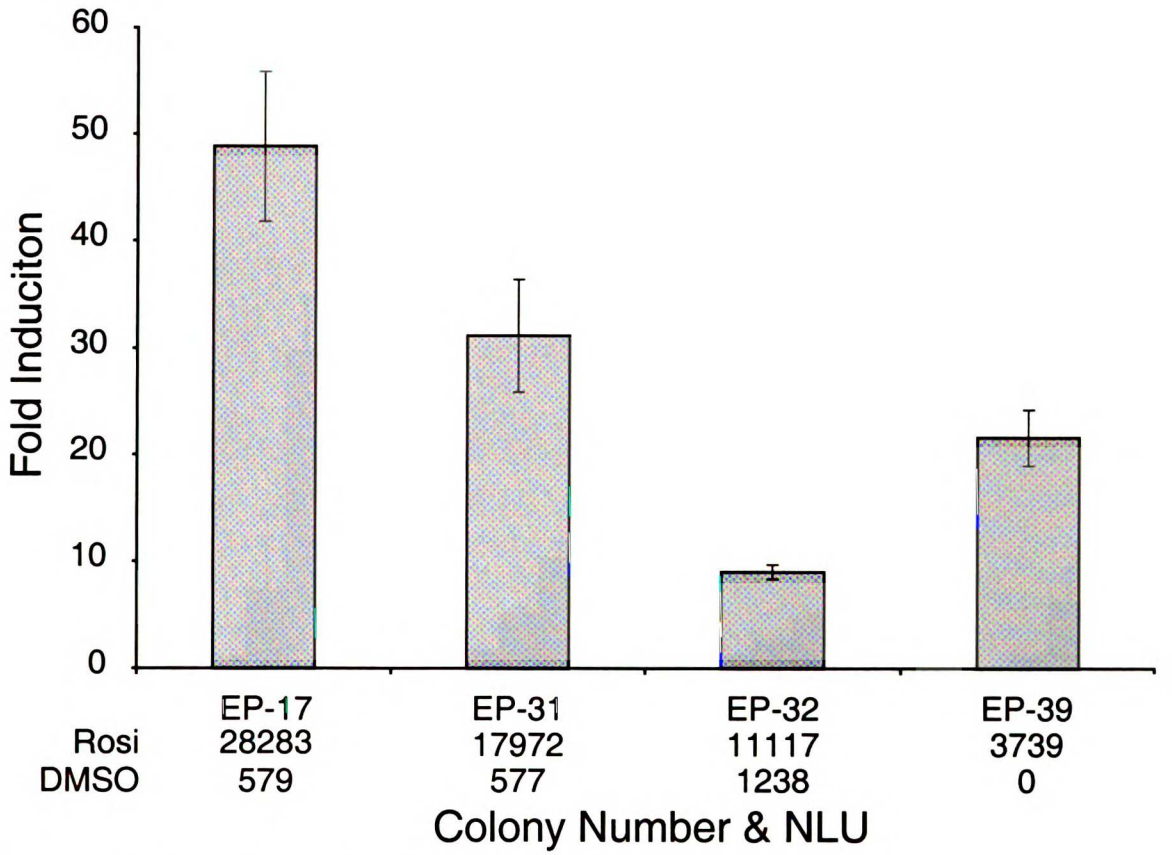

Figure 4.4: Error Determination

12 wells of stable cell lines were incubated for 16 hours with media containing either 10 μM rosiglitazone or vehicle alone (0.1% DMSO). Fold induction was calculated after subtracting background, and plotted on the vertical axis. The normalized light units, after subtraction of background, are shown as text below the horizontal axis. Error bars represent the standard deviation of the individual measurements.

cell lines, while both rosiglitazone and $15dJ_2$ showed induction in all four cell lines. The 6-well plates did not perceptibly improve the data and are more cumbersome than the 24-well plates, which were used for the subsequent experiments.

The four cell lines were then tested to see what error levels could be expected. Cells were plated into 24 well plates, and incubated in groups of 12 wells with either 10 μM rosiglitazone or vehicle alone (0.1% DMSO) (Figure 4.4).

Next, the cells were tested for a rosiglitazone dose response. Cells were plated in quadruplicate into 24 well plates and incubated with rosiglitazone at concentrations ranging from 1 nM to 10 μM (Figure 4.5). Each of the four cell lines showed increasing

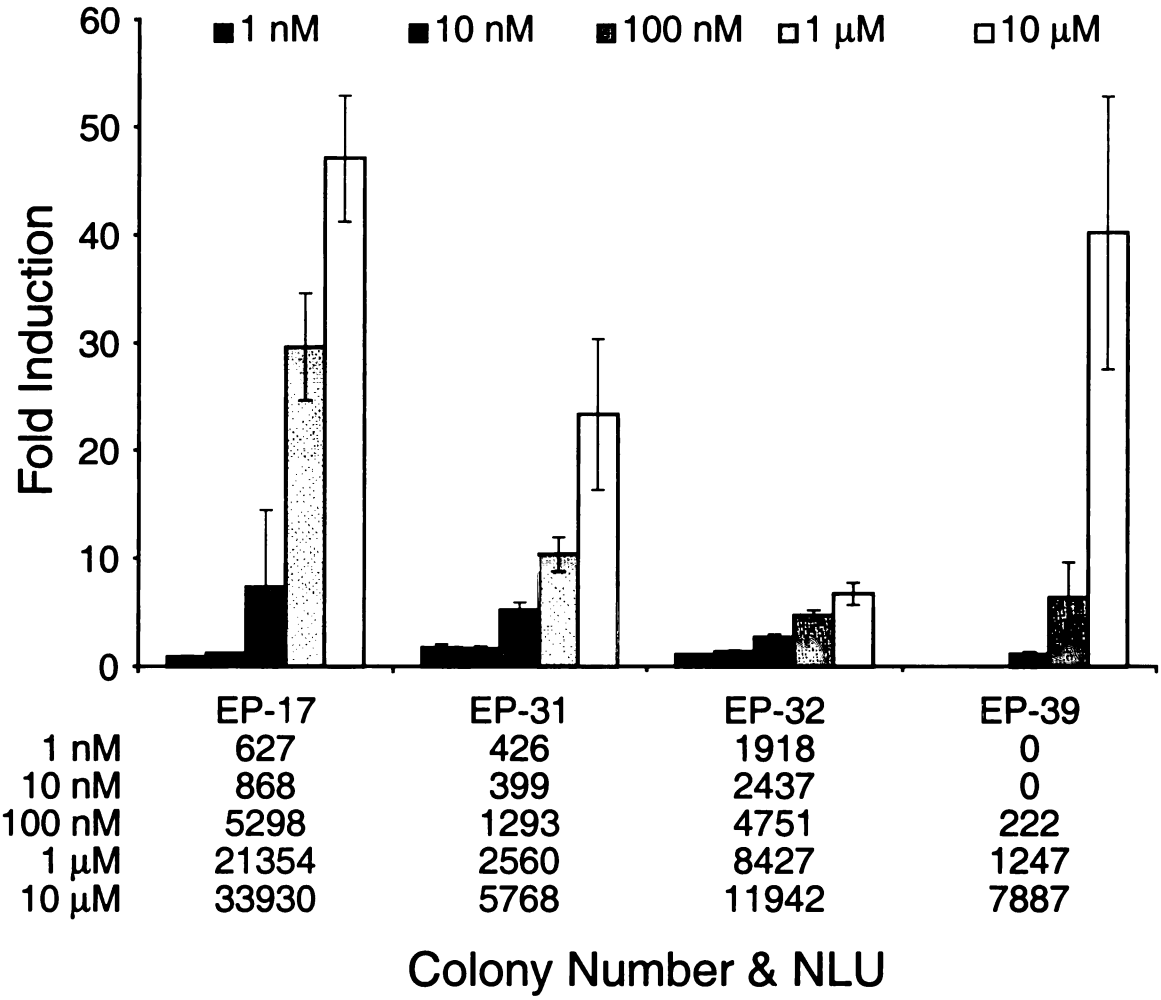

Figure 4.5: Dose Response

Stable cell lines were incubated in quadruplicate for 16 hours with media containing vehicle alone (0.1% DMSO) or rosiglitazone concentrations ranging from 1 nM to 10 μM, as shown in the legend. Fold induction was calculated after subtracting background, and plotted on the vertical axis. The normalized light units, after subtraction of background, are shown as text below the horizontal axis. Error bars represent the standard deviation of the individual measurements.

induction with increasing rosiglitazone concentration, but none showed saturation at the concentrations tested.

The four cell lines were tested to see if several lipids, reported to bind to PPARγ, would show activation in these cells. Cells were plated in triplicate into 24 well plates and incubated for 16 hours with media containing the specified ligand. 10 μM rosiglitazone and 1 μM $15dJ_2$ were included on each plate as controls. Each lipid was

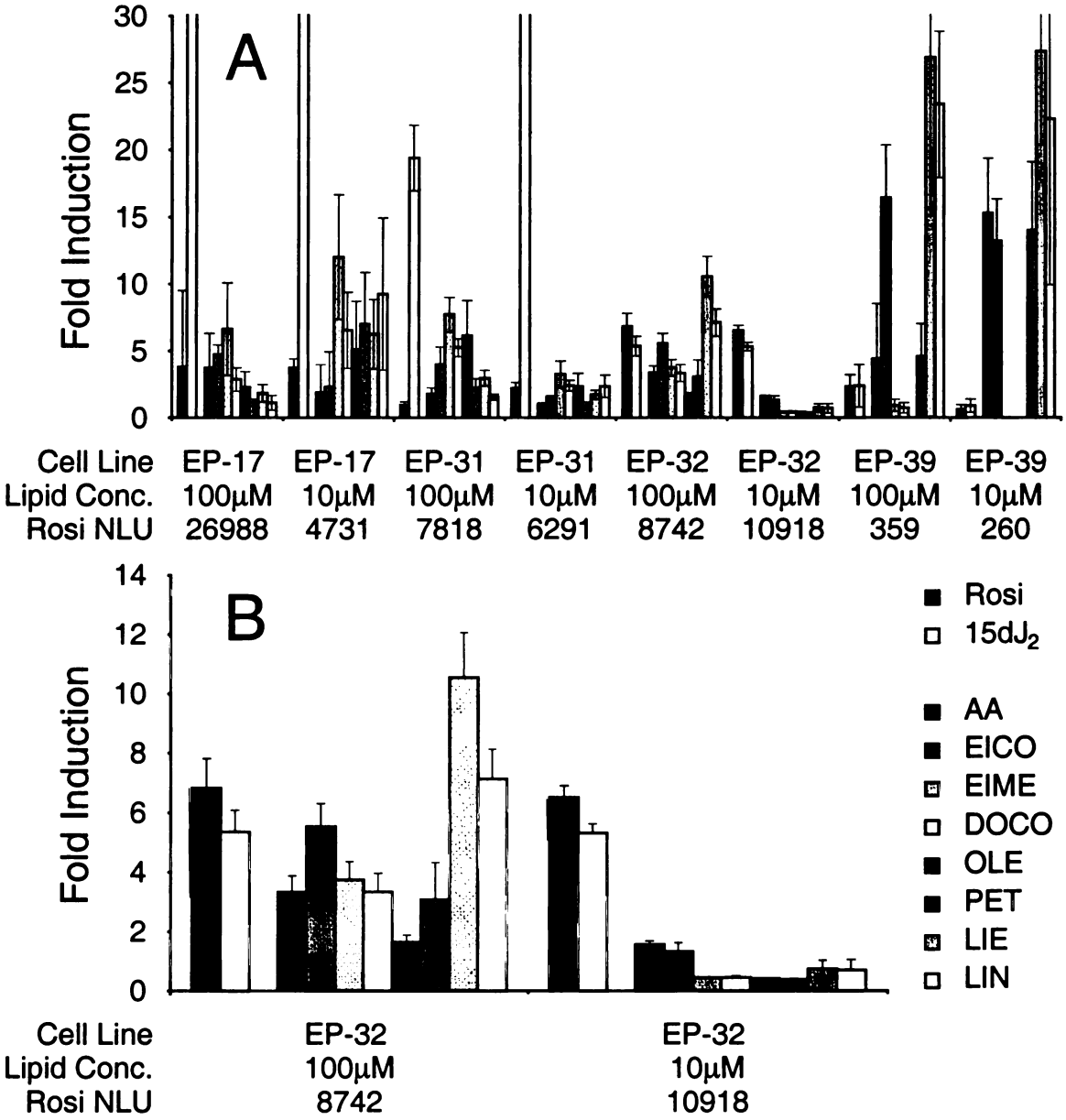

Figure 4.6: Lipid Screen

Stable cell lines were incubated in triplicate for 16 hours with media containing 10 μM rosiglitazone (Rosi), 1 μM $15dJ_2$, vehicle alone (0.1% EtOH), or the specified concentration of lipid. The following fatty acids were tested at 100 μM and 10 μM: arachidonic acid (AA), eicosapentaenoic acid (EICO), eicosapentaenoic acid methyl ester (EIME), docosahexaenoic acid (DOCO), oleic acid (OLE), petroselinic acid (PET), linoleic acid (LIE), and linolenic acid (LIN). Panel A shows the data for all four cell lines, while panel B shows an expansion of the data for EP-32 cells, the cell line with the most consistent response. Fold induction was calculated after subtracting background, and plotted on the vertical axis. The normalized light units for rosiglitazone, after subtraction of background, are shown as text below the horizontal axis. Error bars represent the standard deviation of the individual measurements.

Compound	100 μM Exp. Fold Induction	10 μM Exp. Fold Induction	Reported Binding	Ref.
rosiglitazone	7 ± 1 (10 μM)	6.5 ± 0.4 (10 μM)	40 nM	(50)
$15dJ_2$	5.4 ± 0.7 (1μM)	5.3 ± 0.3 (1μM)	6.4 ± 0.9 μM	(228)
Arachidonic Acid	3.3 ± 0.5	1.6 ± 0.1		
Eicosapentanoic Acid	5.5 ± 0.8	1.3 ± 0.3	3.1 ± 0.2 μM	(228)
Eicosapentanoic Acid Methyl Ester	3.8 ± 0.6	0.43 ± 0.03		
Docosahexaenoic Acid	3.3 ± 0.6	0.43 ± 0.08	2.9 ± 0.3 μM	(228)
Oleic Acid	1.7 ± 0.2	0.40 ± 0.03	11.7 ± 0.5 μM	(228)
Petroselinic Acid	3 ± 1	0.36 ± 0.05		
Linoleic Acid	10 ± 2	2.1 ± 0.3	8.4 ± 0.8 μM	(228)
Linolenic Acid	7 ± 1	0.7 ± 0.4	2.3 ± 0.1 μM	(228)

Table 4.1: Binding and PPARγ Induction of Some Fatty Acids

The induction of PPARγ in EP-JEG cells reported in Figure 4.6 is shown in the second and third columns. The literature binding constants and the appropriate references are listed in the fourth and fifth column.

tested at both 10 and 100 μM, comparable to the reported PPARγ binding of each ligand (Table 4.1). Figure 4.6A shows all of the lipid data for the four cell lines, while Figure 4.6B shows only the data for EP-32, which was later selected as the line showing the greatest consistency. Most of the lipids showed moderate activation,

To help determine which of the four cell lines should be selected for further study, the data from figures 4.1-4.5, which were expected to lead to full induction, were plotted together (Figure 4.7). Though the induction seen with the EP-32 cell line was lower than some of the data from other cell lines, the response was much more consistent and showed lower error levels in Figure 4.4 and most experiments. As the overall levels of activation and error were also desirable, EP-32 cells were selected as the most desirable cell line for subsequent studies and are henceforth referred to as EP-JEG cells to clarify their origin as a JEG-3 derived stable cell line.

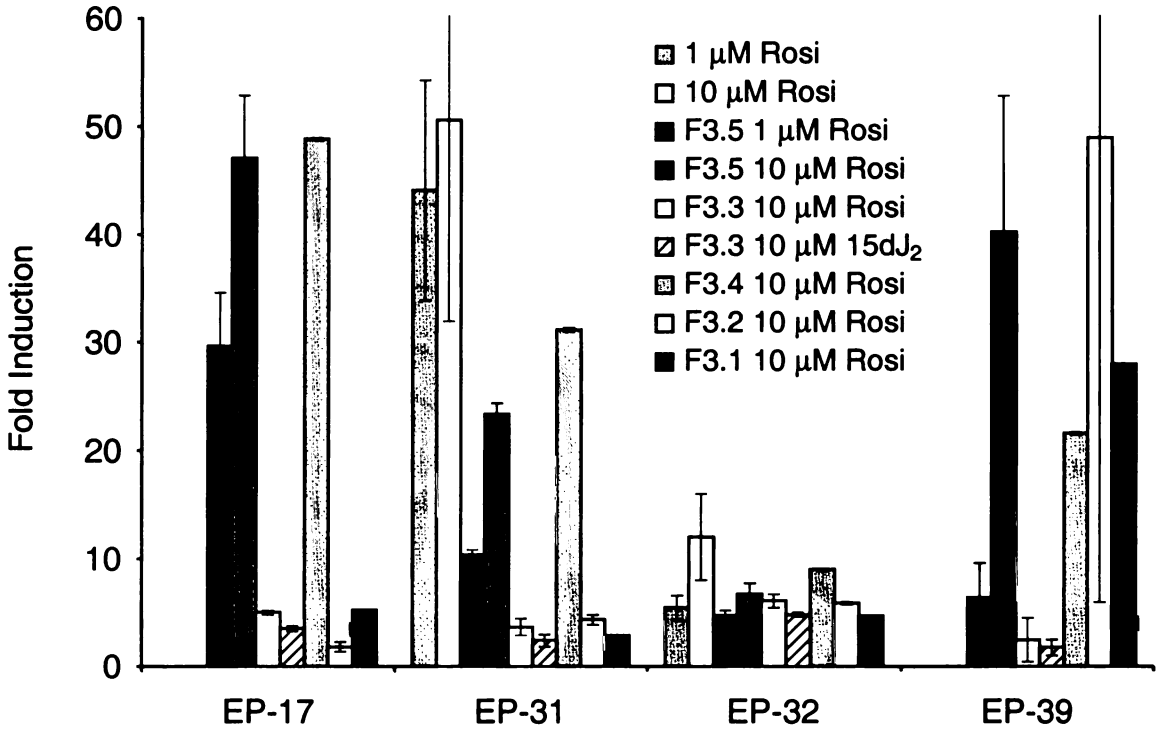

Figure 4.7: Variability in Induction Level

All of the conditions expected to give saturating activation from either rosiglitazone of $15dJ_2$ in Figure 4.1, Figure 4.2, Figure 4.3, Figure 4.4, and Figure 4.5 are plotted together to show the variability of induction levels. The source of data is specified by figure number in the legend with the exception of those obtained in a duplicate dose response experiment, conducted under the same conditions, for the EP-31 and EP-32 cell lines. Fold induction was calculated after subtracting background, and plotted on the vertical axis. Error bars represent the standard deviation of the individual measurements.

As part of continued characterization of these cell lines I looked for PPARγ expression in the stable cell lines, as was observed in the JEG-3 cells they were derived from (Figure 3.1). Western blot analysis shows high levels, comparable to that seen in the JEG-3 control, of full length PPARγ expression in all four stable cell lines (Figure 4.8).

HeLa Stable Cell Line Attempt

The tk-$PPRE_3$-LUC reporter gene construct, which I used to generate the EP-JEG cell line, also responds to cotransfected PPAR α and δ in transient transfection assays (58, 102). Dr. Leslie Waite has also observed substantial levels of mRNA for both

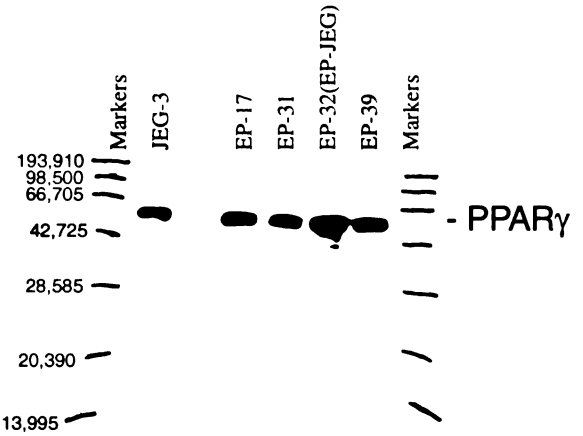

Figure 4.8: JEG-3 and the Stable Cell Lines Cells Express High Levels of PPARγ

JEG-3 (lane 2), EP-17 (lane 4), EP-31 (lane 5), EP-32 (lane 6), and EP-39 (lane 7) cells were grown in 10 cm dishes and lysed. Total protein in the lysate was quantified and 20 μg was added to each well of an SDS-PAGE gel. Protein was visualized after blotting using a PPARγ specific mouse antibody and an anti-mouse peroxidase chemical visualization system. Markers were run both in lanes 1 and 8, their positions were transferred to the film by hand using a pen, and the molecular weights are noted on the left side. The observed band is consistent with the full length PPARγ receptor, which has a molecular weight of 58 kilodaltons.

PPARα and PPARδ in EP-JEG cells (81). Together these observations suggest that the response observed in EP-JEG cells may not limited to the PPARγ activity of the ligands. To complement the EP-JEG cells I attempted to generate a HeLa stable cell line containing only PPARγ. HeLa cells were selected because I had successfully seen useful levels of activity in transient transfection assays, they are of human origin, and I did not observe detectable levels of PPARγ expression by western blot (Figure 3.1), making them a good candidate for PPAR overexpression.

HeLa cells were transfected with the tk-PPRE$_3$-LUC reporter plasmid along pCI-hPPARγ, a PPARγ mammalian expression plasmid, and pGK-Neo, a neomycin resistance plasmid. After G418 selection, 36 well-separated colonies were isolated and grown up. Yeast contamination (small needle like growths) limited the screening of the isolated colonies for induction of PPARγ by rosiglitazone. The 13 colonies without contamination were grown up into 10 cm dishes and then plated into 12-well plates and screened. 7 of the 13 colonies showed high luciferase activity, but none of the colonies showed ligand induction of luciferase expression (Figure 4.9).

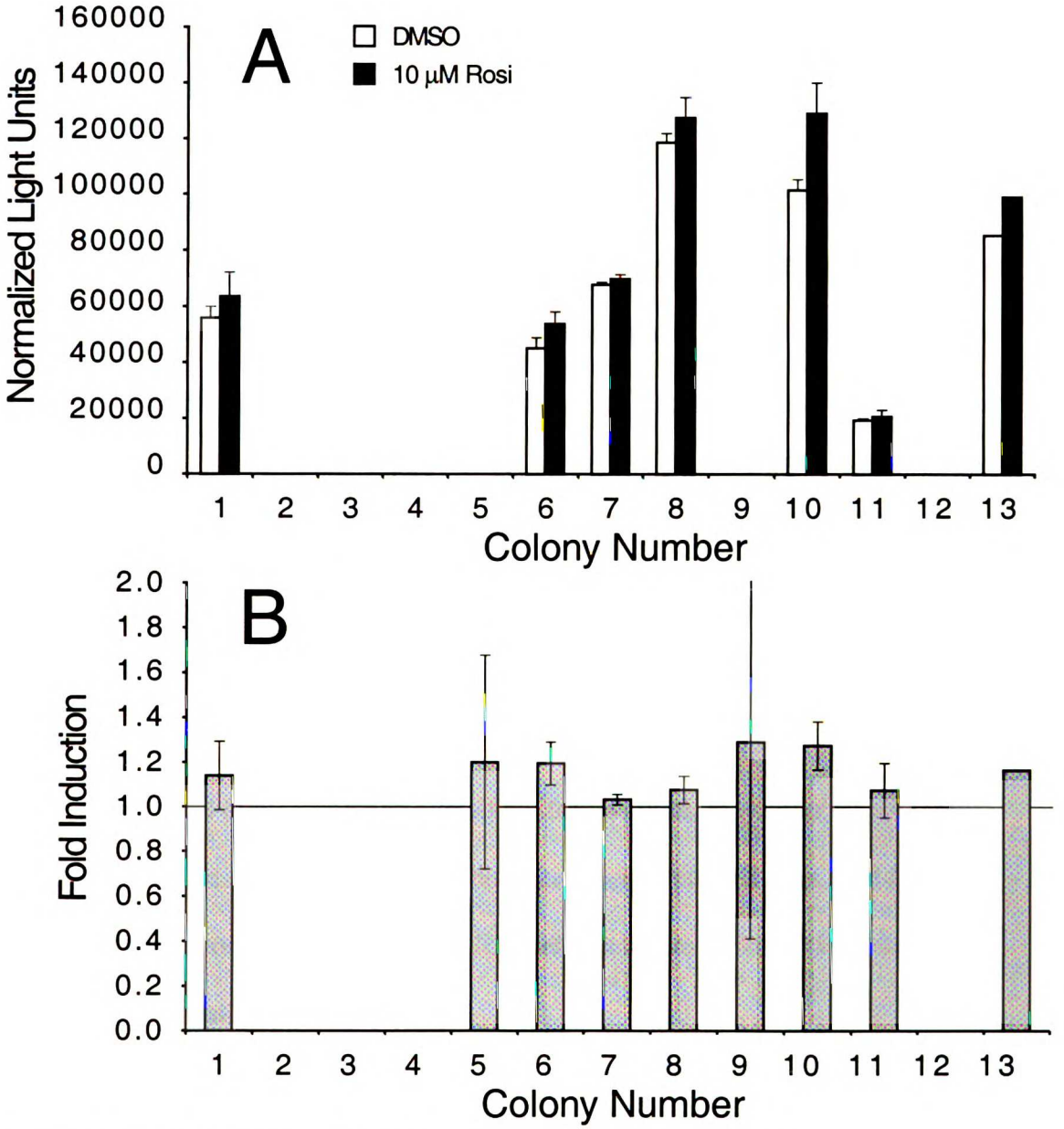

Figure 4.9: Initial Screen of HeLa Derived Stable Cell Colonies

Isolated colonies were incubated in triplicate for 24 hours with media containing either 10 μM rosiglitazone (black) or vehicle alone (0.1% DMSO) (white). Panel A shows normalized light units, after subtraction of background. Panel B shows the corresponding rosiglitazone fold induction, calculated relative to vehicle after subtracting background. Error bars represent the standard deviation of the individual measurements.

As the cell lines were not useful for my experiments without ligand induction of transcription, they were discarded. Attempts at similar HeLa derived stable cell lines were made with the same plasmids at lower concentrations, and with a pCIneo-hPPARγ

plasmid containing both a neomycin resistance and the PPARγ expression properties. In both of these attempts no colonies survived G418 selection.

Discussion

EP-JEG cells provide a useful tool to measure the activity of ligand and serum samples in an endogenous PPARγ response. While complicated by the possibility of activation through other receptor subtypes, the EP-JEG cell line allows the evaluation of PPARγ activation in a cell line where the receptor is in balance with other transcription factors and coactivators. While EP-JEG induction levels are relatively low compared to some of the other stable cell lines, and the JEG-3 transient transfection assays, the levels are sufficient for my needs, and the increased overall luciferase levels offer a distinct advantage.

Due in part to the increased overall luciferase levels, they offer significantly improved error and reproducibility over both the other stable cell lines, and JEG-3 transient transfection assays. I view EP-JEG cells as the most desirable endogenous assay currently available in our lab.

EP-JEG's maximal induction is obtained after 8 hours, but based on the profiles of the other cell lines and for convenience, a time of 16-24 hours has been used typically. EP-JEG cells are inducted by both rosiglitazone and $15dJ_2$, but are not induced by estradiol as expected for a PPAR reporter gene system.

I have not obtained reproducible saturation at high ligand concentrations in my dose response experiments with EP-JEG cells or transiently transfected JEG-3 cells, though I do see reproducibility in the ligand concentrations where I see the increasing induction begin. This lack of saturation may be due in part to increased expression of

PPARγ at high ligand concentrations in this endogenous PPARγ response. Dr. Leslie Waite has observed an increase in the PPARγ mRNA levels, as measured by reverse transcriptase-polymerase chain reaction (RT-PCR), upon treatment of JEG-3 cells with rosiglitazone (81). She does not observe an increase in the protein levels, as observed by Western Blot (81), perhaps due to the increased degradation of PPARγ upon treatment of cells with PPARγ ligands (241). While this alone is not sufficient to account for the lack of saturation, along with the toxicity of high ligand concentrations to both JEG-3 and EP-JEG, cells this could explain the increasing activation seen in my dose response experiments.

Dr. Waite's observation of PPARα and PPARδ mRNA in JEG-3 and EP-JEG cells (81), along with the reporter plasmid responding to these subtypes in transient transfection assays, raises the concern that they may be part of the endogenous response I observe in EP-JEG cells. While this does not pose a problem if I am testing the effects of ligands known to be specific for the PPARγ subtype, such as rosiglitazone and $15dJ_2$, it complicates the interpretation of screening experiments for ligands that may also function through one of the other PPAR subtypes.

In order to accurately screen ligands for activity at specific subtypes of PPAR, it would be useful to generate a series of stable cell lines with the individual PPAR subtypes overexpressed along with an appropriate reporter plasmid. These cell lines along with EP-JEG cells would provide a useful system, not only for screening ligands for activity at the PPAR subtypes, but also for studying the natural PPAR response in the JEG-3 and EP-JEG cells.

In pursuit of a cell line for PPARγ, I have attempted several times to stably transfect a PPARγ expression plasmid and the tk-$PPRE_3$-LUC reporter plasmid into HeLa cells, which do not express PPARγ endogenously. I was not successful in initial attempts at incorporating these plasmids simultaneously. As the level of PPARγ expression may be important for obtaining a useful cell line, a more lengthy procedure for incorporating them one at a time may be required.

Chapter 5: PPARγ Binding Assays and the Expression and Purification of hPPARγ LBD

A his-tagged hPPARγ LBD construct can be expressed and purified in a simple procedure yielding sufficiently pure protein in high yield after a single purification step. Binding of the fluorescent PPARγ ligand cis-parinaric acid demonstrates that the PPARγ LBD construct is in an active conformation. While a fluorescent competitive binding assay may be possible for some ligands, the intrinsic fluorescence of rosiglitazone and its derivatives interferes with the evaluation of these ligands using the fluorescence binding assay.

Introduction

To evaluate the PPARγ activity of ligands it is first necessary to be able to measure binding constants, or at least show that candidate ligands bind to PPARγ. While activation of a reporter gene in a cell assay is an important evaluation of ligands it alone does not show that the ligands act directly through the receptor. For instance, a compound could act through cell surface receptors, by phosphorylation of transcription factors, or by stimulating the synthesis or release of a nuclear receptor ligand. If a candidate ligand can be shown to bind tightly to the receptor in addition to activating or inhibiting activation of a receptor, it is reasonable to assume that that compound is a bona fide ligand for the receptor.

The most common PPARγ binding assay used in the literature for evaluation of PPARγ ligands is a competitive binding assay using a PPARγLBD construct and tritiated rosiglitazone (Figure 5.1) (50, 51, 75, 77). This type of assay would serve our purposes

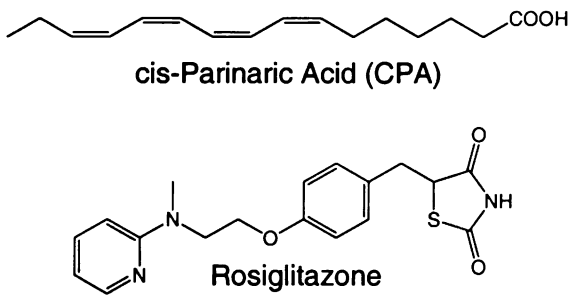

Figure 5.1: Chemical Structures of Ligands

The chemical structures of ligands discussed in this chapter are shown. Rosiglitazone, a PPARγ agonist, was synthesized as described in Chapter 2. cis-Parinaric Acid is a fluorescent probe that was purchased from Molecular Probes.

well, but unfortunately, we do not have appropriate synthetic equipment to generate the tritiated rosiglitazone.

Another class of binding assays takes advantage of the receptors recruitment of coactivators by the receptor upon agonist binding (85, 242). In this type of assay, a radiolabeled coactivator peptide and a GST-PPARγLBD fusion protein are incubated with the candidate ligands. The amount of radioactive peptide that coprecipitates with the LBD fusion protein is then measured and related to the amount of ligand bound to the receptor. This binding assay is a useful measure of the ability of an agonist to recruit coactivator and hence induce transcription, but is not useful for the evaluation of ligands which may bind to the receptor, but not allow coactivator binding, such as antagonists and partial agonists.

A spectrophotometric PPARγ binding assay has been reported by Palmer (228). This assay takes advantage of changes in the spectrophotometric and fluorescent properties of cis-parinaric acid (CPA) (Figure 5.1), a commercially available fluorescent membrane probe, depending on the polarity of its environment. CPA binds specifically to PPARγ with a binding constant (K_d) of 670 ± 70 (228). As the PPARγ binding site places CPA in the hydrophobic core of the receptor, binding results in a measurable shift in both the spectrophotometric and fluorescent properties of the ligand. These spectral changes reverse when CPA is displaced from the binding site by the candidate ligand in a

competitive binding assay. Though the relatively weak affinity of CPA prevents the measurement of binding constants below 1 μM, it allows the qualitative determination of whether a candidate ligand binds to the receptor.

In this study, I report the expression and purification of Palmer's hPPARγ LBD construct and evaluation of the utility of the binding assay in evaluating the PPARγ binding of thiazolidinedione derivatives.

Experimental Procedures

Reagents

Unless otherwise specified, all chemicals were obtained from Fisher Scientific (Pittsburgh PA) or Sigma-Aldrich (St. Louis MO). 15-Deoxy-$\Delta^{12,14}$-prostaglandin J_2 ($15dJ_2$) was obtained from Cayman Chemical Company (Ann Arbor MI). Rosiglitazone (BRL 49653) was synthesized as described in Chapter 2. cis-Parinaric acid (CPA) was obtained from Molecular Probes (Eugene OR).

PPARγ LBD Expression and Purification

The plasmid pET15b-hPPARγLBD, a bacterial expression vector containing a his-tagged LBD construct of human PPARγ, was a gift of Dr. Colin Palmer (228). The LBD construct was expressed and purified with the assistance of Russ Huber from the Fletterick lab using modifications of his protocol based on suggestions from Dr. Palmer.

The plasmid was transformed into competent Novagen (Madison WI) BL21 (DE3) cells and plated on ampicilin LB plates according to Novagen's supplied protocol. A single well-formed colony was picked with a pipette tip, grown up, and restreaked on a fresh ampicilin LB plate. This plate was incubated overnight at 37°C and a single well-

formed colony was selected. This colony was used to inoculate 100 mL of LB, which was then grown overnight. 25mL of the overnight culture was added to each of 4 1-liter LB cultures, equilibrated at 30°C. Cells were grown at 30°C until OD_{600}=1, when they were induced with 0.5 mM IPTG for 3 hours.

Cells were spun down (divided between six 500 mL bottles and spun at 4k in a GS3 rotor, 2000 x g) and resuspended in start buffer (500 mL bottle of PBS (UCSF Cell Culture), 10% glycerol, 1 mM PMSF, 1 mM Benzamidine, 5 mM BME). 25 mL of buffer was used to resuspend each pellet (150 mL total). The cell suspension was divided between four 50 mL centrifuge tubes and flash frozen in liquid nitrogen to assist in lysing the cells.

Protein was thawed on ice for 30 minutes, after which 1 mg/mL lysozyme was stirred in with the cells for one hour. Lysate was sonicated until the thick consistency generated by addition of the lysozyme had dissipated, after which it was sonicated for ten, two-minute bursts with a fifty percent duty cycle at sixty percent power. The solution turned a nut brown and lost the viscosity gained during the lysozyme treatment.

The solution was then divided equally between ultracentrifuge tubes and spun in an ultracentrifuge at 35-40 K for one hour to pellet the cell debris. The cleared lysate was decanted from the pelleted cell debris and filtered through a 0.45 μm pore filter.

The cleared and filtered lysate was purified using an AKTA-Explorer (Amersham Pharmacia, Piscataway NJ) protein purification system with a column packed with Talon (Clonetech, Palo Alto CA) media at a 1 mL/min flow rate. The lysate was loaded onto the cobalt column equilibrated with buffer A (same as start buffer, but with 1 mM BME). The column was washed with 3.3% buffer B (same as buffer A with 300 mM imidazole)

until the OD_{280} returned to less than 0.01. A gradient was then applied to the column, increasing the imidazole concentration to 300 mM (100% buffer B) over 2 hours. Samples were collected every 5 mL using the AKTA's automated fraction collector. Samples 1-9, which showed a significant increase of OD_{280}, were run out on a SDS-PAGE gel along with BSA, molecular weight markers, the lysate, the pellet, the loading buffer, and the wash fraction to determine the protein content and purity of the samples. The wash and samples 3-9 were pooled, and then desalted and concentrated using 1K cutoff Millipore (Bedford MA) Ultrafree-15 protein concentrators (spinning at 7.5 K in an SS-34 rotor, 6700 x g) to a concentration of 4 mg/mL, as estimated by a crude Bradford assay. The concentrated protein sample was then spun at 100K to remove any aggregated protein, aliquoted for use in assays, flash frozen in liquid nitrogen, and then transferred for long term storage at -80°C.

Absorbance and Fluorescence Measurements

Unless otherwise specified all fluorescence and absorbance measurements were made in 25 mM Tris-HCl buffer, pH 7.5 in quartz cuvettes. Absorbance measurements were performed on a Kontron Instruments UVIKON 930 Spectrophotometer. Fluorescence measurements were performed on a Perkin Elmer LS 50 B Luminescence Spectrometer.

PPARγ Fluorescence Binding Assays

The fluorescent binding assay was based on the assay reported by Dr. Palmer (228). Briefly, purified hPPARγLBD was mixed with CPA in 25 mM Tris-HCl buffer, pH 7.5, at room temperature. The resulting fluorescence (excitation wavelength of 318,

emission wavelength of 410) was measured after mixing by inverting the cuvette 3-4 times. The fluorescence from the protein alone was measured independently, and subtracted from the fluorescence of the protein with CPA.

Determination of the Concentration of Active hPPARγLBD

To determine the concentration of active hPPARγLBD in the LBD stock solution the binding of CPA was monitored using the fluorescence binding assay described above. The fluorescence intensity data was fit using a modification of the equation reported by Swillens for the binding of radioligand at high receptor concentrations (243). Starting with Equation 5.1, substitution for free ligand using the expression $L_T = L + B$, where L_T is the total ligand concentration, L is the free ligand concentration, and B is the concentration of bound ligand, followed by substitution for the maximum bound ligand (B_{max}) with the total concentration of LBD (C_{LBD}) gives Equation 5.2. As the fluorescence intensity (I) is proportional to the bound ligand ($I = \beta B$), with β being the proportionality constant,

Equation 5.1

$$B = \frac{B_{\max} L}{K_d + L} = \frac{C_{LBD} L}{K_d + L}$$

Equation 5.2

$$B = \frac{C_{LBD}(L_T - B)}{K_d + (L_T - B)}$$

Equation 5.3

$$I = \frac{\beta C_{LBD}(L_T - I/\beta)}{K_d + (L_T - I/\beta)}$$

Equation 5.4

$$\frac{I^2}{\beta} + (-C_{LBD} - L_T - K_d)I + \beta C_{LBD} L_T = 0$$

Equation 5.5

$$I = \frac{C_{LBD} + L_T + K_d - \sqrt{(-C_{LBD} - L_T - K_d)^2 - 4C_{LBD}L_T}}{2/\beta}$$

multiplying both sides of the equation by β followed by substitution for the fluorescence intensity (I) gives Equation 5.3. Rearrangement gives a quadratic equation (Equation 5.4) which can then be solved for the measured fluorescence intensity giving Equation 5.5. This equation was fit to the experimental data using the EXCEL Solver function and the least squares method, with the literature value for CPA's K_d as a constant, to determine the total protein concentration.

PPARγ Spectrophotometric Binding Assays

The spectrophotometric binding assay was based on the assay reported by Dr. Palmer (228). Briefly, CPA (500 nM) was added to 25 mM Tris-HCl buffer, pH 7.5, at room temperature and scanned against a buffer reference between 312 and 340 nm. All additions of protein were added equally to both the sample and the reference cuvettes and mixed by inverting the cuvette 3-4 times before measuring the absorbance spectrum. The ratio of absorbance at 319 and 329 nm was calculated, but was not fit to a binding equation because of the poor signal to noise ratio and poor reproducibility.

Results

The logical first step in establishing a working binding assay to complement the cell assays described in the previous chapters in the characterization of PPARγ ligands was to express and purify a PPARγLBD construct. Palmer reported high levels of expression of a His-tagged hPPARγLBD construct (228). Using the His-tagged hPPARγLBD expression construct and a modification of Russ Huber's expression protocol based on the suggestions of Dr. Palmer, 4 L of transfected BL21(DE3) cells

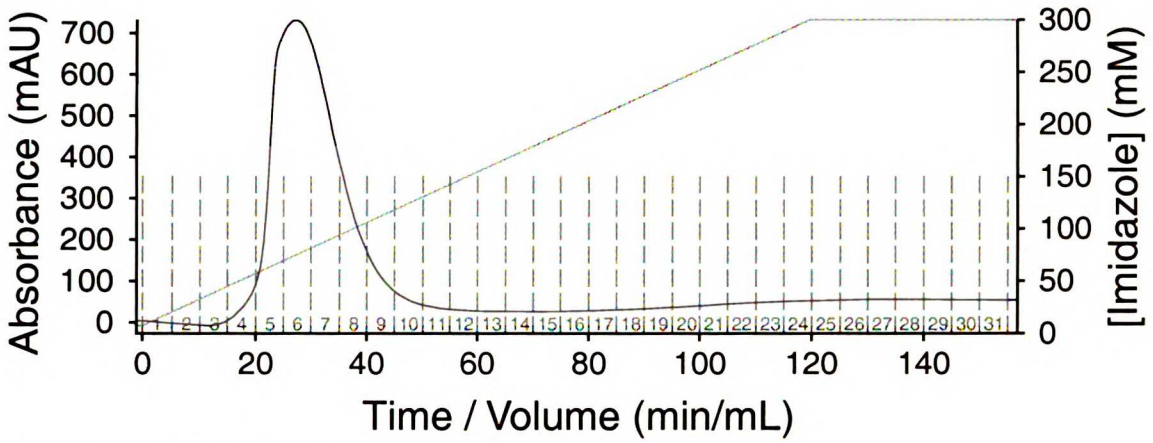

Figure 5.2: hPPARγLBD Purification

The His-tagged hPPARγLBD was purified from the cleared lysate using an AKTA-Explorer protein purification system. The lysate was loaded onto a Talon cobalt column, washed with 10 mM imidazole, and then eluded with a gradient of increasing imidazole concentration to 300 mM after 2 hours (120 mL). 5 mL fractions were collected. The black trace shows the UV absorbtivity at 280 nm and is plotted on the left axis. The imidazole gradient is plotted as the gray trace on the right axis. The time, in minutes, and volume of eluent, in mL (a flow rate of 1 mL/min), is plotted on the bottom axis. The 5 mL fraction divisions are marked with gray dashed lines, and are numbered immediately above the bottom axis.

were grown up and induced. Lysis of these cells showed very high expression levels of hPPARγLBD.

The lysate containing the His-tagged LBD was cleared by ultracentrifugation and loaded onto a TALON cobalt column. The column was washed with 10 mM imidazole to remove proteins not bound specifically to the column, and then the LBD construct was eluted as a single well-formed peak under an imidazole gradient (Figure 5.2).

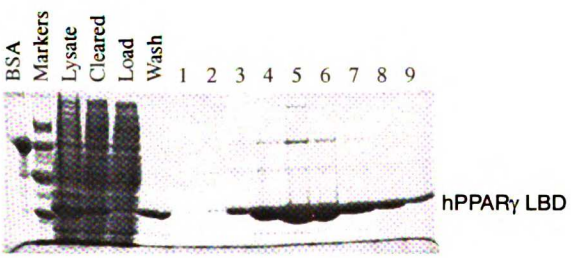

Figure 5.3: SDS-PAGE Analysis of Washes and Fractions

Wash and fractions were run on a SDS-PAGE gel and stained with Coomassie Blue to determine content and purity of the collected fractions. The lanes were loaded with BSA (lane 1), molecular weight markers (lane 2), cell lysate (lane 3), cleared lysate (lane 4), load flow through (lane 5), wash (lane 6), and samples 1-9 (lanes 8-16). The LBD construct has a molecular weight of 35 kilodaltons. The wash and samples 3-9 showed a significant concentration of hPPARγLBD, and were pooled and concentrated, and then ultracentrifuged to remove aggregate.

Samples saved from the purification procedure, standards, and the first nine column fractions were run on a

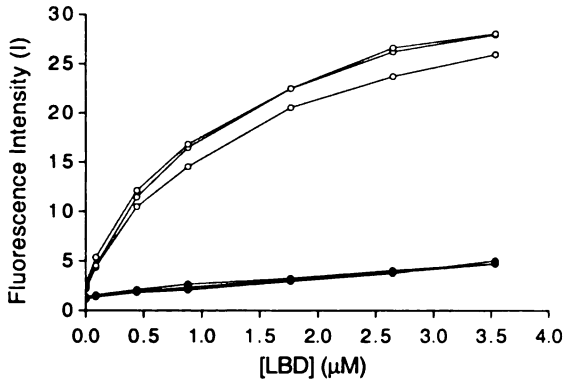

Figure 5.4: CPA Fluorescence Binding Assay (raw data)

The fluorescence of increasing concentrations of hPPARγLBD was monitored in the presence (open circles) and absence (closed circles) of CPA (300 μM). Three independent experiments are plotted together.

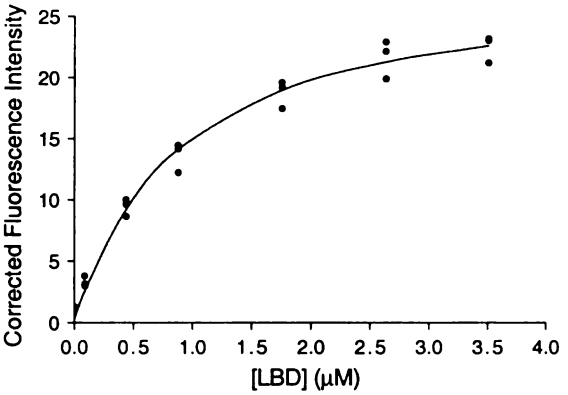

Figure 5.5: CPA Fluorescence Binding Assay / Protein Concentration Determination

The intrinsic protein fluorescence shown in Figure 5.4 (closed circles) was subtracted from the fluorescence in the presence of CPA shown in Figure 5.4 (open circles) for each of the three independent experiments. A fit of Equation 5.5 to all three data sets using the EXCEL Solver function, with a least squares method, with the reported K_d of 670 nM as a constraint was used to determine the concentration of active LBD in the stock solution (350 μM or 11 mg/mL). Using the EXCEL Solver function did not allow the determination of error values for the fit.

SDS-PAGE gel (Figure 5.3). The wash fraction and fractions 3-9 showed significant levels of pure PPARγ-LBD. The bands at higher molecular weight most likely represent aggregates of the LBD construct (244). These fractions were pooled and concentrated to an approximate concentration of 4 mg/mL based on a crude Bradford assay. This stock solution was dispensed into 100 μL to 1 mL fractions and flash frozen in liquid nitrogen before transferring to an -80°C freezer for long-term storage.

To determine the concentration of active hPPARγ LBD the fluorescent binding assay of Dr. Colin Palmer was reproduced (228). Increasing concentrations of LBD were added to a cuvette containing 300 μM cis-Parinaric Acid (CPA). After correction for the changing concentrations as a result of the protein additions, the fluorescence intensity

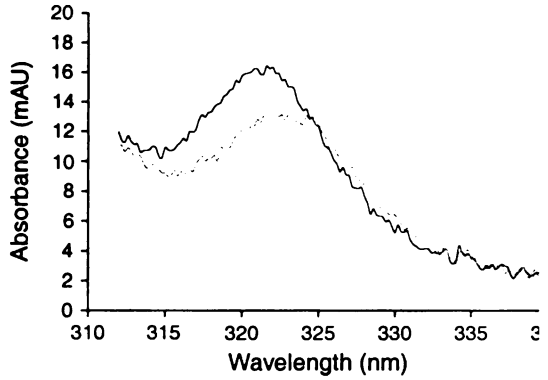

Figure 5.6: cis-Parinaric Acid's Spectra Change upon PPARγ Binding

The UV spectrum of CPA shifts upon binding to hPPARγLBD. The UV spectra for CPA alone (500 nM) (black) and CPA (500 nM) with 2.5 μM hPPARγLBD relative to a reference cuvette with 2 μM LBD but no CPA (gray) are superimposed.

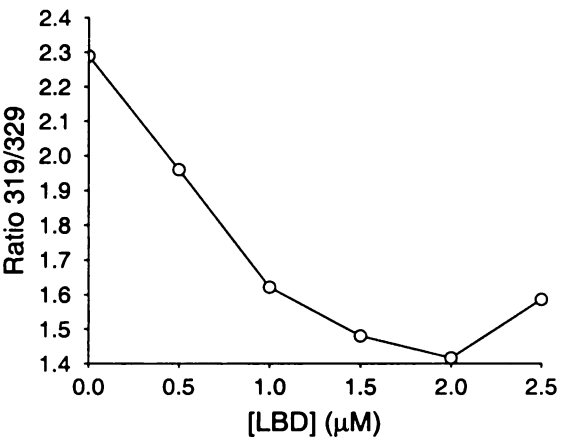

Figure 5.7: Spectrophotometric Data

Increasing concentrations of hPPARγLBD were added to 500 nM CPA and the absorption ratio of 319 nm/ 329 nm was determined relative to a reference cuvette with the same additions of LBD but without CPA. These experiments showed poor reproducibility and erratic results, presumably due to the poor signal to noise observed in the spectra (Figure 5.6).

from three independent experiments were plotted against the total LBD concentration (Figure 5.4). These experiments showed good reproducibility along with the expected curve shape.

The intrinsic protein fluorescence was subtracted and the CPA fluorescence was replotted against the total LBD concentration (Figure 5.5). All three sets of data were fit collectively using the EXCEL Solver function and Equation 5.5, an equation for a single binding site derived in the Experimental Procedures section. The published K_d for PPARγ binding of CPA of 670 ± 70 nM was used as a constraint (228). This fit gave a concentration of 350 μM or 11 mg/mL for the LBD stock solution. This concentration would indicate a yield of 19.5 mg/L of active hPPARγLBD.

We next attempted to reproduce the spectral shift of CPA reported by Palmer (228). The absorption spectrum between 312 and 340 nm was measured for 500 nM CPA relative to a buffer blank and for 500 nM CPA and 2.5 μM LBD relative to a 2.5

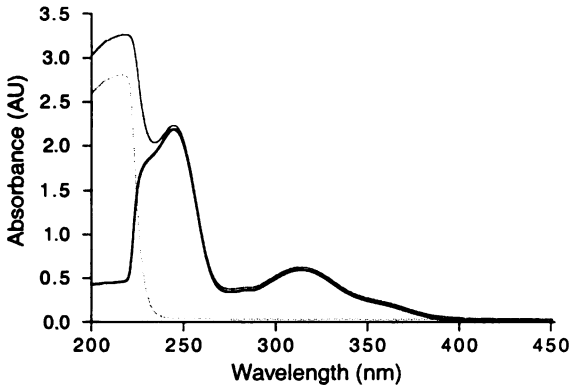

Figure 5.8: Rosiglitazone UV Spectrum

The absorbtivity of DMSO (light gray), rosiglitazone and DMSO (dark gray) and the subtracted rosiglitazone absorbtivity (black) are plotted. The second rosiglitazone peak overlaps with the spectral region used in the CPA Spectrophotometric binding assays, as well as the 318 nm excitation wavelength used in the CPA Fluorescence binding assays.

μM LBD blank (Figure 5.6). This data showed the reported spectral change, but the signal-to-noise ratio was poor.

We attempted to generate a binding curve similar to those reported by Palmer (228), but did not obtain reproducible results, presumably due to the high levels of noise in the spectra. One experiment, the data most similar to the reported binding curve, is shown in Figure 5.7. Increasing LBD concentrations were added to both a sample cuvette with 500 nM CPA and a reference cuvette with buffer alone. After measuring the absorbance spectrum between 312 and 340 nm, the ratio of absorbance at 319/329 nm was calculated and plotted against the protein concentration (Figure 5.7).

The spectrophotometric binding assay was also hindered by the absorbance of rosiglitazone and its derivatives in the required spectral range. While addition of rosiglitazone to the reference cuvette can in theory correct for this, pippeting error along with the proportionately high levels of rosiglitazone absorption in the region (Figure 5.8), relative to that observed for CPA at the concentration used in these assays, produced extremely large error and variability when attempting to measure competitive binding of rosiglitazone with CPA.

Another option for determining the binding constants of the ligands, not reported by Palmer, is the competitive binding with CPA monitored by the CPA fluorescence. As

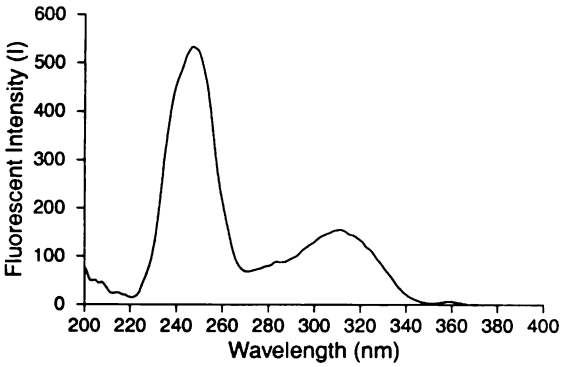

Figure 5.9: Rosiglitazone Fluorescence (Excitation)

The fluorescence intensity of rosiglitazone (1.1 μM) at 410 nm, the emission wavelength used in the CPA fluorescence binding assay, was monitored as a function of excitation wavelength. The observed excitation spectrum is similar to the UV absorption spectrum shown in Figure 5.8.

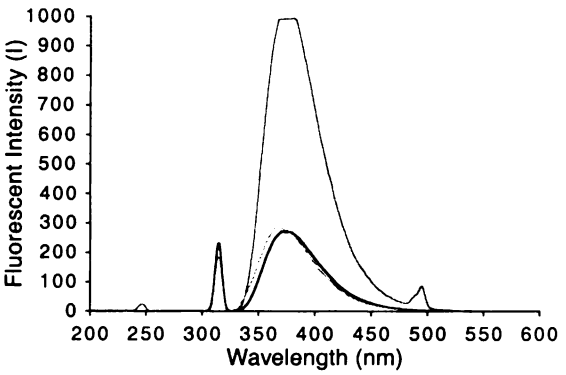

Figure 5.10: Rosiglitazone Fluorescence (Emission)

The fluorescence emission spectrum of rosiglitazone (1 μM) was scanned with excitation at 245 nm (dark gray), 314 nm (black), or 314 nm with 2 μM hPPARγ LBD (light gray). The fluorescence of DMSO (vehicle) was subtracted from each spectrum. The observed emission spectrum overlaps with the 410 nm emission wavelength used in the CPA fluorescence assay.

CPA fluoresces only when bound in a hydrophobic environment, displacement of bound CPA by other ligands would produce a measurable change in the fluorescent intensity. This appears to be more desirable based on my experiments because of the increased signal-to-noise observed in the fluorescence assay relative to the spectrophotometric alternative. Because of rosiglitazone's absorption at the excitation wavelength used in the fluorescence assays, I checked to see if rosiglitazone showed fluorescence that would interfere with the CPA fluorescent binding assay. The fluorescent intensity at 410 nm, the emission wavelength used in the CPA assay, was monitored at excitation wavelengths between 200 and 400 nm (Figure 5.9). This spectrum showed similar structure to the rosiglitazone absorption spectrum (Figure 5.8). The fluorescent intensity between 200 and 600 nm was measured with rosiglitazone and an excitation wavelength of 245 or 314 nm, the maxima observed in the excitation scan, and rosiglitazone with LBD and an excitation wavelength of 314 nm (Figure 5.10). Each

of these excitation wavelengths showed significant fluorescent emission in the region used in the CPA assays.

There was no significant shift in the fluorescence properties of rosiglitazone in the presence of LBD, relative to buffer alone.

Discussion

This study began with attempts to reproduce the binding assay of Palmer (228). While I was able to get good yields of pure protein, I was not able to develop a working binding assay for the evaluation of the binding of rosiglitazone derivatives to PPARγ.

The use of the AKTA Explorer protein purification system equipped with the TALON column offered improved yield and purity relative to nickel-agarose column used by Palmer (228). As the wash fraction contained a substantial quantity of pure PPARγ-LBD, in future purification attempts I would suggest a lower concentration of imidazole for the washing step. The affinity of the His-tagged hPPARγLBD is likely to be lower for the cobalt column than for the nickel, because the support for the cobalt column takes an additional two coordination sites, reducing the sites available for binding the his tag region of the protein construct.

An ultracentrifugation step after concentration of the combined fractions was used to remove any aggregation present in the purification. If the higher molecular weight bands are aggregate as expected this would result in relatively pure protein. The resulting protein is quite pure, and if further purification was required for crystallography studies, a sizing column would likely get the protein pure enough to attempt crystallization if desired (244).

We were able to reproduce the CPA hPPARγLBD fluorescence binding assay reported by Palmer. This experiment gave good signal-to-noise and fit nicely to an equation for a single binding site. This experiment provides a simple measure of the active protein concentration when the reported binding constant of 670 nM for CPA is used as a constraint. In future experiments the Kaleidograph Version 3.08d curve fitting algorithm could be used for fitting the data, which would allow the determination of the error of the fit.

We did not observe adequate signal-to-noise in the spectrophotometric CPA binding experiment reported by Palmer (228) for the assay to be useful in evaluating ligands. Because both the free and PPARγ bound CPA spectra overlap, the protein concentration needs to be kept above the CPA concentration to ensure that the majority of CPA is bound before competitive displacement by candidate ligands. Because of this constraint, increasing the CPA concentration to give higher absorbance levels would require increasing the protein concentration. Increasing the protein concentration in turn would reduce the sensitivity of the binding assay. For this reason, increasing the CPA concentration is not a useful solution to the signal-to-noise problems of this assay.

A second option, which I did not attempt, is to use a smoothing algorithm to reduce the apparent signal-to-noise of the spectrum when calculating the ratio of the absorbance at different peaks. A third way to reduce the error would be by repeating the experiment and obtaining additional points to improve the statistics on the curve fit.

As the fluorescence binding experiment gives better signal-to-noise than the spectrophotometric data, an alternative competitive binding experiment could take advantage of the difference in fluorescent properties of CPA in solution and bound to

PPARγ. Unfortunately, the spectral properties of rosiglitazone and its derivatives interfere with both the spectrophotometric and fluorescent CPA binding assays. As testing the binding of my rosiglitazone derivatives was my primary motivation for finding a working binding assay, I did not pursue CPA binding assays further. They would still be a convenient method for evaluating the PPARγ binding of ligands whose spectral properties do not interfere with the spectral properties of CPA.

The fluorescent and spectral properties of rosiglitazone were not affected by binding to PPARγ, and do not provide an alternate fluorescent or spectral probe for ligand binding. The most promising binding assay system for the evaluation of the rosiglitazone derivatives left at this point is a competitive binding assay with radiolabeled rosiglitazone. The most common method reported in the literature is the use of tritiated rosiglitazone. While the synthetic route for rosiglitazone ends with a reduction, the conditions used in this reduction are not suitable for tritiation with the equipment available to us at this time. If tritiated rosiglitazone were obtained, the described hPPARγLBD expression and purification method would provide a convenient and easy method of LBD preparation for the binding assay.

Chapter 6: Serum Albumin Inhibits Induction of Peroxisome Proliferator-Activated Receptor-γ by 15-deoxy-$\Delta^{12,14}$-Prostaglandin J_2

By binding $15dJ_2$, serum albumin lowers the free concentration of $15dJ_2$ available to activate PPARγ. This results in an observed inhibition of $15dJ_2$ induction of PPARγ. This inhibitory effect can be released by heat treatment of the serum at 80°C for 20 minutes without eliminating the lipid toxicity prevention afforded by serum. Albumin is also likely to bind the high affinity endogenous agonist and may be an important regulator of PPARγ function *in vivo*.

Introduction

Peroxisome proliferator-activated receptors (PPARs) are ligand-inducible transcription factors that belong to the nuclear receptor superfamily (for reviews see 8, 239). There are three different subtypes (α, β/δ/NUC1, and γ), each with distinct ligand specificities and expression patterns. In humans, PPARγ is expressed mainly in brown and white adipose tissue, but is also present in the intestine, skeletal muscle, liver, heart, bone marrow stromal cells, placenta, and spleen (8, 43). PPARγ is the major regulator of adipocyte differentiation, and is also important in glucose and lipid metabolism.

The antidiabetic drugs known as thiazolidinediones are some of the highest affinity synthetic activators of PPARγ. Rosiglitazone (BRL 49653, Avandia™) (Figure 6.1) was the first identified high affinity-PPARγ ligand, and is still one of the most potent ligands, with a K_d of 43 nM, and an EC_{50} of 80 nM for PPARγ-mediated activation of reporter genes controlled by a PPARγ response element (50).

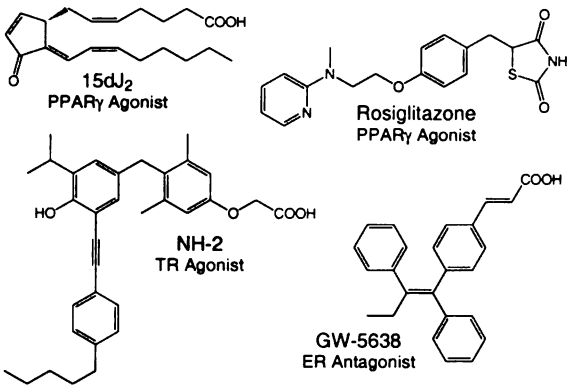

Figure 6.1: Ligand Structures

The chemical structures of ligands discussed in this chapter are shown. $15dJ_2$, an endogenous PPARγ agonist, was purchased from Cayman Chemical Co. Rosiglitazone, a PPARγ agonist, was synthesized as described in Chapter 2. NH-2, a TR agonist, was synthesized and tested by Ngoc-Ha Nguyen. GW-5638, an ER antagonist, was synthesized and tested by Ross Weatherman.

Several natural compounds including metabolites found in oxidized low-density lipoproteins, long chain fatty acids, and the prostaglandin $15dJ_2$ (Figure 6.1), have been proposed as endogenous activators of PPARγ (51, 59, 74, 75, 77, 78). Of these, 15-deoxy-$\Delta^{12,14}$-prostaglandin J_2 ($15dJ_2$) is the most potent natural activator with a EC_{50} of 2 μM for PPARγ-mediated activation of reporter genes controlled by a PPARγ response element and a K_i for competitive binding with rosiglitazone of 2.5 μM (77). While no ligands have conclusively been shown to be an *in vivo* activator of PPARγ, it is reasonable to assume that $15dJ_2$ or structurally similar compounds or metabolites are endogenous *in vivo* activators of PPARγ.

Albumin is the major protein component of human blood, present at about 40 mg/mL (for reviews see 203, 204, 205). While often regarded as a generic stabilizing protein, it has been shown to play many diverse roles. It is a major contributor to the osmotic blood pressure and is involved in the maintenance of blood pH. It binds many fatty acids and small molecules with affinities of 100 nM to 100 μM, plays a major role in the transport of fatty acids that would otherwise be insoluble, and protects cells from polyunsaturated fatty acid induced injury (124, 125). It is involved in the degradation of some prostaglandins and the stabilization of others (79, 80, 219, 220, 245, 246). In fact,

$15dJ_2$ was first reported as an *in vitro* degradation product of prostaglandin D_2 incubated with plasma or serum albumin (79, 80).

In this study I report that serum albumin inhibits $15dJ_2$ induction of PPARγ in *in vitro* EP-JEG cell assays by sequestering $15dJ_2$ in the media making it unavailable for binding to and activation of PPARγ.

Experimental Procedures

Reagents

Unless otherwise specified, all chemicals were obtained from Fisher Scientific (Pittsburgh PA) or Sigma-Aldrich (St. Louis MO). $15dJ_2$ was purchased from Cayman Chemical Company (Ann Arbor MI). Rosiglitazone was synthesized as described in Chapter 2. GW-5638 and NH-2 (Figure 6.1) were synthesized by Ross Weatherman and Ngoc-Ha Nguyen according to their protocols. All forms of bovine serum albumin (BSA) and human serum albumin (HSA) were purchased as powders, dissolved in calcium and magnesium free PBS, and then sterile filtered to give a 500 μM stock solution. Fetal Bovine Serum (FBS) was obtained from Hyclone (Logan UT) or Omega Scientific (Tarzana CA), and Human Male AB Serum was obtained from Omega Scientific. Human sera were collected and analyzed by Leslie Waite according to the Taylor Lab protocols.

Cell Culture

EP-JEG (43) and HeLa cells were cultured at 37°C with 5% CO_2 in Eagle's minimal essential medium with Earle's balanced salt solution (MEM Earle's BSS) containing 10% FBS, penicillin (100 U/mL), and streptomycin (100 μg/mL). Cells were

passaged no more than 10 times after being thawed from a common stock. HeLa cells used in estrogen and thyroid hormone receptor assays were cultured according to the protocols of Ross Weatherman and Ngoc-Ha Nguyen respectively.

EP-JEG Cell Assays

EP-JEG cells were washed with phosphate buffered saline (PBS), incubated with a minimal volume of standard trypsin and versene (STV) for 4 minutes at room temperature, then washed off the plates using media. After counting cells using a hemacytometer, cells were pelleted at 1000g for 3 minutes. Cells were then resuspended in fresh media, and plated onto 12-well plates at a density of $8x10^4$ cells per well. After overnight incubation, cells were washed with PBS, and then treated in triplicate for 24 hours with media containing the specified concentrations of $15dJ_2$, rosiglitazone, or 0.1% vehicle and serum or albumin preparations as specified for each experiment. Rosiglitazone was delivered in dimethyl sulfoxide (DMSO). $15dJ_2$ was delivered in either ethanol or DMSO. I observed no difference in activity among ethanol, DMSO, or media alone (data not shown).

HeLa Transient Transfection Assays

HeLa cells (2 million cells / cuvette) were suspended in electroporation buffer (calcium and magnesium free PBS, 0.1% glucose, 0.01% Biobrene) with pCI-hPPARγ (1 μg / million cells), a CMV driven human PPARγ2 expression plasmid, and tk-$PPRE_3$-LUC (2.5 μg / million cells), a synthetic peroxisome proliferator response element (PPRE) driven luciferase reporter gene. Cells were then electroporated in BioRad (Hercules, California) Gene Pulser Cuvettes (cat# 165-2088, 4 mm electrode gap) using a

BioRad Gene Pulser (0.35V, 960 μFD, 200 Ω). Electroporated cells were promptly resuspended in media and plated into 12-well plates (1.5-2 plates / cuvette). Cells were allowed to attach for 2-4 hours before media was aspirated. Cells were then rinsed with PBS and treated in triplicate for 24 hours with media containing the specified concentrations of $15dJ_2$, rosiglitazone, or 0.1% vehicle and serum or albumin preparations as specified for each experiment. Rosiglitazone was delivered in DMSO. $15dJ_2$ was delivered in either ethanol or DMSO. I observed no difference in activity among ethanol, DMSO, or media alone (data not shown).

Luciferase Activity Assay

Cleared cell lysates were analyzed using a luciferase reporter gene assay (Roche #1 814 036, Indianapolis IN). Briefly, EP-JEG cells were washed with 1 mL of PBS and then lysed with 100 μL of the supplied lysis buffer at room temperature for 15 minutes. HeLa cells were lysed under the same conditions followed by a freeze-thaw cycle and scraping using a rubber policeman.

The lysate was used to wash wells and was then transferred to microcentrifuge tubes and cleared for 6 minutes at maximum speed. 50 μL of the cleared lysate was analyzed for luciferase activity. An aliquot of the cleared lysate was used to determine protein concentration. This was done using the BCA (bicinchoninic acid) Protein Assay (Pierce #23225, Rockford IL). After subtraction of the luciferase activity observed in lysis buffer alone, the luciferase activity was normalized to the protein concentration before averaging and calculation of relative activation as described in the text.

Both cotransfected Promega (Madison WI) dual-luciferase and β-galactosidase (β-gal) were tried as controls for transient transfections in HeLa cells, but resulted in

larger error than the uncorrected data, while normalization to total protein improved the data.

Serum Heat Treatment

Serum was heat treated immediately prior to use by placing serum in a sterile douncer tissue grinder in an 80°C water bath for 20 minutes. Bovine serum remained liquid during this heat treatment, while human serum solidified, resembling a hard-boiled egg. Two or more volumes of media were added to assist in homogenizing and suspending the solids, which were then diluted to a final concentration of 10% in media.

Cell Growth and Toxicity Assay

EP-JEG and HeLa cells were plated into 12 well plates as described above. After allowing cells to attach for 2 hours, the media was removed and cells were washed with PBS before treatment in triplicate with media containing 10% FBS, 10% heat treated FBS, or no serum. The same media formulations were also tested with 1 μM $15dJ_2$ to check for relative ligand toxicity. After 2 hours, 1 day, or 2 days cells were washed twice with PBS to remove loose cells, and incubated with 200 μL of trypsin at room temperature for 3 minutes. Cells were washed off plates with 800 μL of media containing FBS, pelleted in a microcentrifuge for 3 minutes, resuspended in 100 μL of media, and then counted in a hemacytometer.

High Performance Liquid Chromatography

Reverse phase high performance liquid chromatography was performed using Rainin (Emeryville CA) HPXL Pumps, an Altech (Deerfield IL) Nucleosil 100 (C18) 10u 4.6x250 mm column with a 7.5 mm guard column, and a Varian (Walnut Creek CA)

ProStar 330 Photo Diode Array Detector controlled by a Varian Star Chromatography Workstation. The mobile phase was composed of Fisher HPLC grade water and acetonitrile with 0.1% trifluoroacetic acid (TFA) at a flow rate of 1 mL/min.

For the binding assay the column was equilibrated in water for at least 4 minutes before samples were loaded. Samples, dissolved in PBS, were injected using a 500 µL sample loop and run in a mobile phase of water for 5 minutes, ramped linearly over a period of 30 minutes to 100% acetonitrile, followed by 100% acetonitrile for 10 minutes. Progress was monitored at 306 nM. Under these conditions $15dJ_2$ elutes at approximately 33.2 minutes with a peak width of 10 seconds.

For the serum extraction assay the column was run under isocratic conditions at 70% acetonitrile. The column was equilibrated for at least 5 minutes before samples, dissolved in 70% acetonitrile, were loaded. Progress was monitored at 306 nM. Under these conditions $15dJ_2$ elutes at approximately 8.5 minutes and the internal standard of nitrobenzene elutes at approximately 5.2 minutes.

Albumin Binding Assays

A fixed concentration of 2 µM $15dJ_2$ was incubated overnight at 4°C with a range of concentrations of albumin (1 nM to 100 µM) in calcium and magnesium free PBS with a total volume of 400 µL. The incubations were transferred to Microcon 30K cutoff Centrifugal Filter Devices and spun in an Eppendorf (Hamburg, Germany) 5417C microcentrifuge for 12 minutes at full speed to separate $15dJ_2$ free in solution from the albumin-bound fraction. The flow-through was stored at –80°C until 10 minutes before injecting 250 µL into the HPLC. Observed peak areas were converted to concentrations using a calibration curve generated by passing $15dJ_2$, at concentrations ranging from 50

Equation 6.1

$$K_d = \frac{P_f \bullet L_f}{PL}$$

Equation 6.2

$$L_f^2 + (P_T - L_T + K_d)L_f - K_d L_T = 0$$

Equation 6.3

$$L_f = \frac{-(P_T - L_T + K_d) + \sqrt{(P_T - L_T + K_d)^2 + 4K_d L_T}}{2}$$

nM to 2 μM in calcium and magnesium free PBS in the absence of albumin, through the same protocol.

To accurately fit the experimental data I derived an equation for a single binding site allowing for conditions where the total ligand (L_T) rather than the total protein (P_T) is held constant, while allowing for depletion of both the free protein (P_f) and free ligand (L_f). Starting with the equation for dissociation (Equation 6.1) I substituted for free protein using the expression $P_T = P_f + PL$, where PL is the concentration of the protein-ligand complex. I then substituted for bound complex using the expression $L_T = L_f + PL$. After rearrangement, this gives a quadratic equation (Equation 6.2), which can be solved for free ligand (Equation 6.3) and then fit to the experimental data using the Kaleidagraph Version 3.08d curve fitting algorithm.

Serum Extraction

The serum extraction protocol was generated by adaptation of a published serum extraction protocol used to identify $15dJ_2$ as a metabolite of radiolabeled PGD_2 in serum (79). Test tubes containing 3 mL of PBS, 10% serum in PBS, or 50 μM BSA in PBS

with 13 μM $15dJ_2$ were covered with Parafilm™ and incubated for 24 hours in a tissue culture incubator (5% CO_2, 37°C). The incubations were then acidified to below pH 4 by adding 20 μL of formic acid (pK_a = 3.75), and extracted three times with 5 mL of ethyl acetate. The albumin and serum incubations produced significant amounts of precipitate and sticky emulsion, which complicated the extraction and likely led to some loss of material. The extracts were then washed with 5 mL of brine, and evaporated under reduced pressure. Samples were dissolved in 200 μL of HPLC running solvent (70% acetonitrile), 100 μL of which was mixed with 5 μL of 1:1000 nitrobenzene in ethanol as an internal standard and quantified by HPLC.

Ligand Heat Treatment

Serum from a common stock was divided into two 1.3 mL fractions, one of which was heat treated at 80°C for 20 minutes and homogenized using a douncer tissue grinder. The untreated and heat-treated sera were divided into 0.3 mL aliquots to which either 10 μM $15dJ_2$ or 1% DMSO was added (1 μM and 0.1% upon dilution in media). After overnight incubation (37°C) of all aliquots, half of the aliquots (one of each preparation) were again heat treated at 80°C for 20 minutes, while the other half were left untreated. All of the serum preparations were diluted to 3 mL (10%) in serum free tissue culture media, and the heat-treated aliquots were homogenized using a douncer tissue grinder. Media preparations were then incubated with cells as described above.

NH-2 and GW-5638 Experiments

NH-2 and GW-5638 (Figure 6.1) were assayed by Ngoc-Ha Nguyen and Ross Weatherman respectively according to their protocols.

Statistics

Data were derived from multiple independent experiments and are presented as means ± standard deviation of triplicate points. Comparisons among different treatments were analyzed using the Statview 2.0 repeated measures ANOVA function with Fisher post hoc tests and statistically significant differences were accepted at $p < 0.05$.

Results

Serum Inhibits $15dJ_2$ Induction of PPARγ

This study began with an observation from the Taylor lab that serum from pregnant women increases PPARγ expression and induction in both transiently transfected JEG-3 cells and EP-JEG cells (43). While further characterizing the activity of the pregnancy serum they found that human male and both pregnant and non-pregnant female sera, as well as fetal bovine serum, contain a factor(s) that reduces the level of PPARγ induction by $15dJ_2$. To characterize this inhibitory response I have used two cell assay systems. EP-JEG cells (43) are a JEG-3 derived cell line containing a synthetic PPRE driven luciferase reporter. Both JEG-3 and EP-JEG cells express high levels of endogenous PPARγ making them useful for studying native regulation of PPARγ. HeLa cells do not contain detectable levels of PPARγ, and were transiently transfected with both receptor and reporter plasmids.

I first looked at varying serum levels to determine their effects on the luciferase reporter. EP-JEG cells were treated with 1 μM $15dJ_2$ and serum levels ranging from 0 to 10%. At low serum concentrations, below 1%, I observe between 150 and 700 fold induction by $15dJ_2$, a substantial increase over the 2-15 fold induction seen in higher

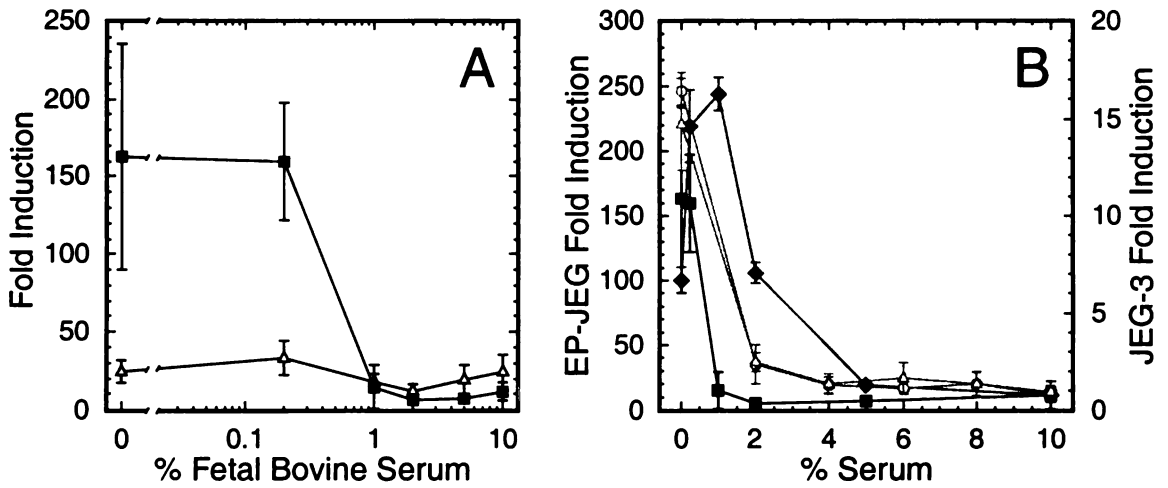

Figure 6.2: Serum Titration

(A) EP-JEG cells were incubated with media containing 1 μM $15dJ_2$ (closed squares) or 1 μM rosiglitazone (open triangles) and the indicated amount of FBS. (B) EP-JEG cells were incubated with media containing 1 μM $15dJ_2$ and the indicated amount of bovine (closed squares) or human male (closed diamonds) sera are reported on the left axis. Data collected by Leslie Waite in transiently transfected JEG-3 cells with 1 μM $15dJ_2$ and the indicated amount of non-pregnant (open triangles) or pregnant (open circles) human female sera are reported on the right axis. Fold induction was calculated relative to 10% serum with 0.1% vehicle.

concentrations of serum (Figure 6.2). Both pregnant and non-pregnant human female sera, tested by Leslie Waite in transiently transfected JEG-3 cells, reduced induction from approximately 15-fold down to approximately 2-fold (Figure 6.2B). All forms of serum tested demonstrated the ability to inhibit $15dJ_2$ induction (Figure 6.2B). In contrast, the induction by rosiglitazone was not affected by the serum concentration (Figure 6.2A).

To investigate the properties of the factor(s) in serum responsible for inhibiting $15dJ_2$ induction I investigated the effect of two heat treatments on the activity of serum. Heat treatment of 56°C for 30 minutes is commonly used to inactivate complement and prepare serum for use in cell culture. A more rigorous heat treatment of 80°C for 20 minutes is suggested for heat inactivation of some heat resistant restriction endonucleases. I incubated EP-JEG cells with 1 μM $15dJ_2$, 1 μM rosiglitazone, or 0.1% vehicle and FBS, FBS treated at 56°C for 30 minutes, or FBS treated at 80°C for 20 minutes. Heat treatment at 56°C for 30 minutes showed a similar level of induction to

Figure STYLEREF 1 \s 6. SEQ Figure * ARABIC \s 1 3: Serum Heat Treatment

EP-JEG cells or transiently transfected HeLa cells were incubated with media containing 0.1% (v/v) vehicle alone (white), 1 _M 15dJ2 (black), or 1 _M rosiglitazone (hatched) and the indicated preparation of FBS. Fold induction was calculated relative to 10% FBS with 0.1% vehicle.

that of untreated serum, while the inhibition of $15dJ_2$ induction is absent when serum is treated at 80°C for 20 minutes (Figure 6.3). Rosiglitazone induction was unaffected by heat treatment of the serum, which is consistent with the unchanged induction levels observed in the serum titration (Figure 6.2). Heat-treated serum allowed induction at similar levels to the induction by 15dJ2 in serum free media.

To see if this was a general effect not limited to the endogenous response of EP-JEG and JEG-3 cells I incubated transiently transfected HeLa cells with 1 _M 15dJ2, 1 _M rosiglitazone, or 0.1% vehicle and FBS or FBS treated at 80°C for 20 minutes. Heat treatment of serum showed a moderate increase in the induction by 15dJ2, and had no effect on the rosiglitazone induction (REF _Ref498423638 \h Figure 6.3). While not as strong an effect, this experiment also showed an inhibition of 15dJ2 induction.

From this point I use the term heat-treated FBS (HTFBS) to refer to serum heated at 80°C for 20 minutes.

To see if the observed differences in 15dJ2 induction could be accounted for by changes in cell growth I evaluated cell growth and ligand toxicity in EP-JEG and HeLa cells. Cells were incubated in media either with or without 1 _M 15dJ2 and with FBS, HTFBS, or no serum. The number of attached cells was quantified as a function of time. After two days no significant differences were observed in the growth rate of EP-JEG or

HeLa cells treated with FBS or HTFBS, HeLa cells treated with serum free media showed decreased cell growth, and EP-JEG cells treated with serum free media showed no significant growth. After two days of treatment with 1 _M 15dJ2, cells treated with FBS showed comparable growth to cells treated with FBS and no ligand. After two days treatment with 1 _M 15dJ2 in HTFBS I observed no increase in the number of attached cells and a substantial number of detached dead cells, while treatment with 1 _M 15dJ2 and serum free media showed almost no surviving cells after two days (REF _Ref498424562 \h Figure 6.4). The observed decrease of cell growth in either serum free or HTFBS media containing 1 μM $15dJ_2$ would lead to lower rather than increased induction in those media preparations.

Identification of Serum Factor

The heat treatment experiment suggests that a serum protein(s) with thermal stability between 56°C and 80°C is responsible for inhibition of $15dJ_2$ induction of PPARγ. Albumin, the most plentiful serum protein, has a reported thermal stability of

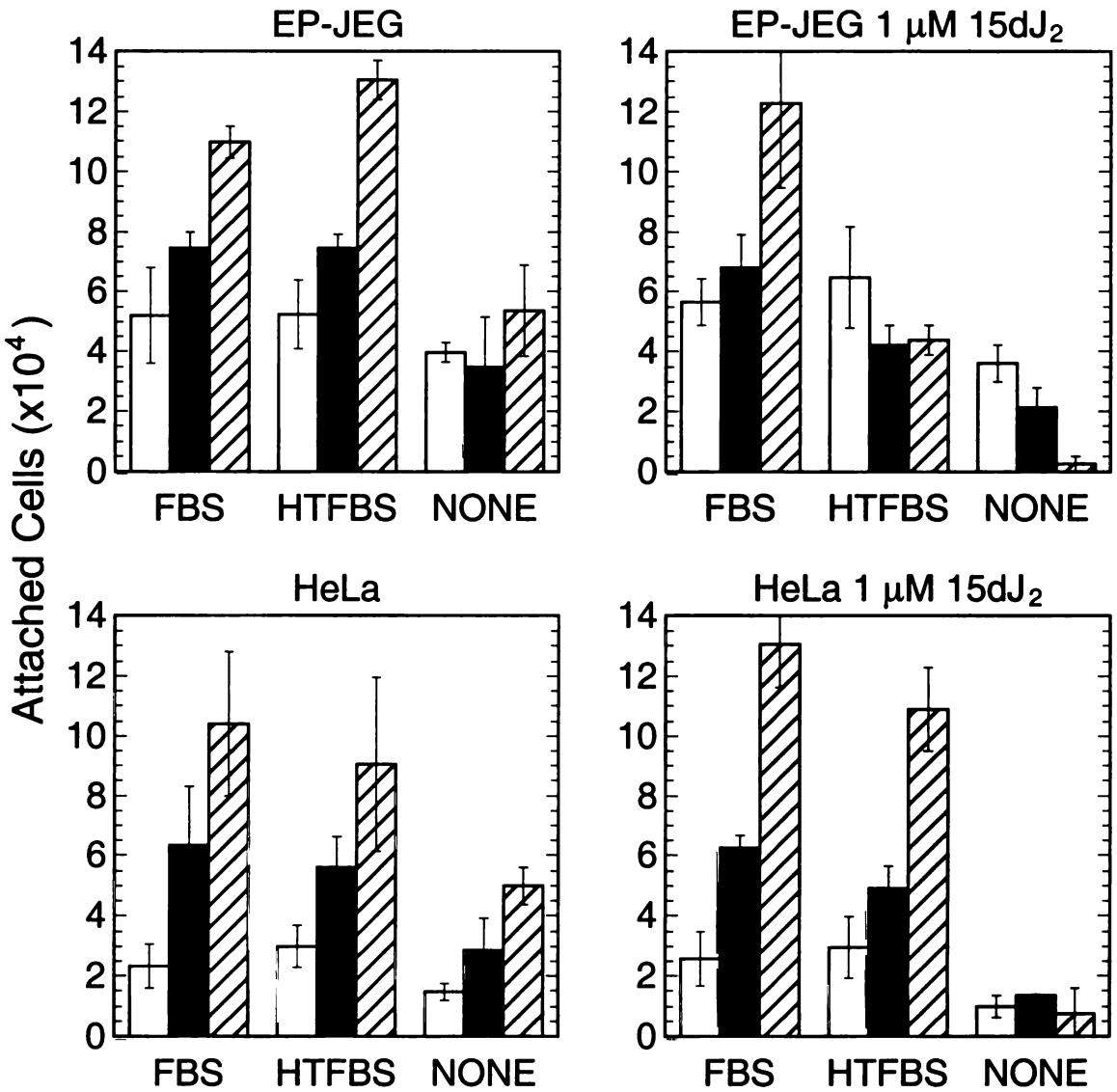

Figure 6.4: Cell Growth

EP-JEG or HeLa cells were treated with media containing untreated FBS, HTFBS, or no serum and either no ligand or 1 μM $15dJ_2$. Attached cells, in ten thousands, were counted after 2 hours (white), 1 day (black), or 2 days (hatched).

60-65°C (247), consistent with the thermal stability observed in the heat treatment experiment, and is reported to catalyze the formation of $15dJ_2$ from prostaglandin D_2 (PGD_2) *in vitro* (79, 80). Knowing that albumin interacts with $15dJ_2$ as the product of a catalytic reaction, I looked to see if albumin had a role in the serum inhibition of$15dJ_2$ induction. I treated EP-JEG cells with $15dJ_2$ and one of four commercial preparations of

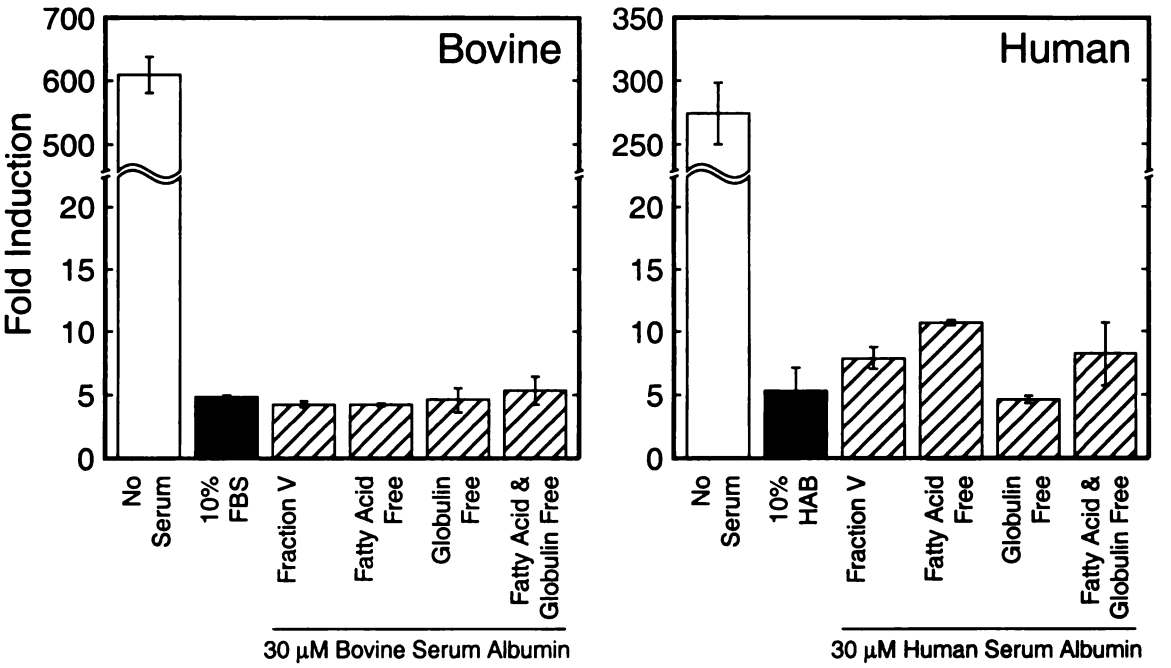

Figure 6.5: Albumin Screen

EP-JEG cells were incubated with media containing 1 µM $15dJ_2$ and either no serum (white), 10% serum (black), or 30 µM of the indicated preparation of albumin (hatched). Fold induction was calculated relative to 10% serum with 0.1% vehicle.

BSA at 30 µM, a concentration comparable to the albumin content of 10% FBS, as reported in the manufacturer's analysis. Both serum-free media, and media with 10% FBS were included as controls. Each BSA preparation reduced the $15dJ_2$ induction to a level comparable to that of 10% FBS (Figure 6.5). In a separate experiment, 30 µM human serum albumin also inhibited $15dJ_2$ induction to levels similar to its serum control (Figure 6.5).

To determine if albumin inhibits $15dJ_2$ induction in a dose-dependent manner similar to that seen for serum, I treated EP-JEG cells with 1 µM $15dJ_2$, 10% HTFBS, and BSA Fraction V levels ranging from 0 to 38 µM. BSA was able to inhibit $15dJ_2$ induction in a dose-dependant manner with an IC_{50} of approximately 2 µM (Figure 6.6).

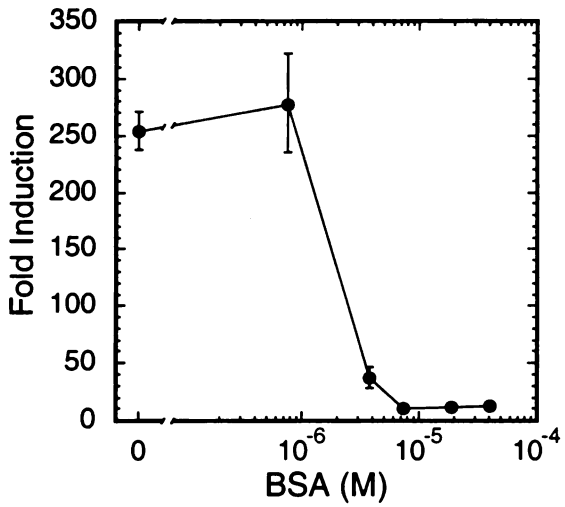

Figure 6.6: Albumin Titration

EP-JEG cells were incubated with media containing 1 μM $15dJ_2$, 10% HTFBS, and the indicated concentrations of BSA Fraction V. Fold induction was calculated relative to 10% HTFBS, 30 μM BSA Fraction V and 0.1% vehicle.

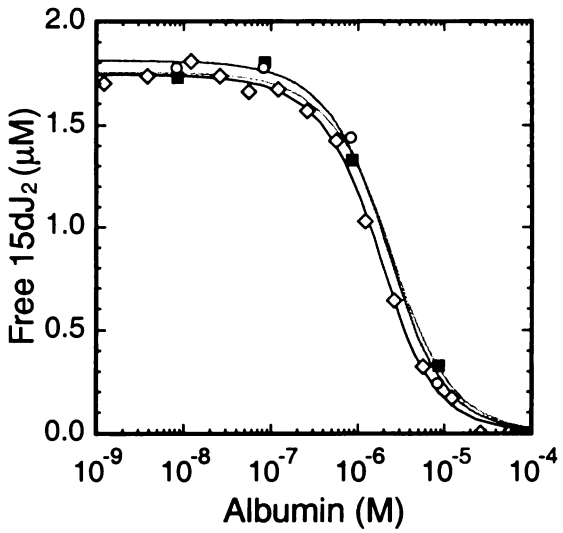

Figure 6.7: Albumin Binding

The concentration of free $15dJ_2$ was measured after incubation of 2 μM $15dJ_2$ with the indicated range of BSA Fraction V (open diamonds, black fit), HSA Fraction V (open circles, dark gray fit), or Glycated HSA (closed squares, light gray fit) as described in Experimental Procedures. Curve fits for single binding sites give K_ds of 870 ± 70 nM, 1.2 ± 0.2 μM, and 1.5 ± 0.3 μM respectively.

These results suggest that serum albumin is responsible for the inhibition of $15dJ_2$ induction of PPARγ. To determine if albumin interacted directly with $15dJ_2$ I incubated 2 μM $15dJ_2$ with BSA Fraction V (concentrations ranging from 1 nM to 100 μM) and isolated free ligand as described in Experimental Procedures. HPLC analysis showed an albumin concentration-dependent reduction in the free $15dJ_2$ concentration (Figure 6.7). Both HSA and glycated HSA showed comparable reductions in free $15dJ_2$ concentration (Figure 6.7). This result suggests that albumin interacts directly with $15dJ_2$.

I next asked whether albumin was simply binding $15dJ_2$, sequestering it from media, or whether albumin is responsible for chemically transforming $15dJ_2$ into an inactive metabolite. To distinguish between catalytic and binding activity I first tested the reversibility of albumin's effect on $15dJ_2$ induction. EP-JEG cells were treated with

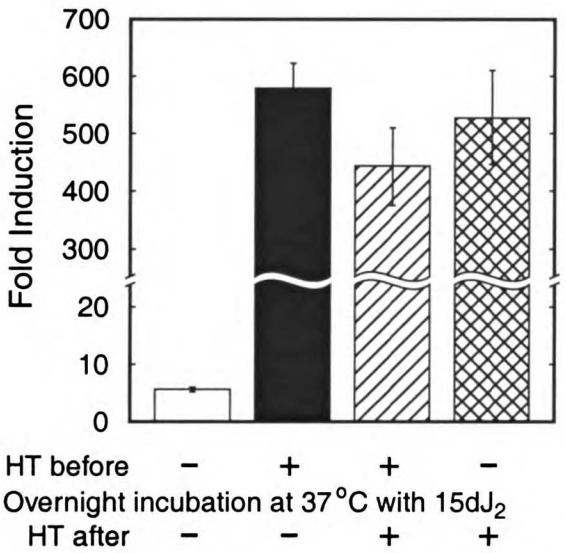

Figure 6.8: Ligand Heat Treatment

$15dJ_2$ was added to either untreated FBS or heat treated FBS to a concentration of 10 μM and incubated overnight at 37°C, after which it was either left untreated or heat treated. These serum preparations were diluted 10-fold into media giving a final serum concentration of 10% and $15dJ_2$ concentration of 1 μM. Fold induction was calculated relative to 0.1% vehicle in untreated serum.

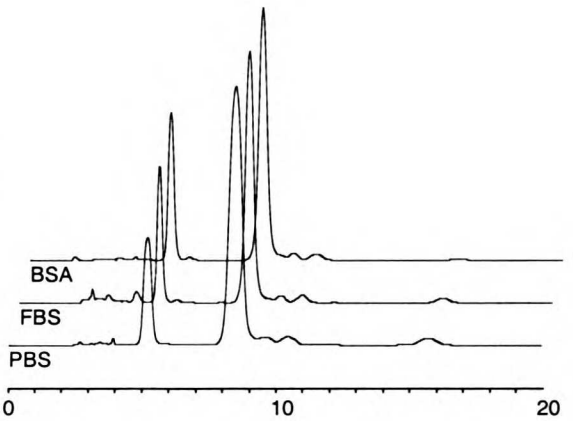

Figure 6.9: Ligand Decomposition

13 μM $15dJ_2$ was incubated in PBS, 10% FBS, or 50 μM BSA overnight at 37°C. The incubation was then acidified, extracted, and analyzed by HPLC. Absorbance was monitored at 306 nM. An internal standard of nitrobenzene elutes at 5.2 minutes, and $15dJ_2$ elutes at 8.5 minutes.

specific serum and ligand preparations as indicated. First, cells were treated with the controls of $15dJ_2$ incubated overnight at 37°C in untreated serum (white) or HTFBS (black). Heat treatment at 80° for 20 minutes after overnight incubation of $15dJ_2$ in HTFBS (hatched) showed comparable levels of induction suggesting that $15dJ_2$ is thermally stable under these conditions. Heat treatment after overnight incubation of $15dJ_2$ in untreated FBS also showed comparable levels of induction (Figure 6.8). If albumin's interaction with $15dJ_2$ resulted in an irreversible change, such as chemical transformation or covalent attachment to albumin, I would expect that heat treatment after incubation with FBS would be unable to recover the high induction seen in the

experiment. As $15dJ_2$ induction is unaffected after overnight incubation with FBS, I conclude that albumin's interaction with $15dJ_2$ is reversible.

A more direct measure of whether $15dJ_2$ is chemically modified by albumin is to look for ligand decomposition using HPLC. I used a published serum extraction protocol (79) followed by HPLC analysis monitored at 306 nM. I observed no detectable shift in the observed $15dJ_2$ peak (Figure 6.9). I observed 93, 70, and 85% of the amount of $15dJ_2$ added in the PBS, BSA, and FBS incubations respectively. Difficulty in the extraction caused by precipitate and sticky emulsions in the presence of both serum and albumin is likely the cause of the observed loss of $15dJ_2$ under those conditions. While not all compounds absorb at 306 nM, the observed reduction in the $15dJ_2$ peak is not sufficient to explain the reduced $15dJ_2$ induction observed in the cell assays.

As albumin interacts reversibly with $15dJ_2$ and does not chemically modify $15dJ_2$, the simplest remaining explanation is that it binds to $15dJ_2$, effectively reducing the free $15dJ_2$ concentration. Fitting the experimental data for BSA, HSA, and glyclated HSA binding of $15dJ_2$ to the equation for a single binding site derived in Experimental Procedures gives equilibrium dissociation constants (K_ds) of 870 ± 70 nM, 1.2 ± 0.2 mM, and 1.5 ± 0.3 μM respectively (Figure 6.7).

Figure 6.10 is a composite of Figure 6.2, Figure 6.6, and Figure 6.7 that shows the correlation of the albumin levels required to reduce the free $15dJ_2$ concentration in the binding experiments with the levels of serum or albumin required to inhibit $15dJ_2$ induction of PPARγ in the EP-JEG cell assay experiments. This correlation suggests that albumin inhibits $15dJ_2$ induction of PPARγ by sequestering $15dJ_2$ effectively reducing the amount available to PPARγ.

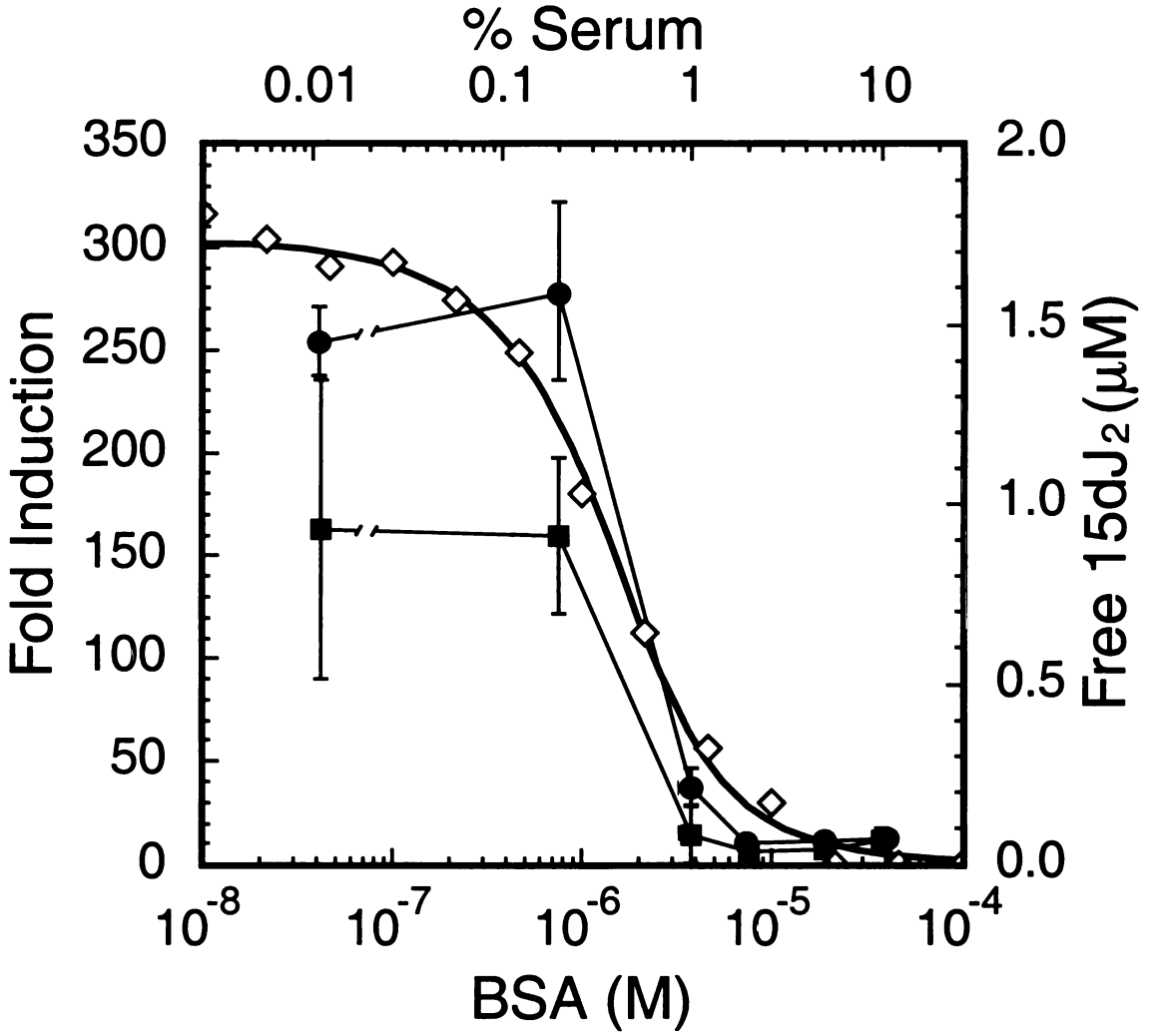

Figure 6.10: Overlay Plot

The data from Figure 6.2, Figure 6.6, and Figure 6.7 are plotted together. The FBS titration from Figure 6.2 and the BSA titration from Figure 6.6 are shown in closed squares and circles respectively on the left axis. The BSA binding curve from Figure 6.7 is shown in open diamonds on the right axis. The leftmost data points on the serum and albumin titration curves are broken off to show that they contain no serum or albumin respectively. The serum levels from Figure 6.2, shown on the top axis, were converted to μM BSA using the BSA level in FBS reported in the manufacturer's analysis.

Unexplained Results and Problems Encountered

To see if albumin binding of $15dJ_2$ led to an apparent shift in the EC_{50} of $15dJ_2$ I incubated EP-JEG cells with $15dJ_2$ (concentrations ranging from 10 nM to 2 μM) and either FBS or HTFBS. I observed higher levels of induction in the heat-treated serum (Figure 6.11), but did not observe a clean enough dose response curve in any of the

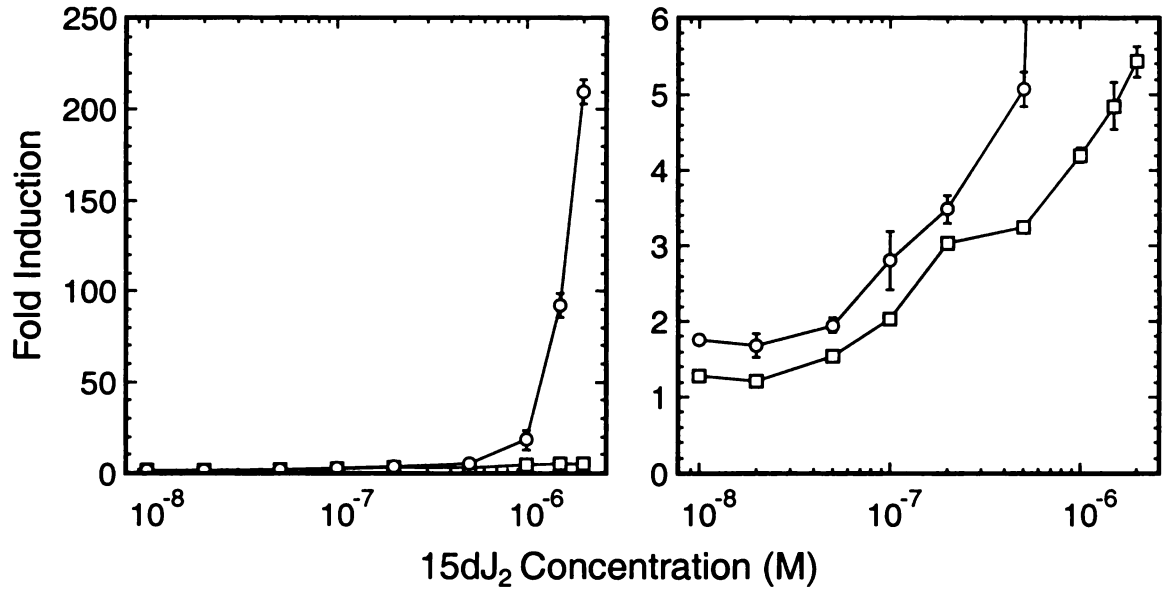

Figure 6.11: $15dJ_2$ Dose Response

EP-JEG cells were incubated with media containing the indicated concentration of $15dJ_2$ and 10% FBS (open squares) or 10% HTFBS (open circles). Fold induction was calculated relative to 0.1% vehicle in untreated FBS.

experiments to observe an apparent EC_{50} shift. Other than increased ligand toxicity at high concentration, it is unclear why saturation of $15dJ_2$ induction is not observed. It should be noted that as the PPARγ in these cells is endogenous, the regulation of its expression and activity is inherently more complicated than it would be in a transiently transfected reporter gene system, where the level of overexpressed receptor is controlled by a viral promoter. A different cell line such as HeLa cells would avoid the complexity of an endogenous response and reduce problems with lipid toxicity.

While unable to obtain clean $15dJ_2$ dose responses in EP-JEG cells, we have discovered that the activities of several other nuclear receptor ligands are affected by albumin in a similar way, and show apparent EC_{50} or IC_{50} shifts.

NH-2 (Figure 6.1) is a thyroid hormone receptor agonist. Ngoc-Ha Nguyen incubated transiently transfected HeLa cells with NH-2 concentrations ranging from 0.1 nM to 10 μM in media containing no serum, newborn calf serum (NCS), heat treated-

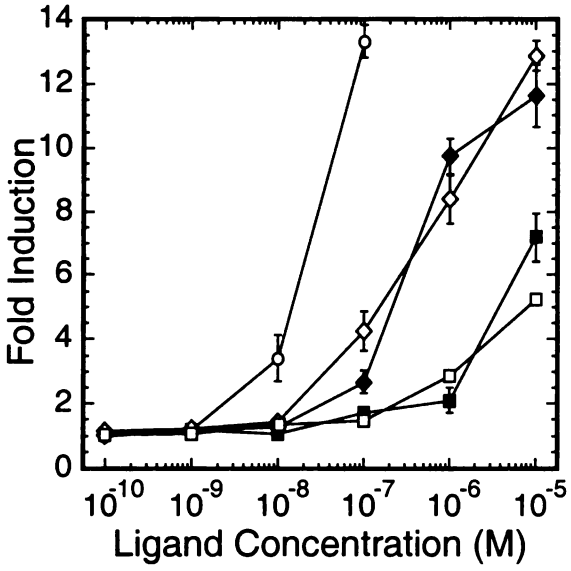

Figure 6.12: EC_{50} Shift of NH-2 in Presence of Albumin

HeLa cells were transiently transfected with TRβ and a TRE driven luciferase reporter. Cells were then incubated with media containing either T3 in NCS (open circles) or NH-2 in NCS (open squares), no serum (open diamonds), 50 μM BSA (closed squares), or HTNCS (closed diamonds). Fold induction was calculated relative to 0.1% vehicle in untreated NCS. This compound was synthesized tested by Ngoc-Ha Nguyen.

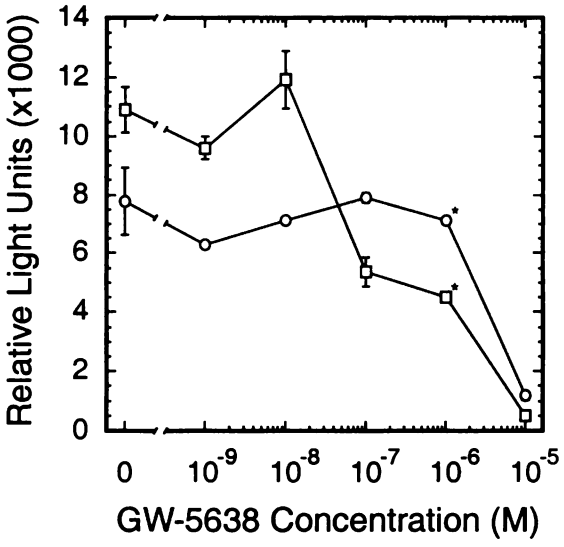

Figure 6.13: IC_{50} Shift of GW-5638 in Heat Treated Serum

HeLa cells were transiently transfected with Era and an ERE driven luciferase reporter. Cells were then incubated with media containing 0.1 nM estradiol, 10% NCS (circles) or10% HTNCS (squares), and the indicated concentration of GW-5638. Data is reported as relative light units. * indicates that only one data point was available, so no error bars are shown. This compound was synthesized and tested by Ross Weatherman.

NCS (HT-NCS), or 50 μM BSA. Both HTNCS and no serum show activation at approximately one order of magnitude lower concentration than in NCS or BSA (Figure 6.12).

GW-5638 (Figure 6.1) is an estrogen receptor antagonist at the classical estrogen receptor response element. Ross Weatherman incubated transiently transfected HeLa cells with GW-5638 concentrations ranging from 0 to 10 μM, 0.1 nM estradiol, and either NCS or HT-NCS. GW-5638 in HTNCS was able to inhibit estradiol induction of estrogen receptor at lower concentrations than those required in NCS (Figure 6.13).

The differences in the induction levels seen in EP-JEG cells for rosiglitazone and $15dJ_2$ in HTFBS (Figure 6.3) suggest that rosiglitazone may be a partial rather than full

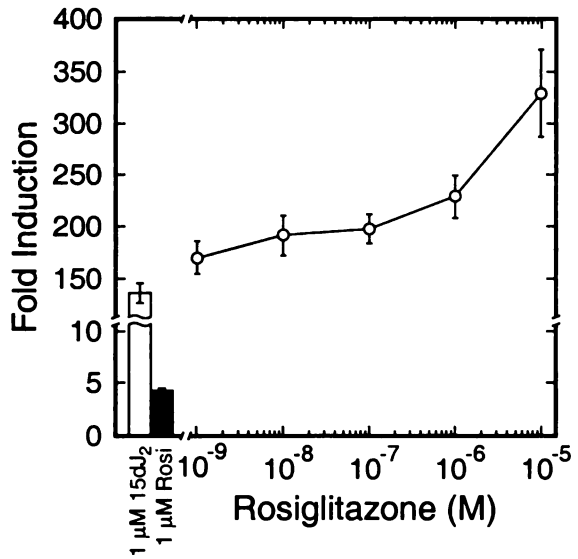

Figure 6.14: Rosiglitazone Competition

EP-JEG cells were treated with media containing 10% FBS and 1 μM $15dJ_2$ (white bar), 1 μM rosiglitazone (black bar), or 1 μM $15dJ_2$ and the indicated concentration of rosiglitazone (open circles). Fold induction was calculated relative to 0.2% vehicle in 10% HTFBS.

agonist of PPARγ. To see if rosiglitazone functioned as a partial antagonist, I incubated EP-JEG cells with rosiglitazone at concentrations ranging from 1 nM to 10 μM, 1 μM $15dJ_2$, and HTFBS. I observed an increase in induction of PPARγ at increasing rosiglitazone concentrations (Figure 6.14). As these two ligands are known to compete for the same binding site (77), I was surprised to see increasing induction with increasing rosiglitazone concentration. Like the unusual dose response this could result from the complexity of the endogenous response in EP-JEG cells arising from endogenous control of receptor expression and the host of other receptors and factors that could mediate activation of the response.

Discussion

Serum Albumin Inhibits $15dJ_2$ Induction of PPARγ

In this work I have shown that albumin interacts directly with $15dJ_2$, a PPARγ agonist, effectively inhibiting induction of PPARγ by $15dJ_2$. I see induction by $15dJ_2$ of between 150 and 700 fold at serum levels below 1%, while at higher serum concentrations I see only 5-20 fold induction by $15dJ_2$. Heat treatment of serum at 80°C

for 20 minutes gives induction levels comparable to those seen with no serum, indicating that a heat labile serum factor(s) inhibits induction of PPARγ. It should be noted that the observed induction levels in serum-free media are extremely high, and I am not aware of any PPARγ reporter systems, which use full length PPARγ, that provide such high levels of ligand induction. Moreover, my system utilized endogenous PPARγ and a physiologically relevant response element. Bishop-Bailey *et al.* have reported serum dependent changes in PPARγ activity in transiently transfected endothelial cells (ECV-304) (127), but see only 10 fold activation in the absence of serum.

Differences in cell growth in different serum preparations cannot account for the observed differences in $15dJ_2$ induction. The cell growth experiment shows a significant decrease in cell growth when cells are treated with HTFBS and 1 μM $15dJ_2$ relative to treatment with FBS with 1 μM $15dJ_2$. The decrease in cell number would lead to a lower observed luciferase activity, so decreased cell growth could not be responsible for the observed increased $15dJ_2$ induction. It has been reported that $15dJ_2$ and PPARγ activation can lead many cell types to differentiate or withdraw from the mitotic cycle and undergo apoptosis (45, 47, 100, 120, 126, 127, 248-251). Induction of these pathways was observed in 10% FBS at $15dJ_2$ concentrations higher than the 1 μM I used in my experiments. My findings suggest that a lower total concentration of $15dJ_2$ may activate the apoptosis and cell cycle withdrawal pathways when albumin is unable to reduce the free $15dJ_2$ concentration. The activation of one or both of these pathways is likely to be responsible for the observed changes in cell growth.

Albumin is the serum factor responsible for inactivation of $15dJ_2$ induction of PPARγ. Albumin preparations reproduced the ability of serum to inhibit $15dJ_2$ induction,

regardless of the method of purification, at concentrations comparable to those in serum that inhibited $15dJ_2$ induction of PPARγ. Along with the observation that thermally denatured albumin was unable to inhibit induction, these data suggest that an active conformation of albumin is required to inhibit $15dJ_2$ induction of PPARγ.

Albumin Inhibits Induction Of PPARγ By Reversibly Binding $15dJ_2$

Albumin plays an important role in regulating the PPARγ response in these cells, by inhibiting the extreme levels of induction observed in its absence. Based on albumin's known role in the transport and metabolism of fatty acids, the two most likely mechanisms of inhibition are by albumin either sequestering $15dJ_2$ or by converting $15dJ_2$ to a less active form. Albumin's interaction with $15dJ_2$ *in vitro* is reversible and analysis by HPLC shows no new products formed after incubation of $15dJ_2$ with serum. This leaves binding as the most likely mechanism for the *in vitro* inhibition of $15dJ_2$ induction by albumin.

Albumin inhibits $15dJ_2$ induction of PPARγ by reversibly binding $15dJ_2$ and reducing the free concentration available to activate PPARγ. By measuring free ligand concentration as a function of albumin concentration I was able to measure an equilibrium dissociation constant for several forms albumin and $15dJ_2$ (870 ± 70 nM (BSA), 1.2 ± 0.2 μM (HSA), and 1.5 ± 0.3 μM (glycated HSA)) assuming a single binding site. This measured value is comparable to the reported K_i of 2.5 μM for $15dJ_2$ displacement of rosiglitazone binding to PPARγ (77). With similar binding constants, the much larger pool of albumin would leave little or no $15dJ_2$ bound to PPARγ and significantly reduce the observed induction. The free ligand concentrations observed in the binding assay correlate well with the reporter gene activity observed at the

corresponding albumin concentrations in the serum and albumin titration experiments. The levels of protein that would be required to inhibit activation through a binding mechanism, along with the observation that albumin purified by several methods shows the same activity, suggest that albumin, rather than a trace impurity, is responsible for the activity.

Implications of Inhibition On Other Ligands

Albumin may also affect the observed activities of other PPARγ ligands. Albumin has been reported to bind to several known PPARγ activators (203), and is likely to bind many of the other fatty acids that activate the receptor, including the putative endogenous activator(s). In addition to inhibiting induction of PPARγ by these ligands, by binding them albumin may affect the observed EC_{50} of these compounds.

It is reasonable to assume, given albumin's known interactions with a wide range of fatty acids, that it will bind other structurally similar PPARγ ligands. It is possible that albumin binding will lead to similar changes in the observed activity or potency of these compounds.

As the endogenous ligand is most likely a fatty acid, possibly another prostaglandin, it is likely that through binding and possibly catalysis, albumin will play an important role in regulating its transport, metabolism and availability to bind PPARγ and activate transcription. Using heat-treated serum to eliminate albumin's inhibition of these compounds would help in the identification of important PPARγ activators whose activity was masked by albumin in previous screening attempts.

Albumin binding and inhibition could also have profound implications for the testing and screening of ligands for other nuclear receptors, as a wide range of

endogenous, xenobiotic, and pharmaceutical compounds are known to bind to albumin (203). I have observed that albumin inhibits ligand for the estrogen and thyroid hormone receptor. In these cases the use of heat-treated serum also lead to an observed increase in the potency of the ligands. In the case of NH-2, the compound only shows agonist activity in the absence of albumin, which could have been missed in a traditional ligand screening experiment.

Heat treatment of serum removes albumin's inhibition of ligand induction, without compromising cell growth or exacerbating ligand toxicity. While albumin's reduction of activity probably parallels the induction I would expect to see with the high albumin levels in vivo, the ability to separate receptor activation and serum protein binding in these assays could prove useful. It would give important insights into the potential pharmacology of ligands for nuclear receptor targets, as well as allowing the design of drugs, which are not prone to these affects.

Medical Implications

Several diseases including cirrhosis of the liver, nephrotic syndrome, protein losing enteropathy, malnutrition, and AIDS (137, 221), are associated with quantitatively reduced levels of serum albumin. Other disorders, such as preeclampsia (124, 227), coronary heart disease (225, 226), and diabetes (223), have been shown to manifest qualitative changes in isoforms of serum albumin, which can alter lipids and lipoprotein transport. Among these the most extensively studied is the pregnancy syndrome preeclampsia. In this condition, elevated circulating concentrations of free polyunsaturated fatty acids bind to and shift the pI of plasma albumin from 5.6 to 4.8(125). Given my observations that albumin reduces the activity of $15dJ_2$ and

potentially decreases the activity of natural PPARγ ligands, quantitative or qualitative changes in circulating albumin could affect the regulation of PPARγ activated genes in these diseases.

Chapter 7: Concluding Remarks

The most significant result of my research has been the observation that albumin binds and inhibits 15-deoxy-$\Delta^{12,14}$-prostaglandin J_2 ($15dJ_2$) induction of peroxisome proliferator-activated receptor-γ (PPARγ) *in vitro*. While this has implications for the *in vivo* function and regulation of PPARγ, we are currently unable to evaluate the role albumin plays *in vivo*. My research has also led to the development and characterization of the EP-JEG cell line, which was a valuable tool in the evaluation of albumin's inhibitory effects. Several of the areas I have touched on in my research have not been brought to a conclusion, as the albumin and EP-JEG projects have been, and many of the major questions for PPARγ function remain.

The synthesis of a series of candidate antagonists was the starting point for my research, and remains incomplete. This part of my research was hampered by solubility problems of the thiazolidinedione class of compounds. In retrospect, it would have made sense to choose more aliphatic extensions because of their increased solubility. The original phenyl extension location remains unaddressed at this point, and appropriate choice of extensions could improve solubility of derivatives and this location as well.

The derivatives I have made have not been as thoroughly tested as would be desirable because of the difficulties that were encountered with generating useful assays for their evaluation. Because EP-JEG and JEG-3 cells contain mRNA for all three PPAR subtypes, they allow for the possibility, though remote, that these derivatives mediate effects through other subtypes. These cells were also showed increased toxicity as a result of treatment with my thiazolidinedione derivatives relative to the CV-1 and HeLa cells used in the transient transfection assays. Unfortunately, these transient transfection

assays did not provide sufficient signal-to-noise and reproducibility to properly evaluate the cellular effect of these ligands. I was also unable to develop a binding assay that would work for these ligands. Both a working reporter gene assay and binding assay are necessary to complete the evaluation of the derivatives I have synthesized and any new derivative that are made.

As mentioned in Chapter 6, albumin also interacts with ligands for other nuclear receptors (Figure 6.12, Figure 6.13). This suggests that the reevaluation of the activities of previously screened and tested ligands for PPARγ as well as other nuclear receptors could yield interesting data. Ligand showing these effects should also be tested for albumin binding. I have not pursued this avenue, but would recommend that heat-treated serum be including in the screening and testing of ligands in the future.

As mentioned in Chapter 6, several of the diseases already connected to PPARγ show altered forms of albumin (124, 125, 223, 225-227). I tested a commercial synthetic preparation of glycated albumin, an albumin modification found in patients with poorly regulated diabetes, and did not see differences in binding (Figure 6.7). However, a more physiologically relevant test of ligand binding to albumin purified from the serum of diseased patients and testing its binding of ligands might show differences in the albumin interaction. This, in turn, would provide clues to the potential role of albumin in these diseases and the mechanism of the PPARγ effects.

While all these topics are interesting, my results and these experiments have not yet addressed the major questions in PPARγ function. Perhaps the most important part of my research is the tools and clues it has given as to how best to approach some of the questions regarding the regulation and function of PPARγ *in vivo*. What is the

endogenous PPARγ agonist? What factor(s) in human pregnancy serum are responsible for induction of the peroxisome proliferator response element (PPRE) reporter gene, and which PPAR subtypes mediate this response? What differences are there between the factor(s), and their levels, present in serum from women with a normal pregnancy relative to those seen in patients with diseases such as preeclampsia? What roles do other proteins, including albumin, play in the regulation of ligand induction of PPARγ *in vivo*? In which tissues does PPARγ play an important role?

What is the endogenous PPARγ agonist?

We have recently reported that serum from pregnant women contains a factor(s) that activates transcription of the tk-$PPRE_3$-LUC reporter gene (43). This factor leads to increased transcription of the PPARγ mRNA, and increased PPARγ protein levels (81). Pregnancy serum also contains a factor, presumably albumin, which inhibits $15dJ_2$ induction of PPARγ (Figure 6.2B), and may inhibit induction by the endogenous factor(s). Heat-treatment of pregnancy serum leads to aggregation and more variability in the data obtained, but shows that the endogenous serum activator(s) is not heat labile (81). Heat treatment appears to lead to higher levels of induction than is seen in untreated serum, consistent with albumin playing a similar role with the endogenous ligand(s) (81).

Based on these experiments we suspect that albumin functions as an inhibitor of the endogenous activator of PPARγ found in pregnancy serum. Based on the heat treatment results and the structures of known synthetic activators for PPARγ, it is likely that the activator is a lipid. Because of the presence of mRNA for the other PPAR

subtypes in the cells used for these experiments, it is possible that part of the response of pregnancy serum is mediated by the other PPAR subtypes.

Isolation of an endogenous PPARγ agonist has been difficult. Hopefully, using pregnancy serum as a known source of detectable levels of an endogenous PPARγ activator, we will be able to isolate and characterize endogenous activators for PPARγ. Due to common problems with anemia during pregnancy, only about 3 mL of blood (~1.5 mL of serum) can be drawn from a patient at one time. Serum from pregnant cows collected at the UC Davis dairy facility did not contain detectable levels of the PPARγ agonist observed in human serum. It is possible that a large animal with PPARγ activators in pregnancy serum could be identified, which would allow the collection of larger serum volumes. I would suggest using human serum, given the clinical relevance, rather than spending time looking for another source.

The isolation of serum agonists should be approached by two methods. First, we need to develop tools to characterize the subtype specificity or profile of the response. This will help in determining if an isolated factor(s) can account for all or part of the activity seen in pregnancy serum. Second, we need to develop tools to isolate the responsible activating factors from human pregnancy serum.

PPAR Subtype Specific Cell Assays

The development of working assays showing specificity for each of the three PPAR subtypes would assist in characterizing the response of pregnancy serum and any isolated serum factors. The endogenous response of JEG-3 and EP-JEG cells are very physiologically relevant, particularly when studying factors in pregnancy serum, but does

not distinguish activation mediated by the different PPAR subtypes when tested with the tk-$PPRE_3$-LUC reporter.

The use of response elements specific for the various PPAR subtypes in these cells would provide an ideal mix of subtype specificity and physiological relevance. Unfortunately, I am not aware of a set of specific response elements, and it is not clear that specific response elements are likely to exist.

The other approach is to develop assays in a cell line, preferably human, that does not express the PPAR subtypes. The mixture of overexpressed PPAR and an appropriate reporter gene would allow characterization of the subtype specific response of samples. Because of the ease of use, improved error, and improved variability, a series of stable cell lines would be useful for characterizing and screening of the serum fractions and isolated factors.

I have unsuccessfully attempted incorporation of the reporter gene and the PPARγ expression vector into HeLa cells simultaneously. Another cell line may work under these conditions, or it may be necessary to add each plasmid individually. Once isolated and characterized a series of stable cell lines overexpressing each of the PPAR subtypes would complement the EP-JEG cells. Together these four cell lines would provide a set of powerful experimental tools for deconvoluting the role of each PPAR subtype in mediating the endogenous response of the EP-JEG cells to activators such as the pregnancy serum.

The activity of activators in these four cell lines, along with RT-PCR or western blot data from JEG-3 cells if desired, would constitute an activation profile. This profile

could be used to compare sera from different diseases, to evaluate isolated serum factors, and evaluate the subtype specificity of new synthetic ligands.

It is possible that the profile of serum activator(s) in pregnancy serum would change during the gestational period. The Taylor lab has recently been able to obtain a series of samples spanning the last two-thirds of the gestational period from a single subject, complementing less extensive samples from other patients. Testing this series of samples with these cells could provide important data on the role of the three PPAR subtypes in pregnancy, as well as providing a way to test for abnormalities and diseases clinically.

Understanding the roles of each PPAR subtype in the endogenous response of JEG-3 and EP-JEG cells could help explain the difficulty in observing saturation of the ligand response in these cells. It appears that albumin affects the EC_{50}s of ligands for other nuclear receptors, but we were unable to observe an EC_{50} shift in EP-JEG cells for $15dJ_2$. If this could be resolved, it would allow the accurate determination of EC_{50}s for PPARγ ligands in these cells.

High Throughput Coactivator Binding Assays

The fluorescence anisotropy coactivator binding assay developed by the Guy lab (252) could be potentially be used as a high throughput screen for the endogenous agonist in pregnancy serum during fractionation experiments. First, the his-tagged hPPARγ LBD construct would need to be tested to confirm that it shows the expected ligand induced coactivator recruitment in these assays with $15dJ_2$ and rosiglitazone. Pregnancy serum could then be tested to see if the observed agonist activity is a ligand that acts directly on the receptor resulting in coactivator recruitment. If treatment with serum results in

coactivator recruitment, this high throughput assay would provide a convenient way to rapidly screen column fractions generated in serum fractionation experiments.

NMR in vivo Structural Studies

The recent development of *in vivo* NMR techniques by the Doetsch lab (253, 254) provides a potential tool to evaluate the structural differences between the receptor bound to rosiglitazone and $15dJ_2$. $15dJ_2$ and rosiglitazone show differences in PPARγ transcriptional activity. Due to the differences in ligand binding pocket size observed in the rosiglitazone bound PPARγ crystal structure and other nuclear receptors, it seems possible that this could be a result in differences in ligand bound receptor conformation. The *in vivo* NMR technique significantly increases the ease of selective amino acid labeling experiments, which could be used to help assign the peaks or to probe a specific region such as a string of amino acids in helix-12.

The PPARγ LBD expression construct described in Chapter 5 may be appropriate for *in vivo* NMR. Spectra of the LBD construct alone and with both $15dJ_2$ and rosiglitazone could be used to evaluate differences in the structure of the ligand bound complexes as well as to demonstrate the expected conformational change of helix-12 upon ligand binding.

If these experiments prove useful, evaluation of the effect of pregnancy serum on the receptor conformation could show whether the agonist in serum acts directly by binding to PPARg. It could also provide insight into which ligands produce a receptor conformation closest to the endogenous ligand.

Protease Treatment

While the heat treatment protocol has proved to be useful in avoiding the albumin inhibition of ligand in bovine serum, heat treatment of human sera produces aggregation resembling a hard-boiled egg. Homogenization of this precipitate using douncer tissue grinders has allowed us to assay heat-treated human sera, but variability and large error values have complicated these experiments.

An alternative approach to the inactivation of albumin would we the use of proteases attached to beads. Incubation of serum with these beads, followed by a centrifugation step to remove them, would allow the destruction of serum proteins without heat treatment. While more expensive and time consuming than the heat treatment of serum, this approach would have several advantages. First, this technique would allow the destruction of serum proteins, including albumin, without disturbing other heat labile serum factors, which may include small molecules and ligands participating in the response. Second, it would likely avoid the aggregation problems associated with the heat treatment of human sera. Third, it might be more easily performed on small serum volumes than heat treatment. Finally, while heat treatment inactivates albumin binding, the aggregation of the denatured serum proteins could provide a nonspecific hydrophobic sink for the types of endogenous ligands we are looking for. Protease treatment might avoid this type of aggregation and allow detection of larger hydrophobic ligand concentrations.

The first step in developing this technique would involve looking for proteolytic degradation of the serum proteins as observed by SDS-PAGE. Albumin is clearly visible with Coomassie Blue staining, as it comprises half of the total serum protein. Once a

digestion procedure has been developed, the results of digestion of $15dJ_2$ induction of PPARγ should be compared to the heat treatment experiment (Figure 6.3).

This technique would be useful in evaluating and characterizing the endogenous activator in pregnancy serum, and may be useful in removing albumin activity before attempts at isolating lipids from the serum.

Albumin and Serum Fractionation

The traditional way to isolate an activator from serum or other liquid sample is to conduct successive fractionations of the material, and assay each fraction for activity. Given the difficulty in obtaining large quantities of human pregnant serum, the efficiency of the fractionation procedure will be important. The information about albumin's potential interactions with the endogenous PPARγ activator(s) gives us several clues as to how to approach this problem.

A simple protein precipitation, such as ammonium sulfate, is commonly used, but may also precipitate protein bound ligands. Because the activator is likely to bind to albumin, it may be important to inactivate albumin before a protein precipitation or lipid extraction. This could be done with heat treatment of the serum or protease treatment. Because of potential nonspecific hydrophobic interactions the ligands we are looking for may have with the aggregated proteins, the protease treatment may be preferable.

Albumin's binding interaction could also be used as an advantage by using it as a handle to pull the ligand out of solution. Either isolating lipids that are precipitated along with proteins in the ammonium sulfate treatment or purification of albumin and its bound ligand using chromatography could afford a useful enrichment of the desired activator. Protease or heat treatment could then be used to release the activator along with a few

albumin bound small molecules. Liquid chromatography-mass spectrometry (LCMS) could then be used to identify these molecules. Comparison to the molecules present in similar treatment of a serum that does not contain an activator, such as non-pregnant human serum, could identify candidates for the activating lipid.

A PPARγ Affinity Column

While albumin may provide a useful handle to pull the activator out of serum, it would also pull many structurally similar molecules out along with it. These may be difficult to fractionate further, and as some lipids are likely to be present in much higher concentrations, detection of the activator by LCMS may be difficult. One potential way to pull the activator out of solution is to use a more specific binding interaction with PPARγ ligand binding domain (LBD).

In order to detect unlabeled lipids we would need 1 ng quantities of ligand, based on the limits of detection of $15dJ_2$ on our HPLC, so we would need at least 100 ng (3 pmol) quantities of protein. Fortunately, the bacterial expression of the His-tagged PPARγ LBD construct described in Chapter 5 provides high expression levels. Although a cobalt column was used for the purification of the construct in Chapter 5, a nickel column will bind the construct with a higher affinity.

If the bacterial cleared cell lysate is run over a nickel column several times, the column could be saturated with PPARγ LBD. Buffer exchange could then wash nonspecific proteins from the column. Given no other protein peaks were seen in the elution of PPARγ (Figure 5.2), the PPARγ bound to this column would be relatively pure. The trick would then be to add ligand to the column in a way that did not disturb the PPARγ binding, and allowing interaction of the ligand and protein over the time scale

required for PPARγ binding of the ligand. The PPARγLBD bound ligand could then be eluted by chemical denaturation of the LBD, proteolitic degradation of the LBD, or imidazole displacement of the LBD followed by LBD degradation.

Serum or cell lysates could potentially be loaded on the column without further purification, but it would be necessary to do a proof of principle experiment to ensure that the PPARγ survives the process and can still bind ligand. Organic extracts redissolved in buffer would likely work. Whatever the mechanism of loading the ligand onto the column, the potential advantage of this approach is the use of large volumes and the enrichment and concentration of the ligand through this process.

Whatever the method of addition, it would be necessary to first characterize the ability to recover ligand from this process. The ability to recover $15dJ_2$ using this process would provide a useful test. Starting with $15dJ_2$ in buffer alone would allow determination of the interaction time required for saturation of the column. If $15dJ_2$ could be recovered, testing of $15dJ_2$ added to serum or cell lysates could determine the stability of these columns under these conditions. A second class of control experiment would be the ability to separate PPARγ ligands such as $15dJ_2$ from larger quantities of other fatty acids such as oleic acid. These control experiments would also help determine the detection limits of this procedure, which would change the size of column and amount of sample that should be used in the experiment.

Optimization of the elution and detection procedure could lead to relatively high ligand concentrations. It would be important to characterize the activity of the ligands in cell assays and potentially in binding assays. The purity of the ligand, and the amount

obtained will affect the most desirable analytical techniques for the structural determination. LCMS is an obvious first candidate for the identification.

Differences in the activation profile of serum from pregnancy diseases

If the endogenous activator(s) in pregnancy serum can be identified, or if a series of PPAR subtype specific assays will allow the determination of an activator profile, it opens options for studying pregnancy disease. For example, comparison of serum taken from patients showing abnormal pregnancies or pregnancy diseases to serum from normal pregnancy could provide important clues to understanding the role of PPAR in these diseases.

One pregnancy disease is preeclampsia, which shows lower levels of PPARγ expression, but higher levels of PPAR induction. A better understanding of which subtypes are involved in the response of EP-JEG and JEG-3 cells to the serum from normal and preeclamptic pregnancies could lead to identification of proteins up or down regulated in the preeclampsia. This could help in understanding the cellular mechanism for this disorder.

Treatment

One basic application of information about the proteins responsible for the symptoms of preeclampsia, and the receptors responsible for their regulation is the development of drugs. Information about the particular changes in activation profiles through the particular PPAR subtypes could lead to the use of PPAR subtype specific agonists and antagonists to treat these diseases. Alternately the proteins regulated by these activators could be targeted directly.

Diagnosis

A second application of these tools would be in the diagnosis of pregnancy disorders. Preeclampsia is a disorder where the placenta does not invade properly and fails to establish adequate blood supply to the fetus. Currently preeclampsia is diagnosed based on the presence of non-specific symptoms including the presence of protein in the urine, high blood pressure, and edema. This diagnosis is broad, and it is likely that more than one disorder leads to symptoms diagnosed as preeclampsia. The activation profile of serum samples as a function of gestational age could be used to compare to patients' samples and allow the distinction of different types of preeclampsia, or possibly the early detection of the disorder. A more accurate diagnosis of preeclampsia, or the specific type of preeclampsia, would be important to improving treatment of this disease.

Characterization of the PPAR signaling pathway *in vivo*

One of the main implications of my albumin experiments is the potential role albumin plays *in vivo* in regulating the function of PPARγ. Unfortunately without knowledge of the natural activator of PPARγ there is very little that can be done to evaluate albumin's role *in vivo*. Once the activator is identified, and techniques are developed to measure its level *in vivo*, the door is opened for a variety of experiments looking at the role of the receptor *in vivo*.

For one, both normal and diseased tissue samples could be screened for the presence of the ligand, bringing the implication that PPARγ signaling plays a role in tissue or function or disease. Perhaps the most important avenue of research that could be pursued with knowledge of the endogenous activator for PPARγ would be the characterization of other proteins involved in the PPARγ signaling pathway. For

instance, if the endogenous PPARγ activator is an endocrine ligand, albumin could play an important role in transport, while if it were an autocrine ligand, albumin would effectively shield neighboring cells and tissues from the effects of the ligand. Knowledge of other factors involved in the signaling pathway increases the number of drug targets related to PPAR activity. They may also provide drug targets for diseases such as diabetes that avoid some of the serious side effects affecting the current class of PPARγ agonist thiazolidinediones that are being used for treatment.

rosiglitazone and Other Thiazolidinediones

Heat-treatment of serum in EP-JEG or JEG-3 cell assay experiments leads to greatly increased levels of PPARγ induction by $15dJ_2$, while rosiglitazone induction remains unaffected by albumin's absence (Figure 6.2A). The observed increase in $15dJ_2$ induction of PPARγ is not as large when transiently transfected HeLa cells are used, but in each case, rosiglitazone appears to be a partial agonist in the absence of albumin.

Because rosiglitazone can compete with $15dJ_2$ for PPARγ binding (50, 51, 75, 77), this data opens the possibility that rosiglitazone could function as an antagonist of PPARγ induction under these conditions. Preliminary competition experiments in EP-JEG cells showed increased activity with increasing rosiglitazone concentrations both in the presence and absence of 1 μM $15dJ_2$, in contrast to the predicted result (Figure 6.14). This may be related to the failure of the endogenous PPARγ response of these cells to show saturation at high ligand concentrations. Once the saturation problems in JEG-3 and EP-JEG cells are understood, accurate measurement of competition may be possible.

The conclusion that rosiglitazone is not a full agonist for the receptor implies that the thiazolidinedione derivatives described in chapters 2 and 3 should be tested against

$15dJ_2$ rather than the rosiglitazone used in the competition experiments (Figure 3.5). Evaluating the ability of these derivatives to antagonize $15dJ_2$ induction of PPARγ could lead to the identification of other PPARγ antagonists. Additionally, the synthesis of thiazolidinedione derivatives with better solubility and synthesis of phenyl ring derivatives could yield useful compounds.

Conclusion

Characterization of the albumin response has dramatic implications for the *in vitro* evaluation of nuclear receptor ligands, and has potential important implications for the function of PPARγ *in vivo*. However, I feel that the most exciting areas arising out of my work are potential tools to assist in the evaluation, detection, and isolation of natural activators such as those in human pregnancy serum.

References

1. **Whitfield GK, Jurutka PW, Haussler CA, Haussler MR** 1999 Steroid hormone receptors: evolution, ligands, and molecular basis of biologic function. Journal of Cellular Biochemistry Suppl 32-33:110-22
2. **Weatherman RV, Fletterick RJ, Scanlan TS** 1999 Nuclear-receptor ligands and ligand-binding domains. Annual Review of Biochemistry 68:559-81
3. **Glass CK, Rose DW, Rosenfeld MG** 1997 Nuclear receptor coactivators. Current Opinion in Cell Biology 9:222-32
4. **Feng W, Ribeiro RC, Wagner RL, Nguyen H, Apriletti JW, Fletterick RJ, Baxter JD, Kushner PJ, West BL** 1998 Hormone-dependent coactivator binding to a hydrophobic cleft on nuclear receptors. Science 280:1747-9
5. **Horwitz KB, Jackson TA, Bain DL, Richer JK, Takimoto GS, Tung L** 1996 Nuclear receptor coactivators and corepressors. Molecular Endocrinology 10:1167-77
6. **Mangelsdorf DJ, Evans RM** 1995 The RXR heterodimers and orphan receptors. Cell 83:841-50
7. **Rosen J, Day A, Jones TK, Jones ET, Nadzan AM, Stein RB** 1995 Intracellular receptors and signal transducers and activators of transcription superfamilies: novel targets for small-molecule drug discovery. Journal of Medicinal Chemistry 38:4855-74
8. **Escher P, Wahli W** 2000 Peroxisome proliferator-activated receptors: insights into multiple cellular functions. Mutation Research 448:121-38

9. **Jpenberg AI, Jeannin E, Wahli W, Desvergne B** 1997 Polarity and specific sequence requirements of peroxisome proliferator-activated receptor (PPAR)/retinoid X receptor heterodimer binding to DNA. A functional analysis of the malic enzyme gene PPAR response element. Journal of Biological Chemistry 272:20108-17

10. **Juge-Aubry C, Pernin A, Favez T, Burger AG, Wahli W, Meier CA, Desvergne B** 1997 DNA binding properties of peroxisome proliferator-activated receptor subtypes on various natural peroxisome proliferator response elements. Importance of the 5'-flanking region. Journal of Biological Chemistry 272:25252-9

11. 1999 A unified nomenclature system for the nuclear receptor superfamily [letter]. Cell 97:161-3

12. **Dreyer C, Krey G, Keller H, Givel F, Helftenbein G, Wahli W** 1992 Control of the peroxisomal beta-oxidation pathway by a novel family of nuclear hormone receptors. Cell 68:879-87

13. **Issemann I, Green S** 1990 Activation of a member of the steroid hormone receptor superfamily by peroxisome proliferators [see comments]. Nature 347:645-50

14. **Mangelsdorf DJ, Thummel C, Beato M, Herrlich P, Schütz G, Umesono K, Blumberg B, Kastner P, Mark M, Chambon P, et al.** 1995 The nuclear receptor superfamily: the second decade. Cell 83:835-9

15. **Schoonjans K, Staels B, Auwerx J** 1996 Role of the peroxisome proliferator-activated receptor (PPAR) in mediating the effects of fibrates and fatty acids on gene expression. Journal of Lipid Research 37:907-25

16. **Oppenheimer JH, Schwartz HL, Strait KA** 1994 Thyroid hormone action 1994: the plot thickens. European Journal of Endocrinology 130:15-24

17. **Sher T, Yi HF, McBride OW, Gonzalez FJ** 1993 cDNA cloning, chromosomal mapping, and functional characterization of the human peroxisome proliferator activated receptor. Biochemistry 32:5598-604

18. **Greene ME, Blumberg B, McBride OW, Yi HF, Kronquist K, Kwan K, Hsieh L, Greene G, Nimer SD** 1995 Isolation of the human peroxisome proliferator activated receptor gamma cDNA: expression in hematopoietic cells and chromosomal mapping. Gene Expression 4:281-99

19. **Yoshikawa T, Brkanac Z, Dupont BR, Xing GQ, Leach RJ, Detera-Wadleigh SD** 1996 Assignment of the human nuclear hormone receptor, NUC1 (PPARD), to chromosome 6p21.1-p21.2. Genomics 35:637-8

20. **Fajas L, Fruchart JC, Auwerx J** 1998 PPARgamma3 mRNA: a distinct PPARgamma mRNA subtype transcribed from an independent promoter. Febs Letters 438:55-60

21. **Fajas L, Auboeuf D, Raspé E, Schoonjans K, Lefebvre AM, Saladin R, Najib J, Laville M, Fruchart JC, Deeb S, Vidal-Puig A, Flier J, Briggs MR, Staels B, Vidal H, Auwerx J** 1997 The organization, promoter analysis, and expression of the human PPARgamma gene. Journal of Biological Chemistry 272:18779-89

22. **Zhu Y, Qi C, Korenberg JR, Chen XN, Noya D, Rao MS, Reddy JK** 1995 Structural organization of mouse peroxisome proliferator-activated receptor gamma (mPPAR gamma) gene: alternative promoter use and different splicing yield two

mPPAR gamma isoforms. Proceedings of the National Academy of Sciences of the United States of America 92:7921-5

23. **Tontonoz P, Hu E, Graves RA, Budavari AI, Spiegelman BM** 1994 mPPAR gamma 2: tissue-specific regulator of an adipocyte enhancer. Genes and Development 8:1224-34

24. **Gelman L, Zhou G, Fajas L, Raspé E, Fruchart JC, Auwerx J** 1999 p300 interacts with the N- and C-terminal part of PPARgamma2 in a ligand-independent and -dependent manner, respectively. Journal of Biological Chemistry 274:7681-8

25. **Juge-Aubry CE, Hammar E, Siegrist-Kaiser C, Pernin A, Takeshita A, Chin WW, Burger AG, Meier CA** 1999 Regulation of the transcriptional activity of the peroxisome proliferator-activated receptor alpha by phosphorylation of a ligand-independent trans-activating domain. Journal of Biological Chemistry 274:10505-10

26. **Adams M, Reginato MJ, Shao D, Lazar MA, Chatterjee VK** 1997 Transcriptional activation by peroxisome proliferator-activated receptor gamma is inhibited by phosphorylation at a consensus mitogen-activated protein kinase site. Journal of Biological Chemistry 272:5128-32

27. **Shalev A, Siegrist-Kaiser CA, Yen PM, Wahli W, Burger AG, Chin WW, Meier CA** 1996 The peroxisome proliferator-activated receptor alpha is a phosphoprotein: regulation by insulin. Endocrinology 137:4499-502

28. **Zhang B, Berger J, Zhou G, Elbrecht A, Biswas S, White-Carrington S, Szalkowski D, Moller DE** 1996 Insulin- and mitogen-activated protein kinase-mediated phosphorylation and activation of peroxisome proliferator-activated receptor gamma. Journal of Biological Chemistry 271:31771-4

29. **Hu E, Kim JB, Sarraf P, Spiegelman BM** 1996 Inhibition of adipogenesis through MAP kinase-mediated phosphorylation of PPARgamma. Science 274:2100-3

30. **Camp HS, Tafuri SR** 1997 Regulation of peroxisome proliferator-activated receptor gamma activity by mitogen-activated protein kinase. Journal of Biological Chemistry 272:10811-6

31. **Rastinejad F, Perlmann T, Evans RM, Sigler PB** 1995 Structural determinants of nuclear receptor assembly on DNA direct repeats [see comments]. Nature 375:203-11

32. **Zechel C, Shen XQ, Chen JY, Chen ZP, Chambon P, Gronemeyer H** 1994 The dimerization interfaces formed between the DNA binding domains of RXR, RAR and TR determine the binding specificity and polarity of the full-length receptors to direct repeats. Embo Journal 13:1425-33

33. **Keller H, Dreyer C, Medin J, Mahfoudi A, Ozato K, Wahli W** 1993 Fatty acids and retinoids control lipid metabolism through activation of peroxisome proliferator-activated receptor-retinoid X receptor heterodimers. Proceedings of the National Academy of Sciences of the United States of America 90:2160-4

34. **Kliewer SA, Umesono K, Noonan DJ, Heyman RA, Evans RM** 1992 Convergence of 9-cis retinoic acid and peroxisome proliferator signalling pathways through heterodimer formation of their receptors. Nature 358:771-4

35. **Tugwood JD, Issemann I, Anderson RG, Bundell KR, McPheat WL, Green S** 1992 The mouse peroxisome proliferator activated receptor recognizes a response element in the 5' flanking sequence of the rat acyl CoA oxidase gene. Embo Journal 11:433-9

36. **Auboeuf D, Rieusset J, Fajas L, Vallier P, Frering V, Riou JP, Staels B, Auwerx J, Laville M, Vidal H** 1997 Tissue distribution and quantification of the expression of mRNAs of peroxisome proliferator-activated receptors and liver X receptor-alpha in humans: no alteration in adipose tissue of obese and NIDDM patients. Diabetes 46:1319-27

37. **Mukherjee R, Jow L, Croston GE, Paterniti JR, Jr.** 1997 Identification, characterization, and tissue distribution of human peroxisome proliferator-activated receptor (PPAR) isoforms PPARgamma2 versus PPARgamma1 and activation with retinoid X receptor agonists and antagonists. Journal of Biological Chemistry 272:8071-6

38. **Palmer CN, Hsu MH, Griffin KJ, Raucy JL, Johnson EF** 1998 Peroxisome proliferator activated receptor-alpha expression in human liver. Molecular Pharmacology 53:14-22

39. **Jain S, Pulikuri S, Zhu Y, Qi C, Kanwar YS, Yeldandi AV, Rao MS, Reddy JK** 1998 Differential expression of the peroxisome proliferator-activated receptor gamma (PPARgamma) and its coactivators steroid receptor coactivator-1 and PPAR-binding protein PBP in the brown fat, urinary bladder, colon, and breast of the mouse. American Journal of Pathology 153:349-54

40. **Lambe KG, Tugwood JD** 1996 A human peroxisome-proliferator-activated receptor-gamma is activated by inducers of adipogenesis, including thiazolidinedione drugs. European Journal of Biochemistry 239:1-7

41. **Saez E, Tontonoz P, Nelson MC, Alvarez JG, Ming UT, Baird SM, Thomazy VA, Evans RM** 1998 Activators of the nuclear receptor PPARgamma enhance colon polyp formation. Nature Medicine 4:1058-61

42. **Vidal-Puig AJ, Considine RV, Jimenez-Liñan M, Werman A, Pories WJ, Caro JF, Flier JS** 1997 Peroxisome proliferator-activated receptor gene expression in human tissues. Effects of obesity, weight loss, and regulation by insulin and glucocorticoids. Journal of Clinical Investigation 99:2416-22

43. **Waite LL, Person EC, Zhou Y, Lim K-H, Scanlan TS, Taylor RN** 2000 Placental Peroxisome Proliferator-Activated Receptor-γ is Up-Regulated by Pregnancy Serum. Journal of Clinical Endocrinology and Metabolism 85:3808-3814

44. **Lefebvre AM, Chen I, Desreumaux P, Najib J, Fruchart JC, Geboes K, Briggs M, Heyman R, Auwerx J** 1998 Activation of the peroxisome proliferator-activated receptor gamma promotes the development of colon tumors in C57BL/6J-APCMin/+ mice. Nature Medicine 4:1053-7

45. **Sarraf P, Mueller E, Jones D, King FJ, DeAngelo DJ, Partridge JB, Holden SA, Chen LB, Singer S, Fletcher C, Spiegelman BM** 1998 Differentiation and reversal of malignant changes in colon cancer through PPARgamma [see comments]. Nature Medicine 4:1046-52

46. **Kilgore MW, Tate PL, Rai S, Sengoku E, Price TM** 1997 MCF-7 and T47D human breast cancer cells contain a functional peroxisomal response. Molecular and Cellular Endocrinology 129:229-35

47. **Mueller E, Sarraf P, Tontonoz P, Evans RM, Martin KJ, Zhang M, Fletcher C, Singer S, Spiegelamn BM** 1998 Terminal differentiation of human breast cancer through PPAR gamma. Mol. Cell 1:465-470

48. **Kersten S, Desvergne B, Wahli W** 2000 Roles of PPARs in health and disease. Nature 405:421-4

49. **Tsubouchi Y, Sano H, Kawahito Y, Mukai S, Yamada R, Kohno M, Inoue K, Hla T, Kondo M** 2000 Inhibition of human lung cancer cell growth by the peroxisome proliferator-activated receptor-gamma agonists through induction of apoptosis. Biochemical and Biophysical Research Communications 270:400-5

50. **Lehmann JM, Moore LB, Smith-Oliver TA, Wilkinson WO, Willson TM, Kliewer SA** 1995 An Antidiabetic Thiazolinedione is a High Affinity Ligand for Peroxisome Proliferator-activated Receptor γ (PPARγ). Journal of Biological Chemsitry 270:12953-12956

51. **Forman BM, Tontonoz P, Chen J, Brun RP, Spiegelman BM, Evans RM** 1995 15-Deoxy-$\Delta^{12,14}$-Prostaglandin J_2 is a Ligand for the Adipocyte Determination Factor PPARγ. Cell 83:803-812

52. 1999 Avandia (Rosiglitazone maleate) Tablets, vol 2000

53. **Willson TM, Brown PJ, Sternbach DD, Henke BR** 2000 The PPARs: from orphan receptors to drug discovery. Journal of Medicinal Chemistry 43:527-50

54. **Elbrecht A, Chen Y, Adams A, Berger J, Griffin P, Klatt T, Zhang B, Menke J, Zhou G, Smith RG, Moller DE** 1999 L-764406 is a partial agonist of human peroxisome proliferator-activated receptor gamma. The role of Cys313 in ligand binding. Journal of Biological Chemistry 274:7913-22

55. **Lehmann JM, Lenhard JM, Oliver BB, Ringold GM, Kliewer SA** 1997 Peroxisome proliferator-activated receptors alpha and gamma are activated by indomethacin and other non-steroidal anti-inflammatory drugs. Journal of Biological Chemistry 272:3406-10

56. **Wang YP, Porter WW, Suh NJ, Honda T, Gribble GW, Leesnitzer LM, Plunket KD, Mangelsdorf DJ, Blanchard SG, Willson TM, Sporn MB** 2000 A synthetic triterpenoid, 2-cyano-3,12-dioxooleana-1,9-dien-28-oic acid (CDDO), is a ligand for the peroxisome proliferator-activated receptor gamma. Molecular Endocrinology 14:1550-1556

57. **Berger J, Leibowitz MD, Doebber TW, Elbrecht A, Zhang B, Zhou G, Biswas C, Cullinan CA, Hayes NS, Li Y, Tanen M, Ventre J, Wu MS, Berger GD, Mosley R, Marquis R, Santini C, Sahoo SP, Tolman RL, Smith RG, Moller DE** 1999 Novel peroxisome proliferator-activated receptor (PPAR) gamma and PPARdelta ligands produce distinct biological effects. Journal of Biological Chemistry 274:6718-25

58. **Kliewer SA, Forman BM, Blumberg B, Ong ES, Borgmeyer U, Mangelsdorf DJ, Umesono K, Evans RM** 1994 Differential expression and activation of a family of murine peroxisome proliferator-activated receptors. Proceedings of the National Academy of Sciences of the United States of America 91:7355-9

59. **Kliewer SA, Sundseth SS, Jones SA, Brown PJ, Wisely GB, Koble CS, Devchand P, Wahli W, Willson TM, Lenhard JM, Lehmann JM** 1997 Fatty acids and eicosanoids regulate gene expression through direct interactions with peroxisome proliferator-activated receptors α and γ. PNAS 94:4318-4323

60. 1999 ACTOS (Pioglitazone Hydrochloride) Tablets. FDA, vol 2000

61. 1999 Rezulin (Troglitazone) Tablets, vol 2000

62. **Jiang C, Ting AT, Seed B** 1998 PPAR-gamma agonists inhibit production of monocyte inflammatory cytokines. Nature 391:82-6

63. **Ricote M, Li AC, Willson TM, Kelly CJ, Glass CK** 1998 The peroxisome proliferator-activated receptor-gamma is a negative regulator of macrophage activation. Nature 391:79-82

64. **Berger J, Bailey P, Biswas C, Cullinan CA, Doebber TW, Hayes NS, Saperstein R, Smith RG, Leibowitz MD** 1996 Thiazolidinediones produce a conformational change in peroxisomal proliferator-activated receptor-gamma: binding and activation correlate with antidiabetic actions in db/db mice. Endocrinology 137:4189-95

65. **Oberfield JL, Collins JL, Holmes CP, Goreham DM, Cooper JP, Cobb JE, Lenhard JM, Hull-Ryde EA, Mohr CP, Blanchard SG, Parks DJ, Moore LB, Lehmann JM, Plunket K, Miller AB, Milburn MV, Kliewer SA, Willson TM** 1999 A peroxisome proliferator-activated receptor gamma ligand inhibits adipocyte differentiation. Proceedings of the National Academy of Sciences of the United States of America 96:6102-6

66. **Brown PJ, Smith-Oliver TA, Charifson PS, Tomkinson NC, Fivush AM, Sternbach DD, Wade LE, Orband-Miller L, Parks DJ, Blanchard SG, Kliewer SA, Lehmann JM, Willson TM** 1997 Identification of peroxisome proliferator-activated receptor ligands from a biased chemical library. Chemistry and Biology 4:909-18

67. **Xu HE, Lambert MH, Montana VG, Parks DJ, Blanchard SG, Brown PJ, Sternbach DD, Lehmann JM, Wisely GB, Willson TM, Kliewer SA, Milburn MV** 1999 Molecular recognition of fatty acids by peroxisome proliferator-activated receptors. Molecular Cell 3:397-403

68. **Brzozowski AM, Pike AC, Dauter Z, Hubbard RE, Bonn T, Engström O, Ohman L, Greene GL, Gustafsson JA, Carlquist M** 1997 Molecular basis of agonism and antagonism in the oestrogen receptor. Nature 389:753-8

69. **Pike AC, Brzozowski AM, Hubbard RE, Bonn T, Thorsell AG, Engström O, Ljunggren J, Gustafsson JA, Carlquist M** 1999 Structure of the ligand-binding domain of oestrogen receptor beta in the presence of a partial agonist and a full antagonist. Embo Journal 18:4608-18

70. **Shiau AK, Barstad D, Loria PM, Cheng L, Kushner PJ, Agard DA, Greene GL** 1998 The structural basis of estrogen receptor/coactivator recognition and the antagonism of this interaction by tamoxifen. Cell 95:927-37

71. **Wright HM, Clish CB, Mikami T, Hauser S, Yanagi K, Hiramatsu R, Serhan CN, Spiegelman BM** 2000 A synthetic antagonist for the peroxisome proliferator-activated receptor gamma inhibits adipocyte differentiation. Journal of Biological Chemistry 275:1873-7

72. **Nolte RT, Wisely GB, Westin S, Cobb JE, Lambert MH, Kurokawa R, Rosenfeld MG, Willson TM, Glass CK, Milburn MV** 1998 Ligand binding and co-activator assembly of the peroxisome proliferator-activated receptor-gamma. Nature 395:137-43

73. **Kim JB, Wright HM, Wright M, Spiegelman BM** 1998 ADD1/SREBP1 activates PPARgamma through the production of endogenous ligand. Proceedings of the National Academy of Sciences of the United States of America 95:4333-7

74. **Huang JT, Welch JS, Ricote M, Binder CJ, Willson TM, Kelly C, Witztum JL, Funk CD, Conrad D, Glass CK** 1999 Interleukin-4-dependent production of PPAR-γ ligands in macrophages by 12/15-lipoxygenase. Nature 400:378-382

75. **Nagy L, Tontonoz P, Alvares JGA, Chen H, Evans RM** 1998 Oxidized LDL REgulates Macrophage Gene Expression through Ligand Activation of PPARγ. Cell 93:229-240

76. **Ma H, Sprecher HW, Kolattukudy PE** 1998 Estrogen-induced production of a peroxisome proliferator-activated receptor (PPAR) ligand in a PPARgamma-expressing tissue. Journal of Biological Chemistry 273:30131-8

77. **Kliewer SA, Lenhard JM, Willson TM, Patel I, Morris DC, Lehmann JM** 1995 A Protaglandin J_2 Metabolite Binds Peroxisome Proliferator-Activated Receptor γ and Promotes Adipocyte Differentiation. Cell 83:813-819

78. **Gilroy DW, Colville-Nash PR, Willis D, Chivers J, Paul-Clark MJ, Willoughby DA** 1999 Inducivle cycloxygenase may have anti-inflammatory properties. Nature Medicine 5:698-701

79. **Fitzpatrick FA, Wynalda MA** 1983 Albumin-catalyzed Metabolism of Prostaglandin D_2. Journal of Biological Chemsitry 258:11713-11718

80. **Kikawa Y, Narumiya S, Fukushima M, Wakatsuka H, Hayaishi O** 1984 9-Deoxy-Δ^9,Δ^{12}-13,14-dihydroprostaglandin D2, a metabolite of protaglandin D2

formed in human plasma. Procedings of the National Acadamy of Sciences USA 81:1317-1321

81. **Waite LL** *Unpublished Results*

82. **Uppenberg J, Svensson C, Jaki M, Bertilsson G, Jendeberg L, Berkenstam A** 1998 Crystal structure of the ligand binding domain of the human nuclear receptor PPARgamma. Journal of Biological Chemistry 273:31108-12

83. **Wagner RL, Apriletti JW, McGrath ME, West BL, Baxter JD, Fletterick RJ** 1995 A structural role for hormone in the thyroid hormone receptor. Nature 378:690-7

84. **Bogan AA, Cohen FE, Scanlan TS** 1998 Natural ligands of nuclear receptors have conserved volumes. Nature Structural Biology 5:679-81

85. **Krey G, Braissant O, L'Horset F, Kalkhoven E, Perroud M, Parker MG, Wahli W** 1997 Fatty acids, eicosanoids, and hypolipidemic agents identified as ligands of peroxisome proliferator-activated receptors by coactivator-dependent receptor ligand assay. Molecular Endocrinology 11:779-91

86. **Oñate SA, Tsai SY, Tsai MJ, O'Malley BW** 1995 Sequence and characterization of a coactivator for the steroid hormone receptor superfamily. Science 270:1354-7

87. **Bannister AJ, Kouzarides T** 1996 The CBP co-activator is a histone acetyltransferase. Nature 384:641-3

88. **Ogryzko VV, Schiltz RL, Russanova V, Howard BH, Nakatani Y** 1996 The transcriptional coactivators p300 and CBP are histone acetyltransferases. Cell 87:953-9

89. **Spencer TE, Jenster G, Burcin MM, Allis CD, Zhou J, Mizzen CA, McKenna NJ, Onate SA, Tsai SY, Tsai MJ, O'Malley BW** 1997 Steroid receptor coactivator-1 is a histone acetyltransferase. Nature 389:194-8

90. **Chakravarti D, LaMorte VJ, Nelson MC, Nakajima T, Schulman IG, Juguilon H, Montminy M, Evans RM** 1996 Role of CBP/P300 in nuclear receptor signalling. Nature 383:99-103

91. **Onate SA, Boonyaratanakornkit V, Spencer TE, Tsai SY, Tsai MJ, Edwards DP, O'Malley BW** 1998 The steroid receptor coactivator-1 contains multiple receptor interacting and activation domains that cooperatively enhance the activation function 1 (AF1) and AF2 domains of steroid receptors. Journal of Biological Chemistry 273:12101-8

92. **Näär AM, Beaurang PA, Zhou S, Abraham S, Solomon W, Tjian R** 1999 Composite co-activator ARC mediates chromatin-directed transcriptional activation. Nature 398:828-32

93. **Rachez C, Lemon BD, Suldan Z, Bromleigh V, Gamble M, Näär AM, Erdjument-Bromage H, Tempst P, Freedman LP** 1999 Ligand-dependent transcription activation by nuclear receptors requires the DRIP complex. Nature 398:824-8

94. **Yuan CX, Ito M, Fondell JD, Fu ZY, Roeder RG** 1998 The TRAP220 component of a thyroid hormone receptor- associated protein (TRAP) coactivator complex interacts directly with nuclear receptors in a ligand-dependent fashion [published erratum appears in Proc Natl Acad Sci U S A 1998 Nov 24;95(24):14584].

Proceedings of the National Academy of Sciences of the United States of America 95:7939-44

95. **Zhu Y, Qi C, Jia Y, Nye JS, Rao MS, Reddy JK** 2000 Deletion of PBP/PPARBP, the gene for nuclear receptor coactivator peroxisome proliferator-activated receptor-binding protein, results in embryonic lethality. Journal of Biological Chemistry 275:14779-82

96. **Kodera Y, Takeyama K-i, Murayama A, Suzawa M, Masuhiro Y, Kato S** 2000 Ligand type-specific Interactions of Peroxisome Proliferator-activated Receptor gamma with Transcriptional Coactivators. J. Biol. Chem. 275:33201-33204

97. **Zhu Y, Qi C, Jain S, Rao MS, Reddy JK** 1997 Isolation and characterization of PBP, a protein that interacts with peroxisome proliferator-activated receptor. Journal of Biological Chemistry 272:25500-6

98. **Barak Y, Nelson MC, Ong ES, Jones YZ, Ruiz-Lozano P, Chien KR, Koder A, Evans RM** 1999 PPAR gamma is required for placental, cardiac, and adipose tissue development. Molecular Cell 4:585-95

99. **Shao D, Rangwala SM, Bailey ST, Krakow SL, Reginato MJ, Lazar MA** 1998 Interdomain communication regulating ligand binding by PPAR-gamma. Nature 396:377-80

100. **Tontonoz P, Hu E, Spiegelman BM** 1994 Stimulation of adipogenesis in fibroblasts by PPARgamma 2, a lipid-activated transcription factor. Cell 79:1147-1156

101. **Deeb SS, Fajas L, Nemoto M, Pihlajamäki J, Mykkänen L, Kuusisto J, Laakso M, Fujimoto W, Auwerx J** 1998 A Pro12Ala substitution in PPARgamma2

associated with decreased receptor activity, lower body mass index and improved insulin sensitivity. Nature Genetics 20:284-7

102. **Brun RP, Tontonoz P, Forman BM, Ellis R, Chen J, Evans RM, Spiegelman BM** 1996 Differential activation of adipogenesis by multiple PPAR isoforms. Genes and Development 10:974-84

103. **Issemann I, Prince R, Tugwood J, Green S** 1992 A role for fatty acids and liver fatty acid binding protein in peroxisome proliferation? Biochemical Society Transactions 20:824-7

104. **Krey G, Keller H, Mahfoudi A, Medin J, Ozato K, Dreyer C, Wahli W** 1993 Xenopus peroxisome proliferator activated receptors: genomic organization, response element recognition, heterodimer formation with retinoid X receptor and activation by fatty acids. Journal of Steroid Biochemistry and Molecular Biology 47:65-73

105. **Schoonjans K, Watanabe M, Suzuki H, Mahfoudi A, Krey G, Wahli W, Grimaldi P, Staels B, Yamamoto T, Auwerx J** 1995 Induction of the acyl-coenzyme A synthetase gene by fibrates and fatty acids is mediated by a peroxisome proliferator response element in the C promoter. Journal of Biological Chemistry 270:19269-76

106. **Osumi T, Wen JK, Hashimoto T** 1991 Two cis-acting regulatory sequences in the peroxisome proliferator-responsive enhancer region of rat acyl-CoA oxidase gene. Biochemical and Biophysical Research Communications 175:866-71

107. **Bardot O, Aldridge TC, Latruffe N, Green S** 1993 PPAR-RXR heterodimer activates a peroxisome proliferator response element upstream of the bifunctional enzyme gene. Biochemical and Biophysical Research Communications 192:37-45

108. **Zhang B, Marcus SL, Sajjadi FG, Alvares K, Reddy JK, Subramani S, Rachubinski RA, Capone JP** 1992 Identification of a peroxisome proliferator-responsive element upstream of the gene encoding rat peroxisomal enoyl-CoA hydratase/3-hydroxyacyl-CoA dehydrogenase. Proceedings of the National Academy of Sciences of the United States of America 89:7541-5

109. **Aldridge TC, Tugwood JD, Green S** 1995 Identification and characterization of DNA elements implicated in the regulation of CYP4A1 transcription. Biochemical Journal 306:473-9

110. **Muerhoff AS, Griffin KJ, Johnson EF** 1992 The peroxisome proliferator-activated receptor mediates the induction of CYP4A6, a cytochrome P450 fatty acid omega-hydroxylase, by clofibric acid. Journal of Biological Chemistry 267:19051-3

111. **Rodríguez JC, Gil-Gómez G, Hegardt FG, Haro D** 1994 Peroxisome proliferator-activated receptor mediates induction of the mitochondrial 3-hydroxy-3-methylglutaryl-CoA synthase gene by fatty acids. Journal of Biological Chemistry 269:18767-72

112. **Castelein H, Gulick T, Declercq PE, Mannaerts GP, Moore DD, Baes MI** 1994 The peroxisome proliferator activated receptor regulates malic enzyme gene expression. Journal of Biological Chemistry 269:26754-8

113. **Tontonoz P, Hu E, Devine J, Beale EG, Spiegelman BM** 1995 PPAR gamma 2 regulates adipose expression of the phosphoenolpyruvate carboxykinase gene. Molecular and Cellular Biology 15:351-7

114. **Simonson GD, Iwanij V** 1995 Genomic organization and promoter sequence of a gene encoding a rat liver-specific type-I transport protein. Gene 154:243-7

115. **Kelly LJ, Vicario PP, Thompson GM, Candelore MR, Doebber TW, Ventre J, Wu MS, Meurer R, Forrest MJ, Conner MW, Cascieri MA, Moller DE** 1998 Peroxisome proliferator-activated receptors gamma and alpha mediate in vivo regulation of uncoupling protein (UCP-1, UCP-2, UCP-3) gene expression. Endocrinology 139:4920-7

116. **Schoonjans K, Peinado-Onsurbe J, Lefebvre AM, Heyman RA, Briggs M, Deeb S, Staels B, Auwerx J** 1996 PPARalpha and PPARgamma activators direct a distinct tissue-specific transcriptional response via a PPRE in the lipoprotein lipase gene. Embo Journal 15:5336-48

117. **Gulick T, Cresci S, Caira T, Moore DD, Kelly DP** 1994 The peroxisome proliferator-activated receptor regulates mitochondrial fatty acid oxidative enzyme gene expression. Proceedings of the National Academy of Sciences of the United States of America 91:11012-6

118. **Krey G, Mahfoudi A, Wahli W** 1995 Functional interactions of peroxisome proliferator-activated receptor, retinoid-X receptor, and Sp1 in the transcriptional regulation of the acyl-coenzyme-A oxidase promoter. Molecular Endocrinology 9:219-31

119. **Sears IB, MacGinnitie MA, Kovacs LG, Graves RA** 1996 Differentiation-dependent expression of the brown adipocyte uncoupling protein gene: regulation by peroxisome proliferator-activated receptor gamma. Molecular and Cellular Biology 16:3410-9

120. **Chawla A, Schwarz EJ, Dimaculangan DD, Lazar MA** 1994 Peroxisome proliferator-activated receptor (PPAR) gamma:adipose-predominant expression and induction early in adipocyte differentiation. Endocrinology 135:798-800

121. **Grimaldi PA, Teboul L, Inadera H, Gaillard D, Amri EZ** 1997 Trans-differentiation of myoblasts to adipoblasts: triggering effects of fatty acids and thiazolidinediones. Prostaglandins Leukotrienes and Essential Fatty Acids 57:71-5

122. **Gimble JM, Robinson CE, Wu X, Kelly KA, Rodriguez BR, Kliewer SA, Lehmann JM, Morris DC** 1996 Peroxisome proliferator-activated receptor-gamma activation by thiazolidinediones induces adipogenesis in bone marrow stromal cells. Molecular Pharmacology 50:1087-94

123. **Spiegelman BM** 1998 PPAR-gamma: adipogenic regulator and thiazolidinedione receptor. Diabetes 47:507-14

124. **Arbogast BM, Leeper SC, Merrick RD, Olive KE, Taylor RN** 1994 Which plasma factors bring about disturbance of endothelial function in pre-eclampsia? Lancet 343:340-1

125. **Vigne JL, Murai JT, Arbogast BW, Jia W, Fisher SJ, Taylor RN** 1997 Elevated nonesterified fatty acid concentrations in severe preeclampsia shift the isoelectric characteristics of plasma albumin. Journal of CLinical Endocrinology and Metabolism 82:3786-92

126. **Keelan JA, Sato TA, Marvin KW, Lander J, Gilmour RS, Mitchell MD** 1999 15-Deoxy-$\Delta^{12,14}$-prostaglandin J_2, a Ligand for Peroxisome Proliferator-Activated Receptor-γ, Induces Apoptosis in JEG3 Choriocarcinoma Cells. Biochemical and Biophysical Research Communications 262:579-585

127. **Bishop-Bailey D, Hla T** 1999 Endothelial Cell Apoptosis Induced by the Peroxisome Proliferator-activated Receptor (PPAR) Ligand 15-Deoxy-$\Delta^{12,14}$-prostaglandin J_2. Journal of Biological Chemistry 274:17042-17048

128. **Straus DS, Pascual G, Li M, Welch JS, Ricote M, Hsiang C-H, Sengchanthalangsy LL, Ghosh G, Glass CK** 2000 15-Deoxy-$\Delta^{12,14}$-prostaglandin J_2 inhibits multiple steps in the NF-KB signaling pathway. Proc. Natl. Acad. Sci. U.S.A. 97:4844-4849

129. **Yang XY, Wang LH, Chen T, Hodge DR, Resau JH, DaSilva L, Farrar WL** 2000 Activation of human T lymphocytes is inhibited by peroxisome proliferator-activated receptor gamma (PPARgamma) agonists. PPARgamma co-association with transcription factor NFAT. Journal of Biological Chemistry 275:4541-4

130. **Tanaka T, Itoh H, Doi K, Fukunaga Y, Hosoda K, Shintani M, Yamashita J, Chun TH, Inoue M, Masatsugu K, Sawada N, Saito T, Inoue G, Nishimura H, Yoshimasa Y, Nakao K** 1999 Down regulation of peroxisome proliferator-activated receptorgamma expression by inflammatory cytokines and its reversal by thiazolidinediones. Diabetologia 42:702-10

131. **Zhang B, Berger J, Hu E, Szalkowski D, White-Carrington S, Spiegelman BM, Moller DE** 1996 Negative regulation of peroxisome proliferator-activated receptor-

gamma gene expression contributes to the antiadipogenic effects of tumor necrosis factor-alpha. Molecular Endocrinology 10:1457-66

132. **Xing H, Northrop JP, Grove JR, Kilpatrick KE, Su JL, Ringold GM** 1997 TNF alpha-mediated inhibition and reversal of adipocyte differentiation is accompanied by suppressed expression of PPARgamma without effects on Pref-1 expression. Endocrinology 138:2776-83

133. **Hill MR, Young MD, McCurdy CM, Gimble JM** 1997 Decreased expression of murine PPARgamma in adipose tissue during endotoxemia. Endocrinology 138:3073-6

134. **Vamecq J, Latruffe N** 1999 Medical significance of peroxisome proliferator-activated receptors. Lancet 354:141-8

135. **Bishop-Bailey D** 2000 Peroxisome proliferator-activated receptors in the cardiovascular system. British Journal of Pharmacology 129:823-34

136. **Marx N, Sukhova G, Murphy C, Libby P, Plutzky J** 1998 Macrophages in human atheroma contain PPARgamma: differentiation-dependent peroxisomal proliferator-activated receptor gamma(PPARgamma) expression and reduction of MMP-9 activity through PPARgamma activation in mononuclear phagocytes in vitro. American Journal of Pathology 153:17-23

137. **Goldman L, Bennett JC, Cecil RL** 2000 Cecil textbook of medicine 21st ed. W.B. Saunders, Philadelphia

138. **Tontonoz P, Nagy L, Alvarez JG, Thomazy VA, Evans RM** 1998 PPARgamma promotes monocyte/macrophage differentiation and uptake of oxidized LDL. Cell 93:241-52

139. **Berliner JA, Heinecke JW** 1996 The role of oxidized lipoproteins in atherogenesis. Free Radical Biology and Medicine 20:707-27

140. **Seed B** 1998 PPARgamma and colorectal carcinoma: conflicts in a nuclear family [news; comment]. Nature Medicine 4:1004-5

141. 1998 PPAR--the good news and the bad [editorial]. Nature Medicine 4:981

142. **Weisburger JH** 1997 Dietary fat and risk of chronic disease: mechanistic insights from experimental studies. Journal of the American Dietetic Association 97:S16-23

143. **Wasan HS, Novelli M, Bee J, Bodmer WF** 1997 Dietary fat influences on polyp phenotype in multiple intestinal neoplasia mice. Proceedings of the National Academy of Sciences of the United States of America 94:3308-13

144. **Giovannucci E, Willett WC** 1994 Dietary factors and risk of colon cancer. Annals of Medicine 26:443-52

145. **Nolan JJ, Ludvik B, Beerdsen P, Joyce M, Olefsky J** 1994 Improvement in glucose tolerance and insulin resistance in obese subjects treated with troglitazone [see comments]. New England Journal of Medicine 331:1188-93

146. **Sarraf P, Mueller E, Smith WM, Wright HM, Kum JB, Aaltonen LA, de la Chapelle A, Spiegelman BM, Eng C** 1999 Loss-of-function mutations in PPAR gamma associated with human colon cancer. Molecular Cell 3:799-804

147. **Zou Z, Anisowicz A, Hendrix MJ, Thor A, Neveu M, Sheng S, Rafidi K, Seftor E, Sager R** 1994 Maspin, a serpin with tumor-suppressing activity in human mammary epithelial cells [see comments]. Science 263:526-9

148. **Jacoby RF, Marshall DJ, Newton MA, Novakovic K, Tutsch K, Cole CE, Lubet RA, Kelloff GJ, Verma A, Moser AR, Dove WF** 1996 Chemoprevention of

spontaneous intestinal adenomas in the Apc Min mouse model by the nonsteroidal anti-inflammatory drug piroxicam. Cancer Research 56:710-4

149. **Oshima M, Dinchuk JE, Kargman SL, Oshima H, Hancock B, Kwong E, Trzaskos JM, Evans JF, Taketo MM** 1996 Suppression of intestinal polyposis in Apc delta716 knockout mice by inhibition of cyclooxygenase 2 (COX-2). Cell 87:803-9

150. **Thun MJ, Namboodiri MM, Heath CW, Jr.** 1991 Aspirin use and reduced risk of fatal colon cancer. New England Journal of Medicine 325:1593-6

151. **Willson TM, Cobb JE, Cowan DJ, Wiethe RW, Correa ID, Prakash SR, Beck KD, Moore LB, Kliewer SA, Lehmann JM** 1996 The structure-activity relationship between peroxisome proliferator-activated receptor gamma agonism and the antihyperglycemic activity of thiazolidinediones. Journal of Medicinal Chemistry 39:665-8

152. **Yen CJ, Beamer BA, Negri C, Silver K, Brown KA, Yarnall DP, Burns DK, Roth J, Shuldiner AR** 1997 Molecular scanning of the human peroxisome proliferator activated receptor gamma (hPPAR gamma) gene in diabetic Caucasians: identification of a Pro12Ala PPAR gamma 2 missense mutation. Biochemical and Biophysical Research Communications 241:270-4

153. **Hallakou S, Doaré L, Foufelle F, Kergoat M, Guerre-Millo M, Berthault MF, Dugail I, Morin J, Auwerx J, Ferré P** 1997 Pioglitazone induces in vivo adipocyte differentiation in the obese Zucker fa/fa rat. Diabetes 46:1393-9

154. **Tontonoz P, Graves RA, Budavari AI, Erdjument-Bromage H, Lui M, Hu E, Tempst P, Spiegelman BM** 1994 Adipocyte-specific transcription factor ARF6 is a

heterodimeric complex of two nuclear hormone receptors, PPAR gamma and RXR alpha. Nucleic Acids Research 22:5628-34

155. **Zierath JR, Ryder JW, Doebber T, Woods J, Wu M, Ventre J, Li Z, McCrary C, Berger J, Zhang B, Moller DE** 1998 Role of skeletal muscle in thiazolidinedione insulin sensitizer (PPARgamma agonist) action. Endocrinology 139:5034-41

156. **Burant CF, Sreenan S, Hirano K, Tai TA, Lohmiller J, Lukens J, Davidson NO, Ross S, Graves RA** 1997 Troglitazone action is independent of adipose tissue. Journal of Clinical Investigation 100:2900-8

157. **Rebrin K, Steil GM, Getty L, Bergman RN** 1995 Free fatty acid as a link in the regulation of hepatic glucose output by peripheral insulin. Diabetes 44:1038-45

158. **Rebrin K, Steil GM, Mittelman SD, Bergman RN** 1996 Causal linkage between insulin suppression of lipolysis and suppression of liver glucose output in dogs. Journal of Clinical Investigation 98:741-9

159. **Spiegelman BM, Flier JS** 1996 Adipogenesis and obesity: rounding out the big picture. Cell 87:377-89

160. **Hotamisligil GS, Shargill NS, Spiegelman BM** 1993 Adipose expression of tumor necrosis factor-alpha: direct role in obesity-linked insulin resistance. Science 259:87-91

161. **Kallen CB, Lazar MA** 1996 Antidiabetic thiazolidinediones inhibit leptin (ob) gene expression in 3T3-L1 adipocytes. Proceedings of the National Academy of Sciences of the United States of America 93:5793-6

162. **De Vos P, Lefebvre AM, Miller SG, Guerre-Millo M, Wong K, Saladin R, Hamann LG, Staels B, Briggs MR, Auwerx J** 1996 Thiazolidinediones repress ob gene expression in rodents via activation of peroxisome proliferator-activated receptor gamma. Journal of Clinical Investigation 98:1004-9

163. **Müller G, Ertl J, Gerl M, Preibisch G** 1997 Leptin impairs metabolic actions of insulin in isolated rat adipocytes. Journal of Biological Chemistry 272:10585-93

164. **Cantello BC, Cawthorne MA, Cottam GP, Duff PT, Haigh D, Hindley RM, Lister CA, Smith SA, Thurlby PL** 1994 [[ω-(Heterocyclylamino)alkocy]benzyl]-2,4-thazolidinediones as Potent Antihyperglycemic Agents. Journal of Medicinal Chemistry 37:3977-3985

165. **Sohda T, Mizuno K, Momose Y, Ikeda H, Fujita T, Meguro K** 1992 Studies on antidiabetic agents. 11. Novel thiazolidinedione derivatives as potent hypoglycemic and hypolipidemic agents. Journal of Medicinal Chemistry 35:2617-26

166. **Sohda T, Mizuno K, Tawada H, Sugiyama Y, Fujita T, Kawamatsu Y** 1982 Studies on antidiabetic agents. I. Synthesis of 5-[4-(2-methyl-2-phenylpropoxy)-benzyl]thiazolidine-2,4-dione (AL-321) and related compounds. Chemical and Pharmaceutical Bulletin 30:3563-73

167. **Sohda T, Mizuno K, Imamiya E, Sugiyama Y, Fujita T, Kawamatsu Y** 1982 Studies on antidiabetic agents. II. Synthesis of 5-[4-(1-methylcyclohexylmethoxy)-benzyl]thiazolidine-2,4-dione (ADD-3878) and its derivatives. Chemical and Pharmaceutical Bulletin 30:3580-600

168. **Sohda T, Mizuno K, Imamiya E, Tawada H, Meguro K, Kawamatsu Y, Yamamoto Y** 1982 Studies on antidiabetic agents. III. 5-Arylthiazolidine-2,4-diones

as potent aldose reductase inhibitors. Chemical and Pharmaceutical Bulletin 30:3601-16

169. **Sohda T, Meguro K, Kawamatsu Y** 1984 Studies on antidiabetic agents. IV. Synthesis and activity of the metabolites of 5-[4-(1-methylcyclohexylmethoxy)benzyl]-2,4-thiazolidinedione (ciglitazone). Chemical and Pharmaceutical Bulletin 32:2267-78

170. **Tawada H, Sugiyama Y, Ikeda H, Yamamoto Y, Meguro K** 1990 Studies on antidiabetic agents. IX. A new aldose reductase inhibitor, AD-5467, and related 1,4-benzoxazine and 1,4-benzothiazine derivatives: synthesis and biological activity. Chemical and Pharmaceutical Bulletin 38:1238-45

171. **Sohda T, Momose Y, Meguro K, Kawamatsu Y, Sugiyama Y, Ikeda H** 1990 Studies on antidiabetic agents. Synthesis and hypoglycemic activity of 5-[4-(pyridylalkoxy)benzyl]-2,4-thiazolidinediones. Arzneimittel-Forschung 40:37-42

172. **Sohda T, Mizuno K, Kawamatsu Y** 1984 Studies on antidiabetic agents. VI. Asymmetric transformation of (+/-)-5-[4-(1-methylcyclohexylmethoxy)benzyl]-2,4-thiazolidinedione(ciglitazone) with optically active 1-phenylethylamines. Chemical and Pharmaceutical Bulletin 32:4460-5

173. **Meguro K, Tawada H, Sugiyama Y, Fujita T, Kawamatsu Y** 1986 Studies on antidiabetic agents. VII. Synthesis and hypoglycemic activity of 4-oxazoleacetic acid derivatives. Chemical and Pharmaceutical Bulletin 34:2840-51

174. **Momose Y, Meguro K, Ikeda H, Hatanaka C, Oi S, Sohda T** 1991 Studies on antidiabetic agents. X. Synthesis and biological activities of pioglitazone and related compounds. Chemical and Pharmaceutical Bulletin 39:1440-5

175. **Shoda T** 1995 Studies on antidiabetic agents. XII. Synthesis and activity of the metabolites of (+/-)-5(-)[p(-)[2-(5-ethyl-2-pyridinyl)ethoxy]benzyl]-2,4-thiazolidinedione (pioglitazone). Chem. Pharm. Bull. 43:2168-2172

176. **Harris PK, Kletzien RF** 1994 Localization of a pioglitazone response element in the adipocyte fatty acid-binding protein gene. Molecular Pharmacology 45:439-45

177. **Copp AJ** 1995 Death before birth: clues from gene knockouts and mutations. Trends in Genetics 11:87-93

178. **Lim H, Gupta RA, Ma WG, Paria BC, Moller DE, Morrow JD, DuBois RN, Trzaskos JM, Dey SK** 1999 Cyclo-oxygenase-2-derived prostacyclin mediates embryo implantation in the mouse via PPARdelta. Genes and Development 13:1561-74

179. **Matsuo H, Strauss JF, 3rd** 1994 Peroxisome proliferators and retinoids affect JEG-3 choriocarcinoma cell function. Endocrinology 135:1135-45

180. **Waisman H, Kerr G** 1965 Amino acid and protein metabolism in the developing fetus and newborn infant. Pediatr Clin North Am 12:551-572

181. **Hay WW, Jr.** 1994 Placental transport of nutrients to the fetus. Hormone Research 42:215-22

182. **Blackburn ST, Loper DL** 1992 Maternal, fetal, and neonatal physiology : a clinical perspective. Saunders, Philadelphia

183. **Potter JM, Nestel PJ** 1979 The hyperlipidemia of pregnancy in normal and complicated pregnancies. American Journal of Obstetrics and Gynecology 133:165-70

184. **Ogburn PL, Jr., Johnson SB, Williams PP, Holman RT** 1980 Levels of free fatty acids and arachidonic acid in pregnancy and labor. Journal of Laboratory and Clinical Medicine 95:943-9

185. **Ogburn PL, Jr., Williams PP, Johnson SB, Holman RT** 1984 Serum arachidonic acid levels in normal and preeclamptic pregnancies. American Journal of Obstetrics and Gynecology 148:5-9

186. **Arbogast BW, Leeper SC, Merrick RD, Olive KE, Taylor RN** 1996 Plasma Factors That Determine Endothelial Cell Lipid Toxicity in Vitro Correctly Identify Women with Preeclampsia in Early and Late Pregnancy. Hypertension in Pregnancy 15:263-279

187. **Roberts JM, Redman CW** 1993 Pre-eclampsia: more than pregnancy-induced hypertension [published erratum appears in Lancet 1993 Aug 21;342(8869):504] [see comments]. Lancet 341:1447-51

188. **Taylor RN, de Groot CJ, Cho YK, Lim KH** 1998 Circulating factors as markers and mediators of endothelial cell dysfunction in preeclampsia. Seminars in Reproductive Endocrinology 16:17-31

189. **Brosens IA, Robertson WB, Dixon HG** 1972 The role of the spiral arteries in the pathogenesis of preeclampsia. Obstetrics and Gynecology Annual 1:177-91

190. **Kitzmiller JL, Benirschke K** 1973 Immunofluorescent study of placental bed vessels in pre-eclampsia of pregnancy. American Journal of Obstetrics and Gynecology 115:248-51

191. **Meekins JW, McLaughlin PJ, West DC, McFadyen IR, Johnson PM** 1994 Endothelial cell activation by tumour necrosis factor-alpha (TNF-alpha) and the development of pre-eclampsia. Clinical and Experimental Immunology 98:110-4

192. **Vince GS, Starkey PM, Austgulen R, Kwiatkowski D, Redman CW** 1995 Interleukin-6, tumour necrosis factor and soluble tumour necrosis factor receptors in women with pre-eclampsia [see comments]. British Journal of Obstetrics and Gynaecology 102:20-5

193. **Kupferminc MJ, Peaceman AM, Wigton TR, Rehnberg KA, Socol ML** 1994 Tumor necrosis factor-alpha is elevated in plasma and amniotic fluid of patients with severe preeclampsia. American Journal of Obstetrics and Gynecology 170:1752-7; discussion 1757-9

194. **Hara N, Fujii T, Okai T, Taketani Y** 1995 Histochemical demonstration of interleukin-2 in decidua cells of patients with preeclampsia. American Journal of Reproductive Immunology 34:44-51

195. **Taylor RN** 1997 Review: immunobiology of preeclampsia. American Journal of Reproductive Immunology 37:79-86

196. **van Beck E, Peeters LL** 1998 Pathogenesis of preeclampsia: a comprehensive model. Obstetrical and Gynecological Survey 53:233-9

197. **Roberts JM, Taylor RN, Musci TJ, Rodgers GM, Hubel CA, McLaughlin MK** 1989 Preeclampsia: an endothelial cell disorder [see comments]. American Journal of Obstetrics and Gynecology 161:1200-4

198. **Perloe M** 2000 Polycystic Ovary Syndrome..... Treatment with Insulin Lowering Medications. ivf.com, vol 2000

199. **Gasic S, Bodenburg Y, Nagamani M, Green A, Urban RJ** 1998 Troglitazone inhibits progesterone production in porcine granulosa cells. Endocrinology 139:4962-6

200. **Lemberger T, Braissant O, Juge-Aubry C, Keller H, Saladin R, Staels B, Auwerx J, Burger AG, Meier CA, Wahli W** 1996 PPAR tissue distribution and interactions with other hormone-signaling pathways. Annals of the New York Academy of Sciences 804:231-51

201. **Nuñez SB, Medin JA, Braissant O, Kemp L, Wahli W, Ozato K, Segars JH** 1997 Retinoid X receptor and peroxisome proliferator-activated receptor activate an estrogen responsive gene independent of the estrogen receptor. Molecular and Cellular Endocrinology 127:27-40

202. **Keller H, Givel F, Perroud M, Wahli W** 1995 Signaling cross-talk between peroxisome proliferator-activated receptor/retinoid X receptor and estrogen receptor through estrogen response elements. Molecular Endocrinology 9:794-804

203. **Carter DC, Ho JX** 1994 Structure of Serum Albumin. Advances in Protein Chemistry 45:153-203

204. **Curry S, Brick P, Franks NP** 1999 Fatty acid binding to human serum albumin: new insights from crystallographic studies. Biochimica et Biophysica Acta 1441:131-140

205. **Peters TJ** 1985 Serum Albumin. Advances in Protein Chemistry 37:161-245

206. **Ancell H** 1839 Lancet 1:222-231

207. **Gürber A** 1894 Sitzunberger. Phys.-Med. Ges. Wurzburg 143

208. **Low BW, Richards FM** 1954 J. Am. Chem. Soc. 76:2511-2518

209. **Low BW, Weichel EJ** 1951 J. Am. Chem. Soc. 73:3911-3916

210. **Curry S, Mandelkow H, Brick P, Franks N** 1998 Crystal structure of human serum albumin complexed with fatty acid reveals an asymmetric distribution of binding sites [see comments]. Nature Structural Biology 5:827-35

211. **Sugio S, Kashima A, Mochizuki S, Noda M, Kobayashi K** 1999 Crystal structure of human serum albumin at 2.5 A resolution. Protein Engineering 12:439-46

212. **Figge J, Rossing TH, Fencl V** 1991 The role of serum proteins in acid-base equilibria. Journal of Laboratory and Clinical Medicine 117:453-67

213. **Peters TJ, Anfinsen CB** 1950 J. Biochem. (Tokyo) 86:805-813

214. **Waldmann TA** 1977. In: Rosenoer VM, Oratz M, Rothschild MA (eds) Albumin structure, function and uses 1st ed. Pergamon Press, Oxford ; New York:255-273

215. **Kakizoe T, Sugimura T** 1988 Chemical carcinogenesis in analbuminemic rats. Japanese Journal of Cancer Research 79:775-84

216. **Nagase S, Shimamune K, Shumiya S** 1979 Albumin-deficient rat mutant. Science 205:590-1

217. **Emerson TE, Jr.** 1989 Unique features of albumin: a brief review. Critical Care Medicine 17:690-4

218. **Stamler JS, Jaraki O, Osborne J, Simon DI, Keaney J, Vita J, Singel D, Valeri CR, Loscalzo J** 1992 Nitric oxide circulates in mammalian plasma primarily as an S-nitroso adduct of serum albumin. Proceedings of the National Academy of Sciences of the United States of America 89:7674-7

219. **Fitzpatrick FA, Wynalda MA** 1981 Albumin-Lipid Interactions: Prostaglandin Stability as a Probe for Characterizing Binding Sites on Vertebrate Albumins. Biochemsitry 20:6129-6134

220. **Watanabe T, Narumiya S, Shimizo T, Hayaishi O** 1982 Characterization of the Biosynthetic Pathway of Prostaglandin D_2 in Human Platelet-rich Plasma. Journal of Biological Chemistry 257:14847-14853

221. **McNurlan MA, Garlick PJ, Frost RA, Decristofaro KA, Lang CH, Steigbigel RT, Fuhrer J, Gelato M** 1998 Albumin synthesis and bone collagen formation in human immunodeficiency virus-positive subjects: differential effects of growth hormone administration. Journal of Clinical Endocrinology and Metabolism 83:3050-5

222. **Guthrow CE, Morris MA, Day JF, Thorpe SR, Baynes JW** 1979 Enhanced nonenzymatic glucosylation of human serum albumin in diabetes mellitus. Proceedings of the National Academy of Sciences of the United States of America 76:4258-61

223. **Shaklai N, Garlick RL, Bunn HF** 1984 Nonenzymatic glycosylation of human serum albumin alters its conformation and function. Journal of Biological Chemistry 259:3812-7

224. **Koizumi K, Ikeda C, Ito M, Suzuki J, Kinoshita T, Yasukawa K, Hanai T** 1998 Influence of glycosylation on the drug binding of human serum albumin. Biomedical Chromatography 12:203-10

225. **Arbogast BW, Dreher NJ** 1987 Coronary disease prediction using a new atherogenic index. Atherosclerosis 66:55-62

226. **Nelson JJ, Liao D, Sharrett AR, Folsom AR, Chambless LE, Shahar E, Szklo M, Eckfeldt J, Heiss G** 2000 Serum albumin level as a predictor of incident coronary heart disease: the Atherosclerosis Risk in Communities (AIRC) study. American Journal of Epidemiology 151:468-77

227. **Dekker GA, Sibai BM** 1998 Etiology and pathogenesis of preeclampsia: current concepts. American Journal of Obsetrics and Gynecology 179:1359-75

228. **Palmer CN, Wolf CR** 1998 cis-parinaric acid is a ligand for the human peroxisome proliferator activated receptor gamma: development of a novel spectrophotometric assay for the discovery of PPARgamma ligands. Febs Letters 431:476-80

229. **Roberts-Thomson SJ** 2000 Peroxisome proliferator-activated receptors in tumorigenesis: targets of tumour promotion and treatment. Immunology and Cell Biology 78:436-41

230. **Tanis SP, Parker TT, Colca JR, Fisher RM, Kletzein RF** 1996 Synthesis and Biological Activity of Metabolites of the Antidiabetic, Antihyperglycemic Agent Pioglitazone. Journal of Medicinal Chemistry 39:5053-5063

231. **Cantello BCC, Cawthorne MA, Haigh D, Hindley RM, Smith SA, Thurlby PL** 1994 The Synthesis of BRL 49653 - A Novel and Potent Antihyperglycaemic Agent. Bioorganic and Medicinal Chemistry Letters 4:1181-1184

232. **Greene TW, Wuts PGM** 1991 Protective Groups in Organic Synthesis 2 ed. John Wiley & Sons, Inc., New York

233. **Sheehan JC, Bolhofer WA** 1950 An Improved Procedure for the Condensation of Potassium Phthalimide with Organic Halides. Journal of the American Chemical Society 72:2786-2788

234. **Alami M, Ferri F, Linstrumelle G** 1993 An Efficient Palladium-Catalysed Reaction of Vinyl and Aryl Halides or Triflates with Terminal Alkynes. Tetrahedron Letters 34:6403-6406

235. **Mayer JM, Schneemeyer LF, Siegrist T, Waszczak JV, Vandover B** 1992 New Layered Iron-Lanthanum-Oxide-Sulfide and Iron-Lanthanum-Oxide-Selenide Phases - Fe2la2o3e2(E = S,Se). Angewandte Chemie-International Edition in English 31:1645-1647

236. **Hertz R, Berman I, Keppler D, Bar-Tana J** 1996 Activation of gene transcription by prostacyclin analogues is mediated by the peroxisome-proliferators-activated receptor (PPAR). European Journal of Biochemistry 235:242-7

237. **Elbrecht A, Chen Y, Cullinan CA, Hayes N, Leibowitz M, Moller DE, Berger J** 1996 Molecular cloning, expression and characterization of human peroxisome proliferator activated receptors gamma 1 and gamma 2. Biochemical and Biophysical Research Communications 224:431-7

238. **Darimont BD** *Personal Communication*

239. **Michalik L, Wahli W** 1999 Peroxisome proliferator-activated receptors: a nuclear receptor signaling pathway in lipid physiology. Ann. Rev. Cell Dev. Biol. 12:335-363

240. **Miesfeld R, Godowski PJ, Maler BA, Yamamoto KR** 1987 Glucocorticoid receptor mutants that define a small region sufficient for enhancer activation. Science 236:423-7

241. **Hauser S, Adelmant G, Sarraf P, Wright HM, Mueller E, Spiegelman BM** 2000 Degradation of the peroxisome proliferator-activated receptor gamma is linked to ligand-dependent activation. Journal of Biological Chemistry 275:18527-33

242. **Desvergne B, A IJ, Devchand PR, Wahli W** 1998 The peroxisome proliferator-activated receptors at the cross-road of diet and hormonal signalling. Journal of Steroid Biochemistry and Molecular Biology 65:65-74

243. **Swillens S** 1995 Interpretation of binding curves obtained with high receptor concentrations: practical aid for computer analysis. Molecular Pharmacology 47:1197-203

244. **Huber R** 1999 personal communication

245. **Fitzpatrick FA, Liggett WF, Wynalda MA** 1984 Albumin-Eicosanoid Interactions. Journal of Biological Chemistry 259:2722-2727

246. **Maclouf J, Kindahl H, Granström E, Samuelsson B** 1980 Interactions of Prostaglandin H_2 and Thromboxane A_2 with Human Serum Albumin. Eur. J. Biochem. 109:561-666

247. **Kosa T, Maruyama T, Otagiri M** 1998 Species DIfferences of Serum Albumins: II. Chemical and Thermal Stability. Pharaceutical Research 15:449-454

248. **Tontonoz P, Singer S, Forman BM, Sarraf P, Fletcher JA, Fletcher CDM, Brun RP, Mueller E, Altiok S, Oppenheim J** 1997 Terminal differentiation of human liposarcoma cells induced by ligands for peroxisome proliferator-activated receptor gamma and the retinoid X receptor. Proc. Natl. Acad. Sci. U.S.A. 94:237-241

249. **Michael LF, Lazar MA, Mendelson CR** 1997 Peroxosome proliferator-activated receptor gamma1 expression is induced during cyclic adenosine monophosphate-

stimulated differentiation of alveolar type II pneumonocytes. Endocrinology 138:3695-3703

250. **Teboul L, Gaillard D, Staccini L, Inadera H, Amri EZ, Grimaldi PA** 1995 Thiazolidinediones and fatty acids convert myogenic cells into adipose-like cells. J. Biol. Chem. 270:28183-28187

251. **Altiok S, Xu M, Spiegelman BM** 1997 PPARgamma induces cell cycle withdrawal: inhibition of E2F/DP DNA-binding activity via down-regulation of PP2A. Genes Dev. 11:1987-1998

252. **Geistlinger T** personal communication

253. **Serber Z** personal communication

254. **Serber Z, Keatinge-Clay A, Ledwidge R, Kelly A, Miller S, Doetsch V** submitted High-Resolution Macromolecular NMR Spectroscopy Inside Living Cells. Journal of the American Chemical Society

Appendix

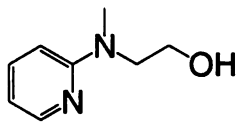

Appendix 2.1: ^{1}H-NMR ($CDCl_3$) 2-methyl-2-pyridinylaminoethanol (1)

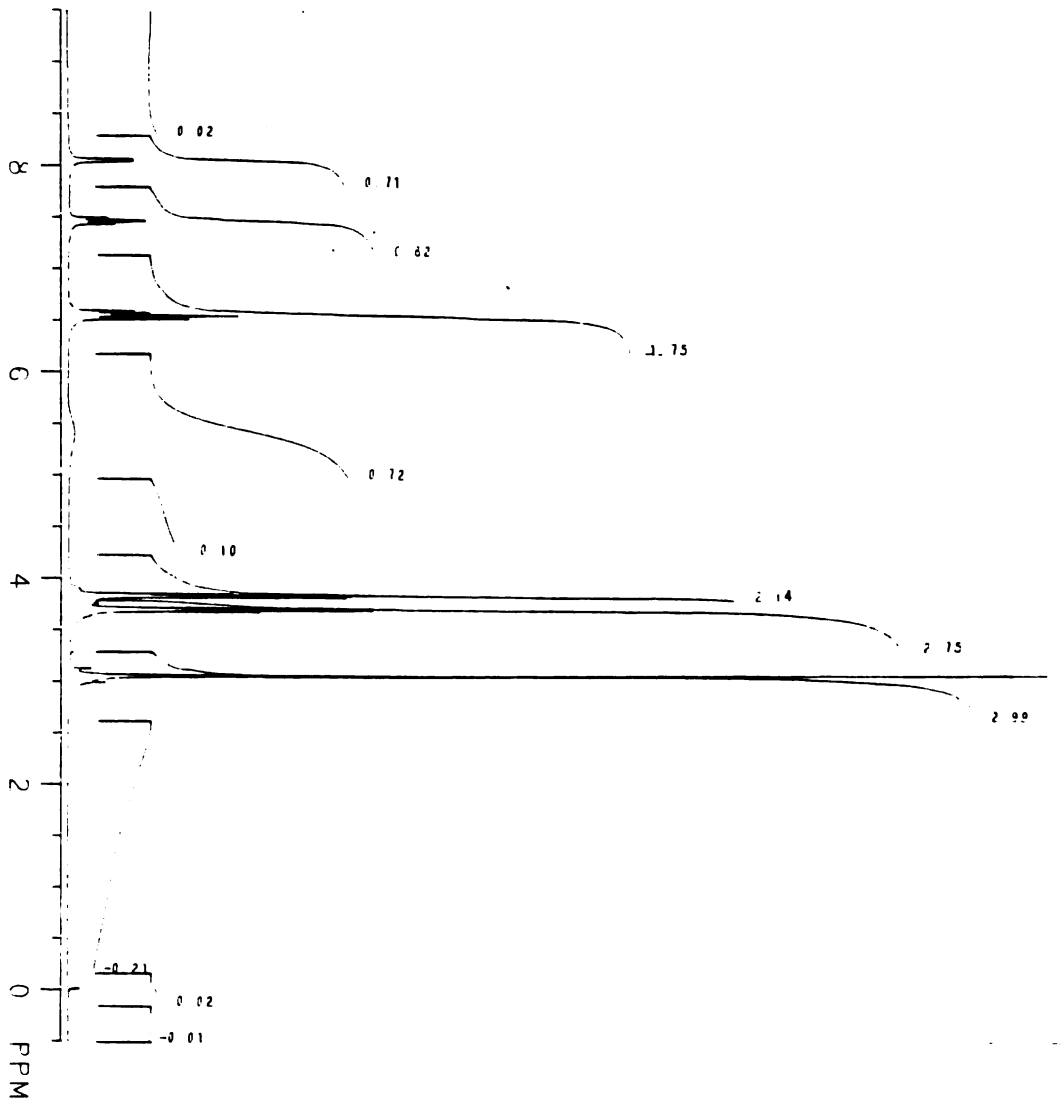

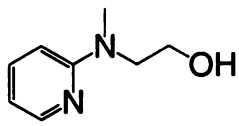

Appendix 2.2: ^{13}C-NMR ($CDCl_3$) 2-methyl-2-pyridinylaminoethanol (**1**)

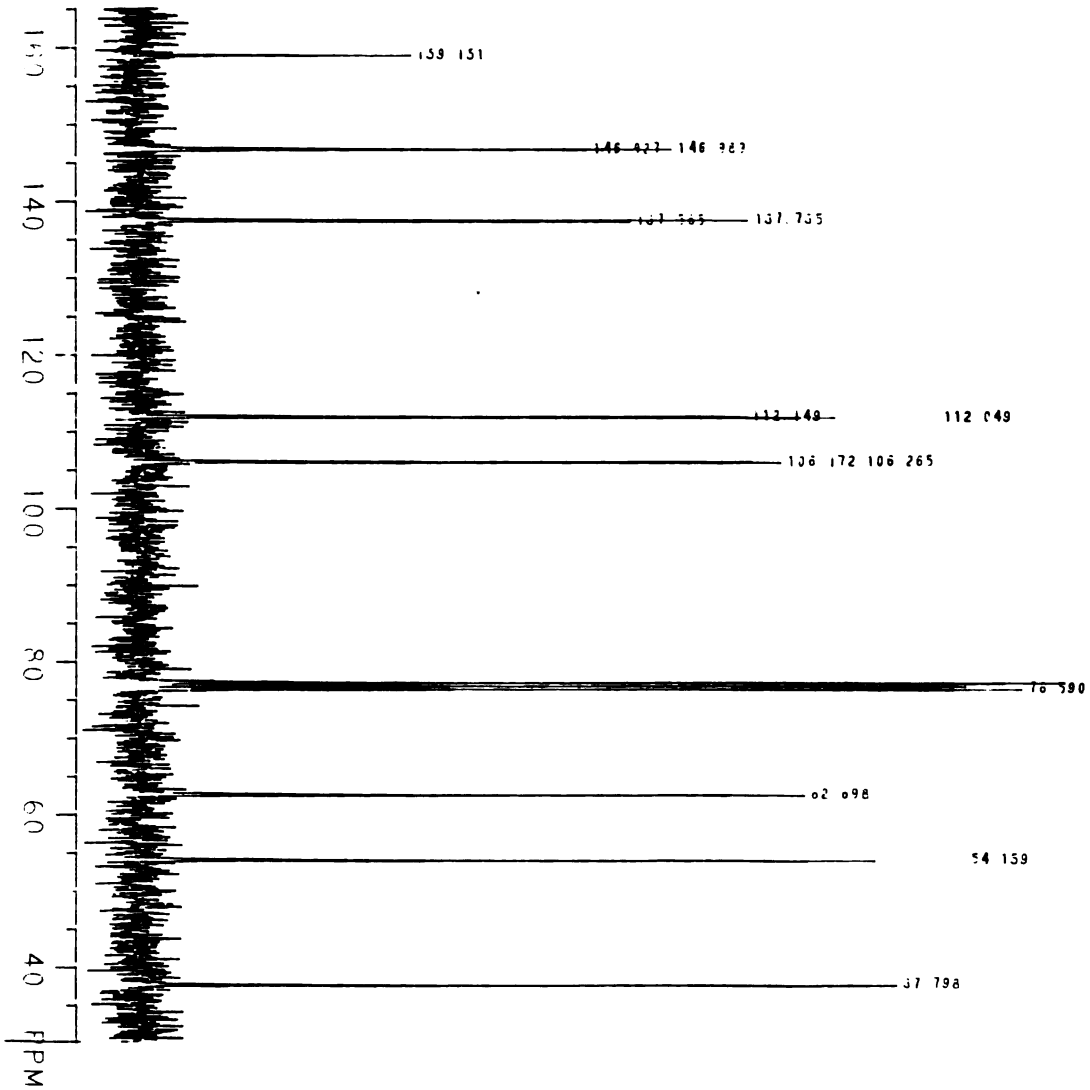

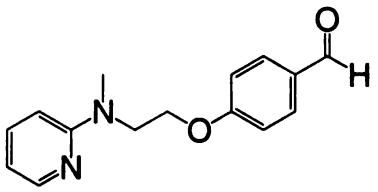

Appendix 2.3: ^{1}H-NMR ($CDCl_3$) 4-(2-(methyl-2-pyridinylamino)ethoxy)benzaldehyde (**2**)

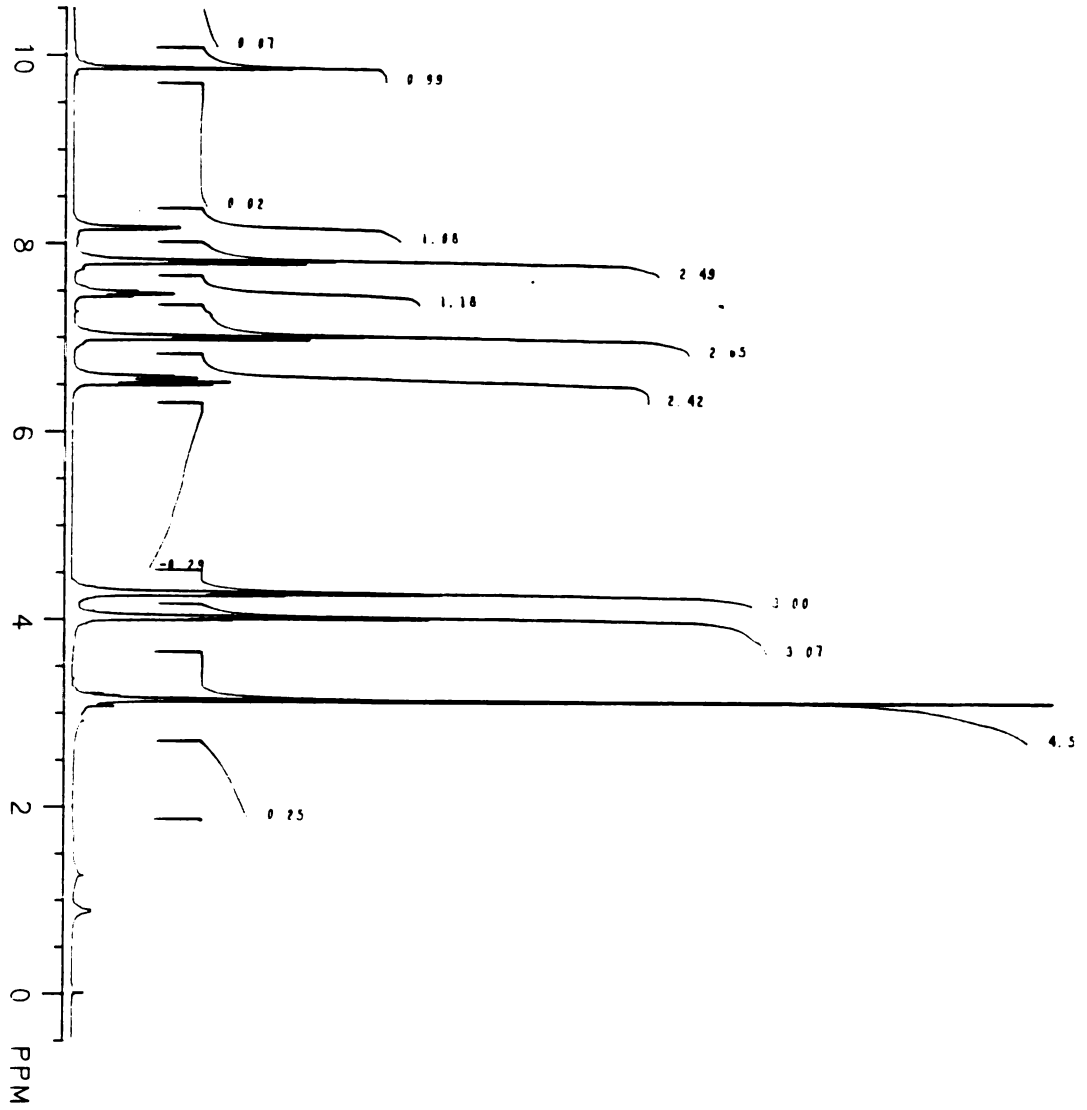

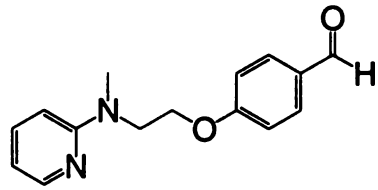

Appendix 2.4: ^{13}C-NMR ($CDCl_3$) 4-(2-(methyl-2-pyridinylamino)ethoxy)benzaldehyde (**2**)

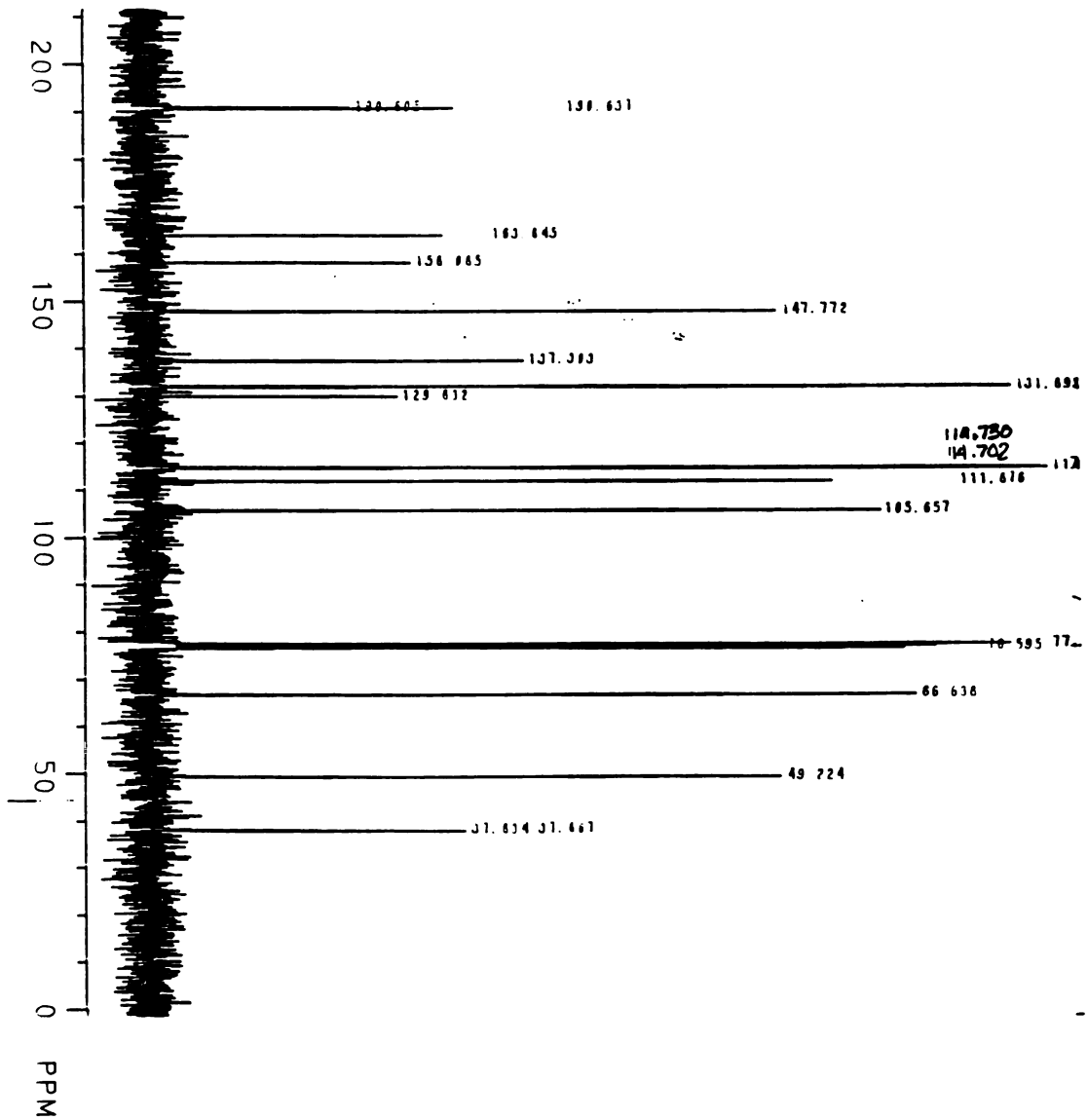

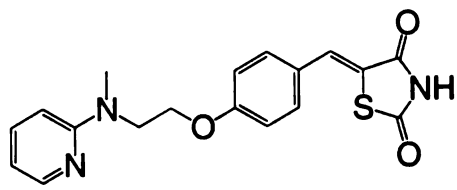

Appendix 2.5: ^{1}H-NMR (DMSO-d_6) (Z)-5-((4-(2-(methyl-2-pyridinylamino)ethoxy)phenyl)-methylene-2,4-thiazolidinedione (**3**)

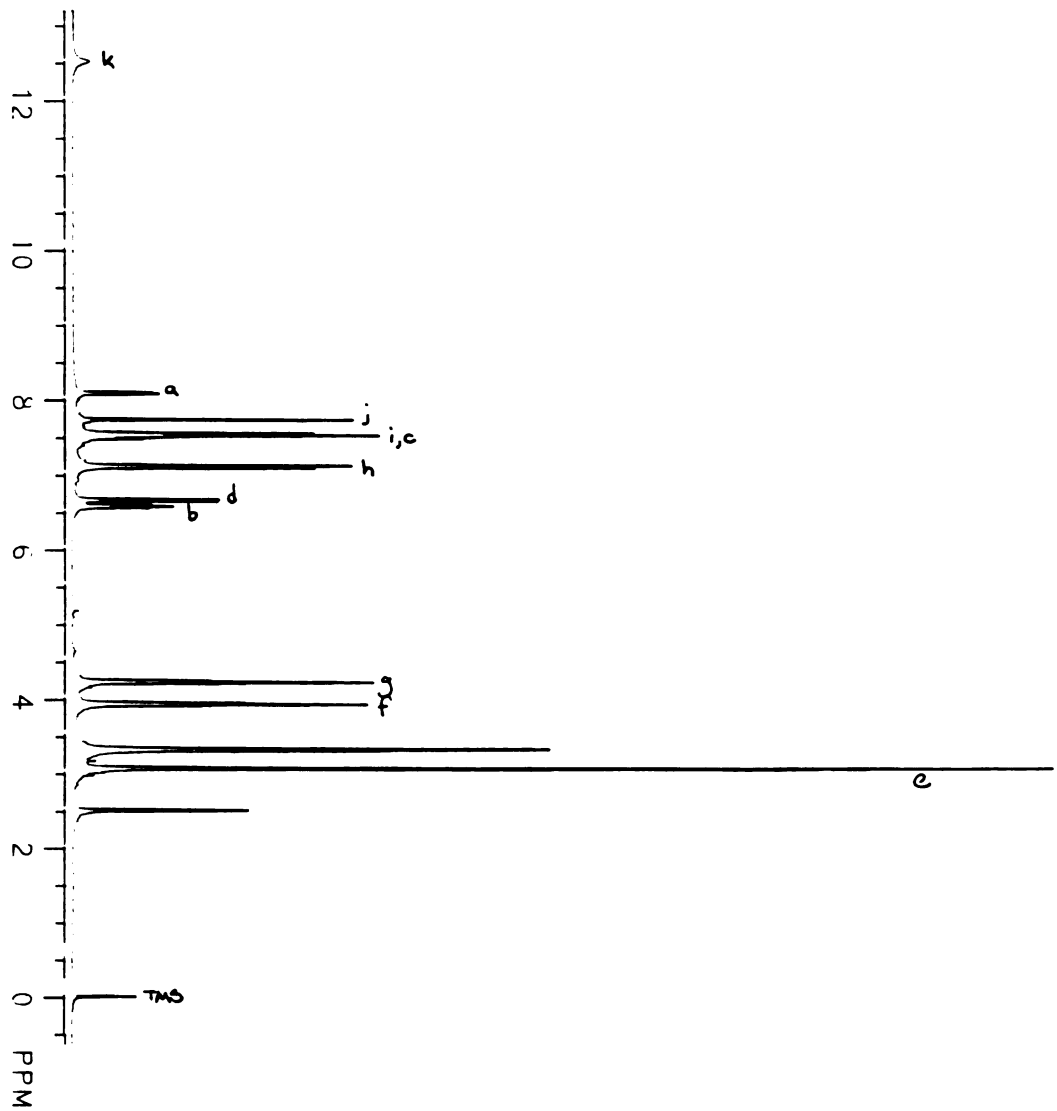

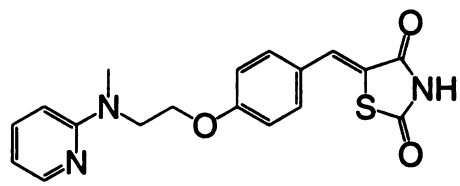

Appendix 2.6: ^{13}C-NMR (DMSO-d_6) (Z)-5-((4-(2-(methyl-2-pyridinylamino)ethoxy)phenyl)-methylene-2,4-thiazolidinedione (3)

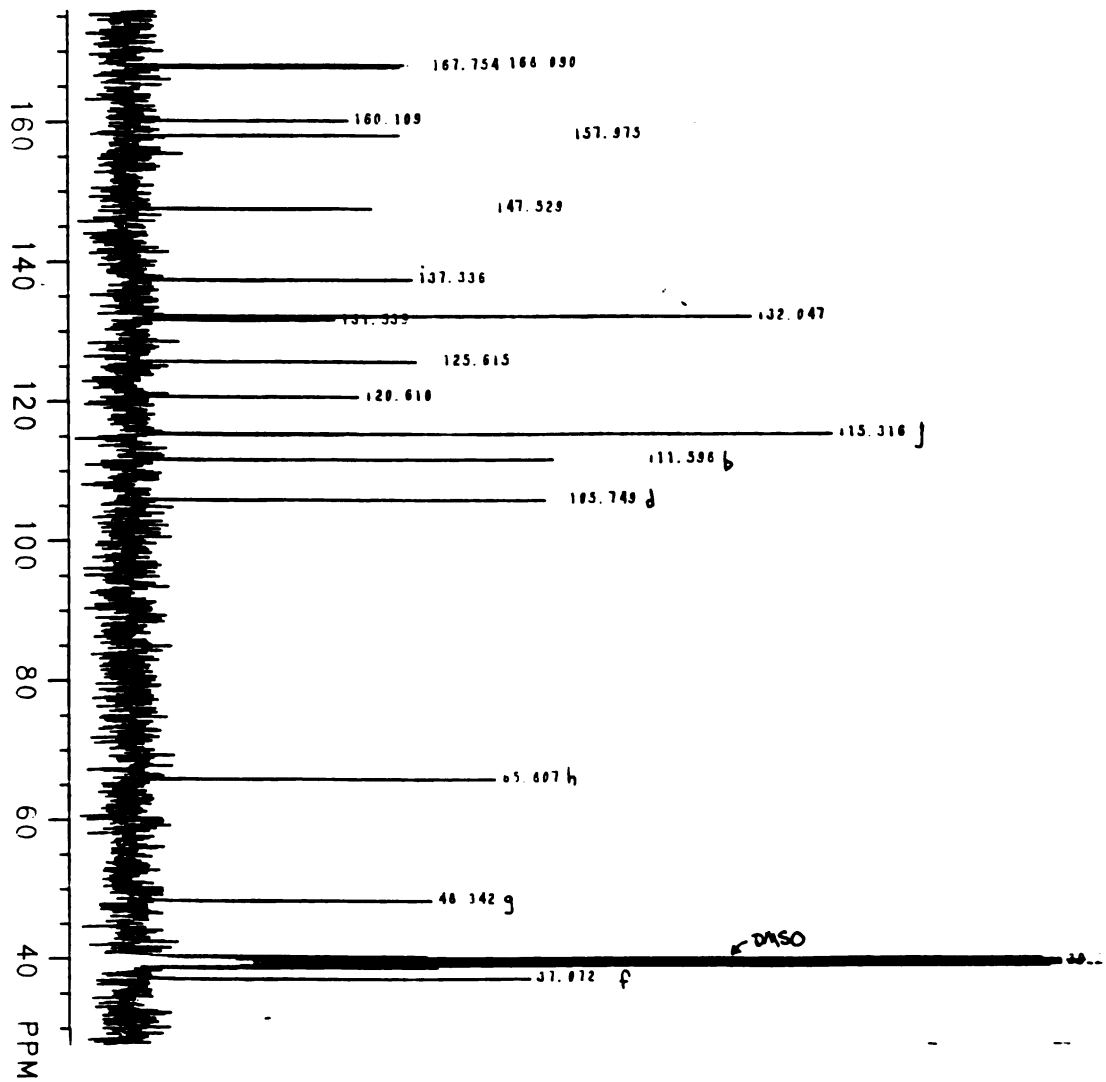

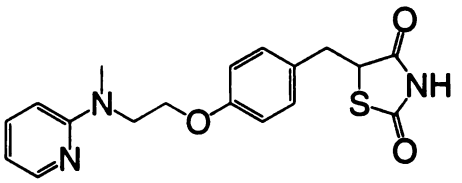

Appendix 2.7: ^{1}H-NMR (DMSO-d_6) 5-(4-(2-(methyl-2-pyridinylamino)ethoxy)benzyl-2,4-thiazolidinedione (**4**)

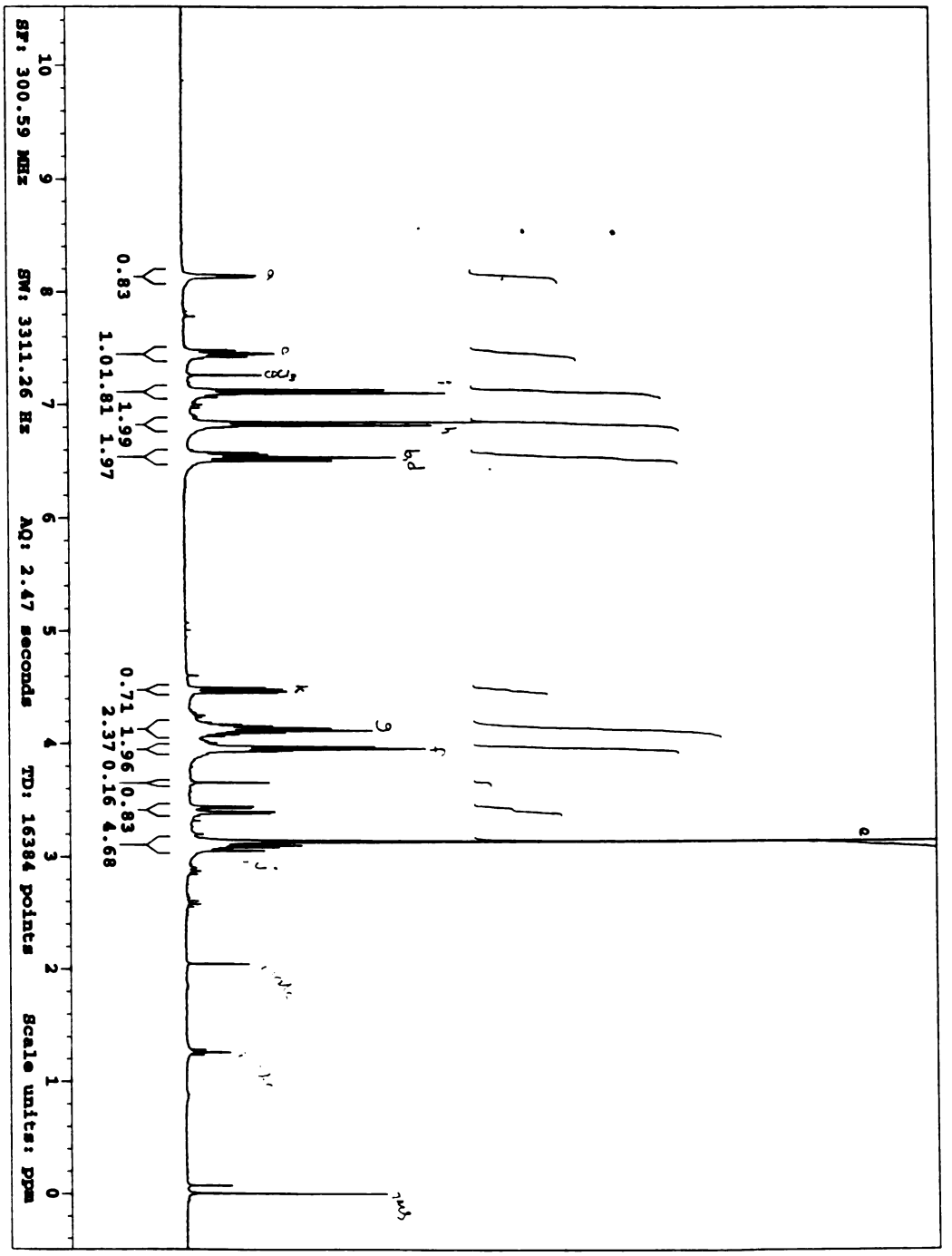

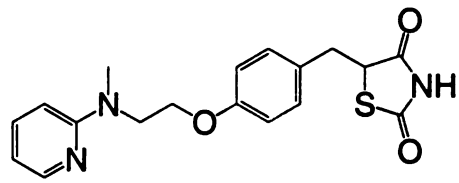

Appendix 2.8: ^{13}C-NMR (DMSO-d_6) 5-(4-(2-(methyl-2-pyridinylamino)ethoxy)benzyl-2,4-thiazolidinedione (**4**)

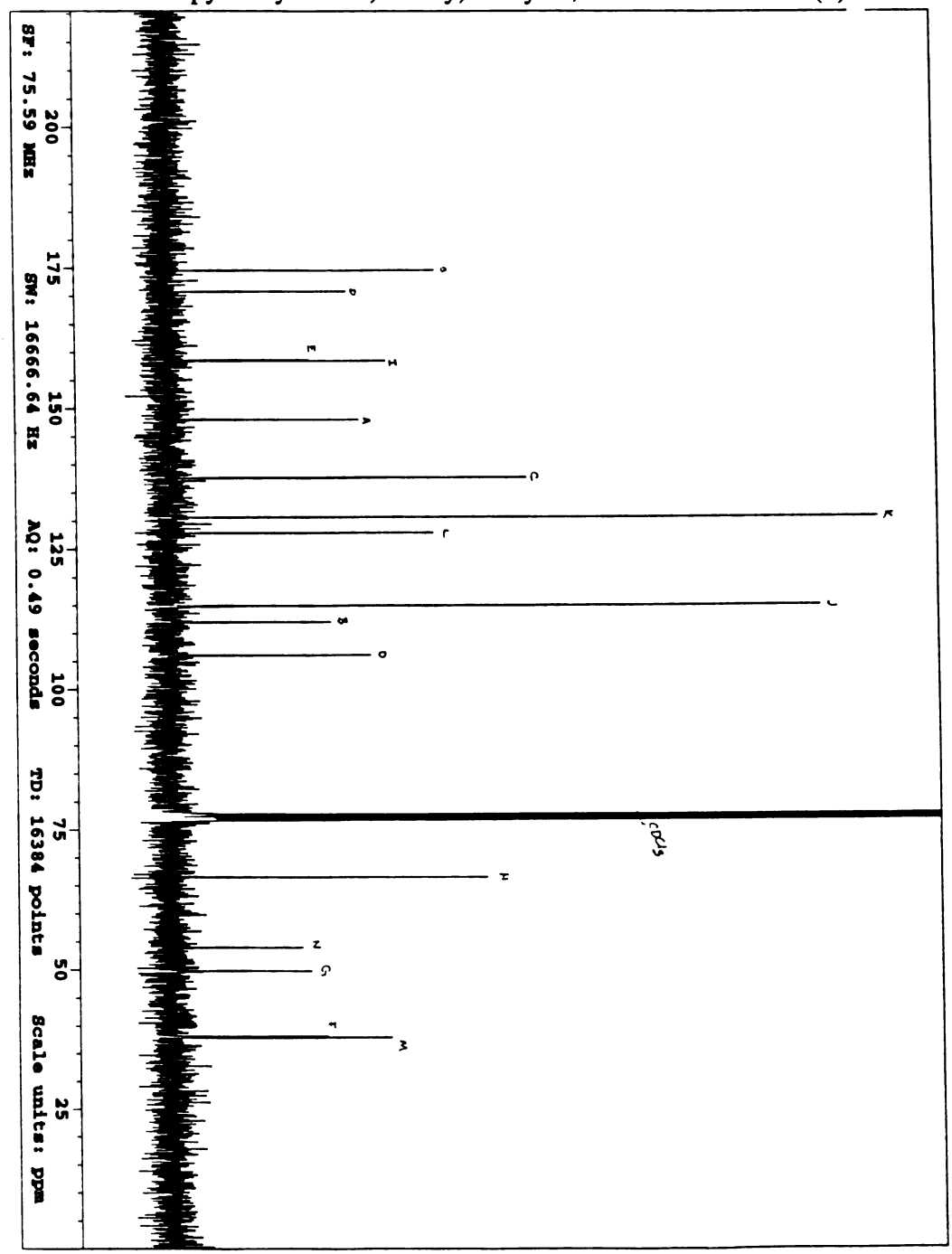

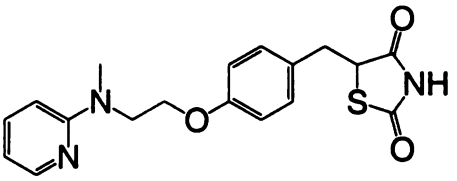

Appendix 2.9: ^{1}H-NMR (DMSO-d_6) 5-(4-(2-(methyl-2-pyridinylamino)ethoxy)benzyl-2,4-thiazolidinedione (**4**) Acetate Salt

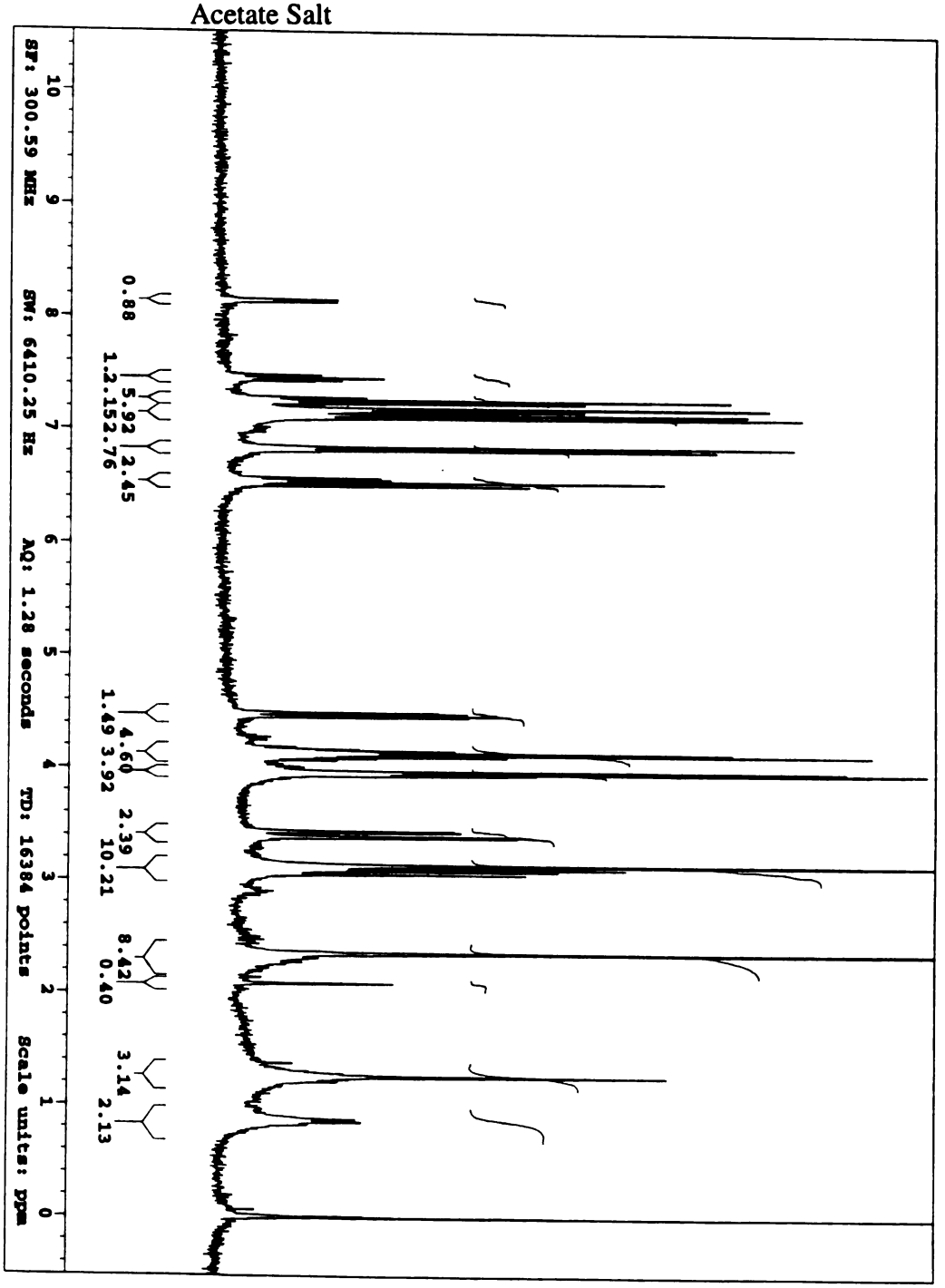

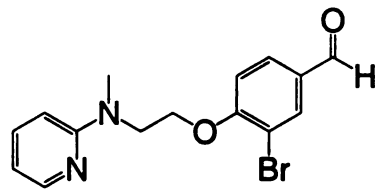

Appendix 2.10: ^{1}H-NMR ($CDCl_3$) 3-bromo-4-(2-(methyl-2-pyridinylamino)ethoxy)-benzaldehyde (**2Br**)

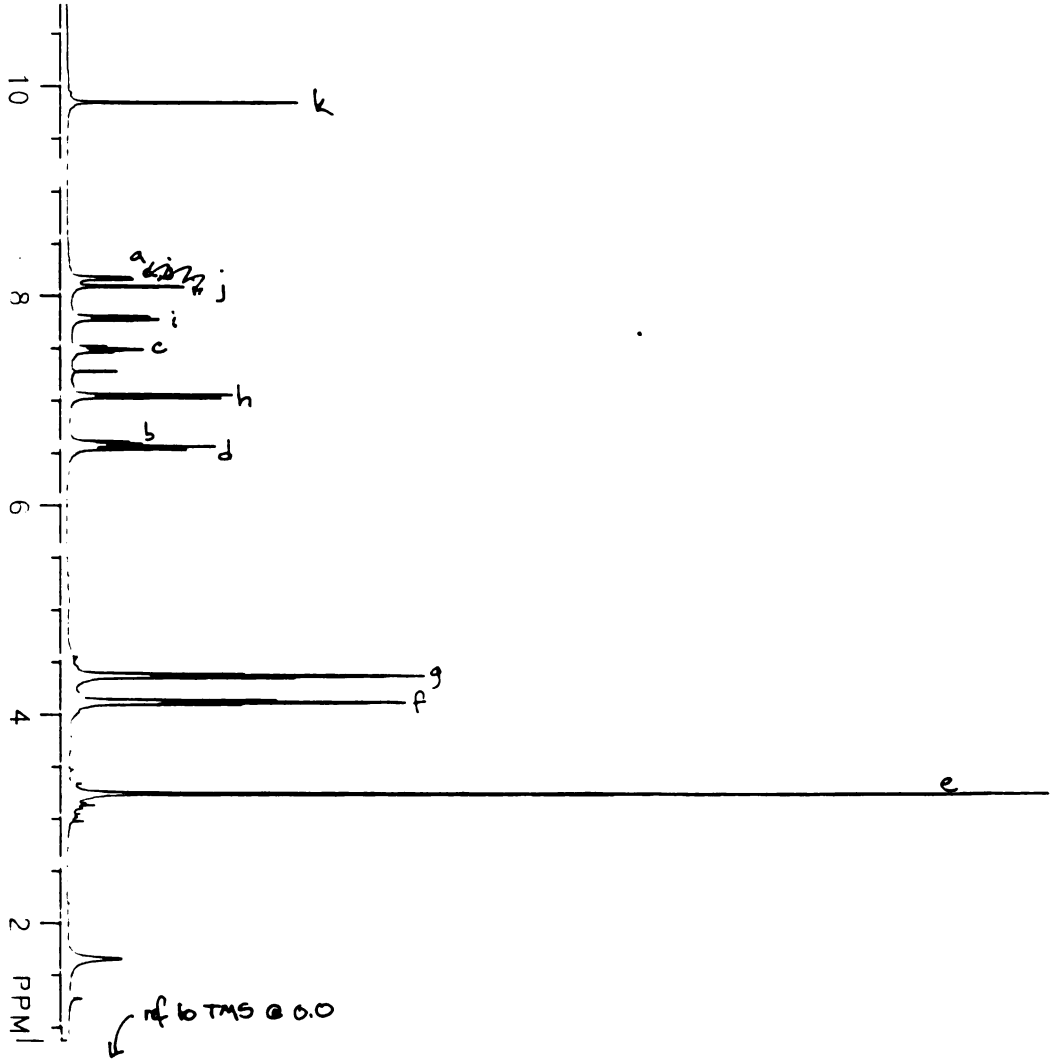

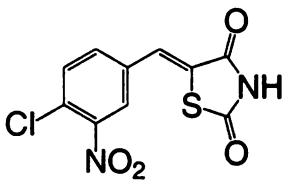

Appendix 2.11: ^{1}H-NMR (DMSO-d_6) (Z)-5-((4-chloro-3-nitrophenyl)methylene)-2,4-thiazolidinedione (**5**)

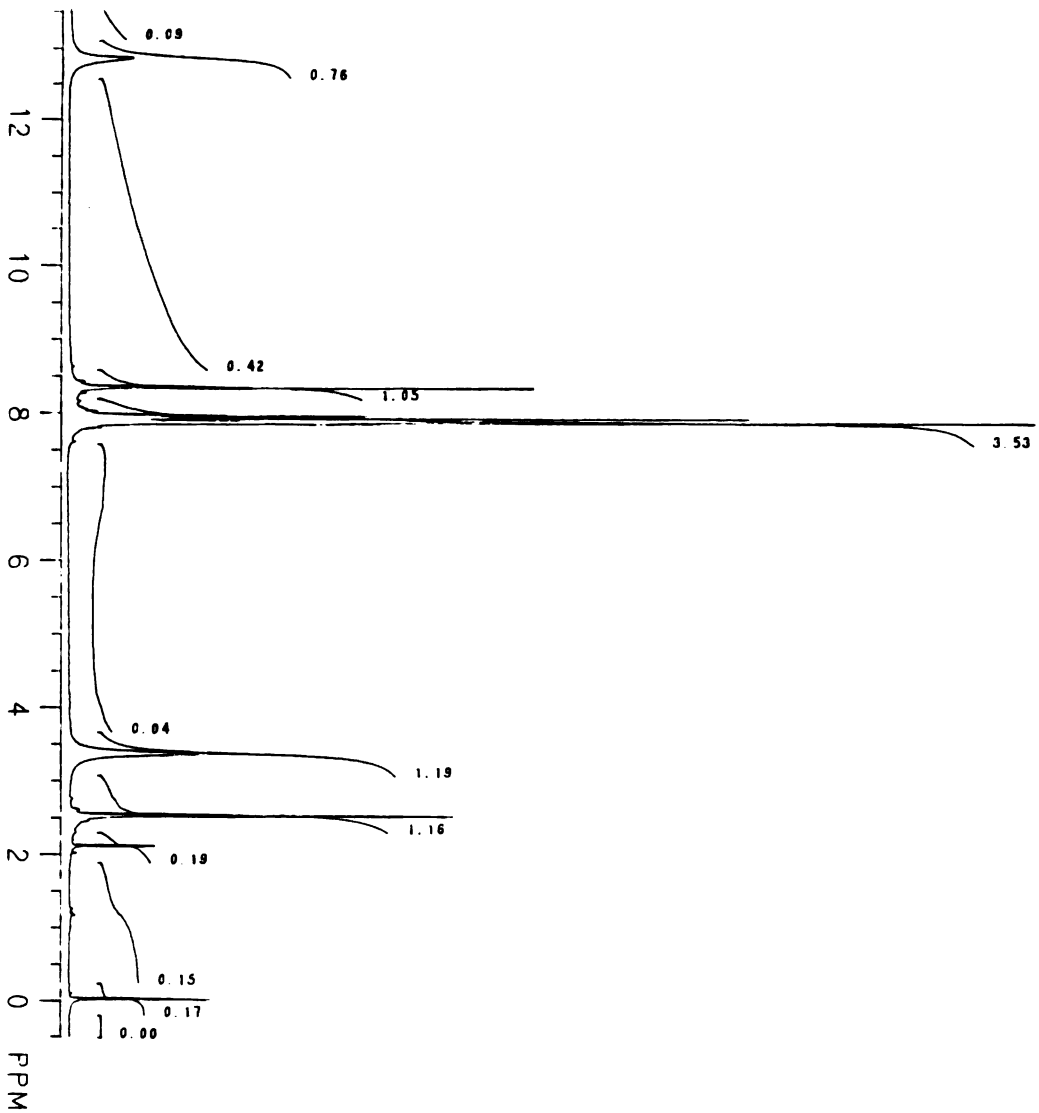

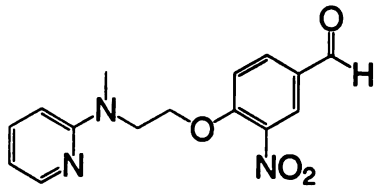

Appendix 2.12: ^{1}H-NMR (Acetone-d_6) 4-(2-(methyl-2-pyridinylamino)ethoxy)-3-nitrobenzaldehyde (**8**)

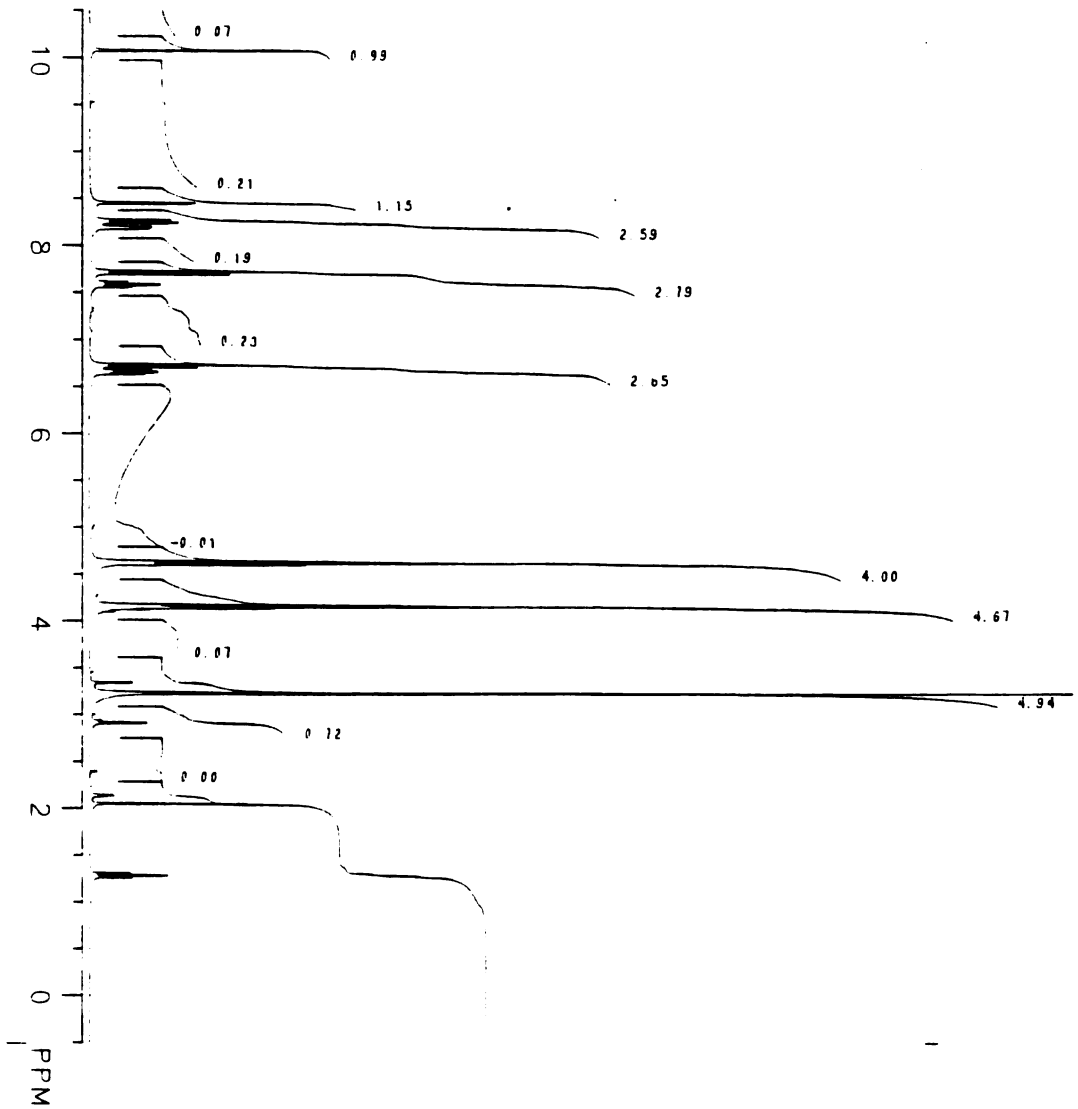

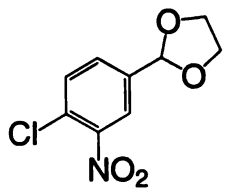

Appendix 2.13: ^{1}H-NMR (Acetone-d_6) 4-chloro-3-nitrophenyl-1,3-dioxolane (**9**)

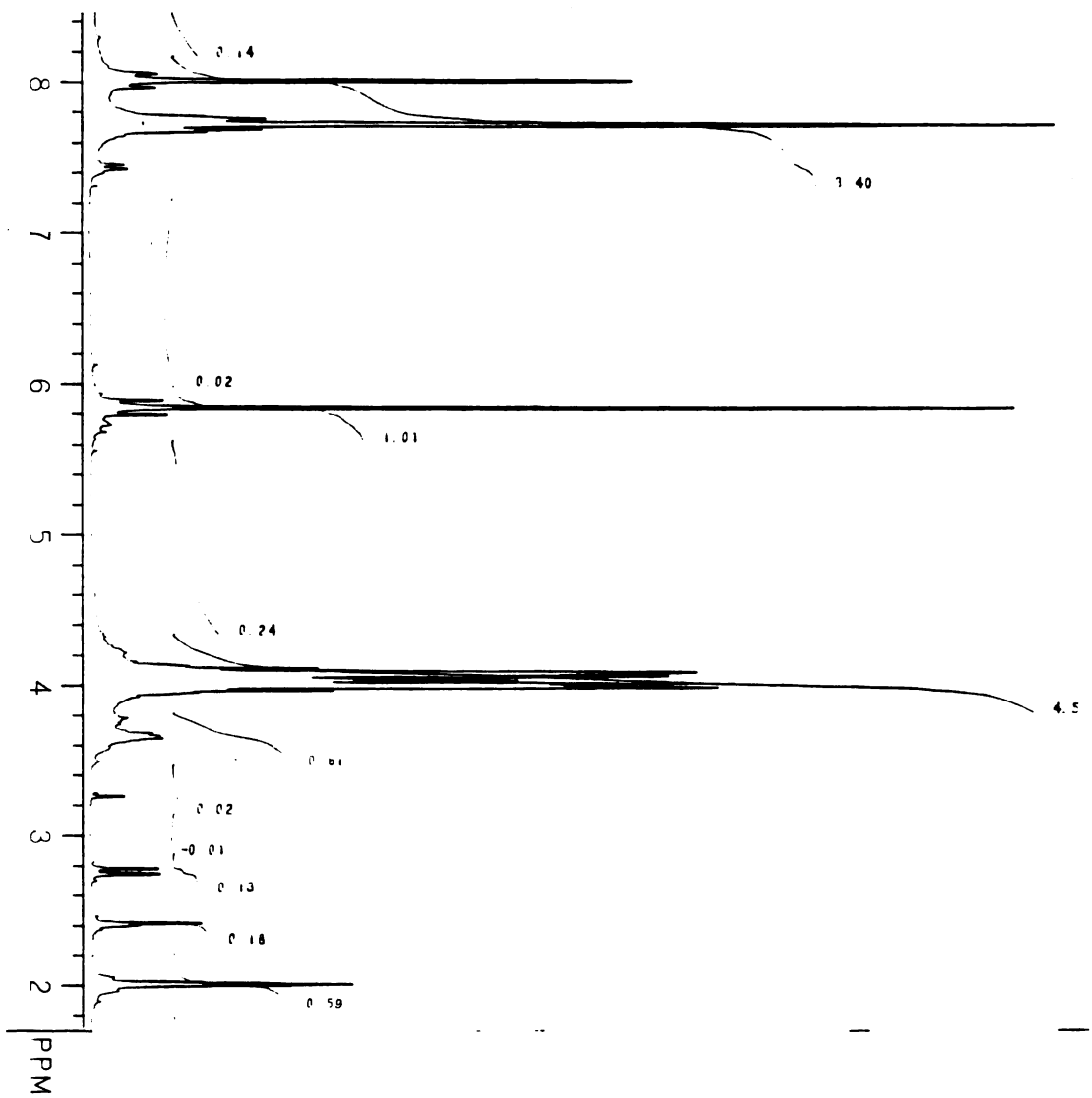

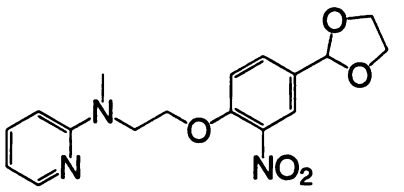

Appendix 2.14: ^{1}H-NMR (Acetone-d_6) 4-(2-(methyl-2-pyridinylamino)ethoxy)-3-nitrophenyl-1,3-dioxolane (**10**)

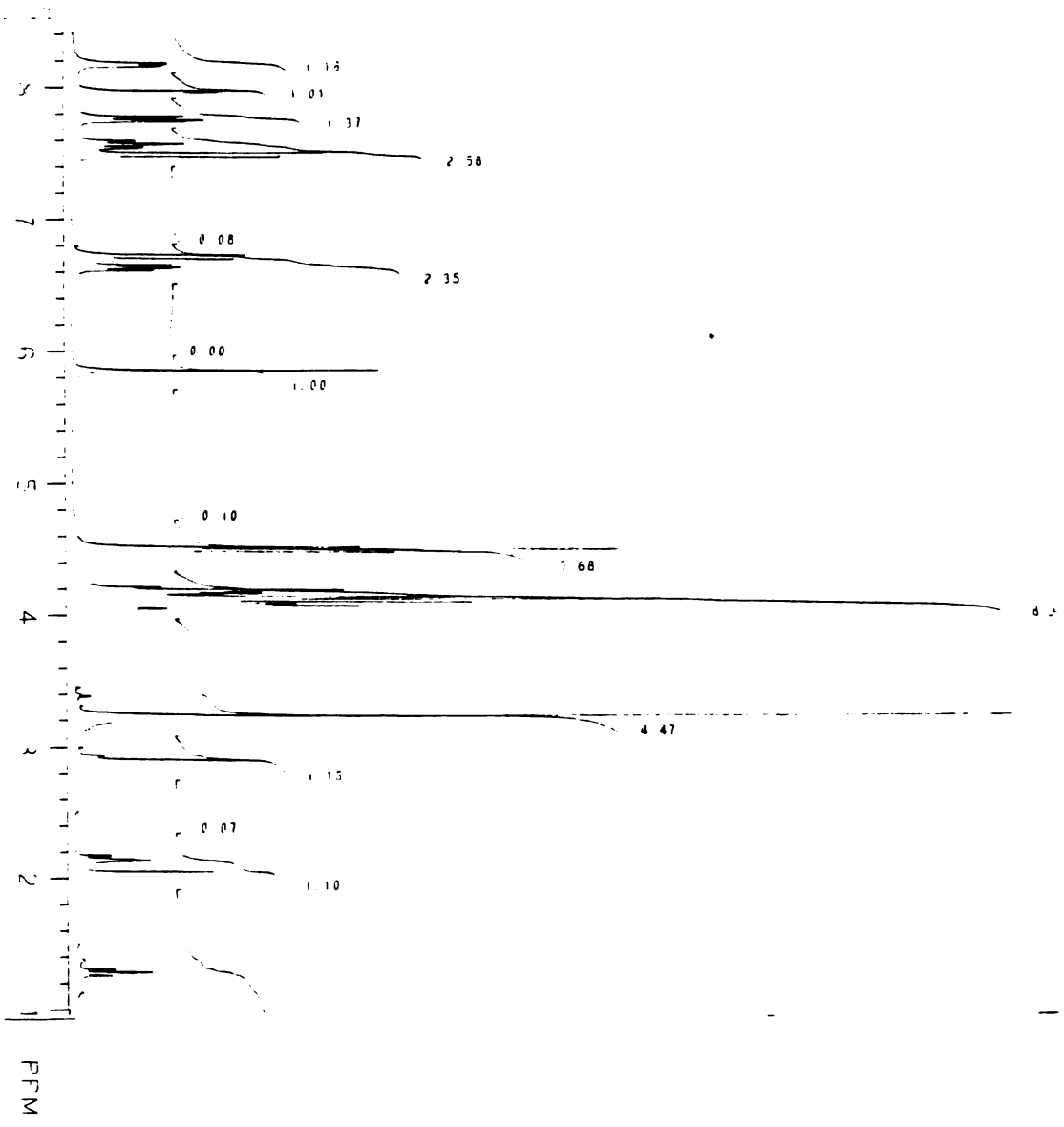

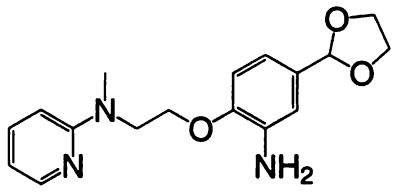

Appendix 2.15: ^{1}H-NMR ($CDCl_3$) 4-(2-(methyl-2-pyridinylamino)ethoxy)-3-aminophenyl-1,3-dioxolane (**15**)

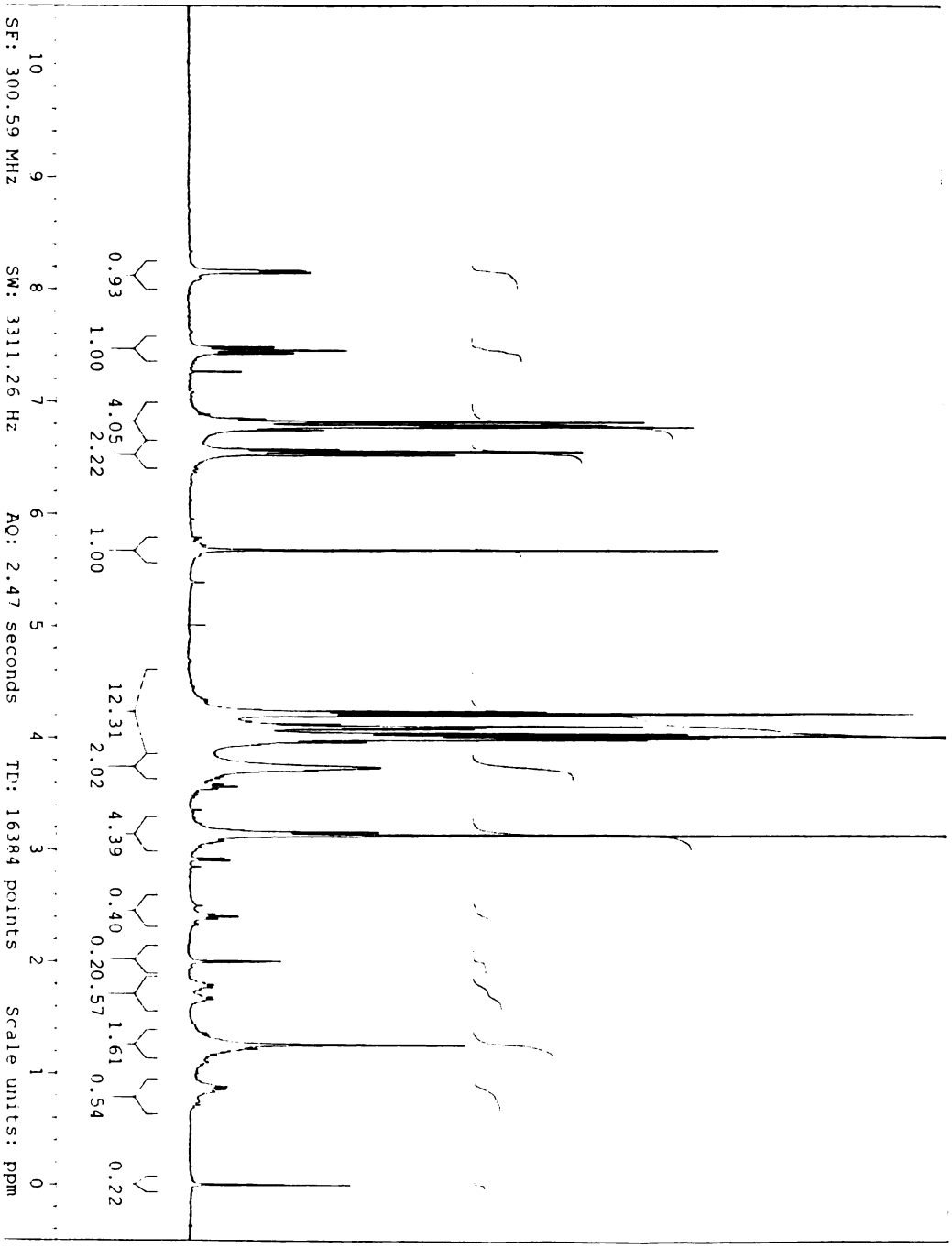

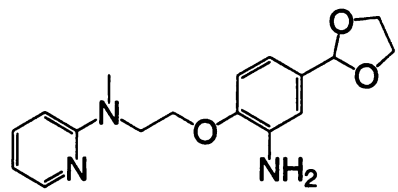

Appendix 2.16: ^{13}C-NMR ($CDCl_3$) 4-(2-(methyl-2-pyridinylamino)ethoxy)-3-aminophenyl-1,3-dioxolane (**15**)

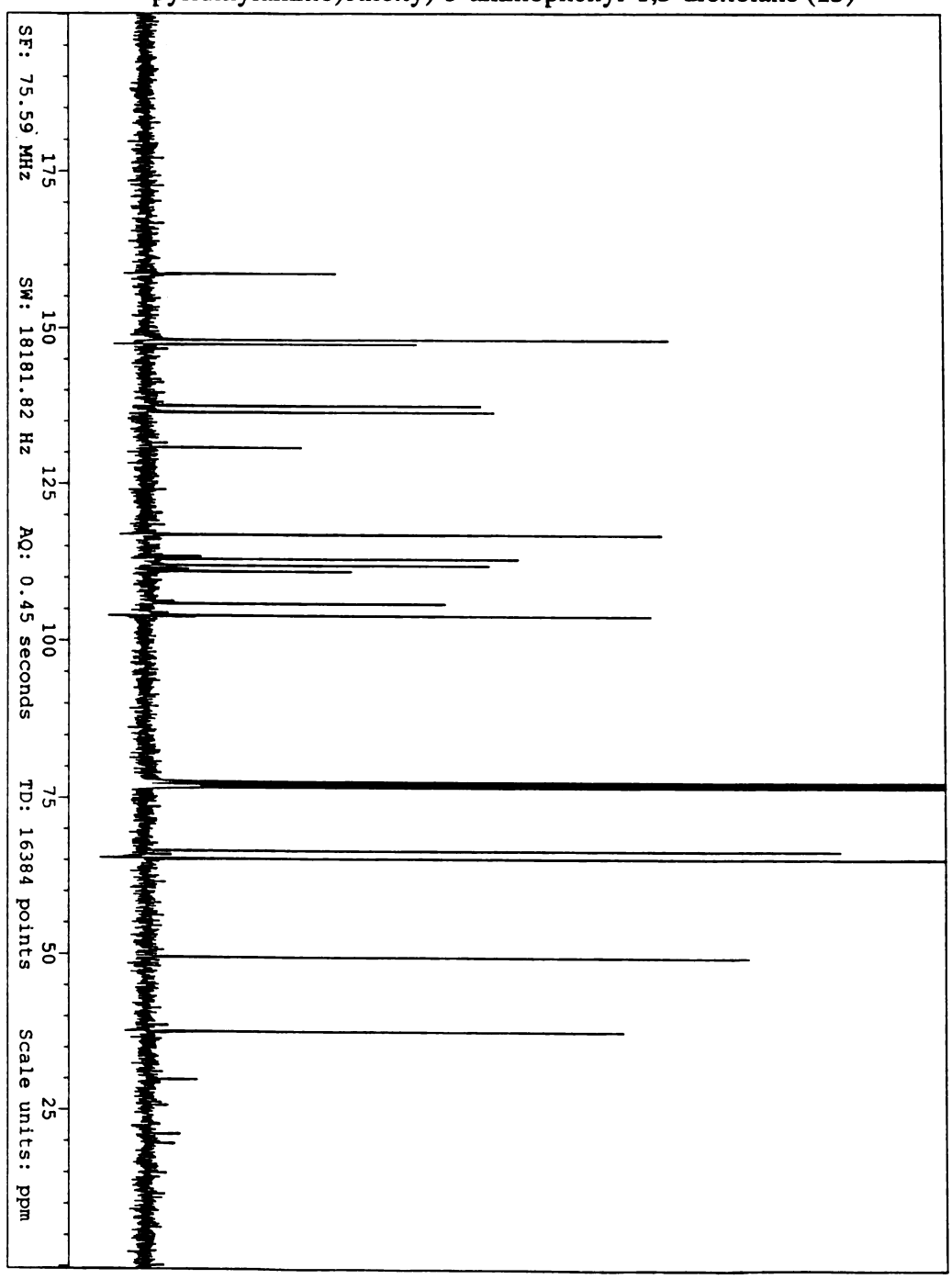

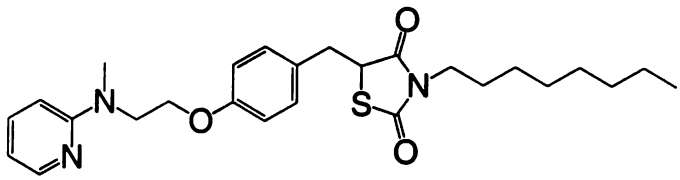

Appendix 2.17: ^{1}H-NMR ($CDCl_3$) 5-(4-(2-(methyl-2-pyridinylamino)ethoxy)benzyl-N-octyl-2,4-thiazolidinedione (**101**)

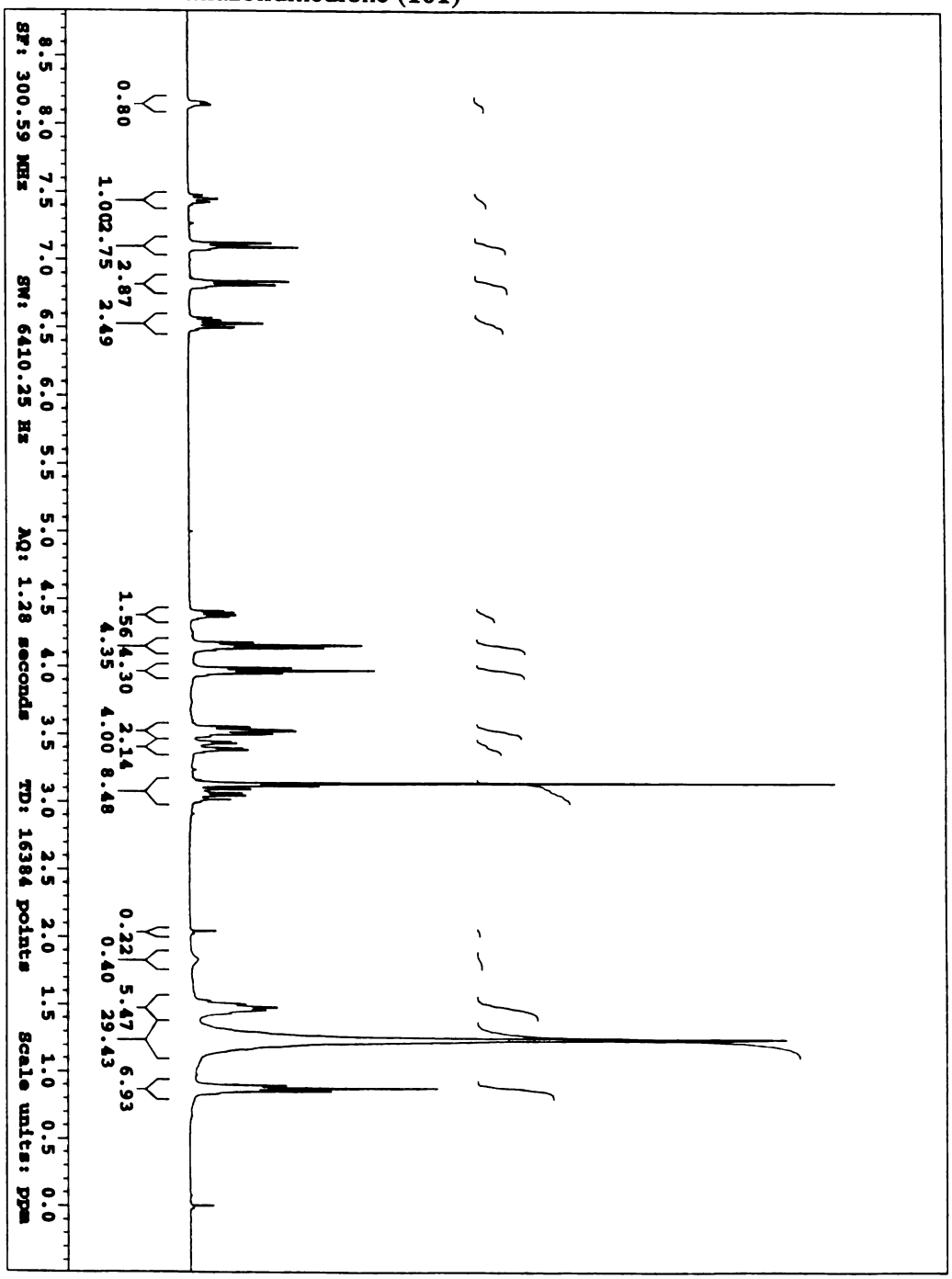

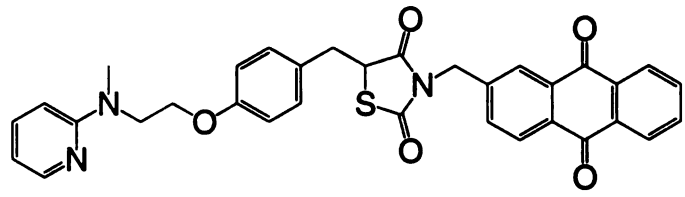

Appendix 2.18: ^{1}H-NMR ($CDCl_3$) 5-(4-(2-(methyl-2-pyridinylamino)ethoxy)benzyl-N-(2-(bromomethyl)anthroquinone)-2,4-thiazolidinedione (**102**)

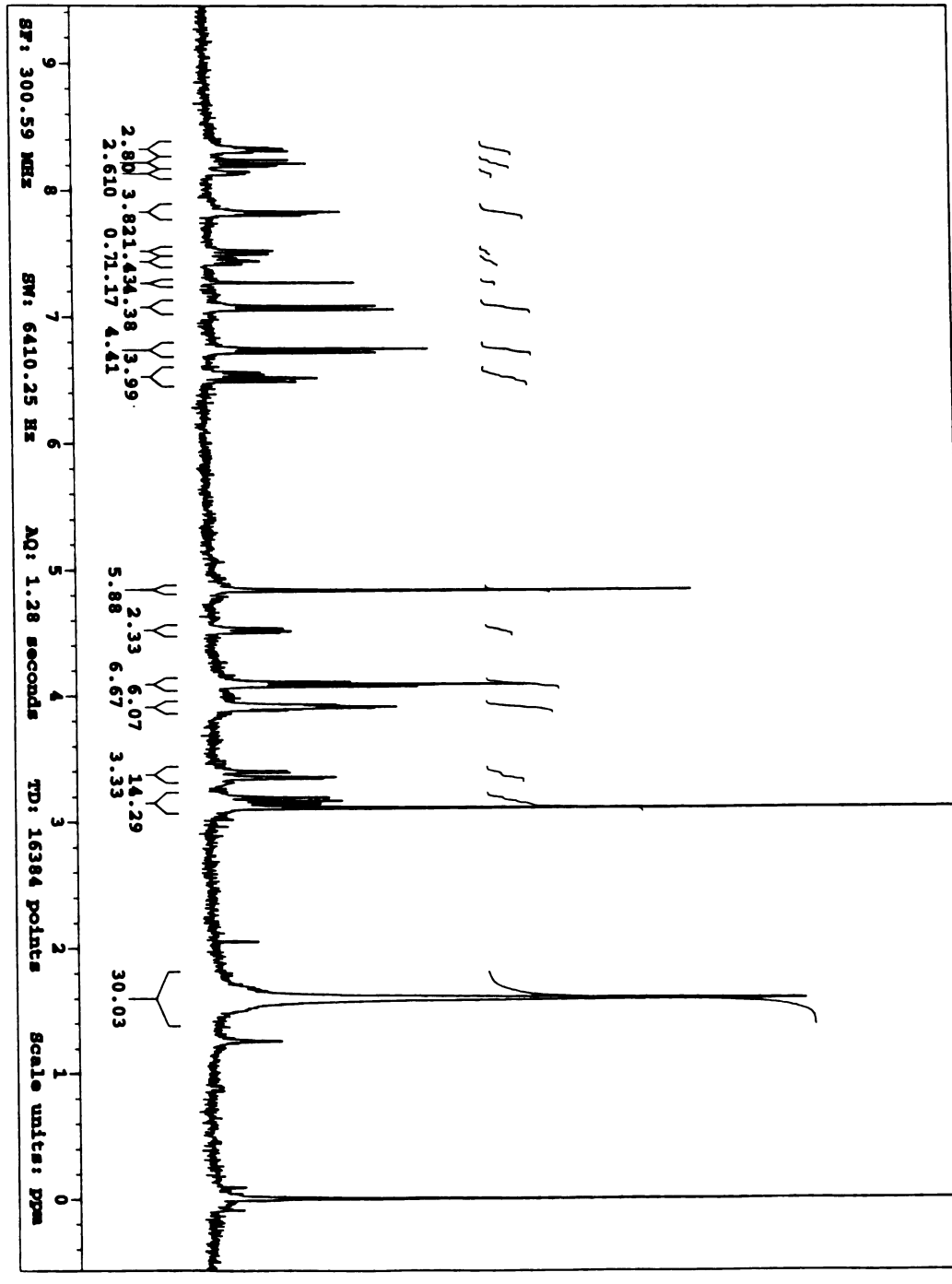

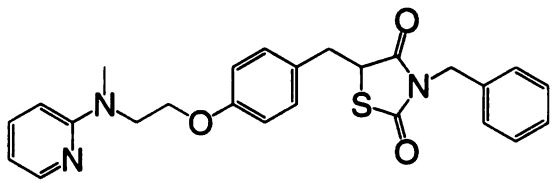

Appendix 2.19: ^{1}H-NMR ($CDCl_3$) 5-(4-(2-(methyl-2-pyridinylamino)ethoxy)benzyl-N-benzyl-2,4-thiazolidinedione (**103**)

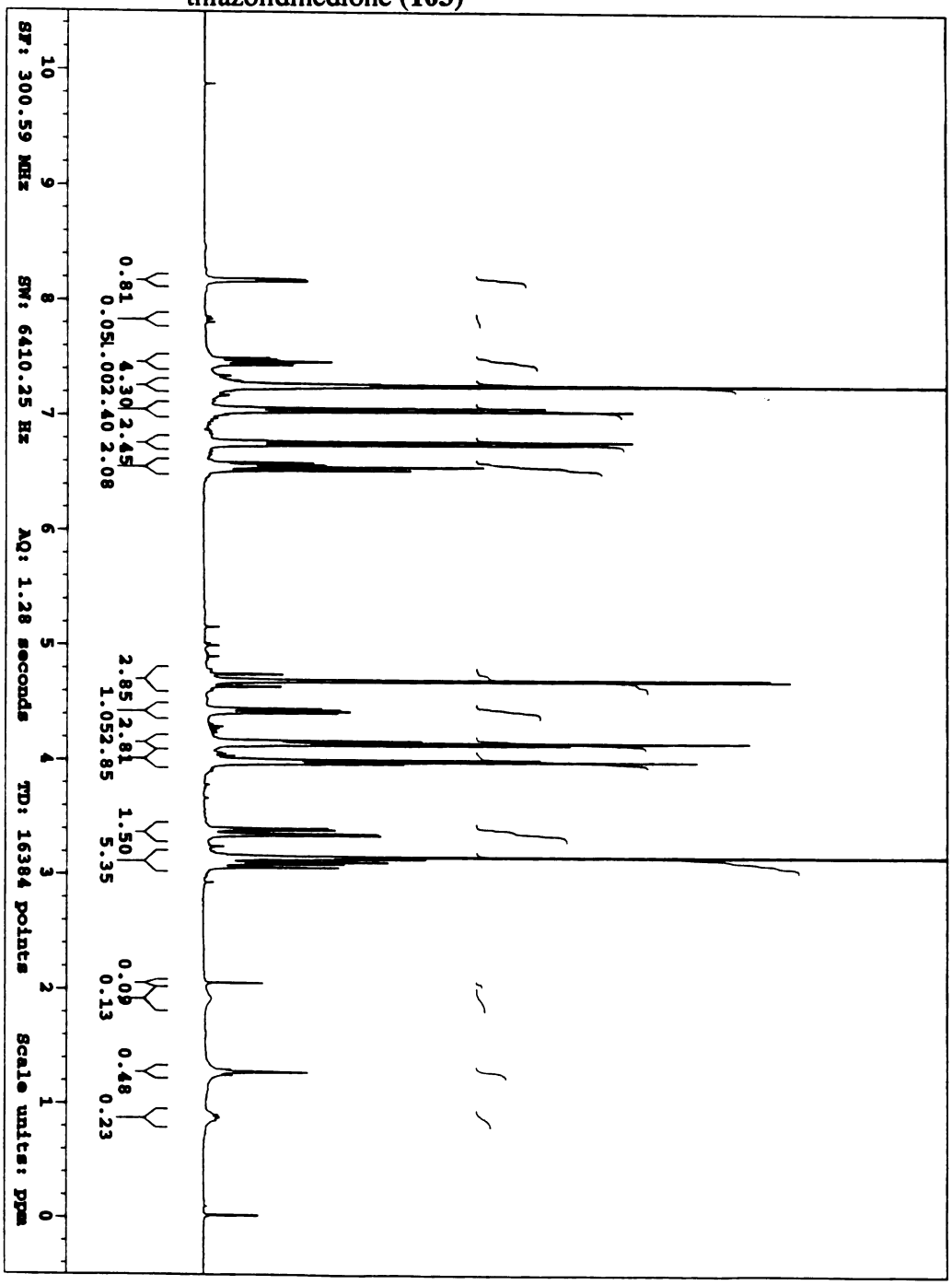

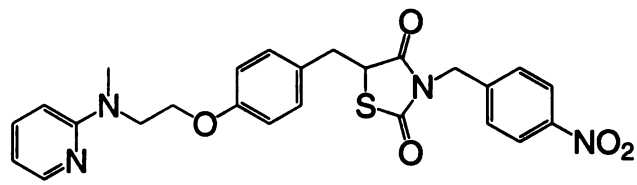

Appendix 2.20: ^{1}H-NMR ($CDCl_3$) 5-(4-(2-(methyl-2-pyridinylamino)ethoxy)benzyl-N-(4-nitrobenzyl)-2,4-thiazolidinedione (**104**)

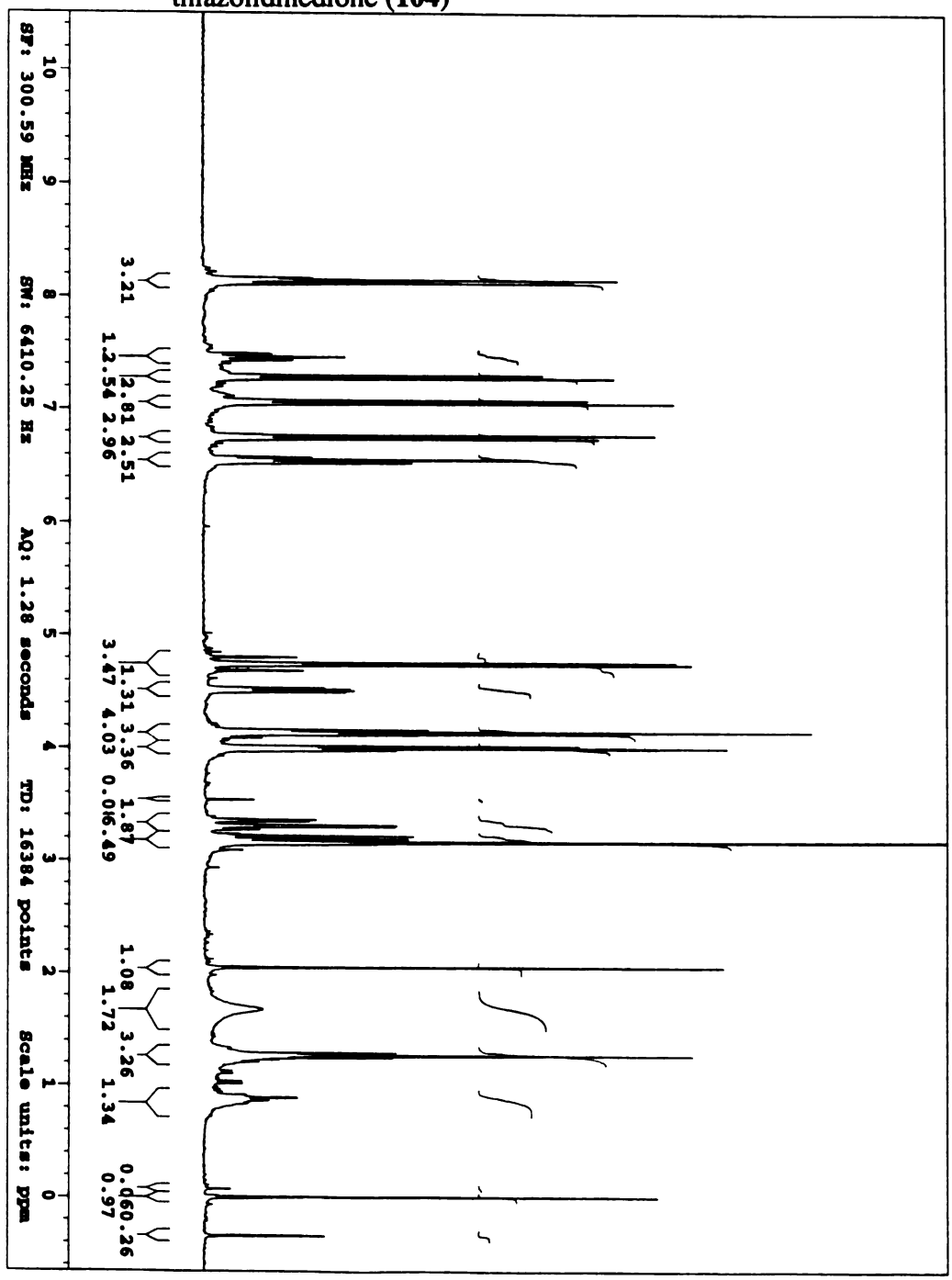

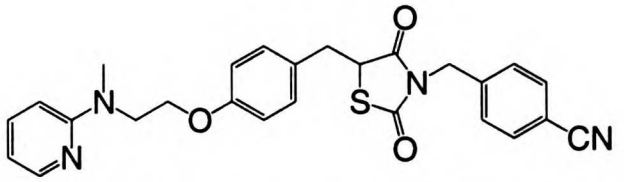

Appendix 2.21: ^{1}H-NMR ($CDCl_3$) 5-(4-(2-(methyl-2-pyridinylamino)ethoxy)benzyl-N-(4-tolunitrile)-2,4-thiazolidinedione (**105**)

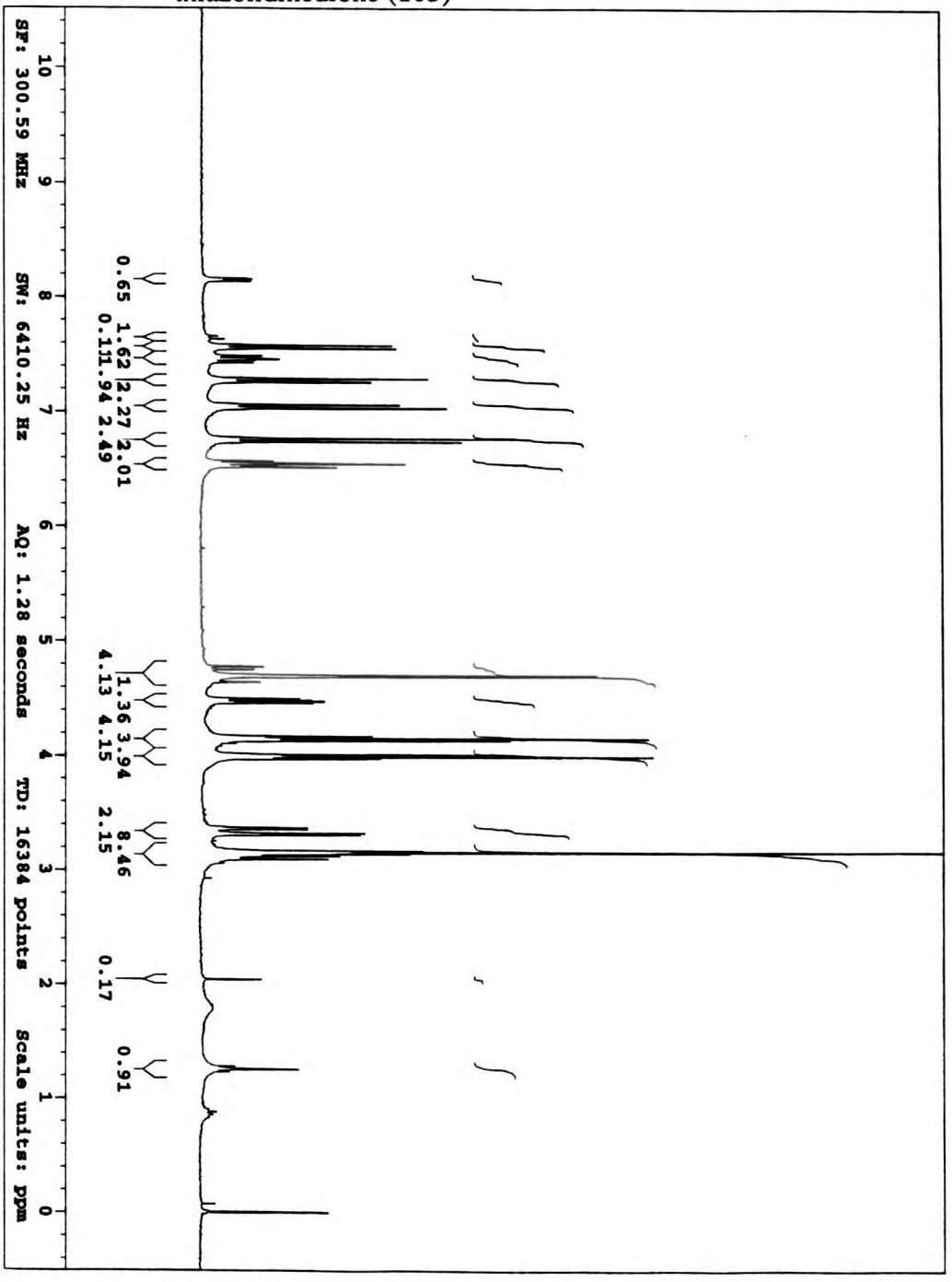

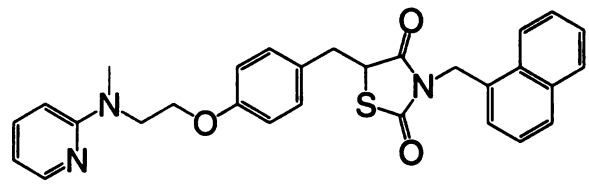

Appendix 2.22: ^{1}H-NMR ($CDCl_3$) 5-(4-(2-(methyl-2-pyridinylamino)ethoxy)benzyl-N-naphthyl-2,4-thiazolidinedione (**107**)

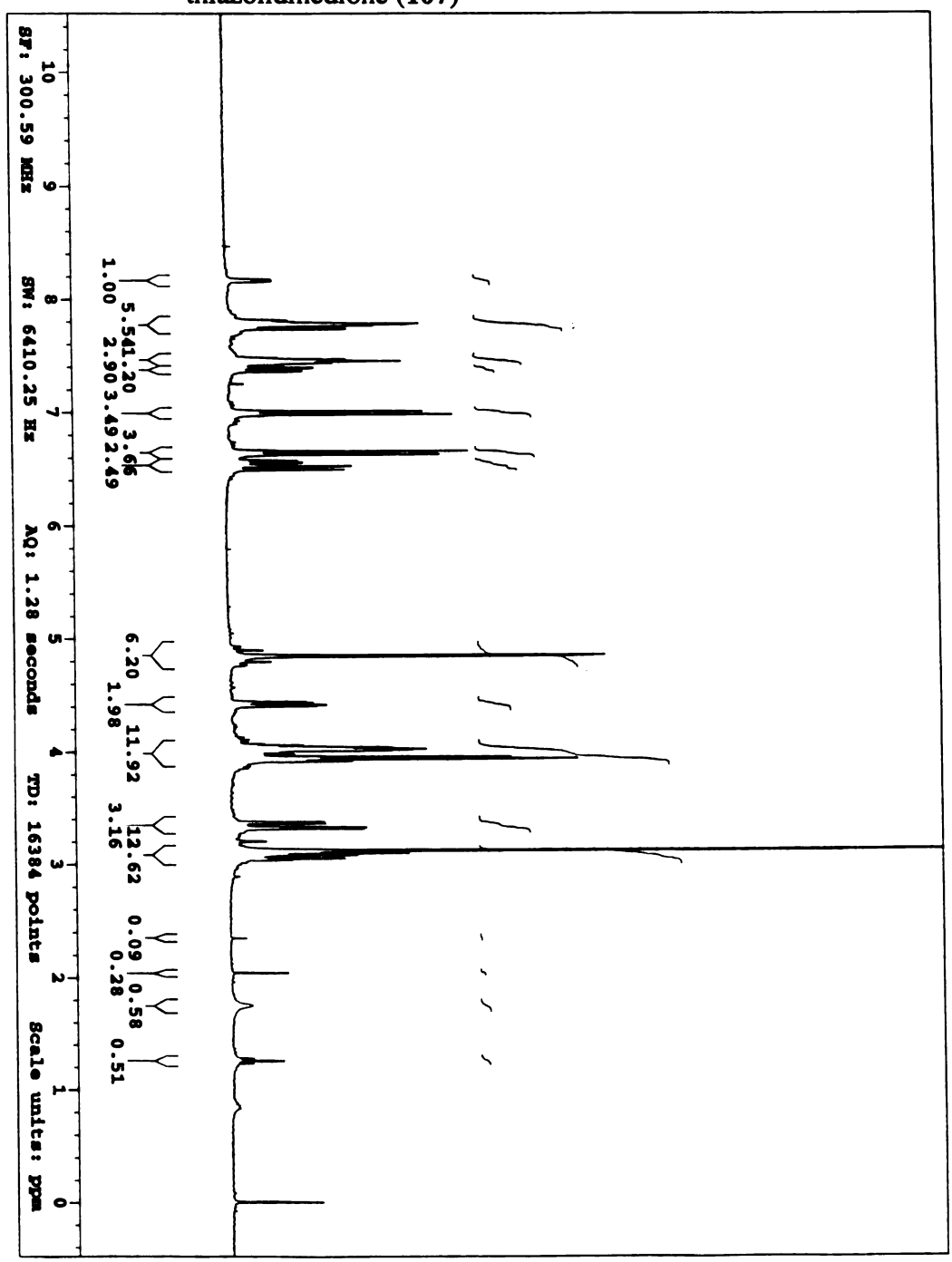

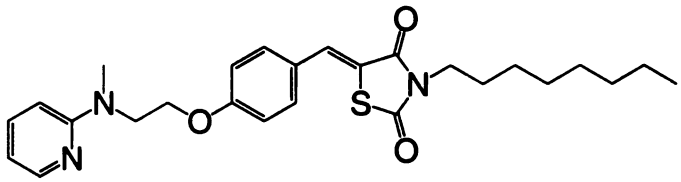

Appendix 2.23: ^{1}H-NMR (DMSO-d_6) (Z)-5-((4-(2-(methyl-2-pyridinylamino)ethoxy)phenyl)-methylene-N-octyl-2,4-thiazolidinedione (**121**)

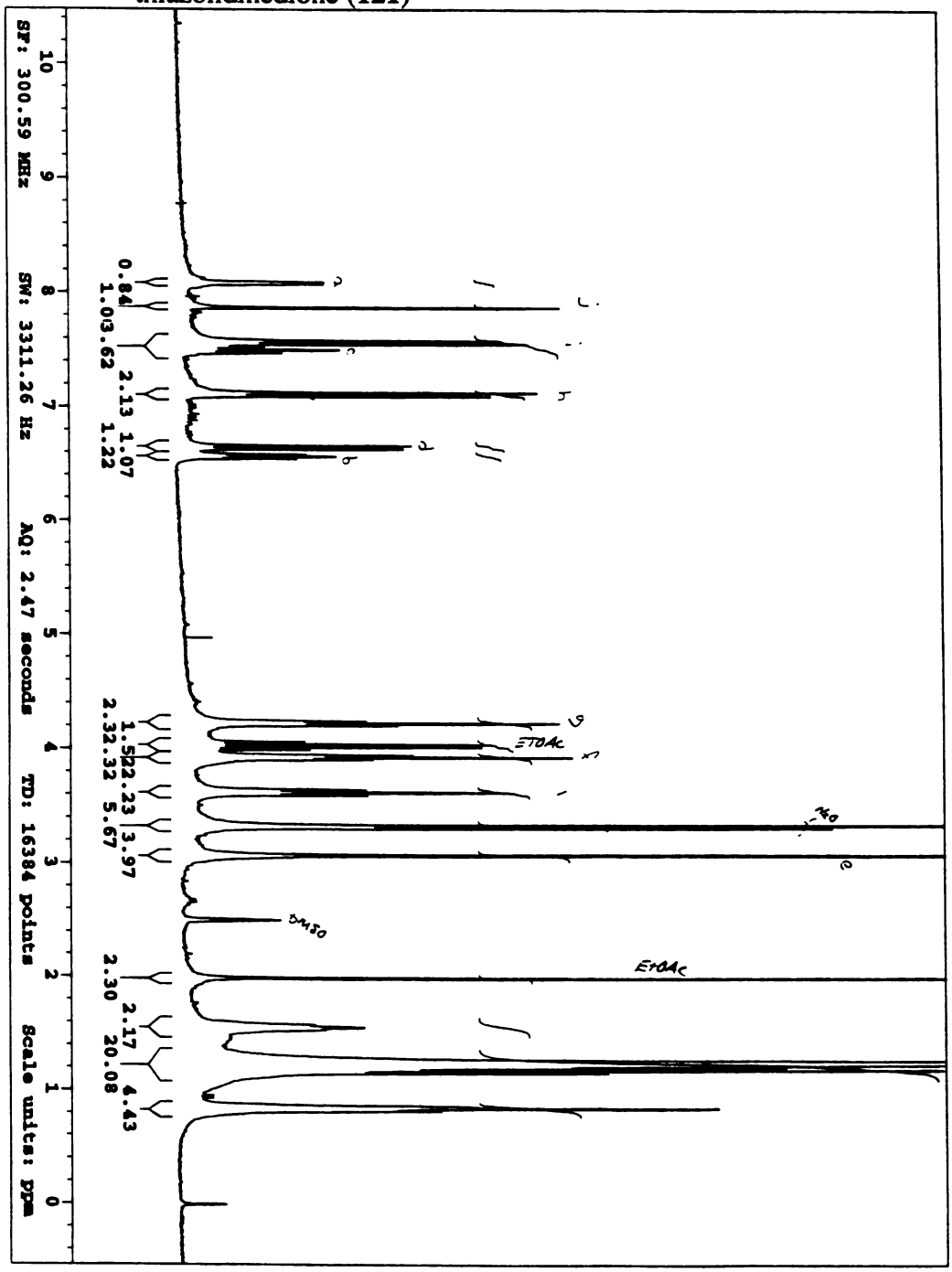

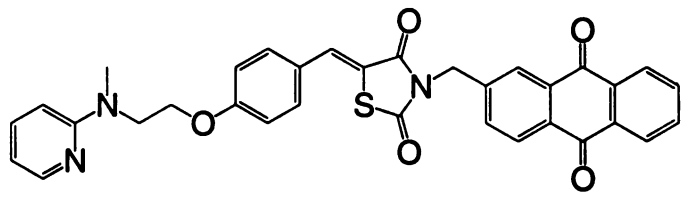

Appendix 2.24: ^{1}H-NMR ($CDCl_3$) (Z)-5-((4-(2-(methyl-2-pyridinylamino)ethoxy)phenyl)-methylene-N-(2-(bromomethyl)anthroquinone)-2,4-thiazolidinedione (**122**)

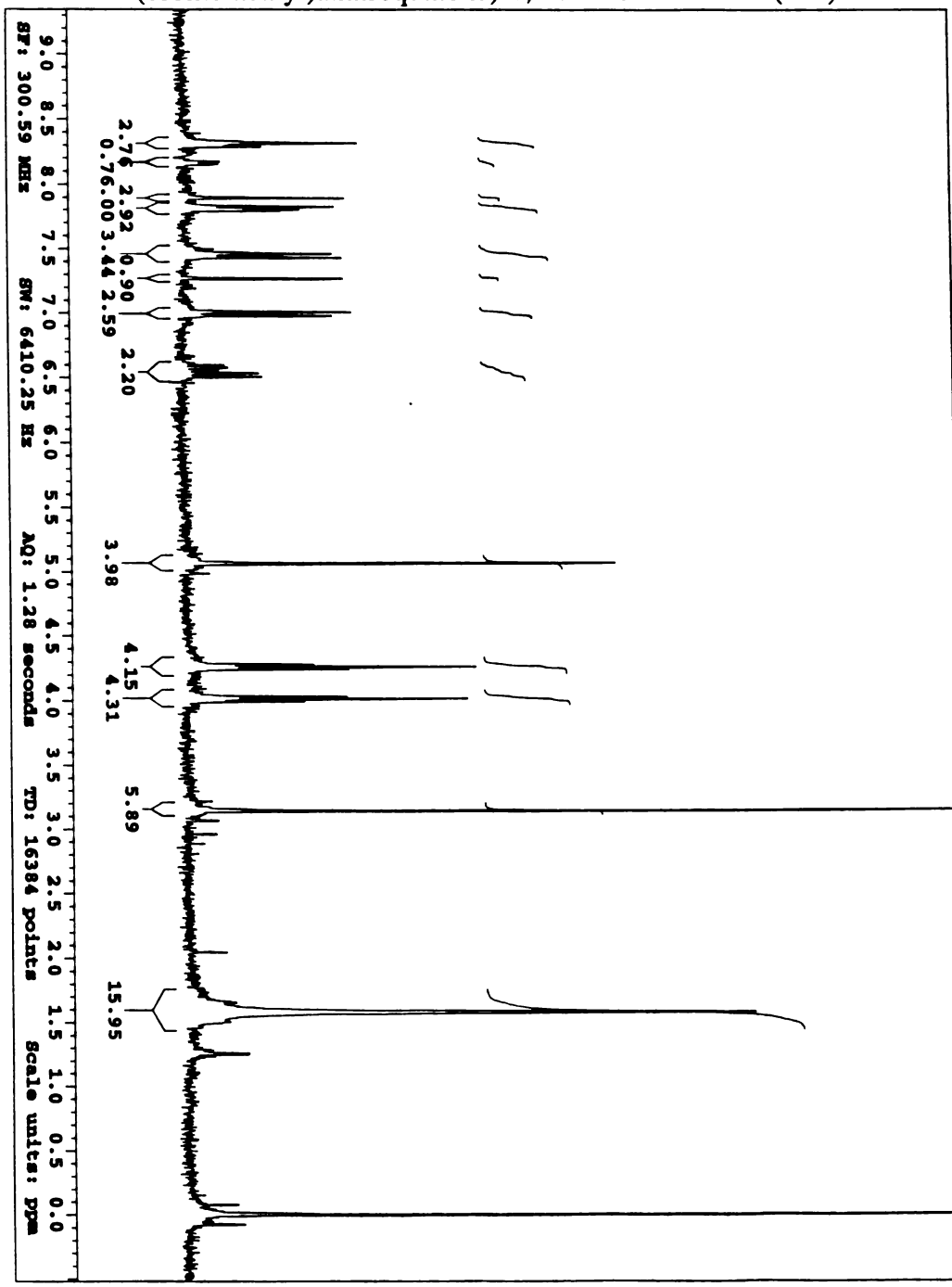

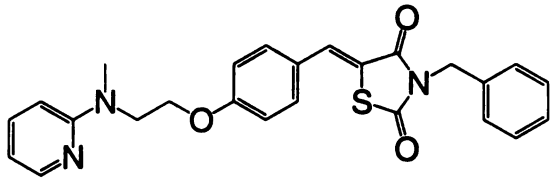

Appendix 2.25: ^{1}H-NMR ($CDCl_3$) (Z)-5-((4-(2-(methyl-2-pyridinylamino)ethoxy)phenyl)-methylene-N-benzyl-2,4-thiazolidinedione (**123**)

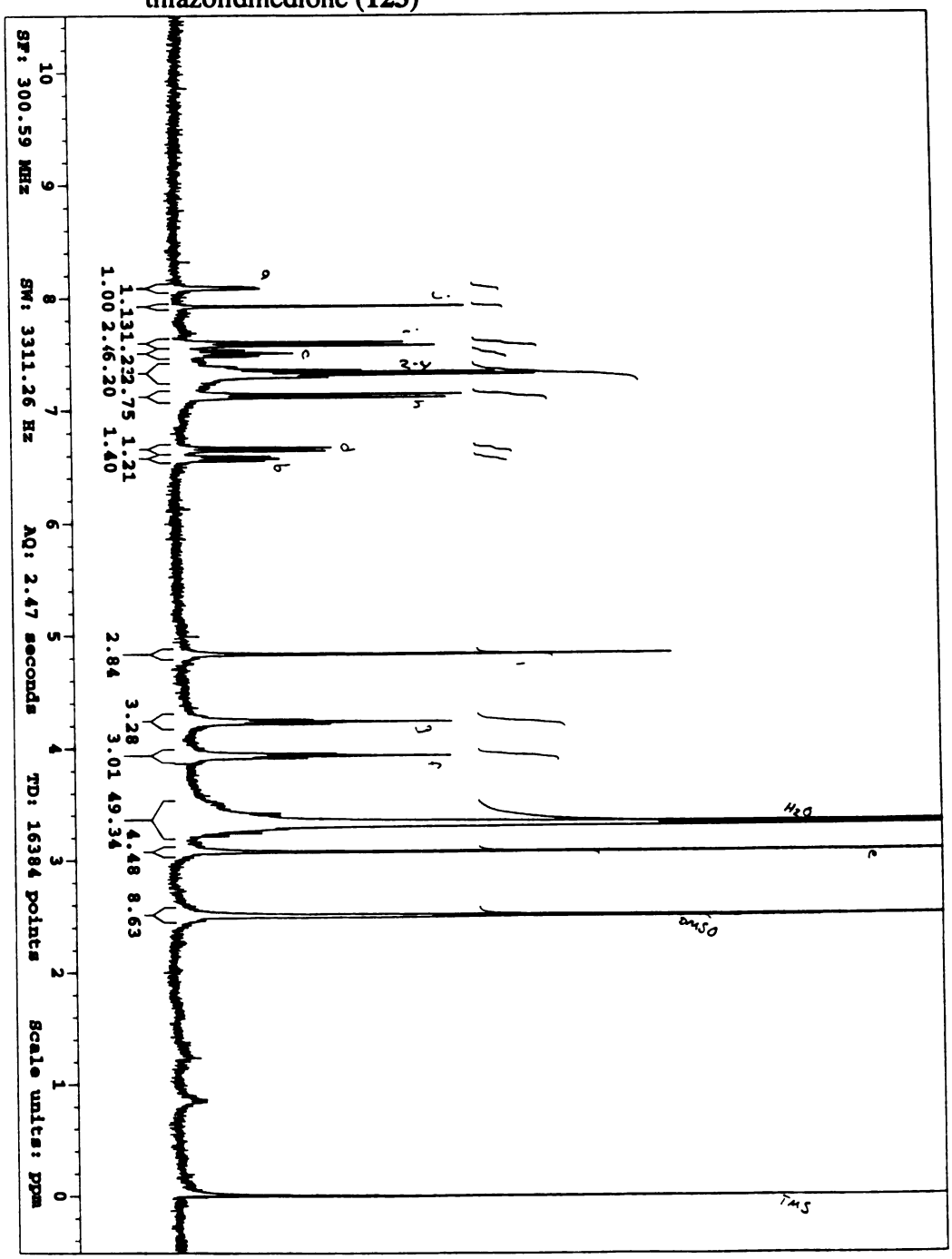

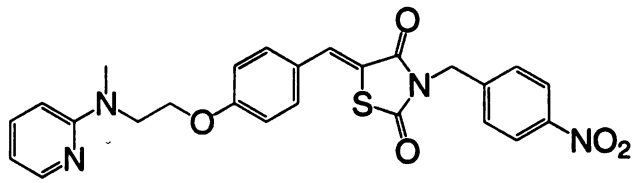

Appendix 2.26: ^{1}H-NMR ($CDCl_3$) (Z)-5-((4-(2-(methyl-2-pyridinylamino)ethoxy)phenyl)-methylene-N-(4-nitrobenzyl)-2,4-thiazolidinedione (**124**)

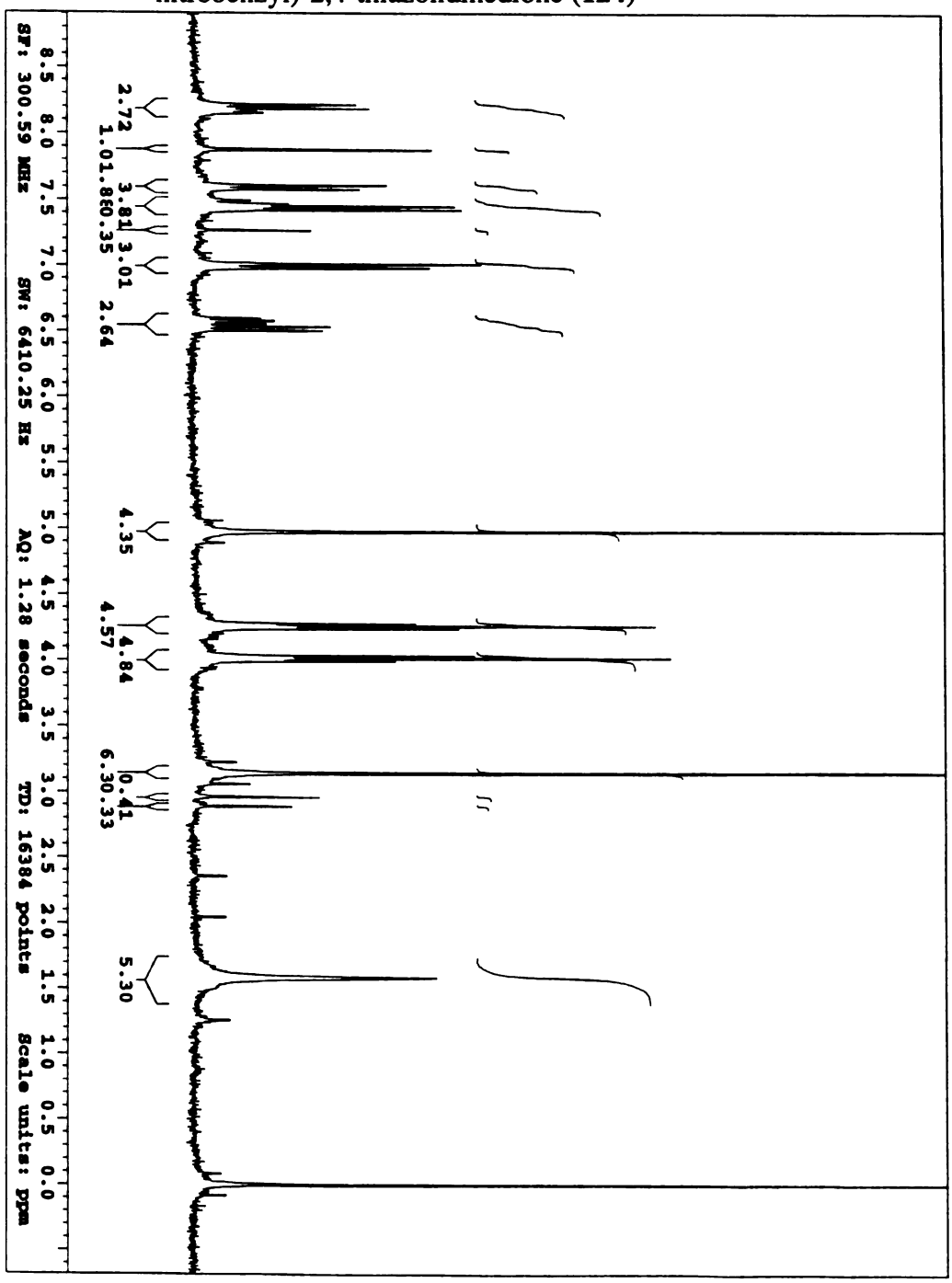

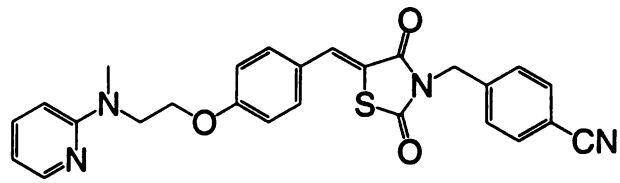

Appendix 2.27: ^{1}H-NMR (DMSO-d_6) (Z)-5-((4-(2-(methyl-2-pyridinylamino)ethoxy)phenyl)-methylene-N-(4-tolunitrile)-2,4-thiazolidinedione (**125**)

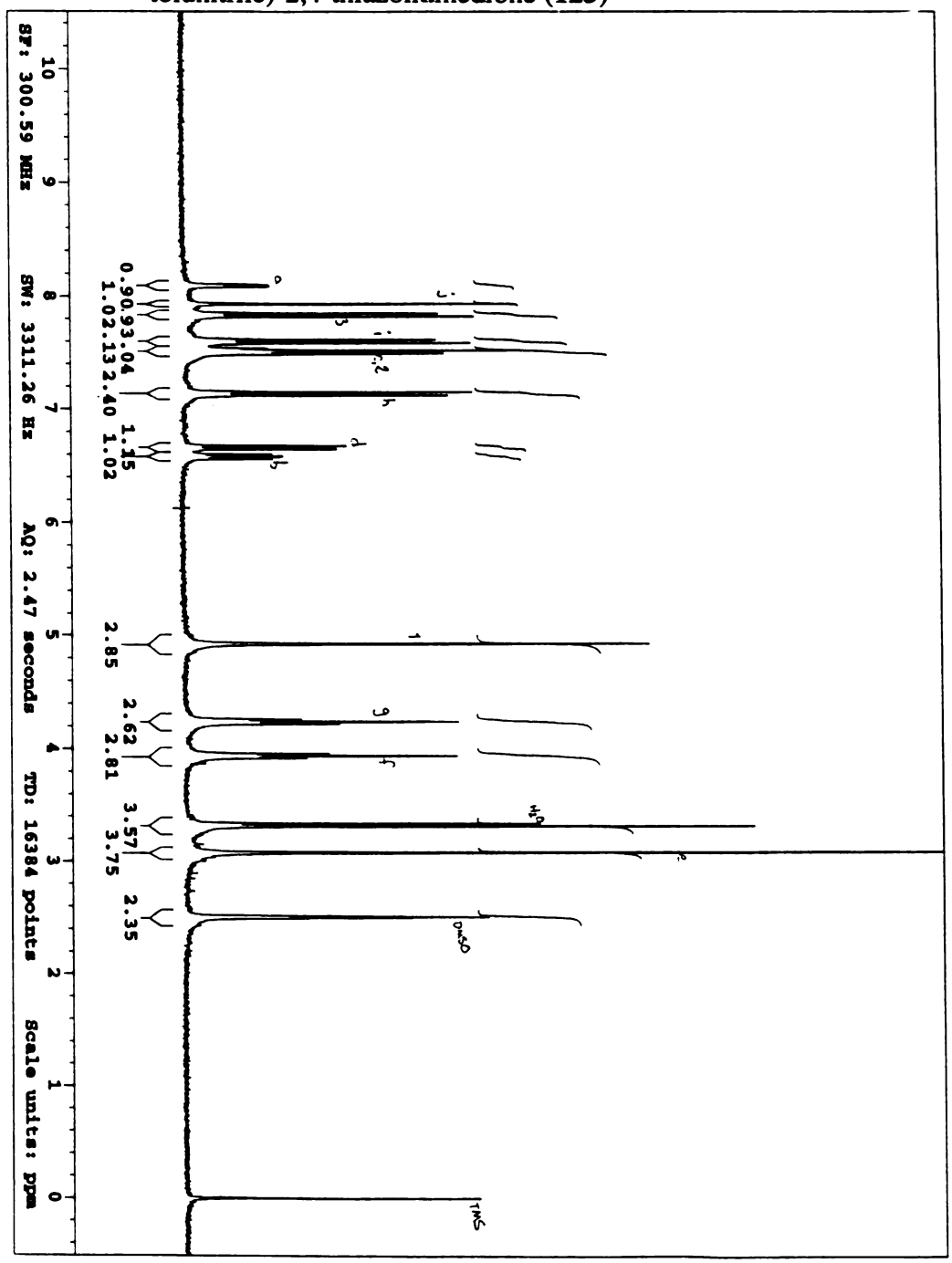

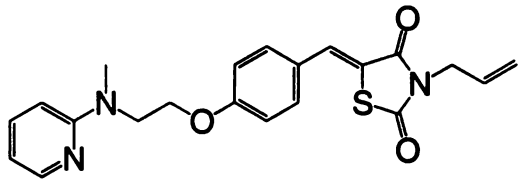

Appendix 2.28: ^{1}H-NMR (DMSO-d_6) (Z)-5-((4-(2-(methyl-2-pyridinylamino)ethoxy)phenyl)-methylene-N-allyl-2,4-thiazolidinedione (**126**)

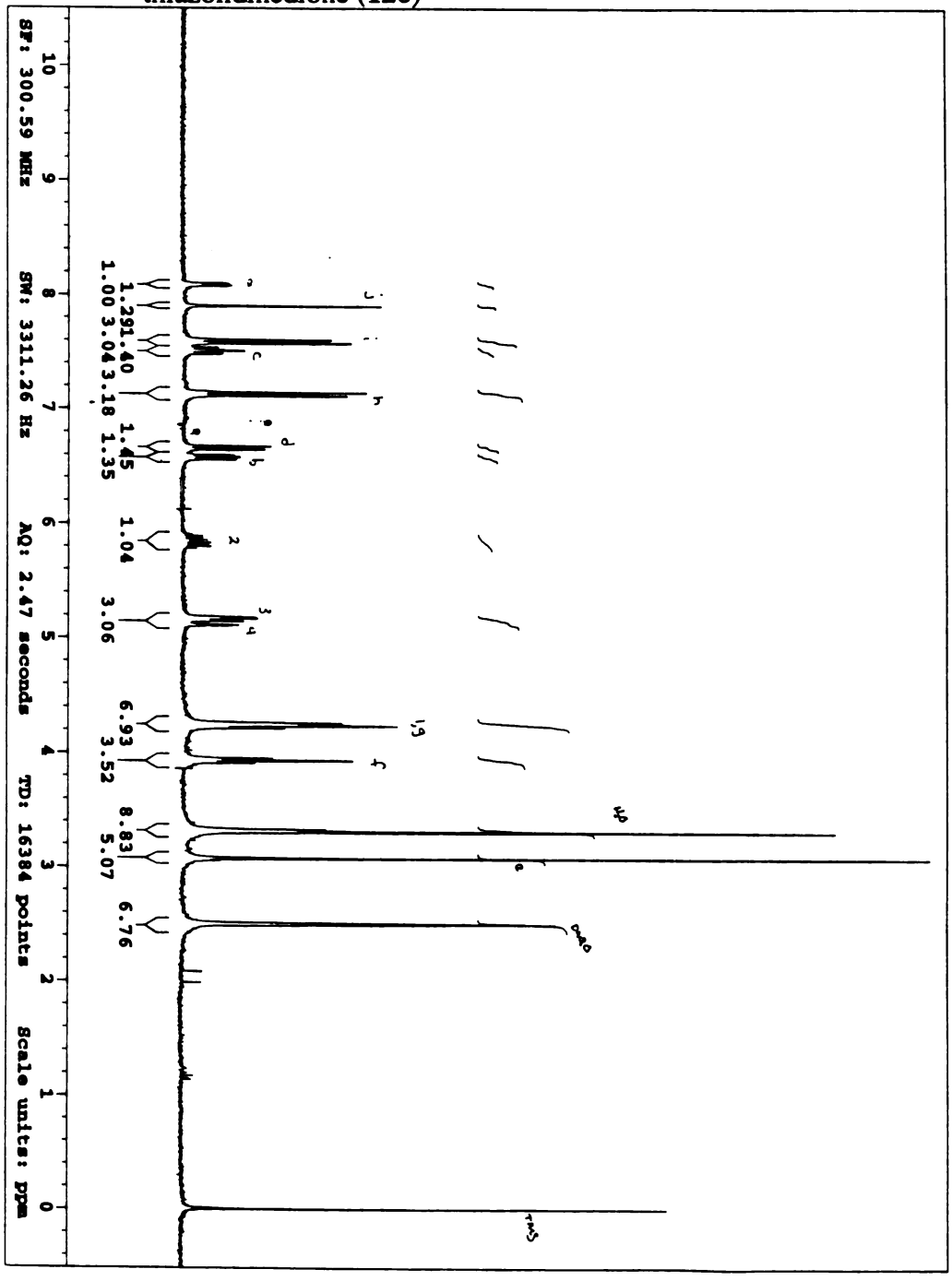

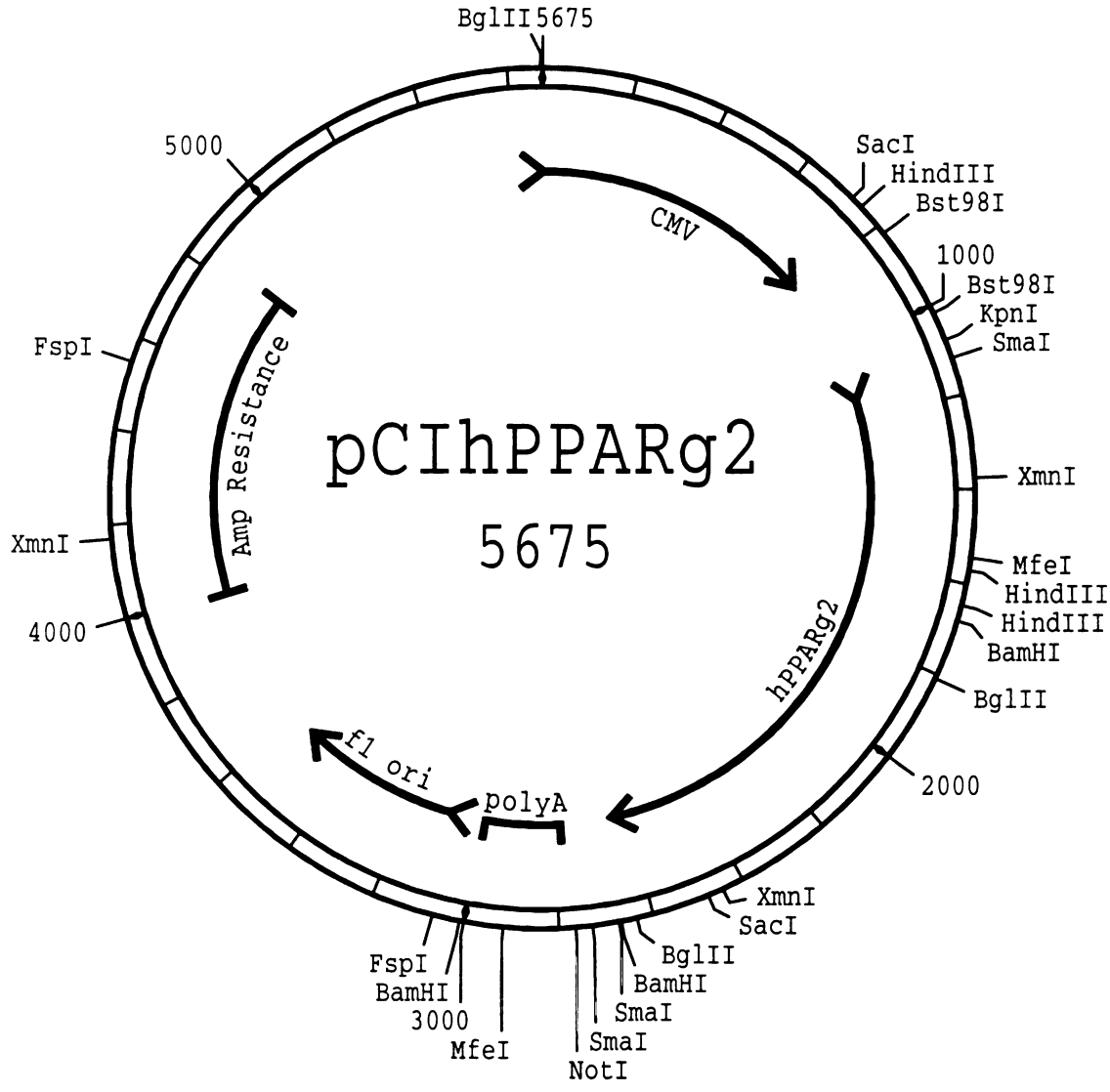

Appendix 3.1: pCIhPPARγ2 - Plasmid Map

The file pCIhPPARγ2.seq is displayed as a plasmid map generated using the GCG Plasmid Map function. This map includes the restriction sites for BamHI, BglII, Bst98I, FspI, HindIII, KpnI, MfeI, NotI, SacI, SmaI, and XmnI. The sequence file, map graphic, and a more extensive list of restriction sites is included on my data CD.

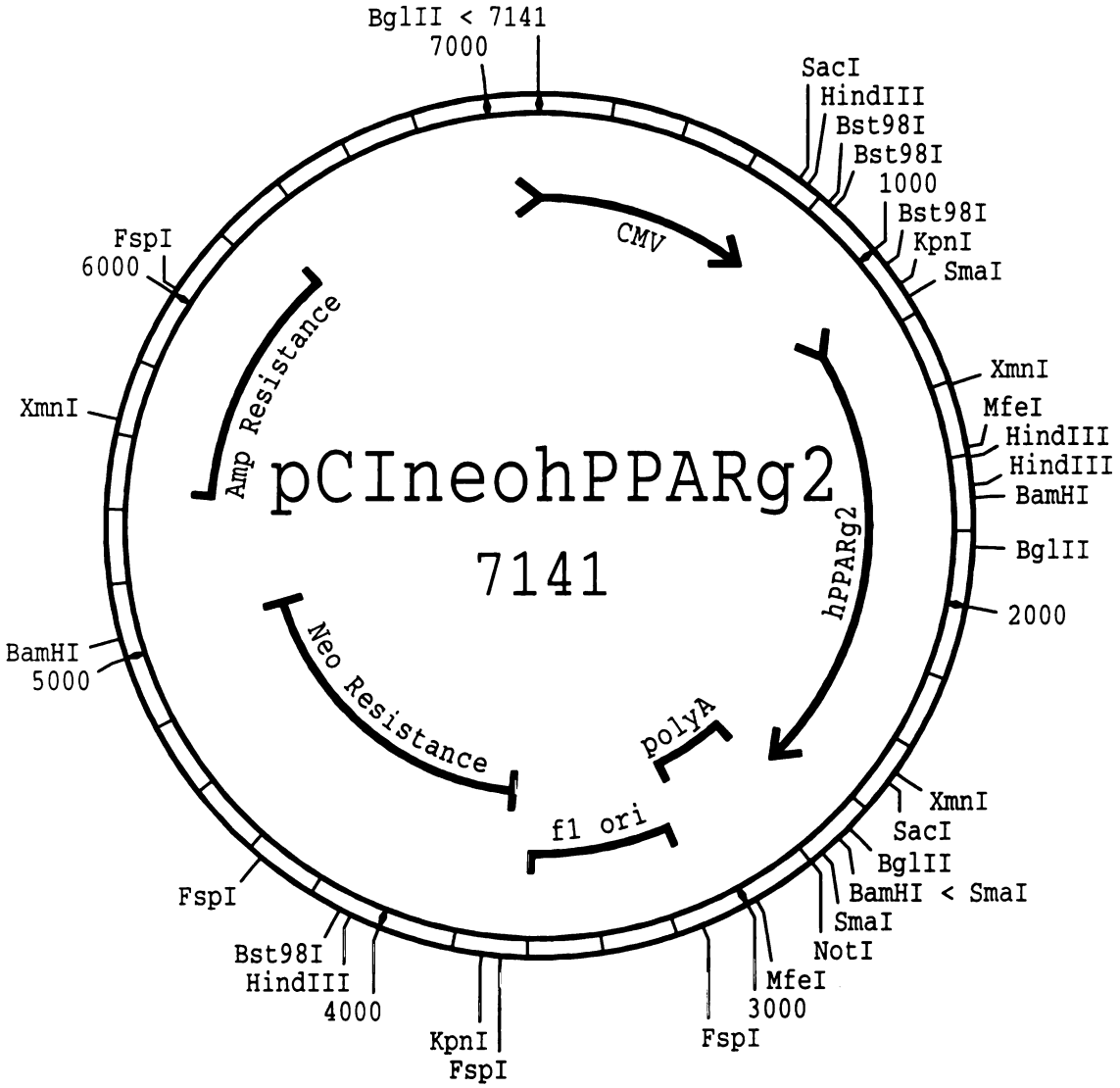

Appendix 3.2: pCIneohPPARγ2 - Plasmid Map

The file pCIneohPPARγ2.seq is displayed as a plasmid map generated using the GCG Plasmid Map function. This map includes the restriction sites for BamHI, BglII, Bst98I, FspI, HindIII, KpnI, MfeI, NotI, SacI, SmaI, and XmnI. The sequence file, map graphic, and a more extensive list of restriction sites is included on my data CD.

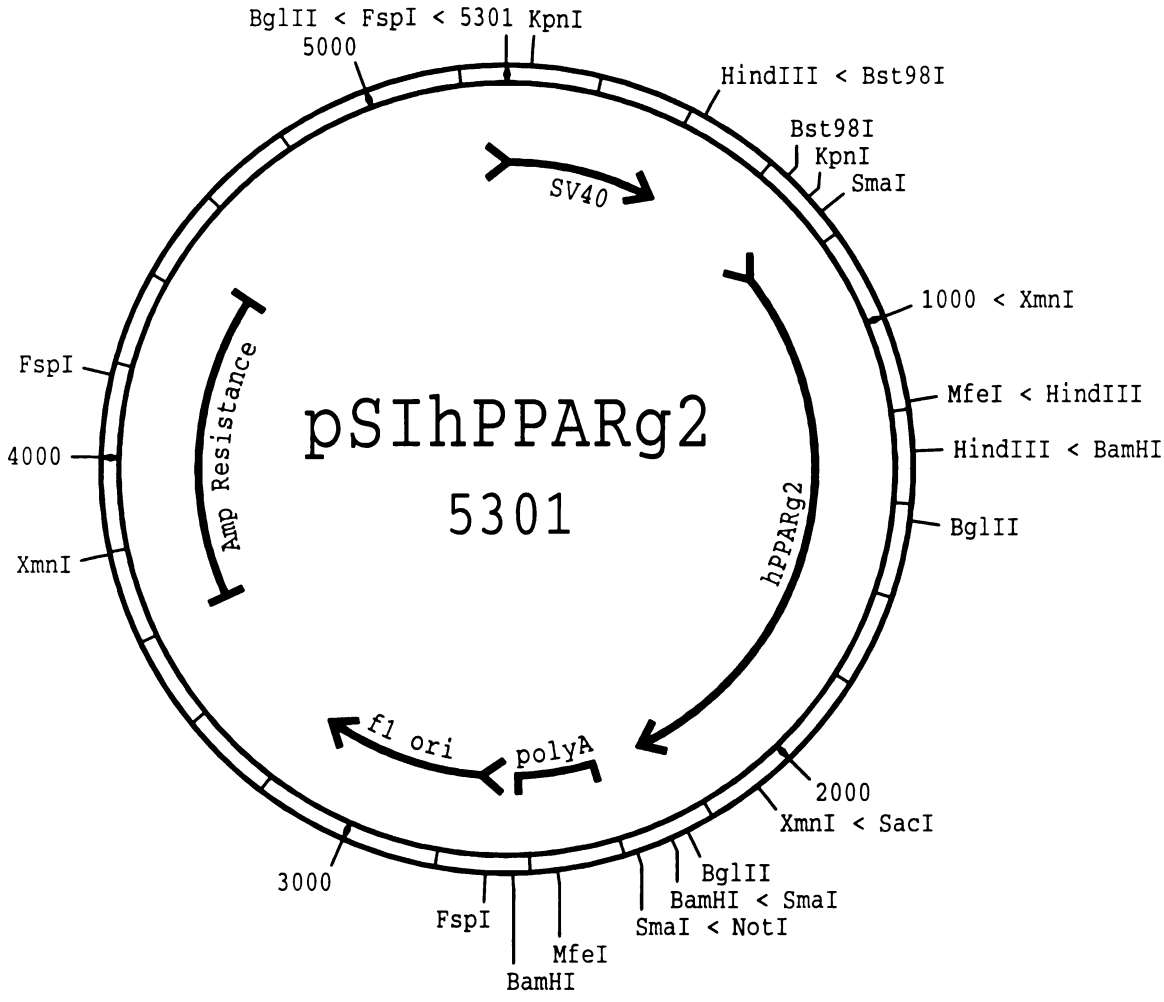

Appendix 3.3: pSIhPPARγ2 - Plasmid Map

The file pSIhPPARγ2.seq is displayed as a plasmid map generated using the GCG Plasmid Map function. This map includes the restriction sites for BamHI, BglII, Bst98I, FspI, HindIII, KpnI, MfeI, NotI, SacI, SmaI, and XmnI. The sequence file, map graphic, and a more extensive list of restriction sites is included on my data CD.

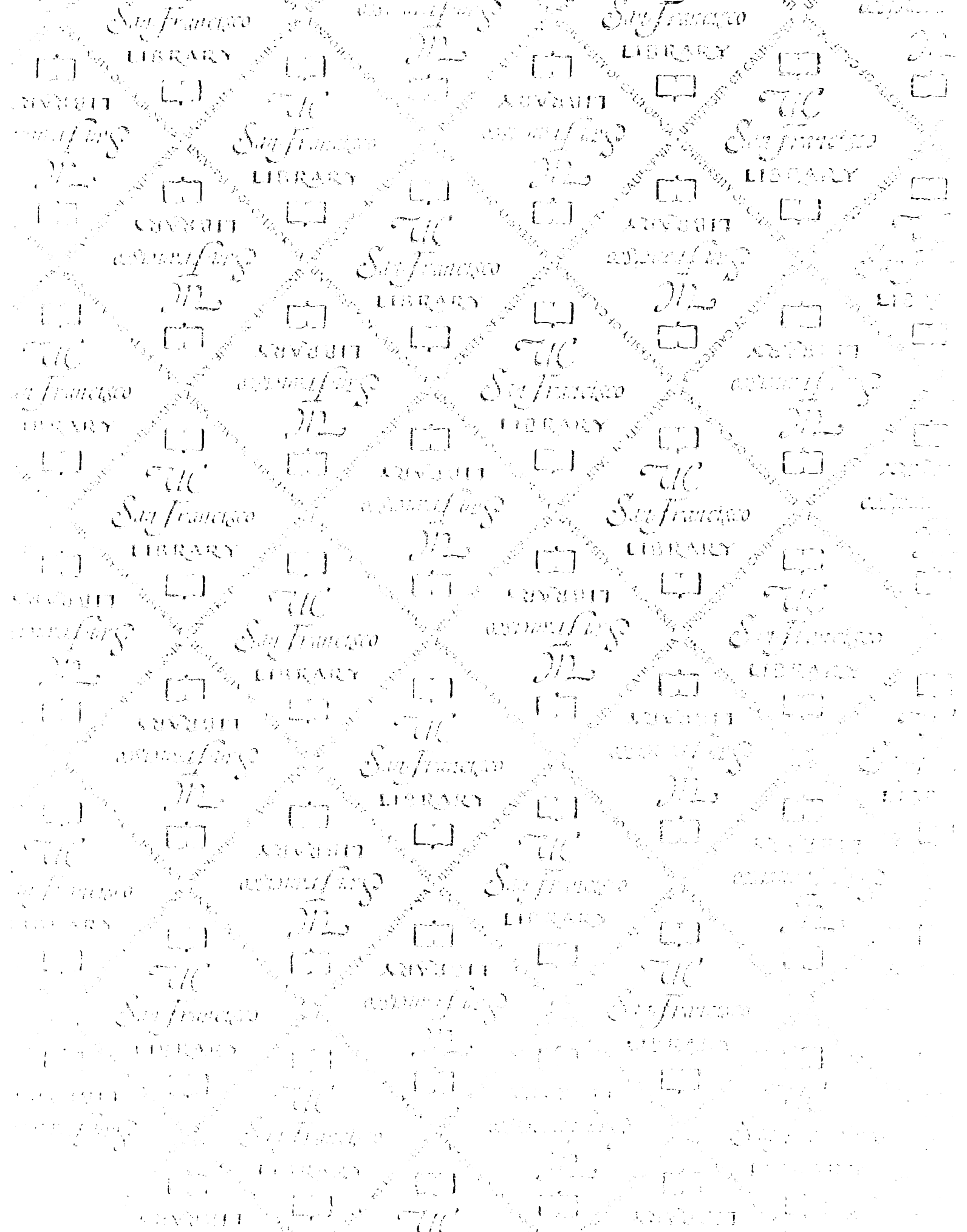
The San Francisco LIBRARY